

INTERACTION OF ANTIMICROBIAL PEPTIDES WITH MODEL LIPID MEMBRANES

Dissertation

zur Erlangung des akademischen Grades
Doctor rerum naturalium (Dr. rer. nat.)

vorgelegt der

Naturwissenschaftlichen Fakultät II - Chemie und Physik
der Martin-Luther-Universität Halle-Wittenberg

von Herrn M.Sc. Ahmad Arouri
geb. am 20. März 1979 in London

Gutachter:

1. Prof. Dr. Alfred Blume
2. Prof. Dr. Karl Lohner

Tag der Verteidigung: 14.04.2009

To my parents

Table of contents

Abbreviations and symbols	iii
1 Bio- and model membranes	1
1.1. Biological membranes.....	1
1.2. Model membranes	4
1.3. Lipid polymorphism.....	6
2 Antimicrobial peptides.....	9
2.1. Introduction.....	9
2.2. Mechanism of action	11
2.3. Bacterial selectivity	15
2.4. Structure activity relationship of antimicrobial peptides	15
3 Motivation.....	17
4 KLA peptides	18
4.1. Introduction	18
4.2 Results and discussion.....	22
4.2.1 Adsorption of KLA1 at the air/water interface.....	22
4.2.2 Adsorption of KLA1 to lipid monolayers.....	25
4.2.3 KLAL π/A isotherm at the air/water interface.....	32
4.2.4 Cospreparing of KLAL/lipid mixtures at the air/water interface.....	34
4.2.5 Adsorption versus cospreparing.....	42
4.2.6 Dynamic Light Scattering (DLS).....	43
4.2.7 Circular Dichroism (CD).....	45
4.2.8 Differential Scanning Calorimetry (DSC).....	47
4.2.9 Fourier Transform Infrared (FT-IR).....	53
4.2.10 Isothermal Titration Calorimetry (ITC)	59
4.3 Summary	74
5 RRWRF peptides	76
5.1 Introduction	76
5.2 Results and discussion.....	80
5.2.1 Dynamic Light Scattering (DLS).....	80
5.2.2 Differential Scanning Calorimetry (DSC).....	80
5.2.3 Fourier Transform Infrared (FT-IR)	92
5.2.4 Isothermal Titration Calorimetry (ITC).....	105
5.3 Summary	113
6 The antimicrobial action on supported lipid bilayers	116
6.1 Supported lipid membranes.....	116
6.2 Vesicle fusion and Langmuir Blodgett/vesicle fusion techniques	117

6.3	Langmuir Blodgett/Langmuir Schaefer technique.....	118
6.4	The interaction of RRWRF peptides with SLB prepared by LB/LS.....	122
6.5	The interaction of KLA peptides with SLB prepared by LB/LS.....	129
6.6	Summary.....	135
7	Conclusions.....	136
8	Zusammenfassung.....	138
9	Experimental procedures.....	140
9.1	Materials.....	140
9.1.1	Peptides.....	140
9.1.2	Lipids.....	140
9.2	Methods.....	141
9.2.1	Monolayer trough and subphase.....	141
9.2.2	Adsorption experiments.....	141
9.2.3	Cospreparing experiments.....	141
9.2.4	Infrared reflection absorption spectroscopy.....	142
9.2.5	Dynamic light scattering.....	142
9.2.6	Circular dichroism.....	143
9.2.7	Differential scanning calorimetry.....	143
9.2.8	Fourier transform infrared.....	143
9.2.9	Isothermal titration calorimetry.....	144
9.2.10	Planar supported bilayers.....	145
9.2.11	Fluorescence microscopy.....	146
9.2.12	Fluorescence recovery after photobleaching.....	147
9.3	Important infrared absorption bands.....	147
10	References.....	149
11	List of Figures and Tables.....	164
11.1	List of Figures.....	164
11.2	List of Tables.....	170
12	Acknowledgement.....	172
13	Curriculum vitae.....	174
13.1	Personal data.....	174
13.2	Education and research experience.....	174
13.3	Publications.....	175
13.4	Oral contributions.....	175
13.5	Poster contributions.....	176
14	Statement of originality.....	178

Abbreviations and symbols

Abbreviations

Methods

BLM	Black lipid membrane
CD	Circular dichroism
DLS	Dynamic light scattering
DSC	Differential scanning calorimetry
ESR	Electron spin resonance
FRAP	Fluorescence recovery after photobleaching
FT-IR	Fourier transform infrared
IR	Infrared
IRRAS	Infrared reflection absorption spectroscopy
ITC	Isothermal titration calorimetry
NMR	Nuclear magnetic resonance
RP-HPLC	Reversed phase high performance liquid chromatography
UV	Ultraviolet

Lipids and amino acids

DMPA	1,2-Dimyristoyl- <i>sn</i> -glycero-3-phosphatidic acid
DMPC	1,2-Dimyristoyl- <i>sn</i> -glycero-3-phosphocholine
DMPG	1,2-Dimyristoyl- <i>sn</i> -glycero-3-phosphoglycerol
DMPG-d ₅₄	Perdeuterated DMPG
DOPC	1,2-Dioleoyl- <i>sn</i> -glycero-3-phosphocholine
DOPE	1,2-Dioleoyl- <i>sn</i> -glycero-3-phosphoethanolamine
DOPG	1,2-Dioleoyl- <i>sn</i> -glycero-3-phosphoglycerol
DPhPC	1,2-Diphytanoyl- <i>sn</i> -glycero-3-phosphocholine
DPPC	1,2-Dipalmitoyl- <i>sn</i> -glycero-3-phosphocholine
DPPE	1,2-Dipalmitoyl- <i>sn</i> -glycero-3-phosphoethanolamine
DPPE-d ₆₂	Perdeuterated DPPE
DPPG	1,2-Dipalmitoyl- <i>sn</i> -glycero-3-phospho- <i>rac</i> -(1-glycerol)
DPPG-d ₆₂	Perdeuterated DPPG
DPSS	1,2-Dipalmitoyl- <i>sn</i> -glycero-3-phospho-L-serine
NBD-DPPE	1,2-Dipalmitoyl- <i>sn</i> -glycero-3-phosphoethanolamine-N-[7-nitro-2-1,3-benzoxadiazol-4-yl]
POPC	1-Palmitoyl-2-oleoyl- <i>sn</i> -glycero-3-phosphocholine
POPE	1-Palmitoyl-2-oleoyl- <i>sn</i> -glycero-3-phosphoethanolamine
POPG	1-Palmitoyl-2-oleoyl- <i>sn</i> -glycero-3-phosphoglycerol
TMCL	1,1',2,2'-Tetramyristoyl cardiolipin
DPG	Diphosphatidylglycerol (cardiolipin)
CL	Cardiolipin (DPG)
LPS	Lipopolysaccharides
PS	Phosphatidic acid
PC	Phosphatidylcholine
PE	Phosphatidylethanolamine

PG	Phosphatidylglycerol	
PS	Phosphatidylserine	
SM	Sphingomyelin	
A	Alanine (Ala)	
F	Phenylalanine (Phe)	
K	Lysine (Lys)	
L	Leucine (Leu)	
R	Arginine (Arg)	
W	Tryptophan (Trp)	
Y	Tyrosine (Tyr)	
<u>Others</u>		
<i>E. coli</i>	<i>Escherichia coli</i>	
<i>S. aureus</i>	<i>Staphylococcus aureus</i>	
<i>B. subtilis</i>	<i>Bacillus subtilis</i>	
<i>S. epidermidis</i>	<i>Staphylococcus epidermidis</i>	
AMP	Antimicrobial peptide	
CAMP	Cationic antimicrobial peptide	
CPP	Cell penetrating peptide	
DTGS	Deuterated triglycine sulphate	
EC ₂₅	Concentration causing 25% effect	
EC ₅₀	Concentration causing 50% effect	
EDTA	Ethylenediaminetetraacetic acid	
FDA	Food and drug administration	
GUV	Giant unilamellar vesicle	
IM	Inner membrane	
L	Lipid	
LB	Langmuir Blodgett	
LS	Langmuir Schaefer	
LUV	Large unilamellar vesicle	
<i>mf</i>	Mobile fraction	
MIC	Minimum inhibitory concentration	μM
MLV	Multilamellar vesicle	
OM	Outer membrane	
P	Peptide	
PMMA	Poly(methyl methacrylate)	
RBC	Red blood cells	
SLB	Supported lipid bilayer	
SUV	Small unilamellar vesicle	
TFE	Trifluoroethanol	
Tris	Tris-(hydroxymethyl) aminomethane	
VF	Vesicle fusion	
<u>Lipid phases in the bulk</u>		
L _α	Lamellar liquid crystalline phase	
P _β (P' _β)	Ripple phase (tilted P _β)	
L _β (L' _β)	Lamellar gel phase (tilted L _β)	
L _C (L' _C)	Lamellar crystalline phase (tilted L _C)	

Lipid phases at the air/water interface

G	Gas analogues phase
LE	Liquid expanded phase
LC	Liquid condensed phase
S	Solid analogues phase

Symbols

A	Area per molecule	$\text{nm}^2 \text{ molecule}^{-1}$
ΔA	Change in area per molecule	$\text{nm}^2 \text{ molecule}^{-1}$
A_0	Initial area per molecule	$\text{nm}^2 \text{ molecule}^{-1}$
$\Delta A/A_0$	Relative change in the molecular area	
a_L	Molecular area per lipid	$\text{nm}^2 \text{ molecule}^{-1}$
a_P	Molecular area per peptide	$\text{nm}^2 \text{ molecule}^{-1}$
$\alpha\%$	Helicity percentage	
β	Compressibility coefficient	m N^{-1}
β_{30}	Compressibility coefficient at 30 mN m^{-1}	m N^{-1}
c	Concentration	mol L^{-1} or g L^{-1}
C_L	Lipid total concentration	mol L^{-1}
C_P	Peptide total concentration	mol L^{-1}
ΔC_p	Constant pressure heat capacity change	$\text{cal mol}^{-1} \text{ K}^{-1}$
D	Lateral diffusion coefficient	$\text{cm}^2 \text{ s}^{-1}$
d	Optical path length	cm
δ	Deformation/scissoring vibration	cm^{-1}
δ_{as}	Antisymmetric bending vibration	cm^{-1}
δ_{s}	Symmetric bending vibration	cm^{-1}
F	Fluorescence	
F_0	Initial fluorescence	
F_∞	Fluorescence after bleaching	
F_{pre}	Fluorescence before bleaching	
Φ/Ψ	Hydrophobic/hydrophilic domain ratio	
G	Conductance	S
ΔG°	Standard free energy change	kcal mol^{-1}
γ	Rocking vibration	cm^{-1}
H	Hydrophobicity	
ΔH	Enthalpy change	kcal mol^{-1}
ΔH°	Standard enthalpy change	kcal mol^{-1}
$\Delta H^\circ_{\text{Helix}}$	Enthalpy change for helix formation per residue	kcal mol^{-1}
K	Partition constant	M^{-1}
K_{app}	Apparent association constant	M^{-1}
K_T	Binding constant at 1M Na^+ concentration	M^{-1}
M.wt.	Molecular weight	g mol^{-1}
M_r	Molecular mass	g mol^{-1}
μ	Hydrophobic moment	
n	Number of events	
N	Stoichiometry of the reaction	
N_A	Number of monomers	
v	Stretching vibration	cm^{-1}
ν_{as}	Antisymmetric stretching vibration	cm^{-1}
ν_{s}	Symmetric stretching vibration	cm^{-1}

p	Stripes period	μm
π	Surface pressure	mN m^{-1}
$\Delta\pi$	Change in surface pressure	mN m^{-1}
π_0	Initial surface pressure	mN m^{-1}
$\Delta\pi/\pi_0$	Relative change in the surface pressure	
Q	Heat flow	$\mu\text{cal s}^{-1}$
Θ	Ellipticity	deg (mdeg)
$[\Theta]_{\text{MRW}}$	Mean residual ellipticity	$\text{deg cm}^2 \text{mol}^{-1}$
$\langle r^2 \rangle$	Mean square displacement	cm^2
R	Universal gas constant	$1.987 \text{ cal mol}^{-1} \text{ K}^{-1}$
ΔS°	Standard entropy change	$\text{cal mol}^{-1} \text{ K}^{-1}$
T	Temperature	K or $^\circ\text{C}$
t	Time	s or min or h
T_m	Transition temperature	K or $^\circ\text{C}$
T_{pre}	Pretransition temperature	K or $^\circ\text{C}$
t_R	Retention time	min
T_{sub}	Subtransition temperature	K or $^\circ\text{C}$
τ	Open dwell time	s
V	Voltage	V
v	Volume	L
w	Wagging vibration	cm^{-1}

1 Bio- and model membranes

1.1. Biological membranes

Biological membranes are complex biphasic aggregates of lipids, proteins, and carbohydrates, consisting of the hydrophobic parts of the molecules, separated from the aqueous phases by polar interfaces, and formed as a result of non-covalent bonding and water exclusion from the hydrophobic core (Gennis 1989; Langner and Kubica 1999). Depending on the type of the membrane, the contribution of the lipids to the total mass of the membrane is between 20 - 80% by weight (Blume 2004). The fluid mosaic model presented by Singer and Nicolson (1972) (**Figure 1.1-1**) is the first comprehensive model describing biological membranes (Singer and Nicolson 1972). The bilayer in biological membranes is a two-dimensional fluid matrix, where the lipid and protein molecules can diffuse freely in the plane of the bilayer. However, this model deals with the lipid bilayer as a passive structure serving two functions: separating the cell from the surrounding and supporting the membrane proteins.

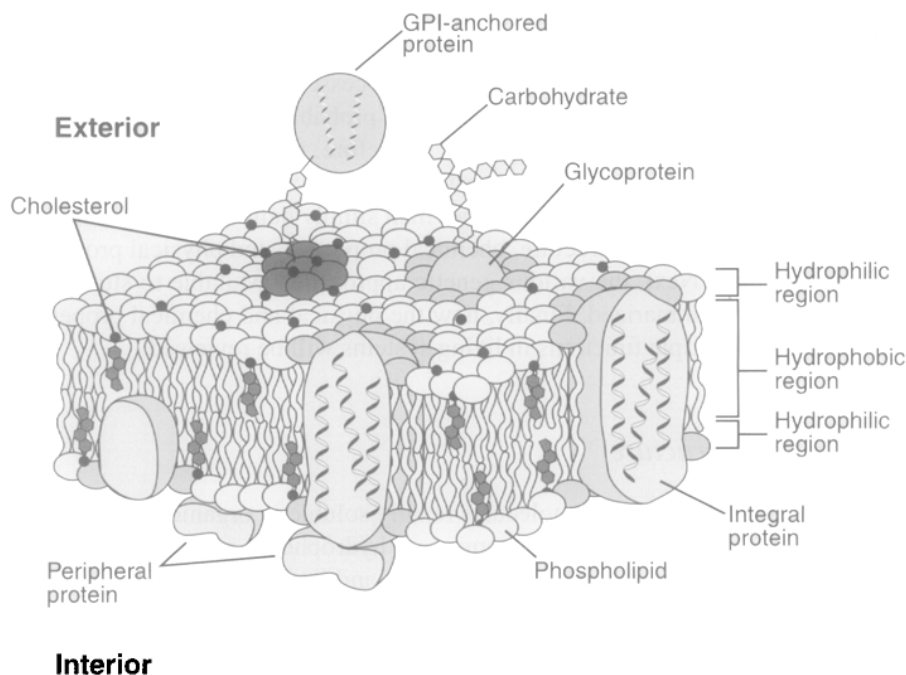


Figure 1.1-1 The plasma membrane structure of eukaryotic cells according to the model of Singer and Nicolson 1972. Adapted from ref. (Dowhan and Bogdanov 2002).

Though the model sufficiently describes the global behaviour of lipid bilayers, it does not take into account the asymmetric transversal and lateral lipid distribution as well as the continuously changing membrane properties according to the environmental conditions and cell state (Zhang and Rock 2008). It is nowadays strongly suggested that biomembranes

contain a mosaic of microdomains (rafts) of certain lipids, rather than the previously assumed homogeneous distribution, assembled according to their intrinsic chemical characteristics and possibly maintained with the support of certain membrane proteins (Engelman 2005; Matsumoto et al. 2006). There is a growing experimental evidence supporting the importance of membrane lipids in several vital cell functions, like regulation of cell activities, cell trafficking, protein orientation and membrane targeting (Langner and Kubica 1999), whereas some lipids are bound invariably to specific sites on proteins supporting their functions (Sanderson 2005). In addition, membrane lipids are now well known to serve as the precursors of many cellular signal molecules which are released intracellularly in response to extracellular stimuli (Langner and Kubica 1999). Furthermore, some drugs, like narcotics, antidepressants, cytotoxic agents, may influence the function of some membrane proteins by their non specific interactions with lipids (Momo et al. 2000).

The membrane lipid composition, i.e. lipid type and fraction, may vary significantly depending on the tissue type, cell function and surrounding conditions (Lohner et al. 2008 and references cited therein). Since each lipid serves specific functions, the phospholipid content in the membrane is well controlled and kept within a window (Cronan 2003). In fact, there are well over 1000 molecular species of all classes of phospholipids in eukaryotic membranes (Huang and Li 1999). The most abundant lipids are cholesterol and the zwitterionic lipids phosphatidylcholine (PC), sphingomyelin (SM), and phosphatidylethanolamine (PE) (Gennis 1989).

Table 1.1-1 Phospholipid composition of red blood cells (percentage of total phospholipid) from various organisms listed according to increasing sphingomyelin content. Adapted from refs. (Lohner et al. 2008; White 1973).

Organism	PC	SM	Total choline phospholipids	PE	PS	Total amino phospholipids	Others
Rat	47.5	12.8	60.3	21.5	10.8	32.3	7.4 ^a
Rabbit	33.9	19.0	52.9	31.9	12.2	44.1	3.0 ^b
Human	34.7	20.1	54.8	28.0	14.3	42.3	2.9 ^c
Pig	22.3	26.5	49.8	29.7	17.8	47.5	2.7 ^a
Sheep	-	51.0	51.0	26.2	14.1	40.3	8.7 ^a

^aMainly phosphatidylinositol. ^bPhosphatidylinositol and phosphatidic acid. ^cMainly phosphatidic acid.

Table 1.1-1 shows the lipid composition of red blood cells (RBC), which serve as an archetype of mammalian cell membranes. The cytoplasmic leaflet of the RBCs contains mostly the amino phospholipids PE and phosphatidylserine (PS), whereas the outer side is composed exclusively of PC and SM. Therefore, a combination of PC, SM and cholesterol

with the proper ratio will suit well to model mammalian cell membranes (Dowhan and Bogdanov 2002; Lohner et al. 2008).

The architecture of bacterial membranes is much more complex as compared to eukaryotic membranes, whereas one should also be aware of the differences between the membrane structure in Gram-positive and Gram-negative bacteria (**Figure 1.1-2**). The cell envelope of Gram-negative bacteria is made of two layers; an outer cell wall and an inner cytoplasmic membrane separated by a periplasmic space filled with peptidoglycan. Lipopolysaccharides exist exclusively in the outer leaflet of the cell wall, whereas lipids form the inner side. Gram-positive bacteria have only a cytoplasmic membrane covered with a peptidoglycan-teichoic acid network for protection.

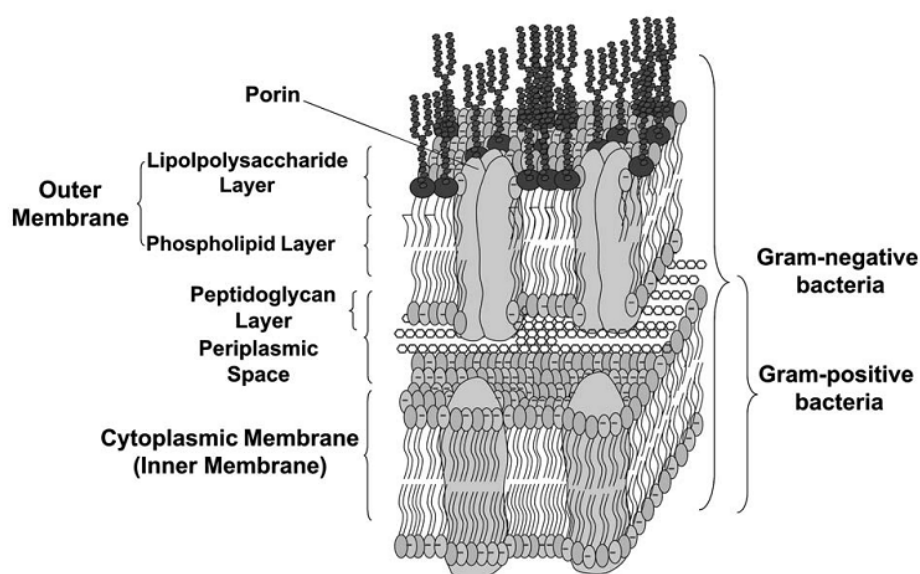


Figure 1.1-2 Schematic presentation of the molecular structure of bacterial cell membranes. Gram-negative bacteria consist of an outer membrane and a cytoplasmic membrane, whereas Gram-positive bacteria possess only a cytoplasmic membrane protected by a peptidoglycan layer that also exists in the periplasmic space of Gram-negative bacteria. Adapted from ref. (Lohner et al. 2008).

As illustrated in **Table 1.1-2**, the outer and cytoplasmic membranes of Gram-negative bacteria consist mainly of PE together with appreciable amounts of the negatively charged phosphatidylglycerol (PG) and cardiolipin (diphosphatidylglycerol DPG). In Gram-positive bacteria, the lipid composition varies to a large extent among the different species. Whereas PG and cardiolipin are the major lipid components in Gram-positive bacteria, PE and aminoacyl derivatives of PG, such as lysyl- and ornithine-PG, can also be found. Although PC is a widely distributed and quantitatively important phospholipid in animals and higher plants, it is generally not found in bacteria (Dowhan and Bogdanov 2002; Lohner et al. 2008). PG/PE lipid mixtures are often used to model bacterial cytoplasmic membranes, particularly the Gram-negative ones. Nonetheless, and due to the diversity in the lipid composition of

bacterial membranes, this model cannot be generalized for all prokaryotes. Besides, the view of bacterial membranes are now changing from homogeneous lipid mixture to one where the lipid molecules are segregated into patches containing specific lipid molecules. This is particularly suggested for PE and cardiolipin molecules, which is facilitated by the tight packing of their hydrocarbon chains and possibly supported by membrane proteins (Matsumoto et al. 2006).

Table 1.1-2 Phospholipid composition of some selected species of Gram-negative and Gram-positive bacteria (percentage of total phospholipid). Adapted from refs. (Lohner et al. 2008; O’Leary and Wilkinson 1988; Wilkinson 1988).

Bacteria species		PG	DPG	L-lysyl PG	PE	Others
Gram-negative						
<i>Erwinia carotovora</i>	OIM ^a	14	8	0	78	0
<i>Escherichia coli</i>	OM ^b	3	6	0	91	0
	CM ^c	6	12	0	82	0
<i>Salmonella typhimurium</i>	OM	17	2	0	81	0
	CM	33	7	0	60	0
<i>Pseudomonas cepacia</i>	OM	13	0	0	87	0
	CM	18	0	0	82	0
Gram-positive						
<i>Bacillus megaterium</i>	CM	40	5	15	40	0
<i>Bacillus subtilis</i>	CM	29	47	7	10	6 ^d
<i>Micrococcus luteus</i>	CM	26	67	0	0	7 ^e
<i>Staphylococcus aureus</i>	CM	57	5	38	0	Trace

^a Phospholipid composition not differentiated between outer and inner membrane. ^b OM, outer membrane. ^c CM, cytoplasmic membrane. ^d Including phosphatidic acid and glycolipids. ^e Almost exclusively phosphatidylinositol.

1.2. Model membranes

Due to the complexity of cell membranes as well as to the diversity in their composition, it is still not easy to study them as one intact entity. Whereas it is more convenient to utilize simpler model lipid systems, the formation of properly structured lipid bilayers and the biological relevance of the model systems limit this approach. Since it is hard to reconstruct cell membranes precisely, a compromise should be made between the model simplicity and accuracy. The biological relevance of the experiments with model membranes and our ability to extrapolate them to biosystems have often been addressed (Blume 2004; Lohner et al. 2008). The main model lipid systems are lipid monolayers, multilamellar and unilamellar vesicles, planar lipid bilayers and black lipid membranes (BLM).

The phospholipids are membrane lipids consisting of a hydrophilic polar headgroup and a hydrophobic tail. Generally, as shown in **Table 1.2-1**, the polar headgroup contains a glycerol backbone, to which two fatty acids are esterified at the sn-1 and sn-2 positions, and a highly polar or charged group attached through a phosphodiester linkage to the third carbon.

as of water on both surfaces vary. Due to the PE smaller headgroup it tends to form membranes with negative curvature.

Charged lipids are common and versatile constituents of biological membranes. In nature, many physiological functions are driven by nonspecific electrostatic interactions with the membrane charged components. PA contains one single charge associated with the phosphate group, where the charge is more exposed to the surrounding as it is not separated by additional moieties. PG and PS also carry one negative net charge which is sterically screened from the bulk by glycerol and serine groups, respectively. Therefore, PA is expected to interact more efficiently with cationic molecules in its vicinity than the other anionic phospholipids (Langner and Kubica 1999 and references cited therein).

The surface of lipid membranes is a complex environment of polar headgroups, ordered water, and ions. Albeit the significant influence of the headgroup environment on bilayer properties, such as its fluidity, thickness and potential, it is not commonly addressed in lipid-peptide/protein interactions (Sanderson 2005).

1.3. Lipid polymorphism

Since membrane phospholipids in cells are exposed extracellularly as well as intracellularly to an aqueous environment, it is of relevance to biological membranes to study the structure and properties of the lipid bilayer composed of well-defined molecular species in the presence of excess water. Lipids have the capacity to show a variety of what are so-called liquid crystalline states (mesophases), which are more ordered than liquid but less than crystalline solid. When phospholipid molecules are placed in water, their hydrophilic heads tend to face water and the hydrophobic tails are forced to stick together. Israelachvili et al. suggested that the adopted lipid structure, e.g. micelles, lamellar, or inverted hexagonal phases, depends on the geometry of the molecules, e.g. cones, cylinders, or inverted cones, respectively (Israelachvili 1992). Manipulating the temperature, pressure, pH, ionic strength, water content, lipid concentration, and the composition of the aqueous dispersing medium can induce phase transitions between these states. Besides, the phase transition is well known to be influenced by many molecular factors, such as the lengths of the two acyl chains, the chain length difference between the sn-1 and sn-2 acyl chains, chain unsaturation, backbone modification, and headgroup structures. The influence of the lipid concentration, vesicle size and lamellarity, thermal history, the preparation procedure, and the incorporation of guest molecules cannot be ignored (Blume 2004; Caffrey and Cheng 1995; Huang and Li 1999; Koynova and Caffrey 1998; Seelig and Seelig 2002).

The one-component phospholipid bilayer in excess water can undergo multiple phase transitions upon heating (thermotropic phase transitions). Of these several transitions, the chain-melting transition or the gel-to-liquid-crystalline phase transition is the main phase transition which is accompanied by the largest entropy and enthalpy changes. Experimentally, this main phase transition is the only one that is observed reproducibly upon repeated reheating. A wide variety of physical techniques, such as DSC, dilatometry, X-ray diffraction, neutron diffraction, dynamic light scattering, NMR, ESR, and fluorescent and vibrational spectroscopies can be used to detect these transitions. Although each of the physical techniques can provide specific information, much of our information concerning the thermodynamic changes accompanying the lipid phase transition have come from DSC (Huang and Li 1999).

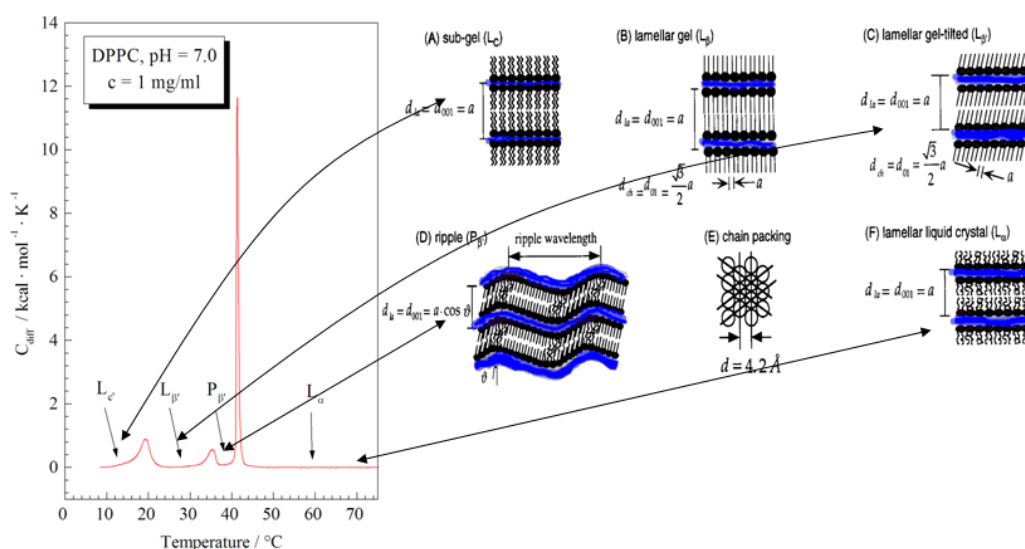


Figure 1.3-1 A DSC thermogram of DPPC showing the various thermotropic phase transitions. The illustrations exhibit the bilayer structure at different phases.

Figure 1.3-1 demonstrates the thermotropic phase transitions of DPPC. After keeping the fully hydrated long chain phospholipids for a long time at low temperature, a phospholipid, such as DPPC, is in the ordered, condensed crystalline subgel phase (L'_c) (The prime ' indicates that the acyl chains are tilted). The hydrocarbon chains are fully extended in all-*trans* conformation and the polar head group ($\sim 0.4 - 0.5 \text{ nm}^2$) is relatively immobile at the water surface. On heating, L'_c state phospholipids undergo a subtransition (usually 30 degrees below the main transition temperature) to the lamellar gel (L_β or L'_β) state, where the chains could be tilted or perpendicular to the bilayer normal. The subtransition is associated with an increase in the head group mobility and in the water penetration into the interfacial region of the bilayer. On further heating, L'_β state phospholipids may undergo a pretransition to the

“ripple” gel (P'_{β}) state (5 - 10 degrees below the main transition) which could be due to the rotation of the polar head group or the co-operative movement of hydrocarbon chains prior to melting. Further heating of P'_{β} state phospholipids results in a co-operative melting of the hydrocarbon chains (the main transition of gel phase to liquid crystalline phase) to give the liquid crystalline (L_{α}) state. In the L_{α} phase, the headgroups ($\sim 0.6 - 0.7 \text{ nm}^2$) are well hydrated, the molecules have high rotational and translational degrees of freedom and the conformation of several carbon-carbon single bonds changes from *trans* to *gauche* conformation (Blume 2004; Nagle and Tristram-Nagle 2000; Taylor and Craig 2003). The phase transition of phospholipid mixtures with different hydrocarbon chains occur over a wider temperature range than pure phospholipids, with asymmetric transitions when the compositions other than equimolar are present. When the hydrocarbon chains differ by only two carbon atoms, ideal mixing of lipids occurs (Garidel and Blume 2000; Garidel et al. 1997a; Garidel et al. 1997b).

2 Antimicrobial peptides

2.1. Introduction

The antimicrobial resistance is a growing problem that threatens our ability to treat infections (Hawkey 2008; Heuer et al. 2006; Teuber 2001), particularly, it is not adequately compensated by the development of new generations of antimicrobials. For instance, 16 new antibiotics were introduced during 1983-1987 as compared to 7 during 1998-2002 (Spellberg et al. 2004). This shows the urgent need to develop novel alternatives for “conventional” antibiotics, which are less susceptible for the development of bacterial resistance. Bacteriophages, bacterial cell wall hydrolases, and antimicrobial peptides are among the most promising candidates (Parisien et al. 2008). The antimicrobial peptides (AMPs) are fundamental components of the innate immune system that conserved their efficiency over billions of years (Gordon et al. 2005; Radek and Gallo 2007). They are produced by almost all species, including microorganisms, plants, animals, and human (Papo and Shai 2003). Besides, the bacteria may produce AMPs to control the colony size when a certain threshold population has been reached, so-called quorum sensing (Rossi et al. 2008). So far, almost 900 eukaryotic AMPs have been identified (<http://www.bbcm.units.it/~tossi/pag1.htm>), in addition to thousands of synthetic variables that have been produced. Therefore, during recent years they have increasingly attracted a lot of interest as a potential solution to the bacterial resistance (Giuliani et al. 2007; Gordon et al. 2005; McDermott 2007; Zhang and Falla 2004). This is due to their ability to disturb biological membranes via non-specific interactions with the membrane lipid components. The most appealing properties of AMPs are their: 1) broad-spectrum activity (antibacterial, antiviral, antifungal), 2) rapid (minutes to a couple of hours (Brogden 2005)) and potent bactericidal activity, 3) low level of induced resistance (Gordon et al. 2005), and 4) vast variety in terms of structures and antimicrobial functionalities (Parisien et al. 2008). Though the use of an AMP as a single therapeutic agent has drawn most of the attention, several other therapeutic strategies exist, such as the use of AMPs for their anti-endotoxin activities through neutralizing LPS (Freceer et al. 2004; Rosenfeld and Shai 2006), as immunostimulatory agents or in combination with conventional antibiotics to promote additive or synergetic effects (Gordon et al. 2005). Many AMPs show a broad spectrum cytotoxic activity against cancer cells (Hoskin and Ramamoorthy 2008). In fact, it has been reported that a single AMP can exhibit all of these functions (Gifford et al. 2005). Some of the cationic AMPs show the capacity to translocate across biological bilayers in a non-disruptive way, and, thus, have been successfully used for drug delivery into mammalian

cells (Deshayes et al. 2006; Henriques et al. 2006). Actually, all membrane active peptides, namely, the AMPs, cell penetrating peptides (CPPs) and fusogenic peptides belong to interrelated families (Henriques et al. 2006).

Most of the pharmaceutical efforts have been devoted to obtain the FDA approval for topically applied antimicrobial agents (Giuliani et al. 2007). In spite of the large efforts undertaken to bring some of the AMPs to the drug market (Giuliani et al. 2007; Gordon et al. 2005; McDermott 2007; Zhang and Falla 2004), thus far no natural or modified AMP obtained the FDA approval for any topical or systematic medical applications (Gordon et al. 2005; Parisien et al. 2008). The major obstacles of the therapeutic use of AMPs are their: 1) low effectiveness as compared to many therapeutically used antibiotics, 2) high toxicity, 3) low in vivo stability, and 4) unfavourable pharmacokinetics. This is in addition to 5) the resistance of some microbial species to AMPs and 6) the high costs of drug development and manufacturing (Giuliani et al. 2007; Gordon et al. 2005; Marr et al. 2006; Parisien et al. 2008). To overcome the stability issue and to increase the half life of an AMP, several strategies have been developed; such as the introduction of D-amino acids and non-natural amino acids, amidation at the N-terminus, and peptide cyclization (Giuliani et al. 2007).

AMPs can be classified according to their 1) origins: eukaryotic AMPs, bacteriocins, and phage-encoded AMPs (Parisien et al. 2008), 2) activity spectrum (Andreu and Rivas 1998), 3) bacterial selectivity (Papo and Shai 2003), 4) secondary structure: β -sheet, α -helical, loop and extended peptides, with the first two classes being the most common in nature (Hancock and Lehrer 1998), and 5) amino acid composition, particularly their content of anionic and cationic residues (Brogden 2005). On a macroscopic level, there are two common and functionally important requirements for the antimicrobial peptide; a net cationic charge and the ability to assume an amphipathic structure, where the hydrophilic and the hydrophobic parts are oriented in opposite directions (Powers and Hancock 2003). The amphipathicity is necessary for their insertion into lipid bilayers and the cationic nature governs the selectivity towards bacterial membranes (Dathe and Wieprecht 1999; Zelezetsky and Tossi 2006). Some peptides require zinc as a cofactor for their antimicrobial activity (Brogden et al. 1996; Dashper et al. 2007). Many studies have already exhibited that the macroscopic properties of the peptide, rather than the primary sequence, determine its activity and selectivity (see for instance (Appelt et al. 2008)). Therefore, there have been several attempts to mimic the essential properties of the antimicrobial peptides by introducing D-amino acids into the peptides (Shai and Oren 1996), by using non-natural amino acids (Liu and DeGrado 2001), and by developing oligomers and polymers with an outstanding

antimicrobial activity and selectivity (Rennie et al. 2005; Som et al. 2008; Tew et al. 2002). Usually, D-amino acid analogues show comparable activity to L-peptides, yet, they are more resistant to the proteolytic degradation. Simple antimicrobial synthetic oligomers and polymers may have an advantage over AMPs, as they are more stable and could be cheaper to produce.

2.2. Mechanism of action

To date, the majority of the scenarios anticipated for the mechanisms of action of AMPs are based on experiments carried out essentially on model lipid systems (Jelinek and Kolusheva 2005). Therefore, many of the tenets of the antimicrobial action of AMPs remain subject to debate. Regardless of the mode of action of AMPs, several steps are necessary for the bactericidal action. Seelig et al. divides the interaction of the cationic antimicrobial peptides (CAMPs) with lipid membranes into three thermodynamic steps: 1) the electrostatic attraction of the cationic peptides to anionic membranes that enhances their concentration on the membrane surface as compared to the bulk, however, binding can also occur between non-charged peptides and neutral membranes, 2) the partitioning of the peptides into lipid membranes, and 3) the conformational changes of the bound peptides, which are induced through hydrophobic interactions (Seelig 2004). It is also noted that antimicrobial peptides may oligomerize in solution and thus may behave different from the peptide monomers (Bechinger and Lohner 2006; Stella et al. 2004). Before the peptide interacts with the bacterial cytoplasmic membrane, it must transverse the outer envelope in Gram-negative bacteria that contains LPS, or the capsular polysaccharides, teichoic acids, and lipoteichoic acids in Gram-positive bacteria. The cationic peptides displace the LPS-stabilizing divalent cations, e.g. Mg^{+2} and Ca^{+2} , which eventually creates defects in the cell wall through which the peptides can translocate in a process termed “self-promoted uptake” (Hancock 1997). Despite the importance of this step, it is rarely addressed in the mechanistic studies, yet, it does not always correlate with the antimicrobial activity (Brogden 2005).

The bioactivity and channel formation are often described as cooperative (all or none). At low peptide/lipid ratios, the peptide lies flat at the surface of the lipid bilayer and causes membrane thinning in proportion to the peptide/lipid ratio. When the ratio is increased above a certain threshold, the peptide goes deeper into the membrane and begins to orientate perpendicular to the membrane. At high peptide/lipid ratios, the peptide is inserted perpendicular in the bilayer forming “stable” transmembrane pores, yet, the membrane thickness remains constant. The formation of transient pores at low peptide/lipid ratios,

induced by fluctuations, is also feasible. Likewise, those steps are also valid for uncharged membranes, however, the threshold peptide/lipid ratio will be orders of magnitude higher than that for charged membranes (Brogden 2005; Huang 2006).

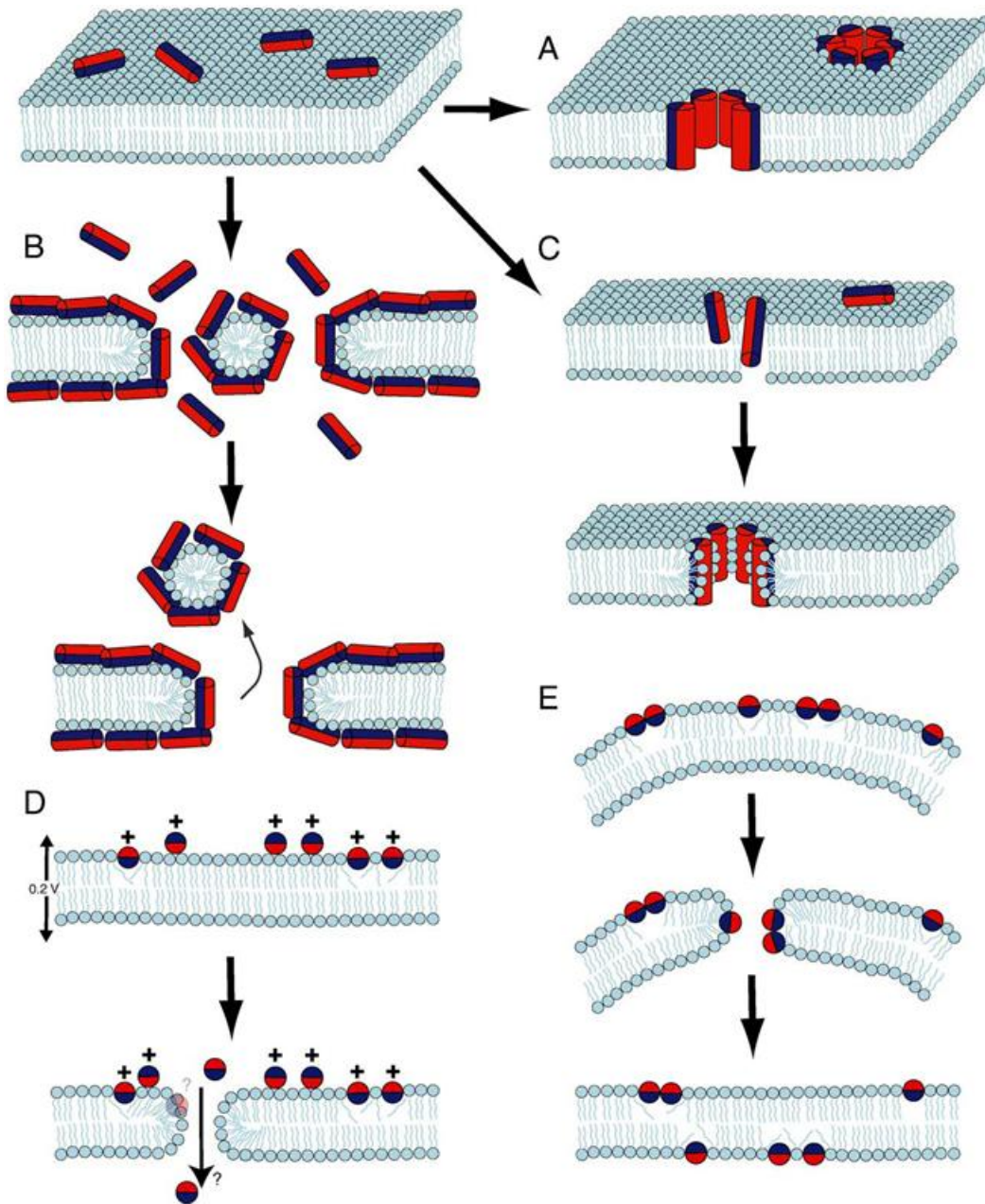


Figure 2.2-1 The classical models for the mode of action of antimicrobial peptides. The red part of the peptides represents the hydrophilic region, whereas the blue shows the hydrophobic part. (A) Barrel-stave model, (B) Carpet model, (C) Toroidal pore model, (D) Molecular electroporation model, (E) Sinking raft model. Adapted from refs. (Chan et al. 2006; Pokorny and Almeida 2005).

As demonstrated in **Figure 2.2-1**, the classical scenarios for the mechanism of action of CAMPs fall into two categories: 1) the formation of pores in lipid membranes through either transmembrane structures (e.g. barrel stave and toroidal pore models) or by disturbing and thinning lipid bilayers (e.g. molecular electroporation and sinking rafts models), 2) by dissolving the membrane in a detergent-like manner (carpet model). By perforating and

breaking down the bacterial membrane, the ion and pH gradient as well as the osmotic regulation are destroyed and eventually the cell is lysed (Bechinger and Lohner 2006; Brogden 2005; Chan et al. 2006; Lohner et al. 2008; Sato and Feix 2006; Shai 2002; Tossi et al. 2000; Yeaman and Yount 2003).

In the carpet model, the peptides are electrostatically accumulated at the membrane surface covering it in a carpet-like manner. At high peptide concentrations, the peptides disrupt the membrane in a detergent-like manner, eventually leading to its disintegration and the formation of bicelles and micelles. Nevertheless, it is possible that at lower peptide concentrations the peptides micellize some lipid molecules carrying them away from the membrane resulting in transient openings. At a critical threshold concentration, the peptides may form stable transmembrane pores allowing more peptides to access the membrane. In principle, all amphipathic peptides are capable of solubilising lipid membranes when a threshold peptide concentration at the membrane surface is attained (Bechinger and Lohner 2006; Lohner et al. 2008).

In the toroidal pore, the polar lipid headgroup is associated with the peptide polar surface in lining the toroidal pore lumen. Both lipid monolayers are bent in the fashion of the toroidal pore and connected. The lipid molecules are necessary to screen the cationic charges of the peptides and to help them assemble (Bechinger 1999). Magainins, melittin and protegrins induce this type of pores (Hallock et al. 2003; Matsuzaki 1998; Matsuzaki et al. 1996; Yang et al. 2001). However, using fluorescence correlation spectroscopy it was found that magainin and melittin interact with lipid vesicles in different ways. Whereas melittin forms channels in lipid membranes, magainin damages the lipid vesicles (Pramanik et al. 2000). The formation of disordered toroidal pores was also proposed, where the peptide binds primarily to the edge of the pore and does not have a specific orientation as in the case of the classical toroidal pore (Sengupta et al. 2008).

The transmembrane pore in the barrel-stave model is assembled merely from the oligomerization of a bundle of peptide helices and no threshold concentration is required (Lohner et al. 2008). This model is unique to alamethicin (Vogel 1987), where the peptide hydrophobic regions attach to the lipid core and a central lumen is formed from the peptide hydrophilic regions. The alamethicin-induced pore is composed of 3-11 molecules, and the inner and outer diameters are estimated as ~ 1.8 and ~ 4.0 nm, respectively (He et al. 1995; Spaar et al. 2004). The magainin-induced toroidal pores are larger and have a more variable pore size as compared to alamethicin-induced pores (Yang et al. 2001).

In the sinking raft model, the AMP induces a mass imbalance in the cell membrane and thereby introduces a strong membrane curvature. Consequently, the peptide sinks in the membrane and causes transient pores which results in the peptide residing in both leaflets of the membrane (Pokorny and Almeida 2004). Comparably, the AMP creates transient pores in the molecular electroporation model, however, by generating a difference in the electrical potential across the membrane (Miteva et al. 1999).

The micellar aggregate channel is an alternative model proposed to fill the gap between the antimicrobial assays and the results with model membranes. After the binding to the lipid headgroups, the peptides penetrate the membrane and then cluster into unstructured aggregates. The collapse of the aggregate-like structures creates transient pores that span the bilayer through which the peptides can translocate (Hancock and Chapple 1999).

Other less well investigated mechanisms based on the formation of lipid-peptide domains (Erand and Erand 2008; Hasper et al. 2006; Jean-Francois et al. 2008; Latal et al. 1997; Lohner et al. 1997), the segregation of anionic lipids from the zwitterionic ones (Erand et al. 2008a; Erand et al. 2006; Erand et al. 2008b), and the induction of non-lamellar phases (El Jastimi and Lafleur 1999; Staudegger et al. 2000; Yang et al. 2007) were also reported (Lohner et al. 2008). A peptide that works solely by one of those mechanisms is not very common and the actually observed mechanism depends on the detailed condition, most importantly the lipid composition and the peptide/lipid ratio (Bechinger 1999; Bechinger and Lohner 2006). Therefore, the possibility exists that an AMP induces a certain action upon interacting with the membrane of a certain organism, but a different action when the peptide interacts with a different species. In addition, numerous antimicrobial peptides have targets inside the bacterial cell, where they may alter the cell membranes, bind to DNA, or inhibit enzymatic activities and protein synthesis (Brogden 2005; Hale and Hancock 2007). As supported by the extensive information about AMPs, the mode of their action is equally modulated by peptide properties and the microbial surface composition.

Despite the non-specific mode of action of AMPs, many bacterial species have already evolved counter mechanisms to limit their effectiveness. This involves: 1) reducing the net negative charge of bacterial membranes, which helps repelling the cationic AMPs, e.g. through the transport of basic amino acids or by masking the charge of PG by producing lysyl- and ornithine-PG, 2) reducing the membrane fluidity, 3) expelling the peptide using energy-driven efflux pumps, and 4) the degradation of the peptides by proteolytic enzymes (Brogden 2005; Peschel 2002).

2.3. Bacterial selectivity

The antimicrobial peptides interact specifically with the lipid components of cell membranes and thereby exert their action. A key feature of the cationic peptides is their capability to distinguish bacterial from mammalian cells because the lipid composition of their membranes is different. The outer leaflet of human erythrocytes, as a representative model for mammalian cell membranes, is composed of uncharged lipid components, mainly PC, PE, sphingomyelin, and cholesterol (Virtanen et al. 1998). In contrast, the inner membrane of *Escherichia coli*, as a model membrane of Gram-negative bacteria, contains mainly PE together with substantial amounts of negatively charged phospholipids, namely PG and cardiolipin (Garidel and Blume 2000; Lohner et al. 2008; Pozo Navas et al. 2005; Sanderson 2005). The bacterial selectivity of CAMPs is based on their preferential non-specific electrostatic-driven attraction to the negatively charged bacterial membranes. The selectivity is further enhanced for some peptides as they interact specifically with lipid components exclusively exist in prokaryotic membranes such as PG, cardiolipin and PG-PE mixture (Arnt et al. 2006; Jing et al. 2005). SM and cholesterol were found to strongly attenuate the perturbations of AMPs through altering the fluidity and packing in lipid bilayers, thereby protecting eukaryotic membranes (Leuschner and Hansel 2004; Matsuzaki et al. 1995; McIntosh 2004; Sood et al. 2008; Sood and Kinnunen 2008). In addition, the outer glycocalyx of erythrocytes formed of glycoproteins and glycosphingolipids, which are rich in acidic moieties, offers a strong protection against the lytic effects of AMPs (Papo and Shai 2003). In accordance with this notion, some peptides are found non-haemolytic despite the fact that they strongly interact and permeabilize zwitterionic model membranes (Papo et al. 2002).

In comparison to healthy cells, malignant cells have higher fluidity and typically carry a net negative charge due to the higher than normal expression of the anionic molecules PS and O-glycosylated mucins. Therefore, many AMPs show the ability to kill cancer cells, most probably via one of the aforementioned mechanisms as well as the induction of apoptosis following the peptide uptake into the cytoplasm (Hoskin and Ramamoorthy 2008).

2.4. Structure activity relationship of antimicrobial peptides

Several studies were carried out to inspect the correlation between the structural properties of the AMPs and their antimicrobial activity and selectivity, based on the fact that the activity is determined by the macroscopic properties of the peptides rather than the exact sequence or order of amino acids (Dathe and Wieprecht 1999; Frecer 2006; Tossi et al. 2000; Zelezetsky and Tossi 2006). The activity of an AMP depends on the interplay between a

number of physicochemical properties: the amino acid sequence, net charge, amphipathicity, hydrophobicity, hydrophobic moment, structural folding in membranes (includes secondary structure, dynamics and orientation), oligomerization, peptide concentration, and membrane composition (Shai 1999; Tossi et al. 2000; Zelezetsky and Tossi 2006). However, those parameters are intimately interrelated, so that modifications aiming to alter one of the properties usually significantly affect the other properties (Dathe and Wieprecht 1999; Tossi et al. 2000). The bactericidal concentration of the most potent AMP is $\sim 1 \mu\text{M}$, whereas the reported studies show that our ability to optimize the antimicrobial activity by tweaking the structure of AMPs is limited (Dathe and Wieprecht 1999).

The size of the vast majority of AMPs is shorter than 100 amino acids and their sequences show considerable variations, yet, the physicochemical properties are somewhat conserved. A well-defined helical amphipathic structure of the CAMP allows an optimal interaction with lipid membranes. Increasing the helical content or stabilizing the helical structure pronouncedly enhances the activity towards anionic and non-ionic vesicles as well as the antimicrobial and haemolytic activities (Andrushchenko et al. 2008; Dathe et al. 1996; Tossi et al. 2000; Zelezetsky and Tossi 2006). However, the effect on uncharged membranes was more pronounced than on the charged ones, which decreases the peptide selectivity. The high intrinsic helicity can be associated with the helical structuring in bulk, which may make it sterically difficult for the peptides to reach the bacterial cytoplasmic membrane (Tossi et al. 2000). Generally, AMPs are cationic (usually carry a charge of +4 to +9), mainly due to the positively charged residues Arg and Lys. The peptide cationic charge is essential for a selective and potent antimicrobial action. Increasing the peptide cationicity enhances its activity upon anionic membranes, yet, highly charged peptides show less ability for helical structuring as well as less ability to penetrate and permeabilize the membranes. CAMPs are rich (40 – 60%) in substantially hydrophobic residues, such as leucine, alanine, phenylalanine and tryptophan, which is consistent with the requirement for an amphipathic structure. Increasing the hydrophobicity enhances the activity towards uncharged and charged membranes, and as a result, the selectivity decreases (Dathe et al. 1996; Tossi et al. 2000; Zelezetsky and Tossi 2006).

3 Motivation

In spite of the significant amount of experimental data, many of the issues concerning antimicrobial peptides are still not well understood. This includes their molecular-based mechanism of action, the role of the membrane architecture, the importance of the structure and properties of the antimicrobial peptides, the extent and significance of the pore formation and membrane micellization processes, and others.

We carried out several biophysical experiments to understand the interplay between the conformation and helical propensity of the 18-mer KLA peptides, the lipid composition of model membranes, the experimental conditions, and the mode of action of the peptides. In addition, we tried to correlate the results we obtained with model membranes with the antimicrobial tests of the peptides.

We also investigated the influence of the small hexapeptides Ac-RW and C-RW on model membranes in order to explain the discrepancy in their behaviour. In addition, we carried out systematic experiments with mixed membranes in an attempted to get insights into the mode of action of the peptides.

Using epifluorescence microscopy on supported lipid bilayers, we studied the morphological changes of the lipid bilayer that takes place upon the interaction of KLA and RW peptides with the membrane. In addition, we were interested to inspect the influence of the membrane composition on the morphological changes induced by the peptides.

4 KLA peptides

4.1. Introduction

KLA peptides are model antimicrobial peptides that assume upon the interaction with lipid membranes an amphipathic α -helical conformation. They were synthesized and intensively investigated by Dathe and co-workers (Dathe et al. 2002; Dathe et al. 1996; Dathe et al. 1997; Krause et al. 1995). The peptides were designed to establish a quantitative relationship between the peptide structural properties and its bacterial activity and selectivity. In addition, KLAL (see **Table 4.1-1**) is a cell penetrating peptide and, therefore, a potential delivery vector for pharmacologically interesting substances (Hallbrink et al. 2004; Oehlke et al. 2005). The nomenclature and sequence of the KLA peptides used here **Table 4.1-1**, and their activities and properties are exhibited in **Table 4.1-2**.

Table 4.1-1 The nomenclature and sequence of KLA peptides. The modified amino acids as compared to KLAL are underlined. The one letter code is used to give the sequence; K: lysine, L: leucine, A: alanine, W: tryptophan. The capital and small letters are used to show L-amino acids and D-amino acids, respectively. Adapted from refs. (Dathe et al. 1996; Krause et al. 1995).

Peptide	Sequence
KLAL	KLAL KLAL KAL KAAL KLA-NH ₂
KLA1	KLAL KLAL <u>KAW</u> KAAL KLA-NH ₂
k _{1,12} -KLAL	<u>k</u> LAL KLAL KAL KAAL KLA-NH ₂
k _{9,a10} -KLAL	KLAL KLAL <u>ka</u> L KAAL KLA-NH ₂
l _{11,k12} -KLAL	KLAL KLAL KA <u>l</u> <u>k</u> AAL KLA-NH ₂

KLAL peptide was the reference to which all modifications and comparisons were done. The peptide is composed of 18 amino acids (5 Lys, 7 Leu, and 6 Ala residues), where the N-terminus is uncapped and the C-terminus is amidated. The peptide has a nominal charge of +6 provided by the 5 Lys residues, which cover a 90° angle of the peptide interface, and the uncapped N-terminus, while the Leu and Ala groups form the hydrophobic part of the amphipathic peptide. The α -helix and β -strand structures of KLAL are illustrated in **Figure 4.1-1**, showing the amphipathic arrangement of the amino acids. KLA1 has a similar sequence to KLAL but with Leu11 being replaced with Trp, which reduces the peptide hydrophobicity and the helicity, however, the other properties are kept nearly unaltered (see **Table 4.1-2**). Double D-substitution, where two consecutive L-amino acids are replaced with their D-analogues, is utilized to disturb, or sometimes improve, the intrinsic helicity of KLA peptides without affecting other properties. The double D-substitution in the middle of the chain pronouncedly disturbs the peptide helicity as in k_{9,a10}-KLAL and l_{11,k12}-KLAL, whereas the

double D-substitution at the C-terminus enhances the peptide helicity (k_{1,l_2} -KLAL). Besides the helicity (α), the peptide charge, amphipathicity, hydrophobicity (H), hydrophobic moment (μ) and the hydrophobic/hydrophilic domain ratio (Φ/Ψ) were investigated.

Generally, the KLA peptides are unstructured in buffer, whereas they assume an α -helical structure in TFE or when mixed with POPG, POPG/POPC 1:3 and POPC lipid vesicles. The helicity induced by TFE and POPC is prominently reduced when the two consecutive D-amino acids are in the middle of the chain. As shown in (Table 4.1-2), the helicity order of KLA peptides in TFE is different from that upon interaction with lipid vesicles. The helicity order of the peptides determined in POPG LUV suspension is k_{1,l_2} -KLAL > KLAL > KLA1 > $k_{9,a_{10}}$ -KLAL \geq $l_{11,k_{12}}$ -KLAL.

Table 4.1-2 The different properties and activities of KLA peptides. Adapted from refs. (Dathe et al. 1996; Dathe et al. 1997; Krause et al. 1995)

Peptide	H	μ	Helicity ($\alpha\%$)			Dye release (μM)		MIC (μM)		EC ₅₀ (μM)
			TFE	POPG	POPC	POPG EC ₅₀	POPC EC ₅₀	<i>E. coli</i>	<i>S. epidermidis</i>	RBC
k_{1,l_2} -KLAL	-0.016	0.334	68	74 ^a	50 ^a	0.24	0.015	4	4	7
KLAL	-0.016	0.334	72	62 ^a /62 ^b	54 ^a /65 ^b	0.18	0.03/0.25 ^c	4	2	10
KLA1	-0.025	0.329	73	54 ^b	59 ^b	0.25	0.009 ^c	5.2	-	11
$k_{9,a_{10}}$ -KLAL	-0.016	0.334	43	48 ^a	3 ^a	0.12	1.3	16	16	56
$l_{11,k_{12}}$ -KLAL	-0.016	0.334	34	47 ^a	5 ^a	0.22	1.2	32	32	540

The hydrophobicity (H) and hydrophobic moment (μ) were calculated as described by Eisenberg (1984) (Eisenberg 1984). The helicity of the peptides in 50% TFE (v/v) or in lipid SUV suspension were determined in Tris buffer using 10 μM peptide concentration. EC₂₅ and EC₅₀ are peptide concentrations causing 25% and 50% effect, respectively. ^a $c_{\text{lipid}}/c_{\text{peptide}} = 230$. ^b $c_{\text{lipid}}/c_{\text{peptide}} = 500$. ^c EC₂₅.

The peptides show also the tendency to form β -structures in acidic media or at high peptide concentrations, high peptide to lipid ratios, or high temperatures (see below). This is particularly true for the peptides with the lower helical propensity.

The helical structure is induced by the hydrophobic interaction of the peptide side chains with the lipid core, and is found to be independent of the surface charge of lipid vesicles. The primary function of the surface charge of lipid membranes is to increase the affinity of the peptides and, consequently, their surface concentration.

As observed from CD experiments, KLAL and the less helical analogue $k_{9,a_{10}}$ -KLAL show similar affinities towards POPG. The binding to POPG/POPC 1:3 vesicles is weaker and more differentiated than to POPG. The apparent binding constant of the binding of KLAL and $k_{9,a_{10}}$ -KLAL to POPG/POPC 1:3 vesicles is 2.6×10^4 and $1.5 \times 10^4 \text{ M}^{-1}$, respectively. The

binding affinity of KLAL towards POPC is much weaker ($\sim 10^3 \text{ M}^{-1}$) and, therefore, a higher lipid/peptide ratio (500) is required for complete binding. In the case of $k_{9,a_{10}}$ -KLAL, a ratio of 1100 is not enough to obtain a complete binding to POPC. This indicates the importance of the peptide helicity for interactions with partially charged and uncharged vesicles.

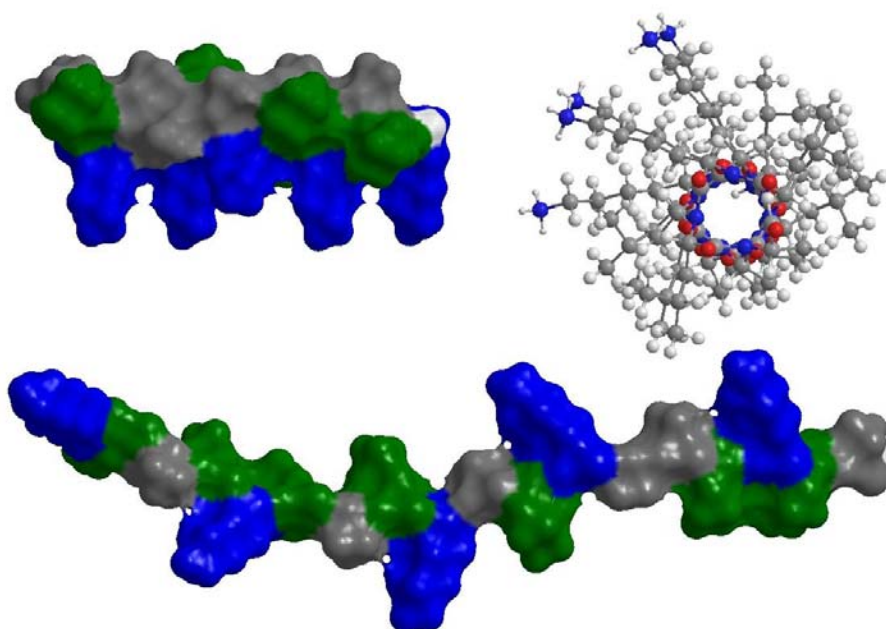


Figure 4.1-1 View of the α -helix (top) and the twisted β -sheet single strand (bottom) structures of KLAL. In the side view of the α -helix, the atoms N, O, C and H are coloured blue, red, dark gray, and light gray, respectively. In the Connolly surface of the peptide, Lys (K) is coloured blue, Leu (L) is coloured green, Ala (A) is coloured grey, and the backbone is coloured light gray.

As shown in **Table 4.1-2**, the helicity of KLA peptides is essential for their membrane permeabilizing activity on neutral membranes. Nevertheless, the permeabilization of highly charged membranes is barely influenced by distorting the peptide helicity. Despite the low affinity of the cationic peptides towards neutral membranes in comparison to negatively charged membranes, the peptides show a much higher permeabilizing activity against neutral membranes.

The helical structuring enhances the antimicrobial and haemolytic activities of the peptides, but the helicity is more crucial for the haemolytic activity. The enhanced antimicrobial and haemolytic activities are related to the greater disturbance of the lipid headgroups and hydrocarbon chains, respectively. The hydrophobicity of the peptides enhances their ability to penetrate the outer bacterial membranes (wall) of Gram negative bacteria. It is suggested that the reduced activity of the peptides with the low intrinsic helicity is due to the decrease in the actual hydrophobicity of the peptides.

The KLA peptides are poorly selective, as evident by their high haemolytic activity as well as by their high permeabilizing activity of uncharged vesicles. Enhancing the antimicrobial activity reduces the peptide selectivity. The peptide selectivity is also decreased with increasing the hydrophobicity, however, the antibacterial activity is not affected. Optimum selectivity was found for peptides with moderate hydrophobicity, reduced hydrophobic moment and a low angle subtended by the charged residues.

The surface activity and the behaviour of KLA peptides were studied at the air/water interface by means of infrared reflection absorption spectroscopy (IRRAS) (Kerth et al. 2004). The main findings of this work are: 1) The KLA peptides adopt a helical structure at low surface pressure and high surface area per peptide, 2) The peptides undergo an α -helix to intermolecular β -sheet transition, which is a concentration and time driven process, 3) From the simulations of IRRA spectra, the secondary structures are arranged almost parallel to the water surface. The adsorption of the peptides into lipid monolayers was also investigated (Erbe 2001). It was found that the peptides interact selectively with charged lipid films where they assume a helical structure. The results of the monolayer experiments will be discussed again in details in the results and discussion section.

4.2 Results and discussion

4.2.1 Adsorption of KLA1 at the air/water interface

Monolayer techniques have been widely employed as potent tools to study interactions of water soluble molecules with lipid monolayers at the molecular level. The possibility of coupling the monolayer technique to various methods (e.g. epifluorescence spectroscopy, infrared spectroscopy, Brewster angle microscopy, atomic force microscopy, and grazing-incidence X-ray diffraction) improves the usability of the technique (Maget-Dana 1999; Mendelsohn and Flach 2002; Volinsky et al. 2006). Infrared reflection absorption spectroscopy (IRRAS) is a unique means to acquire information about the conformation and orientation of lipid chains as well as the secondary structure and orientation of peptides and proteins in situ in monolayers at the air/water interface (see (Flach et al. 2006; Mendelsohn and Flach 2002)).

The behaviour of KLA peptides at the air/water interface was investigated by Kerth et al. (2004). In the π /time experiments, where the peptide was injected in the subphase and the change in the surface pressure (π) was observed over time, a higher peptide bulk concentration drove a faster adsorption and a higher π was attained. A certain ionic strength was required for the surface activity of KLA peptides, since no adsorption was noticed for KLAL in pure water. Nonetheless, and as reported by others, the surface activity of peptides on pure water surface as compared to buffer surface could be minor (Bringezu et al. 2007a) or comparably pronounced (Maltseva and Brezesinski 2004). KLAL assumed a helical structure at low π and at high are per one peptide molecule (A). A concentration- and time-dependent α -helix to antiparallel β -sheet transformation was observed, which was associated with a pressure relaxation. The formation of β -structures was most probably driven by the energy gain, and an area of 6 nm² per β -dimer was anticipated. From the simulations of IRRA spectra, it was shown that the α -helices and β -sheets of the different KLA peptides were aligned almost parallel to the water surface (Kerth et al. 2004).

We used IRRAS on a Langmuir trough to study the adsorption of KLA1 to the air/water interface as well as its incorporation into different lipid monolayers. Monitoring the adsorption of KAL peptides at the air/water interface and the resulting increase in π gave a clear indication about the surface activity of the peptide.

In order to study the incorporation of KLA1 peptide into lipid films, it was unavoidable to study the behaviour of KLA1 at the air/water surface (without lipid) as well. As shown in **Figure 4.2-1A**, the accumulation of KLA1 at the air/water interface increased π

over time. The concentration of KLA1 in the subphase was 100 nM. An immediate, however, very slow, two-step increase in π was observed, with a maximum of 14.3 mN m^{-1} after 40 hours. We anticipate that 97% of KLA1 peptide in the subphase adsorbed to the water surface. The calculations were based on an approximate area of $\sim 4.3 \text{ nm}^2$ per a β -sheet KLA1 at 14.3 mN m^{-1} , which was estimated using the surface pressure/area (π/A) isotherm of KLAL (discussed later).

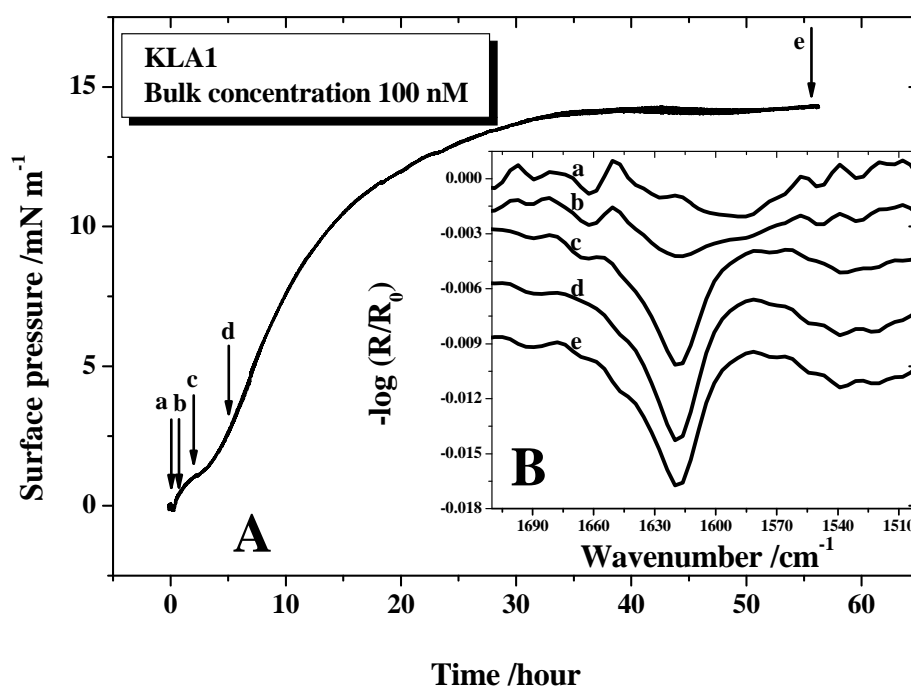


Figure 4.2-1 (A) The development of surface pressure over time after the injection of KLA1 in the subphase (10 mM Tris, 154 mM NaCl, pH 7.4) at 20°C . The starting bulk concentration was 100 nM. (B) The IRRA spectra of KLA1 film at the respective positions a-e. The IRRA spectra were recorded with *p*-polarized light at an angle of incidence of 40° .

Similar experiments were carried out before with KLAL and two D,L-amino acid analogues (Kerth et al. 2004). KLAL (100 nM) showed a fast one-step rise in the surface pressure followed by a relatively slow surface pressure relaxation. KLA1 behaved similarly to KLAL and the maximum π for both peptides was comparable for the same bulk concentration, yet, the adsorption of KLA1 to the air/water interface was ~ 40 times slower. In addition, no post-adsorption pressure relaxation was noticed in the case of KLA1. The D,L-amino acid analogues showed a two-step increase in the surface pressure, however, it was still much faster than the KLA1 case.

The IRRA spectra at different times during the experiment are presented in **Figure 4.2-1B**. Since the experiments were carried out on H_2O subphase, the H_2O bending mode

centred $\sim 1640\text{ cm}^{-1}$ overlaps with the amide I bands and hampers their proper analysis. This is in addition to interferences due to water vapour at the water surface, through which the IR beam passes (Flach et al. 2006; Mendelsohn and Flach 2002). At the beginning of the adsorption of KLA1, an amide I band at $\sim 1662\text{ cm}^{-1}$ and an amide II band at $\sim 1547\text{ cm}^{-1}$ were observed that indicated an α -helical secondary structure (Goormaghtigh et al. 1994; Tamm and Tatulian 1997). Further accumulation of the peptide on the air/water interface was accompanied by an α -helix to antiparallel β -sheet transformation, which was evident by the disappearance of the amide I band at $\sim 1662\text{ cm}^{-1}$ and the appearance of two amide I bands at ~ 1620 and $\sim 1689\text{ cm}^{-1}$. The amide I bands at low wavenumbers ($1611 - 1630\text{ cm}^{-1}$) are characteristics for aggregated strands rather than for normal β -sheets (Tamm and Tatulian 1997; Zandomenighi et al. 2004). We anticipate that the first step in the adsorption curve represents the accumulation of the peptide at the air/water interface, as an α -helix, and the induction of an α -helix to β -sheet transition, whereas the second step is merely due to the adsorption of KLA1 as a β -sheet. It is known that β -structures usually diffuse and adsorb slower than α -helices (Maget-Dana et al. 1999), which is accordance with our notion.

A similar two-phase adsorption process accompanied by an α -helix to β -sheet conversion was also obtained with islet amyloid polypeptide (IAPP), a process that was followed by fibril formation (Lopes et al. 2007). Although KLA1 existed as a helical structure at high peptide surface area, it favoured the anti-parallel β -sheet structure upon its interaction with the neighbouring peptide molecules. KLAL behaved similarly, however, mere β -strands were observed upon the adsorption of the D,L-amino acid analogues to the air/water interface (Kerth et al. 2004). Similar observations were reported in the literature for other peptides. Amyloid (1-40) peptide in solution was poor in β -structures, whereas it formed irreversibly monolayers with a high β -sheet content when spread at the air/water interface (Schladitz et al. 1999). A reversible (Mendelsohn and Flach 2002) and irreversible (Cai et al. 2003) pressure-driven conversion into β -structures was also reported for pulmonary surfactant proteins and their analogues.

The intensity of the water OH stretching vibration $\sim 3600\text{ cm}^{-1}$ can be correlated to the thickness of the film at the air/water interface (Dyck et al. 2006; Hussain et al. 2004). The thickness of KLA1 film increased rapidly upon the accumulation of the peptide at the interface and reached the maximum after ~ 5 hours (data not shown). However, a quantitative description of the film thickness in our case was not possible.

4.2.2 Adsorption of KLA1 to lipid monolayers

We investigated the affinity of KLA1 towards lipid films of different compositions to check the degree of interaction/insertion with/into lipid monolayers. We performed A /time experiments, in which the surface pressure of the lipid film was kept constant ($\pi = \text{const}$) at 30 mN m^{-1} and the change in the area per lipid molecule (ΔA) due to the adsorption of KLA1 was followed over time. We chose a surface pressure of 30 mN m^{-1} since it resembles the bilayer-monolayer equivalent pressure (Blume 1979; Tamm 2002). In A /time ($\pi = \text{const}$) experiments, the limited surface area of the trough restricts the amount of lipid and peptide that can be used. On one hand, by applying a small amount of lipid, a surface pressure of 30 mN m^{-1} cannot be attained. On the other hand, the spreading of high amount of lipid will force us to start with an already high surface pressure. In addition, the technique is relatively insensitive for low peptide bulk concentrations, whereas high peptide concentrations will induce ΔA that is larger than the trough measuring range.

Pressure/time ($A = \text{const}$) binding studies of KLAL to POPG, POPC and POPG/POPC films were performed before by Erbe (2001) using 30 mN m^{-1} as a starting pressure (Erbe 2001). The insertion of KLAL into POPG monolayer induced a 12 mN m^{-1} increase in π . Reducing the surface charge density (using PG/PC mixtures) caused a smaller increase in π . The peptide formed a helical structure after binding to POPG (Erbe 2001). In comparison to the A /time method, the π /time procedure has some drawbacks, namely 1) the increase in the surface pressure cannot be directly correlated to the amount adsorbed of the peptide and 2) the affinity of the peptide to the lipid film does not remain constant during the experiment, but decreases upon increasing the surface pressure.

The electrostatic attraction of the positively charged KLA peptides to anionic lipid components is the origin of their activity (Dathe et al. 1996). Therefore, we studied the interaction of KLA1 with PG lipids (POPG, DPPG, and DMPG), the zwitterionic lipids POPC and POPE, as well as a number of POPG/POPC and POPG/POPE mixed monolayers. Simultaneously, the recorded IRRA spectra could be used to monitor the secondary structure and the orientation, if possible, of the peptides during the adsorption experiments. Moreover, any possible changes in the packing order of the hydrocarbon chains of the lipids, in the orientation of the lipid headgroup, in the hydration and hydrogen bonding with the lipid headgroups, and in the monolayer thickness were checked. In fact, we performed angle-dependent experiments to determine the orientation of the peptides in the different lipid films. However, the IRRA spectra were of poor quality and, therefore, we refrained from analyzing them.

Figure 4.2-2A demonstrates the area change ΔA of POPG, DPPG, POPC and POPE lipid monolayers after the injection of KLA1 (49 nM as a starting bulk concentration) into the subphase and **Figure 4.2-2B** shows the recorded IRRA spectra after 10 hours.

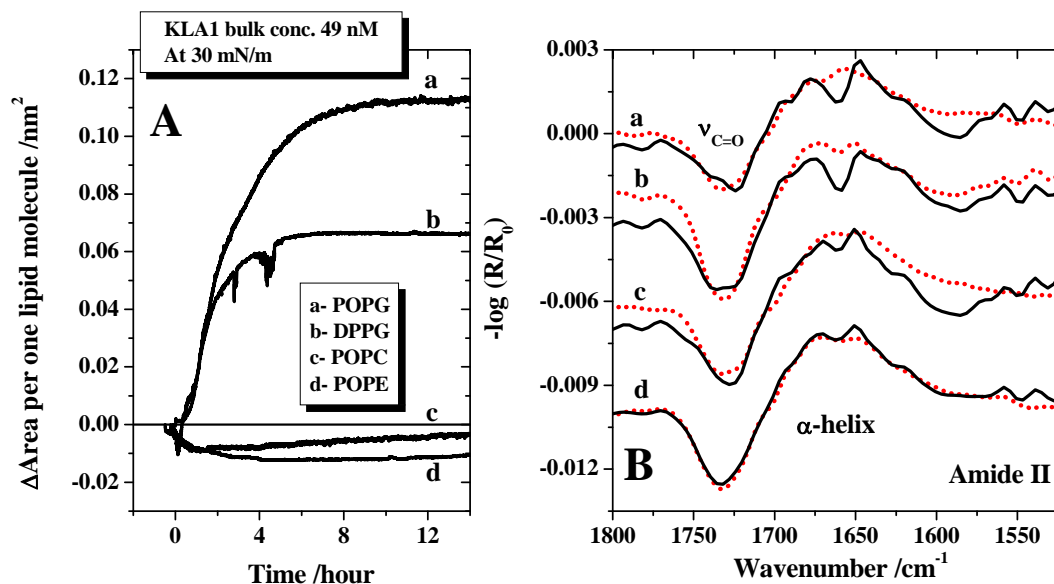


Figure 4.2-2 (A) ΔA versus time course of various lipid monolayers after the injection of KLA1 in the subphase (10 mM Tris, 154 mM NaCl, pH 7.4) at 20°C. The surface pressure of the lipid films was kept at 30 mN m^{-1} , and the starting bulk concentration of KLA1 was 49 nM. (B) The IRRA spectra of the different films at the respective positions a-d. The solid black lines belong to the peptide-associated lipid films, whereas the dotted red lines are from pure lipid films. The IRRA spectra were recorded with *p*-polarized light at an angle of incidence of 40°.

KLA1 showed no adsorption to the zwitterionic lipids POPC and POPE. The carbonyl stretching mode of the POPC carbonyl groups ($\nu(\text{CO})$) was shifted from $\sim 1733 \text{ cm}^{-1}$ to a lower wavenumber $\sim 1728 \text{ cm}^{-1}$. This indicates possible hydrogen bonding between KLA1 and the PC headgroups at the monolayer surface without peptide insertion (Blume et al. 1988). No such effect was observed for POPE. The higher chain packing of PE as compared to PC could explain this difference. KLA peptides showed modest interactions with uncharged membranes (Dathe et al. 1996, and our observations). Therefore, we believe that the interactions with POPC and POPE were too small to be detected with this technique. The drop in ΔA of POPC and POPE films could be explained by the relaxation or peptide-induced condensation of the lipid film. The possibility that the peptide dragged some of the lipid molecules into the subphase, which reduced ΔA , cannot be ruled out. The consequent increase in the ΔA could be due to the evaporation of water from the subphase during the experiment. The effect of the water evaporation and the degree of the lipid film relaxation varied among the experiments and remained, therefore, hard to predict.

The increase in ΔA of the POPG monolayer, which is in the liquid-expanded phase at 30 mN m^{-1} at room temperature, started promptly after the peptide injection and reached the maximum of $0.11 \text{ nm}^2 \text{ molecule}^{-1}$ after 10 hours. A delayed-onset was observed for the incorporation of the peptide into DPPG film, which exists in the liquid-condensed phase at 30 mN m^{-1} at room temperature, and a ΔA of $0.066 \text{ nm}^2 \text{ molecule}^{-1}$ was obtained after 6.5 hours.

The amount of lipid spread in both cases was similar (17 nmol), however, the accumulation of the peptide at the fluid lipid film (POPG) was faster and almost twice as much in comparison to the liquid-condensed lipid film (DPPG). A similar experiment was carried out using DMPG and only small differences were observed between DPPG and DMPG films (data not shown). The higher penetration into fluid monolayers was also reported elsewhere (Gidalevitz et al. 2003). As illustrated in **Figure 4.2-2B**, KLA1 assumed an α -helix upon interaction with PG films as evident by the appearance of the amide I band at $\sim 1660 \text{ cm}^{-1}$ and the amide II band at $\sim 1548 \text{ cm}^{-1}$. For KLAL, the peptide helix was found to be tilted in the POPG monolayer with an angle of $> 54.6^\circ$ with respect to the surface normal (Erbe 2001). We believe that the orientation of KLA1 in POPG monolayers will be similar to that of KLAL. Due to the hydrogen bonding between KLA1 and the ester moieties of POPG headgroups, the $\nu(\text{CO})$ \sim was broadened and down-shifted from 1733 (free POPG) to $\sim 1724 \text{ cm}^{-1}$. The antisymmetric stretching mode of PO_2^- ($\nu_{\text{as}}(\text{PO}_2)$) remained unaltered at $\sim 1209 \text{ cm}^{-1}$. On the other hand, the interaction of the peptide with DPPG increased the $\nu(\text{CO})$ from ~ 1732 to $\sim 1736 \text{ cm}^{-1}$ and the $\nu_{\text{as}}(\text{PO}_2)$ from ~ 1205 to $\sim 1210 \text{ cm}^{-1}$ pointing to a dehydration of the carbonyl and phosphate groups (Hübner and Blume 1998; Mantsch and McElhaney 1991; Tamm and Tatulian 1997). The lipid chain packing, as indicated by the wavenumber of the CH_2 stretching vibrational modes (see FT-IR section), and the thickness of PG monolayers, as indicated by the intensity of the water OH stretching band, remained unchanged upon the adsorption of KLA1 (data not shown).

The effect of the peptide bulk concentration on the ΔA of POPG is illustrated in **Figure 4.2-3A**. A higher peptide bulk concentration led to a faster onset of adsorption and a higher accumulation of the peptide at the lipid monolayer. **Figure 4.2-3B** shows the correlation between the peptide bulk concentration and the relative increase in the molecular area of the lipid film, namely $\Delta A/A_0$, where A_0 is the initial area per lipid.

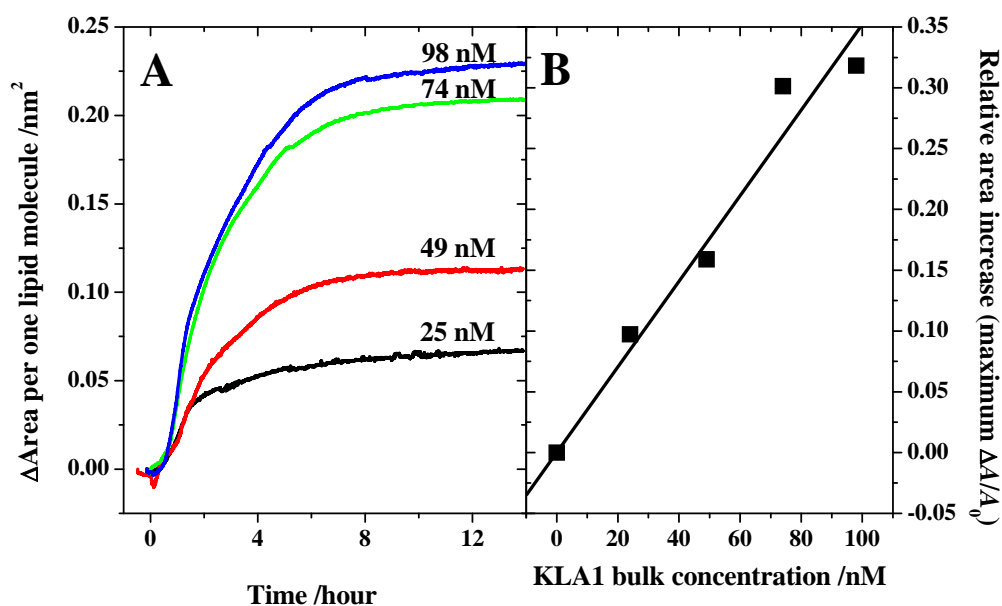


Figure 4.2-3 (A) The influence of KLA1 bulk concentration (25 – 98 nM) on ΔA versus time course of POPG monolayers after the injection of the peptide in the subphase (10 mM Tris, 154 mM NaCl, pH 7.4) at 20°C. **(B)** The dependence of the relative area increase ($\Delta A/A_0$) of POPG monolayers on the KLA1 bulk concentration, where A_0 is the initial area per lipid. During the experiments, the surface pressure of the films was kept constant at 30 mN m^{-1} .

The relation was linear, as observed with other peptide-lipid monolayer interactions (Castano et al. 2000; Tamm et al. 1989), and could be described with simple peptide partition equilibrium between the aqueous phase and the lipid monolayer (Tamm 1986, 2002). We employed the equation $\Delta A/A_0 = (a_p/a_L)KC_p/(1+KC_L)$ to analyze the binding isotherm, where $\Delta A/A_0$ is the relative increase in the molecular area of the lipid monolayer, a_p and a_L are the molecular areas of the peptide and lipid in the monolayer, respectively, K is the partition constant (with a unit of M^{-1}) and C_p and C_L are the peptide and lipid total concentrations, respectively (Tamm 1986, 2002).

To calculate K , we used an average POPG area at 30 mN m^{-1} of 0.7 nm^2 , and 9.1 nm^2 as an estimate of the molecular area per a helical KLA1 (discussed later). K was $2.9 \times 10^5 \text{ M}^{-1}$, and this was one order of magnitude lower than the apparent binding constant towards lipid vesicles determined with ITC. This exhibits a tenfold enhanced peptide binding to the larger hydrophobic core in lipid bilayers as compared to monolayers (Papo and Shai 2003). Since the POPG surface concentration remained unaltered in the experiments, the direct correlation between $\Delta A/A_0$ and the peptide bulk concentration suggests the lack of any POPG/KLA1 complex with a specific ratio in the studied concentration range (discussed later).

To check the influence of the surface charge density of the monolayer on the peptide adsorption, we studied POPG/POPC and POPG/POPE mixed monolayers. As illustrated in **Figure 4.2-4**, the negative surface charge density enhanced the accumulation of KLA1 at the lipid monolayer. In POPG/POPC films, the incorporation of the peptide correlated linearly with the POPG fraction. Other peptides can behave differently. For instance, the penetration of β -amyloid peptide β AP(1-40) into POPG/POPC monolayers was weak in the range of 0-50% POPG, but increased very strongly above 50% POPG (Terzi et al. 1997).

When POPG/POPC and POPG/POPE mixtures are compared, up to 25% POPG no differences were observed in the affinity of KLA1 towards POPG/POPC and POPG/POPE mixed films. At 50% POPG, however, the adsorption of KLA1 into the POPG/POPE monolayer ($\Delta A = 0.109 \text{ nm}^2$) was 50% more than for the POPG/POPC monolayer ($\Delta A = 0.072 \text{ nm}^2$). The smaller headgroup of POPE in comparison to POPC may explain this difference. It has been also reported that POPE-containing monolayers are characterized by an increased fluidity (Malcharek et al. 2005). Our experiments with lipid bilayers revealed many differences between the interaction of KLA peptides with PC and PE containing vesicles (discussed later). From the adsorption experiments, we observed differences between POPG/POPC and POPG/POPE mixed films only at high POPG content. This could be due the different properties or geometries of PC and PE headgroups.

Additionally, the affinity of KLA1 towards a monolayer made of *E. coli* polar lipid extract (67% PE, 23.2% PG, 9.8% cardiolipin) was examined and the result is shown in **Figure 4.2-4**. In *E. coli* membranes, both PG and cardiolipin provide the negative charge, namely -1 and -2, respectively. Therefore, the *E. coli* extract has a total negative charge of 39%. Unexpectedly, the incorporation into the *E. coli* monolayer resembled that for POPG/POPE mixed monolayer with $\sim 23\%$ charge content rather than 39%. This finding suggests that the peptide affinity was not enhanced by the presence of cardiolipin. The preferential interaction of our peptides with the PG headgroup may explain this behaviour. This concurs with our calorimetry data (data not shown), which showed that the KLA peptides interacted preferentially with the PG headgroup, whereas their influence on the other negatively charged phospholipids including cardiolipin was modest. Moreover, this could be due to the higher rigidity of cardiolipin membranes (Lewis et al. 2007) or the formation of cyclic intramolecular hydrogen-bonded structures in the headgroup region of cardiolipin that renders the cardiolipin molecules unavailable (Kates et al. 1993).

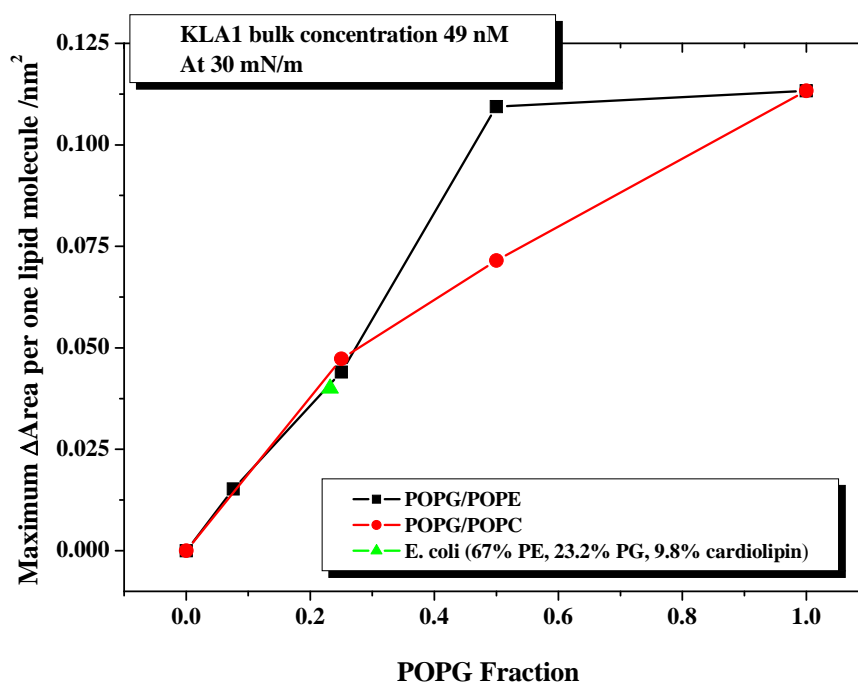


Figure 4.2-4 The influence of POPG fraction in the mixed monolayers on the maximum ΔA achieved after the injection of KLA1 in the subphase (10 mM Tris, 154 mM NaCl, pH 7.4) at 20°C. The surface pressure of the lipid films was kept at 30 mN m⁻¹, and the starting bulk concentration of KLA1 was 49 nM.

During the course of this study, we were interested to see the influence of the lipid fluidity, the lipid surface concentration, the peptide bulk concentration and the surface charge density of the monolayer (POPG/POPC and POPG/POPE) on the adsorption of the peptide and on the attained ΔA . **Table 4.2-1** summarizes the results. Besides, we checked if there was a specific peptide adsorption ratio or a specific lipid/peptide ratio at the air/water interface, and what would be the effect of the former variables on such ratios.

To calculate the adsorption percentage of KLA1 to PG containing monolayers, we needed to determine the area per an α -helical peptide. Since KLA peptides adopted β -strands at the air/water interface even at a very low surface pressure, this gave us no chance to experimentally estimate the area per an α -helix in a pure peptide film. Therefore, we used in our calculations an area per an α -helix of 9.1 nm², which was determined from the π/A isotherm of POPG/KLAL 20:1 premixed film at 30 mN m⁻¹ after subtracting the isotherm of pure POPG (discussed later). Moreover, an approximate value will be sufficient for making comparisons, assuming that the orientation of the peptide does not change dramatically among the different monolayers.

A comparison between POPG and DPPG monolayers (**Table 4.2-1**) would show that the fluidity of the membrane substantially enhanced (almost doubled) the adsorption of KLA1

at the interface. For 17 nmol POPG and 3.5 nmol KLA1, the peptide adsorption ratio (the percentage of the peptide adsorbed at the surface) and the lipid/peptide ratio at the water interface were 6% and 82, respectively. In the case of DPPG and using the same concentrations, only 3% and 158, respectively, were observed.

Table 4.2-1 Summary of ΔA , KLA1 adsorption ratio and L/P ratio at the interface in dependence on film fluidity, KLA1 bulk concentration, POPG fraction in the mixed films, and POPG surface concentration. The surface pressure of the lipid films was kept at 30mN m⁻¹.

Monolayer	Lipid /nmol	KLA1 /nmol	ΔA /nm ²	Adsorption ratio	L/P at the interface
DPPG	17	3.5	0.066	3%	158
POPG	17	7	0.229	6%	41
POPG	17	5.2	0.209	8%	41
POPG*	17	3.5	0.113	6%	82
POPG	17	1.7	0.067	7%	145
POPG*	17	3.5	0.113	6%	82
POPG/POPE 1:1	17	3.5	0.109	6%	83
POPG/POPE 1:3	16	3.5	0.044	2%	225
POPG/POPE 1:9	17	3.5	0.015	1%	475
POPG/POPC 1:1	18	3.5	0.072	4%	127
POPG/POPC 1:3	18	3.5	0.047	3%	171
POPG	24	3.5	0.102	8%	84
POPG*	17	3.5	0.113	6%	82
POPG	11	3.5	0.092	3%	102

*Rows were repeated to ease comparison.

As demonstrated in **Table 4.2-1**, while keeping the amount of POPG on the surface constant (17 nmol), the increase in the KLA1 bulk concentration (1.7 – 7 nmol) was directly associated with a higher ΔA (0.067 – 0.229 nm²) and a smaller POPG/KLA1 ratio (145 – 41), however, the peptide adsorption ratio remained at an average of 6 - 7%. On the other side, while keeping the KLA1 bulk concentration constant (3.5 nmol), increasing the amount of POPG spread at the surface (11 – 24 nmol) caused a higher peptide adsorption ratio, whereas ΔA and the lipid/peptide ratio were not substantially altered and stayed in average at 0.102 nm² and 89, respectively.

Again, the higher surface charge density in mixed monolayers substantially enhanced ΔA and the peptide adsorption and reduced the lipid/peptide ratio at the interface.

Since KLA1 carries a nominal charge of +6, one would expect that the minimal lipid/peptide ratio at the interface would be around 6. However, the lowest attained ratio was still much higher than 6 (**Table 4.2-1**). The reason of this discrepancy could be one or more of the following points: 1) a ratio of 6 will only be observed for surface electrostatic binding, whereas in our experiments the peptide is highly incorporated into the anionic lipid films, 2) when the peptide is inserted, a much larger number of lipids is needed to surround the peptide molecules, 3) the steric hindrance and repulsion between the peptide helices prevent the

presence of one peptide in the close vicinity of the other which then increases the amount of lipid molecules needed to separate the peptide molecules, 4) the charge screening effects of the counter ions hamper the electrostatic-based binding between the peptide and lipid molecules, 5) the possible formation of lipid domains reduces the actually available PG headgroups.

In conclusion, the bulk concentration of KLA1 was directly associated with a higher peptide adsorption (ΔA) and a lower POPG/KLA1 ratio at the interface, however, the peptide adsorption ratio barely changed. On the other hand, the spreading of more POPG at the surface led to a higher peptide adsorption ratio, whereas comparable ΔA values and lipid/peptide ratios were obtained. This indicates that the peptide adsorption ratio is controlled by the lipid properties and surface concentration, whereas it is barely influenced by the peptide bulk concentration. Furthermore, the lipid/peptide ratio at the interface is regulated by the peptide bulk concentration and not by the lipid surface concentration. This all exhibit that in our system neither the peptide adsorption ratio nor the lipid/peptide ratio at the interface is absolutely conserved.

4.2.3 KLAL π/A isotherm at the air/water interface

Amphipathic peptides can aggregate at the air/water interface assuming a certain conformation, which depends not only on the peptide sequence but on the surroundings as well. A very advantageous experiment in monolayer techniques is to determine the pressure/area (π/A) isotherms of amphipathic molecules at the air/water interface. The procedure can be carried out with one component or a mixture of components, where the second case would provide crucial information about the interaction and miscibility of the different molecules. However and since the spread film is meta-stable, one should ensure that the changes during the experiment occur under thermodynamic equilibrium (Kaganer et al. 1999).

We measured the π/A isotherms of KLAL and multiple lipid/KLAL monolayers at the air/water interface as well as investigated the influence of the lipid surrounding on the surface activity and structure of the peptide. We started by inspecting the π/A isotherm of pure KLAL. The experiments were carried out on Tris buffer as subphase, since the peptide showed low surface activity on pure water (Kerth et al. 2004). **Figure 4.2-5A** shows the π/A isotherm of pure KLAL at the air/water interface and **Figure 4.2-5B** demonstrates the development of the various IRRA bands upon the film compression. Amide I and II bands were used to determine

the peptide secondary structure (Goormaghtigh et al. 1994; Tamm and Tatulian 1997). Nevertheless, the interpretation of the amide bands should take into account that the band characteristics depend not only on the peptide structure, but on the peptide orientation, surface concentration and intermolecular interactions as well (Flach et al. 2006; Mendelsohn and Flach 2002). In addition, the lipid surrounding may have an influence (Lewis et al. 1999). The small bands developed at high surface pressure in the $1650 - 1700 \text{ cm}^{-1}$ and amide II regions (see **Figure 4.2-5B**) were most probably due to water vapour. Those bands overlapped with the peptide bands in the same region and hindered their analysis.

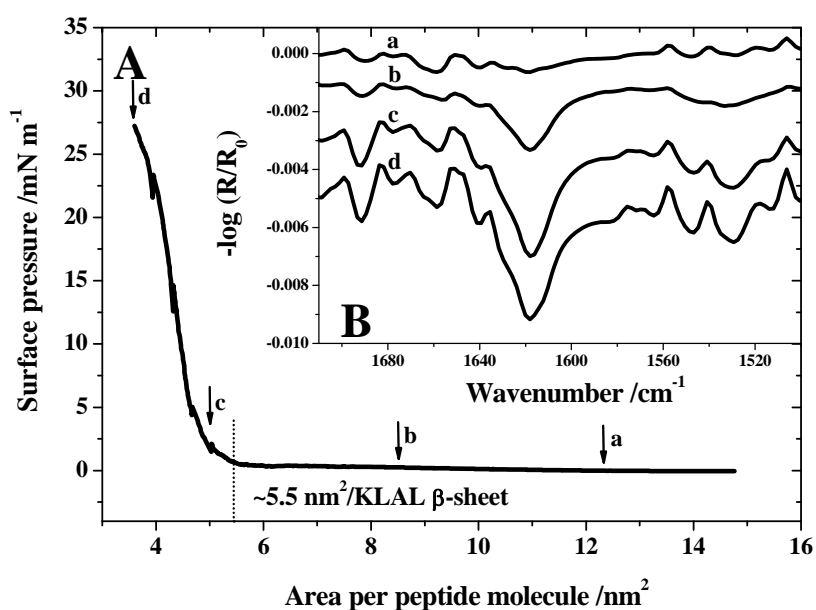


Figure 4.2-5 (A) Surface pressure versus area per one peptide molecule compression isotherm of KLAL spread on the surface of the subphase (10 mM Tris, 154 mM NaCl, pH 7.4) at 20°C . (B) IRRA spectra of the film at the respective positions a-d. The IRRA spectra were recorded with *s*-polarized light at an angle of incidence of 40° .

At high area per peptide ($\sim 12 \text{ nm}^2$) and a surface pressure of $\sim 0 \text{ mN m}^{-1}$, the peptide assumed an α -helical conformation evident by the frequencies of amide I at $\sim 1659 \text{ cm}^{-1}$ and the amide II at $\sim 1547 \text{ cm}^{-1}$. The compression of the peptide film enhanced the interaction between the peptide molecules and consequently increased π . As a result, the peptide transformed to an antiparallel β -sheet (aggregates) as concluded from the amide I bands at ~ 1691 and $\sim 1618 \text{ cm}^{-1}$ and amide II band at $\sim 1529 \text{ cm}^{-1}$. The intensity of the various bands increased upon further compression due to increasing the local peptide concentration under the IRRA beam (Flach et al. 2006; Mendelsohn and Flach 2002). From the isotherm, a liftoff *A* of $\sim 0.31 \text{ nm}^2$ per residue ($\sim 5.5 \text{ nm}^2$ per molecule) of the KLAL β -sheet was determined.

Additionally, a maximum π of $\sim 27.2 \text{ mN m}^{-1}$ and a limiting A of $\sim 0.2 \text{ nm}^2$ per residue ($\sim 3.6 \text{ nm}^2$ per molecule) were achieved before the film collapsed.

Other peptides can have different values. The liftoff and limiting A values of β -amyloid peptide (1-42), which adopted a β -structure, were ~ 0.12 and 0.05 nm^2 per residue, respectively (~ 5 and 2.3 nm^2 per molecule, respectively), and the film collapsed at $\sim 33 \text{ mN m}^{-1}$ (Ambroggio et al. 2005). The limiting area of the helical $\text{K}_2(\text{LA})_x$ ($x = 6$ to 12) varied from 0.04 to 0.16 nm^2 per residue (0.56 to 4.16 nm^2 per molecule), which was explained by the increased helical content for the longer peptides (Dieudonne et al. 1998). The 21-mer helical γ_1 peptide collapsed at $\sim 27 \text{ mN m}^{-1}$ and showed a liftoff and a limiting A of ~ 0.29 and 0.07 nm^2 per residue, respectively (~ 6 and $\sim 1.5 \text{ nm}^2$ per molecule, respectively), (Hinz and Galla 2005). In addition, the head-to-tail cyclised 21-mer microcin J25 achieved a maximum π of $5 - 7 \text{ mN m}^{-1}$ before collapse, whereas the liftoff and limiting A were ~ 0.16 and 0.13 nm^2 per residue, respectively (~ 3.3 and $\sim 2.7 \text{ nm}^2$ per molecule, respectively), (Bellomio et al. 2005). These values and the ones presented in Maget-Dana et al. (1999) (Maget-Dana et al. 1999) demonstrate that the stability of the peptide film and the area occupied by a peptide molecule at a certain surface pressure can vary depending on the peptide size, secondary structure and orientation on the water surface. Additionally, the helical and β -structures at the air/water interface are more stable than the cyclic ones.

Our π/A isotherm and IRRA spectra of KLAL concur well with the results of a similar experiment carried out by Kerth et al. (2004). However, we obtained a larger liftoff and collapse area A of ~ 5.5 and $\sim 3.6 \text{ nm}^2$ per molecule, respectively, in comparison to ~ 4.5 and $\sim 2.9 \text{ nm}^2$ per molecule, respectively (Kerth et al. 2004). This discrepancy can be explained by the different applied spreading techniques of the peptide. We prepared the peptide in chloroform/methanol 4:1 rather than as an aqueous solution (Kerth et al. 2004). Hence, more peptide molecules are retained at the interface and less go into the subphase, therefore, a higher A can be achieved.

4.2.4 Cospreading of KLAL/lipid mixtures at the air/water interface

The next step was to investigate films of premixed lipid and KLAL solutions. The films will be denoted throughout the text as “premixed films”. Ideally, the isotherm of the premixed film will be additive and resembles the superposition of the lipid isotherm and the peptide isotherm. However, deviations due to intermolecular interactions, domain formation,

and squeezing out of lipid/peptide aggregates into the subphase cannot be ruled out (Maget-Dana 1999).

The isotherms of POPG, POPG/KLAL 20:1 and the corresponding IRRA spectra are presented in **Figure 4.2-6A** and **Figure 4.2-6B**. As indicated by the IRRA spectra, the interaction with the PG headgroup induced the formation of an α -helical conformation of the peptide, which was indicated by an amide I and II bands at ~ 1659 and ~ 1547 cm^{-1} , respectively. The peptide in DPPG/KLAL 20:1 film behaved similarly, where amide I and II were observed at ~ 1657 and ~ 1547 cm^{-1} , respectively, (data not shown).

The stretching mode of the POPG ester groups ($\nu(\text{CO})$) was shifted to a lower wavenumber due to the hydrogen bonding between KLAL and the POPG headgroup (Blume et al. 1988; Schwieger and Blume 2007; Tamm and Tatulian 1997). In the adsorption experiments, the KLAL peptide was found to align parallel to the air/water interface in a β -sheet conformation, whereas the α -helix was tilted with an angle $> 54.6^\circ$ with respect to the normal of the interface upon its insertion into POPG films (Erbe 2001). In the case of PG/KLAL premixed films, we expect the peptide to lie flat at the interface in the beginning of the experiment whereas during the film compression reorientation and tilting might take place.

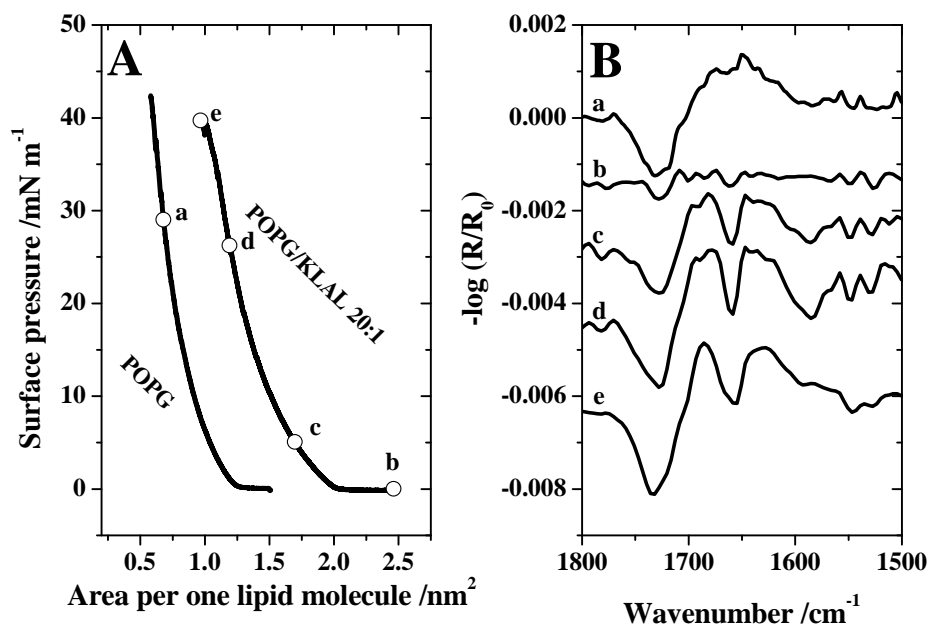


Figure 4.2-6 (A) Surface pressure versus area per one lipid molecule compression isotherm of POPG and POPG/KLAL 20:1 spread on the surface of the subphase (10 mM Tris, 154 mM NaCl, pH 7.4) at 20°C. The area was scaled to the lipid molecular area. **(B)** IRRA spectra of the films at the respective positions a-e. The IRRA spectra were recorded with *p*-polarized light at an angle of incidence of 40°.

The area in the π/A isotherms was scaled to the lipid molecular area. Therefore, the gain in the area per lipid in the premixed films was due to the peptide. As shown in **Figure 4.2-6A**, the interaction with POPG enhanced the peptide stability at the water surface, since the film of the pure peptide collapsed at $\sim 27.2 \text{ mN m}^{-1}$ (**Figure 4.2-5A**), whereas the peptide remained in the premixed film up to $\sim 40 \text{ mN m}^{-1}$. The difference between the two isotherms reduced at high surface pressure. This decrease could be correlated to the compression and/or reorientation of the peptide as well as to the squeezing out of the peptide or lipid/peptide aggregates into the subphase.

We examined also monolayers of KLAL premixed with POPG/POPE 1:3 and *E. coli* polar lipid extract, respectively. In these films, the peptide adopted a helical structure as well, which confirms the connection between the membrane negative charge and the induced helical structuring of KLA peptides.

KLA peptides exhibited a modest affinity towards uncharged membranes (Dathe et al. 1996). In addition, no considerable peptide adsorption was observed for monolayers of the zwitterionic lipids POPC and POPE. Premixing of KLAL with PC and PE and spreading them onto the water surface force them to interact. The study of the interaction with zwitterionic lipids will provide us with crucial information about the influence of the lack of a negative charge on the interaction. A variety of PC and PE lipids were investigated to elucidate the influence of the lipid headgroup on the peptide behaviour.

The isotherms of POPC and POPC/KLAL 20:1 mixture and the corresponding IRRA spectra are shown in **Figure 4.2-7**. The increased area per lipid of the premixed monolayer showed that the peptide remained at the interface till the film collapsed at $\sim 40 \text{ mN m}^{-1}$. Nonetheless, the low intensity amide I and II peaks (at ~ 1659 and $\sim 1547 \text{ cm}^{-1}$, respectively) were not sufficient to make a conclusive conclusion about the peptide secondary structure. This phenomenon, where no substantial amide bands could be detected of peptides/proteins at the interface was observed before in our group as well as in other groups (unpublished observations, personal communications). The difference in the intensity of the amide peaks between POPC and POPG premixed films proposes a different arrangement and orientation of the peptide in the two cases. The difference in the area per lipid between the pure and premixed isotherms decreased continuously during the compression especially at high π ($> 27 \text{ mN m}^{-1}$) suggesting the squeezing out of the peptide into the subphase. Nonetheless, a peptide reorientation cannot be ruled out. The surface-pressure induced squeezing out of unstable lipids (Pastrana-Rios et al. 1994), proteins (Pastrana-Rios et al. 1995), and peptides

(Ambroggio et al. 2005; Bringezu et al. 2007a; Maltseva et al. 2005) at the water surface was presented before in the literature.

We also investigated monolayers of a premixed DOPE/KLAL 20:1 solution (data not shown). Similar to the POPC case, no amide bands of considerable intensities were observed, despite the pronounced expansion of the area per lipid. However, the peptide retained in the DOPE premixed film and no squeezing out into the subphase was noticed.

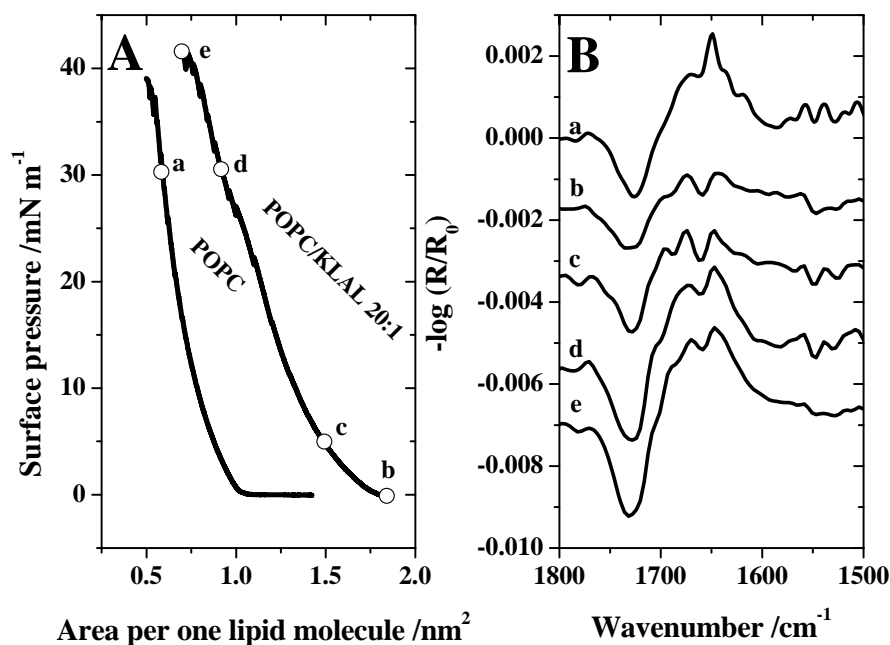


Figure 4.2-7 (A) Surface pressure versus area per one lipid molecule compression isotherm of POPC and POPC/KLAL 20:1 spread on the surface of the subphase (10 mM Tris, 154 mM NaCl, pH 7.4) at 20°C. The area was scaled to the lipid molecular area. **(B)** IRRA spectra of the films at the respective positions a-e. The IRRA spectra were recorded with *p*-polarized light at an angle of incidence of 40°.

Interestingly, KLAL assumed β -strands when premixed with POPE (**Figure 4.2-8**) similarly to pure peptide at the air water interface. However, the small peak at ~ 1691 cm⁻¹ and the shifted amide I band to ~ 1616 cm⁻¹ (~ 1618 cm⁻¹ for pure KLAL) could propose a slightly different peptide orientation from that of pure peptide film. The high surface pressure reached before the film collapsed together with the minor squeezing out of the peptide during the film compression indicated a high stability and a low compressibility of KLAL β -sheets in the POPE/KLAL monolayer (discussed later). Comparably, DPPE induced the formation of β -sheets, which was evident by the amide I and II bands at ~ 1616 and ~ 1527 cm⁻¹, respectively (data not shown).

In the case of DPPC/KLAL 20:1 premixed film, the IRRA spectra exhibited that the peptide adopted concurrently an α -helix (amide I and II at ~ 1660 and ~ 1547 cm⁻¹,

respectively) and an antiparallel β -sheet structures (amide I and II at ~ 1693 , ~ 1614 and ~ 1531 cm^{-1} , respectively) (data not shown).

In the premixed films discussed above, KLAL did not alter the stretching vibrational bands of CH_2 (lipid chain packing) and PO_2^- groups (correspond to the hydration status and the hydrogen bonding with the lipid headgroup). However, the peptide increased the asymmetric stretching mode of PO_2^- ($\nu_{\text{as}}(\text{PO}_2)$) of POPC from ~ 1214 to ~ 1220 cm^{-1} , which revealed possible dehydration of the PC headgroup upon the interaction with the peptide (Mantsch and McElhaney 1991; Tamm and Tatulian 1997). The high noise due to the absorption bands of water vapour centred ~ 1665 cm^{-1} hindered the proper analysis of the carbonyl stretching bands at ~ 1735 cm^{-1} .

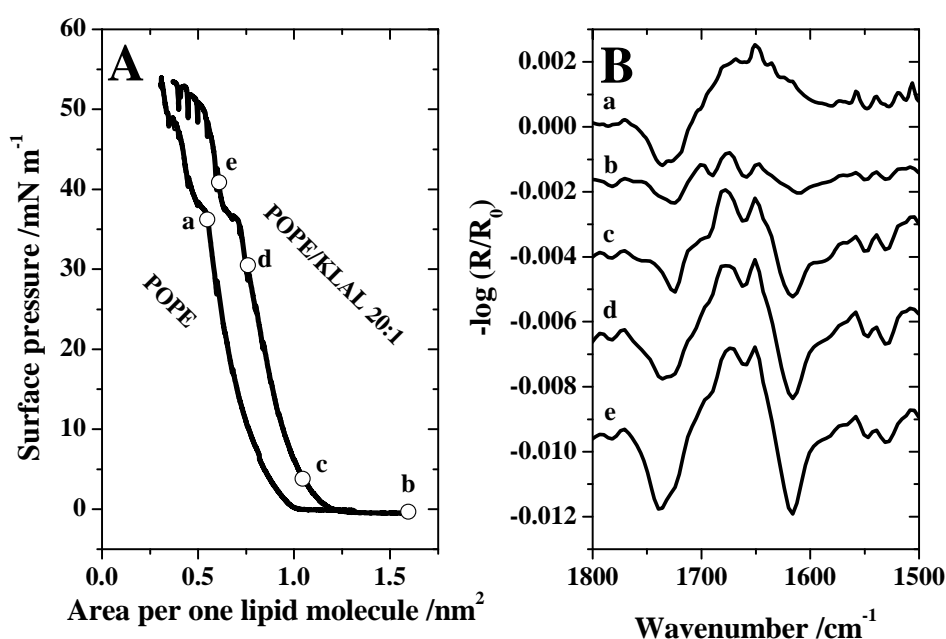


Figure 4.2-8 (A) Surface pressure versus area per one lipid molecule compression isotherm of POPE and POPE/KLAL 20:1 spread on the surface of the subphase (10 mM Tris, 154 mM NaCl, pH 7.4) at 20°C . The area was scaled to the lipid molecular area. **(B)** IRRA spectra of the films at the respective positions a-e. The IRRA spectra were recorded with *p*-polarized light at an angle of incidence of 40° .

KLAL always adopted a helical structure in PG containing monolayers as observed in the cospreading as well as the adsorption experiments. However, the structure adopted in the uncharged monolayers depended on the lipid shape, chain packing, and headgroup structure. The gel to liquid crystalline (L_α) transition temperature of POPC, POPE, DPPE, DPPC and DOPE is ~ -3 , 25, 65, 41.5 and -16°C , respectively (Cevc 1993). At the water surface and at 30 mN m^{-1} and 20°C , POPC, POPE, and DOPE are in the liquid-expanded phase, whereas

DPPE and DPPC are in the liquid-condensed phase. The lipid chain packing of PE lipids is higher than PC lipids with the same acyl chains, which is due to the smaller headgroup of PE.

One can speculate that the peptide tends to form a β -sheet structure in lipid films with high lipid chain packing (POPE, DPPE, and DPPC). One explanation can be that the tightly packed lipids do not mix properly with the peptide at the water surface. This will allow stronger interactions between the peptide molecules that will induce the formation of β -aggregates. Due to the larger headgroup of DPPC, its monolayer is less densely packed as compared to DPPE. Therefore, some miscibility between DPPC and the peptide may take place, and therefore both secondary structures can be formed. The fluid nature of POPC and DOPE enables the lipid molecules to mix well with the peptide molecules at the water surface, which will impede the interaction between the peptide molecules and the formation of β -sheet structures. Nevertheless, the influence of the lipid shape and the experimental procedure cannot be ruled out.

The presence of some discrepancies in the wavenumber, shape, and intensity of the amide bands could indicate that the exact structure and orientation of the peptide may vary among the different monolayers. Besides, the peptide may interact differently with the different monolayers, which will influence the properties of the amide I bands (Lewis et al. 1999). However, our present data are not adequate to make decisive conclusions.

We also determined the peptide isotherm in the different mixtures by subtracting the pure lipid isotherm from the isotherm of the premixed film. The validity of those isotherms is based on the assumption that all the spread lipid and peptide molecules are retained at the surface and that the isotherm of the pure lipid represents that of the lipid in the premixed films. **Figure 4.2-9** illustrates a comparison between the π/A isotherm of pure KLAL and that of the peptide in the different premixed films.

Since the KLAL isotherm of the POPC and DOPE premixed monolayers resembled more the peptide isotherm of the POPG premixed monolayer, we concluded that the peptide in both mixtures, i.e. POPC and DOPE, was mostly α -helix.

The properties of the KLAL isotherms of the different mixtures are summarized in **Table 4.2-2**, including; A of KLAL at the liftoff point and at 30 mN m^{-1} , the max π attained before collapse, and the film compressibility at 30 mN m^{-1} . The film compressibility defined by the compressibility coefficient (β) was calculated using $\beta = -1/A(\partial A/\partial \pi)_{20^\circ\text{C}}$ (Maget-Dana 1999; Maget-Dana et al. 1999).

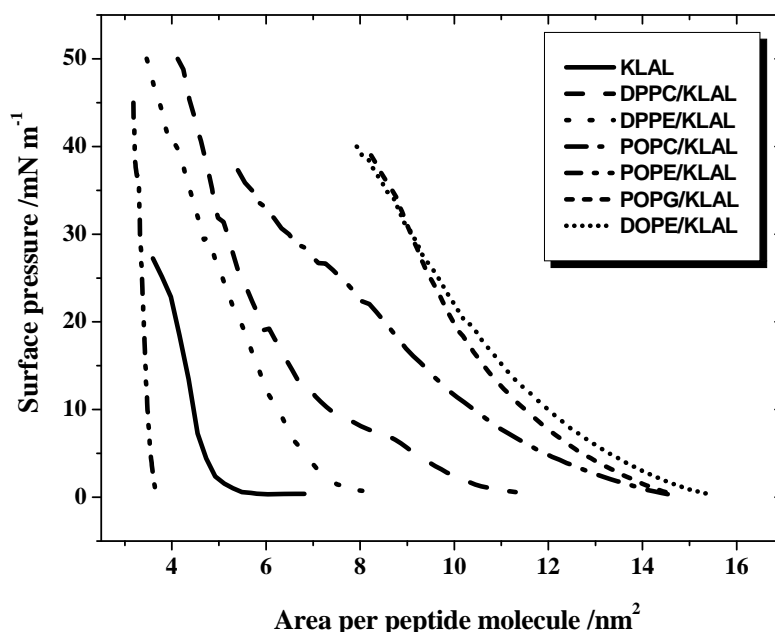


Figure 4.2-9 Comparison of surface pressure versus area per one peptide molecule compression isotherms of pure KLAL and that of the peptide in the different mixed lipid-KLAL films.

As demonstrated in **Table 4.2-2** and **Figure 4.2-9**, the peptide showed a modest influence on the max π of the premixed films, which was comparable to that of pure lipid monolayers.

Table 4.2-2 The different properties of pure KLAL film and of the peptide in the different lipid-KLAL premixed films. The structure of KLAL in POPC and DOPE premixed films was anticipated from the area per peptide molecule (see **Figure 4.2-9**)

Film	Structure	KLAL A / nm ²		Max π / mN m ⁻¹		β_{30} ^b / m N ⁻¹	
		Liftoff ^a	~30 mN m ⁻¹	Lipid	Mixture	Lipid	KLAL
KLAL	Beta	5.5	3.6 ^c	-	27.2	-	16.4
POPE/KLAL	Beta	4	3.3	54	54	24.4	6.5
DPPE/KLAL	Beta	8	4.6	56.5	59	4.8	13.8
DPPC/KLAL	Alpha + Beta	11	5.2	57	60	6.5	14
POPC/KLAL	Alpha	16	6.5	39	41.5	11.1	30.5
POPG/KLAL	Alpha	15.6	9.1	42	39	11.7	11.2
DOPE/KLAL	Alpha	16	9.1	44.5	40.5	9.3	11.8

^a Liftoff A was determined ~ 0.3 mN m⁻¹. ^b β_{30} is the compressibility coefficient at 30 mN m⁻¹. ^c The film of pure KLAL collapsed ~ 27 mN m⁻¹.

The secondary structure of the peptide influences the area occupied by the peptide molecules and the elasticity of the peptide film. Using computer modelling, the area occupied by a β -sheet KLAL was anticipated to be 3.0 nm² (Kerth et al. 2004), whereas the area per a helical KLAL was 3.6 nm² (2.9 nm² of the tilted helical peptide at 54.6°) (Erbe 2001). From

our experiments, the A per a helical peptide was $\sim 16 \text{ nm}^2$ (0.89 nm^2 per residue) at the liftoff point and 9.1 nm^2 (0.51 nm^2 per residue) at 30 mN m^{-1} . On the other hand, the A per a KLAL β -sheet ranged from 4 to 8 nm^2 ($0.22 - 0.44 \text{ nm}^2$ per residue) at the liftoff, and from 3.3 to 4.6 nm^2 ($0.18 - 0.26 \text{ nm}^2$ per residue) at 30 mN m^{-1} . The estimated A per a KLAL β -sheet (pure and mixed) was comparable with the range mentioned in the literature, whereas the area per a KLAL α -helix was much higher than expected (Dieudonne et al. 1998; Maget-Dana 1999; Maget-Dana et al. 1999). The values reported in literature are for experiments carried out with pure peptide films rather than for lipid/peptide premixed films, like in our case. This indicates that the β -structured peptide in mixed monolayers resembles that of pure peptide films. One explanation for the higher-than-expected area per a helical KLAL in premixed monolayers could be that the lipid-peptide miscibility was not ideal and, therefore, their isotherms were not additive. In addition, the difficulties in arranging the helical peptide in the premixed film properly might hamper the optimal use of the surface area and consequently increased the resulting area per peptide.

The A of the peptide in the DPPC/KLAL premixed film had intermediate values, as the peptide in this mixture is anticipated to adopt α -helix and β -sheet structures, simultaneously.

The peptide as an antiparallel β -sheet is anticipated to exist as patches at the air/water interface or in the lipid matrix, and this may explain the similarities between the determined A per a β -sheet and literature. Comparably, X-ray data showed that although PGLa mixed well with PG monolayers, the peptide segregated in PC monolayers and formed peptide separate islands (Konovalov et al. 2002). Additionally, alamethicin, which is believed to assemble into oligomeric channel structures (Vogel 1987), formed discrete domains in DMPC monolayers (Volinsky et al. 2006).

The compressibility of the peptide film in the various monolayers was comparable to that of pure lipid monolayers (see **Table 4.2-2**). In principle, the α -helical peptides are more compressible and less stable than β -sheet peptides (Maget-Dana 1999). Most of the peptide films exhibited a comparable β_{30} of around 13.5 m N^{-1} ($11.2 - 16.4 \text{ m N}^{-1}$). However, the KLAL premixed with POPE, which formed β -sheet, showed the lowest β_{30} (6.5 m N^{-1}). Our compressibility coefficients are comparable to some values for various peptides presented in literature (Maget-Dana et al. 1999).

4.2.5 Adsorption versus cospreading

The comparison between the outcome of both monolayer techniques, i.e. the peptide adsorption to lipid monolayers and the cospreading of premixed lipid-peptide solutions, gives hints about the influence of the experimental procedure on the mode of interaction and on the results. **Table 4.2-3** demonstrates a comparison of the stretching vibrational bands (CH_2 , PO_2^- and CO) of POPG, DPPG, POPC, and POPE between the mixed monolayers at 30 mN m^{-1} and the adsorption experiments, which were carried out at a constant π of 30 mN m^{-1} . In the case of the fluid lipids, namely POPG, POPC, and POPE, no differences in the lipid chain packing ($\nu_{\text{as}}(\text{CH}_2)$) between the adsorption and π/A isotherm experiments were observed. However, DPPG, which existed in the liquid-condensed form at the experimental temperature and surface pressure, was less ordered in the mixed film ($\sim 2922 \text{ cm}^{-1}$) in comparison to the adsorption experiment ($\sim 2920 \text{ cm}^{-1}$).

As illustrated in **Table 4.2-3**, the DPPG premixed film showed a lower $\nu_{\text{as}}(\text{PO}_2^-)$ and $\nu(\text{CO})$ values (~ 1202 and $\sim 1727 \text{ cm}^{-1}$, respectively) in comparison to the adsorption experiment (~ 1210 and $\sim 1736 \text{ cm}^{-1}$, respectively). This indicates a stronger hydrogen bonding of the peptide with the phosphate and carbonyl moieties of DPPG in case of the premixed film as compared to the adsorption experiment. Similar to DPPG, the interaction of the peptide with the phosphate group of POPG in the premixed films was stronger than in the adsorption experiment. The interaction of KLAL with POPC reduced the $\nu_{\text{as}}(\text{PO}_2^-)$ from 1214 to 1220 cm^{-1} proposing the dehydration of the POPC phosphate group. Overall, only modest differences of $\nu_{\text{as}}(\text{PO}_2^-)$ and $\nu(\text{CO})$ were observed between the premixed films and the adsorption experiments of the uncharged lipids POPC and POPE.

Table 4.2-3 Comparison of the stretching vibrational bands (CH_2 , PO_2^- , CO) of the mixed lipid-peptide films at 30 mN m^{-1} and of the peptide adsorbed to lipid monolayers, whose pressure was kept at 30 mN m^{-1} , for the lipids POPG, DPPG, POPC and POPE.

Lipid	$\nu_{\text{as}}(\text{CH}_2) / \text{cm}^{-1}$		$\nu_{\text{as}}(\text{PO}_2^-) / \text{cm}^{-1}$		$\nu(\text{CO}) / \text{cm}^{-1}$	
	Adsorption	π/A	Adsorption	π/A	Adsorption	π/A
POPG	2924	2924	1209	1203	1724	1726
DPPG	2920	2922	1210	1202	1736	1727
POPC	2924	2924	1223	1220	1728	1726
POPE	2923	2923	1216	1215	1733	1733

The cospreading experiments were performed with KLAL, whereas the adsorption experiments were carried out using KLA1. The vibrational bands of the adsorption experiments were recorded of the well-equilibrated system.

4.2.6 *Dynamic Light Scattering (DLS)*

DLS serves as a potent tool to investigate processes that are associated with the aggregation (Wen et al. 2007), fusion (Cummings and Vanderlick 2007), solubilization and degradation (Garidel et al. 2007; Hildebrand et al. 2004; Hildebrand et al. 2002; Sood et al. 2008) of lipid assemblies as well as to follow any morphological changes (Wang et al. 2007). Therefore, static and dynamic light scattering are often used to inspect interactions of membrane-active agents with lipid membranes, which are usually associated with altering the size and shape of lipid vesicles (Domingues et al. 2008). In addition to the aforementioned processes, DLS can detect the adsorption of surfactants (Wang et al. 2007) or peptides (Abraham et al. 2005a, b) to lipid vesicles, in case that the lipid vesicles do not aggregate or break down. As a result, one obtains a direct evidence of the ligand affinity and selectivity.

We utilized DLS to monitor the influence of KLA peptides on the average size of lipid vesicles. To this end, lipid vesicles were titrated into peptide solutions in the cuvette, like in the ITC experiments. This procedure helped us to achieve high peptide to lipid ratios after the first injection of lipid vesicles. However, this caused a massive aggregation of lipid vesicles which hindered the detection of any possible changes in the size of lipid vesicles, for instance due to vesicle solubilization. The further additions of vesicles continuously increased the lipid fraction in the system until the aggregation capacity of the peptides was exceeded. This drove the dissociation of the aggregates. As a result, we could observe the size distribution of the individual vesicles and see the effect of high peptide concentrations.

We studied the effect of KLA1 and $k_{9,a10}$ -KLAL peptides on DPPG and DPPC extruded vesicles (50 nm radius) at 25°C. The average size distribution of the lipid vesicles without peptide was controlled prior to each experiment. **Figure 4.2-10 (left)** demonstrates the unweighted radius size distribution of DPPG without peptide and of DPPG titrated into KLA1 and $k_{9,a10}$ -KLAL solutions, respectively. At L/P ratios of 2, a broad peak with a radius size distribution centred ~ 320 nm was observed. The further addition of DPPG vesicles caused a peak splitting showing two populations with distinct average size distributions. Upon increasing the L/P ratio, the larger structures continued to grow, however, the smaller structures decomposed into, most probably, individual vesicles. At and above L/P of 20, the position of the two peaks remained unaltered whereas their intensity kept changing upon the addition of vesicles in favour of the peak belonging to the individual vesicles.

The origin of the large structures cannot be disclosed by DLS experiments, whether they are aggregates, fused vesicles or a mixture of both, and further investigations are necessary.

After each injection, we gave the sample few minutes to equilibrate before the measurement was started. Due to the generally slow kinetics of vesicle fusion, a much longer time is required for the process to take place. For example, Cummings and Vanderlick (2007) reported that the hemi-fusion of POPG LUVs induced by the antimicrobial peptide cryptdin-4 (Crp4) may take up to 1h to complete (Cummings and Vanderlick 2007). Therefore, we anticipate that the large structures are mainly due to the aggregation of lipid vesicles driven by electrostatic attraction between the cationic peptides and the anionic DPPG.

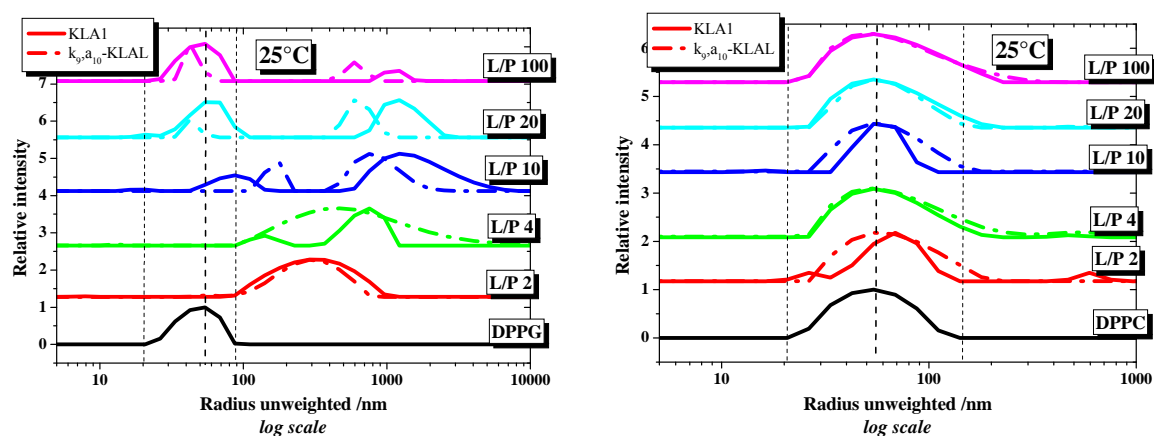


Figure 4.2-10 Unweighted distribution of hydrodynamic radii obtained from DLS measurements of DPPG (left) and DPPC (right) vesicles (1 mM, ~ 50 nm radius) before and after the multi-step addition to KLA1 and $k_{9,a10}$ -KLAL solutions (500 μ l, 10 μ M) at 25°C. The samples were prepared in buffer (10 mM Tris, 154 mM NaCl, pH 7.4).

The aggregation/fusion capacity of KLA1 exceeded that of $k_{9,a10}$ -KLAL, since at L/P ≥ 20 DPPG-peptide structures with the size of ~ 1200 and ~ 600 nm were observed with KLA1 and $k_{9,a10}$ -KLAL, respectively. On the other side, $k_{9,a10}$ -KLAL reduced the average radius of DPPG vesicles from 54 to 42 nm (at L/P of 100) showing a higher solubilization power as compared to KLA1, which did not alter the size of DPPG vesicles. For comparison purposes, carrying out the titrations at temperatures higher than the phase transition temperature of DPPG and DPPC ($> 41^\circ\text{C}$) could be beneficial to examine the influence of the peptides on fluid lipid vesicles. However, heating up the sample provokes the formation of air bubbles that pronouncedly influences the experiment outcome. Although those titrations at high temperatures were performed, and they exhibited a reduced aggregation power of the peptides, we refrained from analyzing them further.

The influence of time on the activity of the peptides towards DPPG vesicles is shown in **Figure 4.2-11**. The addition of DPPG vesicles (43 nm radius) to $I_{11,k12}$ -KLAL solution (L/P of 24) led to the appearance of two populations having an average radius of ~ 80 and ~ 470 nm. The incubation of this complex at 25°C for 12 hours gradually increased the average

radius to ~ 110 and ~ 600 nm, respectively. However, the ratio between the two populations in the solution remained unchanged. The incubation of DPPG vesicles without peptide using the same procedure barely influenced the average size of the vesicles. Because of the slow kinetics of this process, we propose that the increase in the average size distribution was due to vesicle fusion. Based on those observations, one concludes that the aggregation of vesicles is a much faster process and leads to a much larger structures as compared to lipid fusion, however, reversible. Moreover, the aggregation facilitates and accelerates the fusion process.

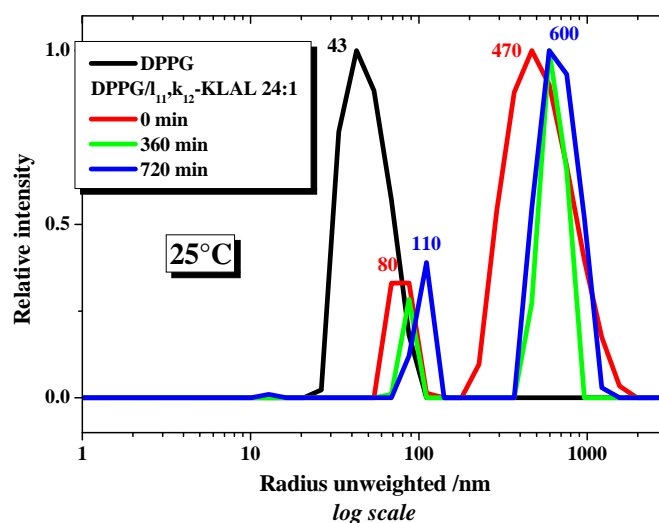


Figure 4.2-11 Unweighted distribution of hydrodynamic radii obtained from DLS measurements of free DPPG vesicles and of $I_{11,k_{12}}$ -KLAL-bound DPPG (L/P 24:1) at 25°C, which shows the changes in the size of DPPG vesicles after 0, 360 and 720 min of the addition of the peptide. The samples were prepared in buffer (10 mM Tris, 154 mM NaCl, pH 7.4).

The effect of KLA1 and $k_{9,a_{10}}$ -KLAL on DPPC vesicles is illustrated in **Figure 4.2-10 (right)**. Essentially, the peptides caused only minor changes in the size distribution of DPPC vesicles as compared to their influence on DPPG vesicles.

4.2.7 Circular Dichroism (CD)

Using CD spectroscopy, the structure of KLA peptides was determined before in buffer as well as under different structure-inducing conditions (Dathe et al. 1996; Krause et al. 1995). As shown in **Figure 4.2-12**, KLAL is unstructured in buffer, whereas the peptide forms an α -helix in 50% TFE and upon binding to POPG and POPC lipids vesicles as evident by the negative ellipticity at 207 and 222 nm and the positive CD band below 200 nm. However, the peptides, and particularly the one with the low helical propensity, showed a tendency to adopt β -structures under certain condition, e.g. at high bulk/surface peptide

concentrations, at high peptide/lipid ratios and with the use of a highly acidic media ((Kerth et al. 2004) and unpublished observations).

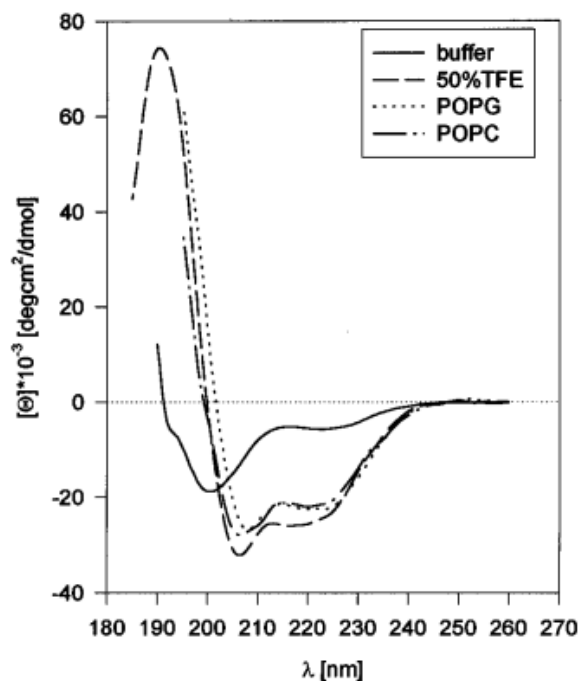


Figure 4.2-12 CD spectra of KLAL (peptide concentration 10^{-5} M) in Tris buffer, 50% TFE in buffer (v/v), buffered POPG SUV suspension (lipid concentration 2.3 mM) and buffered POPC SUV suspension (lipid concentration 2.0 mM). Adapted from ref. (Dathe et al. 1996)

We performed numerous DSC experiments to characterize the interaction of KLA peptides with DPPG and DPPG-containing vesicles, which required the use of high peptide concentrations as well as high peptide/lipid ratios (see below). Therefore, and in order to interpret the DSC experiments properly, we used CD spectroscopy to resolve the secondary structure assumed by the peptides at the concentrations and molar ratios applied in DSC experiments.

Figure 4.2-13 (left) presents the CD spectra observed of KLA peptides mixed with DPPG LUV at L/P ratios of 40 to 10. The high peptide content in the mixture caused more vesicles to aggregate and to precipitate, which increased the scattered light off the sample and decreased the peptide available for the light beam. Therefore, it was not possible to analyze the CD spectra quantitatively.

KLAL1 and k_{1,l_2} -KLAL, the peptides with the higher helical propensity, preserved the α -helix structure when premixed with DPPG, whereas the peptides with the lower intrinsic helicity, $k_{9,a_{10}}$ -KLAL and $l_{11,k_{12}}$ -KLAL, assumed β -strands and aggregated. The CD spectrum of KLAL1 bound to DPPG (see **Figure 4.2-13 (left)**) was comparable to that of

KLAL bound to POPG (see [Figure 4.2-12](#)), whereas the spectrum of k_{1,l_2} -KLAL was somewhat different.

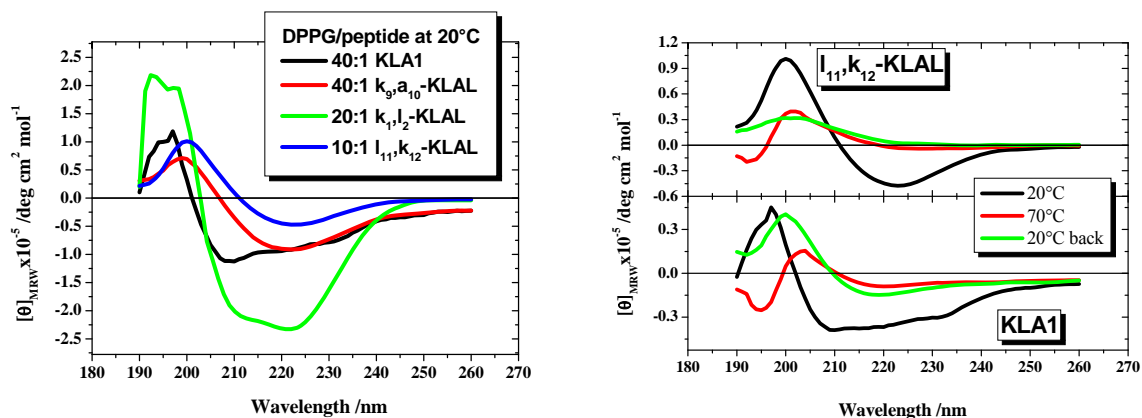


Figure 4.2-13 (Left) CD spectra of KLA peptides (25 – 100 mM) in DPPG LUV suspension (~ 50 nm radius, 1 mM, L/P 10 to 40) at 20°C. **(Right)** The influence of temperature on DPPG/KLA1 and DPPG/ l_{11},k_{12} -KLAL mixtures with L/P ratio of 10. The mixtures were heated from 20 to 70°C and then cooled back to 20°C. The samples were prepared in buffer (10 mM Tris, 154 mM NaCl, pH 7.4).

The influence of temperature on the peptide secondary structure was also inspected. The CD spectra of DPPG/peptide 10:1 mixtures were recorded at 20 and 70°C and again at 20°C after cooling the sample back. KLA1 ([Figure 4.2-13 \(right\)](#)) and k_{1,l_2} -KLAL (spectra not shown) transformed to β -sheets at 70°C, whereas cooling the samples back to 20°C did not reverse this transformation. On the other hand, heating up l_{11},k_{12} -KLAL ([Figure 4.2-13 \(right\)](#)) and $k_{9,a_{10}}$ -KLAL (spectra not shown) caused them to aggregate and their ellipticity to be pronouncedly reduced.

4.2.8 Differential Scanning Calorimetry (DSC)

DSC has been widely used to measure the phase behaviour of phospholipid bilayers, from which information about the phospholipid conformation, bilayer fluidity and ligand-vesicle interaction can be derived. The parameters that can be obtained from DSC analysis are the onset temperature of transition T_o , temperature at the peak maximum T_m , half height width of the transition peak (HHW), and the enthalpy of the process ΔH (by integrating the area under the peak). The width of the transition curves of one-component lipid membranes is correlated with the transition cooperativity.

We used DSC to study the influence of the four KLA peptides on the phase transitions of the anionic DPPG and the uncharged lipids DMPC and DPPE. Concentration-dependent experiments were carried out to follow the effects of the peptides on the lipid vesicles

systematically. The influence of KLA peptides on the zwitterionic lipids DMPC and DPPE was modest in comparison to DPPG.

Figure 4.2-14A to D show the first and second heating DSC curves of DPPG and of DPPG/KLA peptide mixtures at lipid/peptide ratio “L/P” ranging from 10 to 200. The fully hydrated DPPG undergoes a pretransition (T_{pre}) from lamellar gel L_{β} to ripple gel P_{β} at $\sim 33^{\circ}\text{C}$ and a main transition (T_m) to L_{α} at $\sim 41^{\circ}\text{C}$. Our thermograms of pure DPPG revealed pre- and main transitions at ~ 32 and $\sim 40.6^{\circ}\text{C}$, respectively, which agree with literature (Garidel and Blume 2000; Schwieger and Blume 2007). The first heating scan of lipid vesicles through their transition usually abolishes non-equilibrate states of lipids and relieves the stress in vesicles due to ligand binding or to the preparation procedure. It also drives ligand redistribution and entry through the defects between the gel and the fluid domains co-occur during the phase transition (Heimburg 2000).

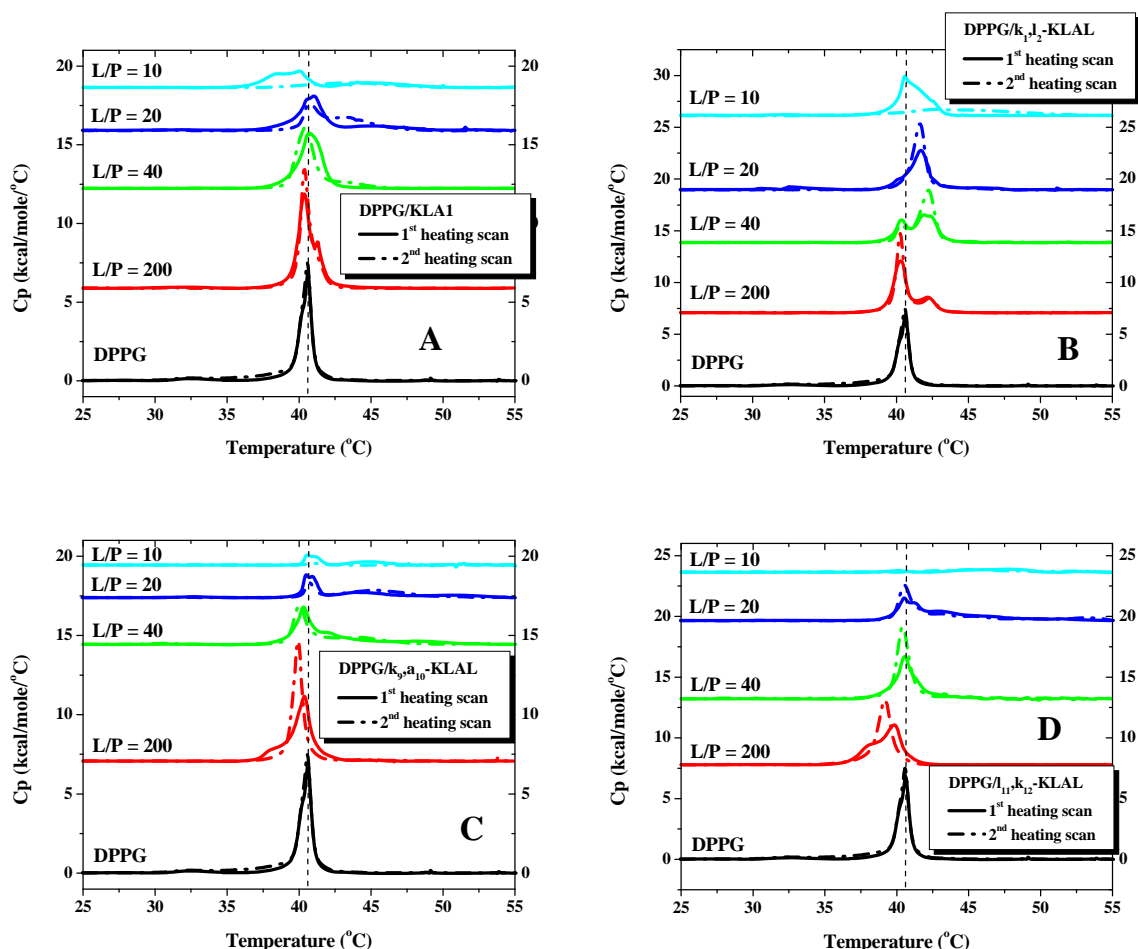


Figure 4.2-14 First (solid lines) and second (dashed lines) heating DSC curves of DPPG LUV (2 mM) before (black lines) and after the addition of (A) KLA1, (B) k_{1,l_2} -KLAL, (C) $k_{9,a_{10}}$ -KLAL, and (D) $l_{11,k_{12}}$ -KLAL peptides with L/P ratios of 200 to 10. The samples were prepared in buffer (10 mM Tris, 154 mM NaCl, pH 7.4).

The pretransition is sensitive to the preparation procedure and it is usually absent or not resolved in SUV (Heimburg 2000). In addition, it can be abolished due to the presence of other components like cholesterol and fatty acids (McElhaney 1982). Also, the interaction of lipid bilayers with surfactants (Hildebrand et al. 2004; Hildebrand et al. 2002), anaesthetics (Engelke et al. 1997) and antimicrobial peptides (Andrushchenko et al. 2007; Prenner et al. 1999; Seto et al. 2007; van Kan et al. 2003) abolishes the pretransition, indicating the untilting of the hydrocarbon chains due to the deeper burial of the bound molecules in the lipid membrane (Lohner and Prenner 1999). KLA peptides suppressed the pretransition of DPPG, particularly at high peptide contents, while they induced a complex transition behaviour.

As shown in **Figure 4.2-14A**, during the first heating scan through the phase transition, KLA1 decreased the enthalpy and cooperativity of DPPG phase transition pronouncedly in a concentration dependent manner. The effect on T_m was modest at L/P of 200 to 20, whereas the phase transition was significantly broadened and T_m was reduced to $\sim 39^\circ\text{C}$ at L/P of 10. The second heating scan was associated with the appearance of a new peak at a higher temperature ($> T_m$), which broadened and up-shifted upon increasing the peptide content, whereas the main peak vanished at L/P of 10.

The interaction of DPPG with k_{1,l_2} -KLAL (**Figure 4.2-14B**) apparently induced the formation of two domains; a k_{1,l_2} -KLAL-poor domain with a transition temperature slightly lower than T_m ($\sim 40^\circ\text{C}$) and a k_{1,l_2} -KLAL-rich domain with a higher transition temperature ($\sim 42^\circ\text{C}$). The ratio between the two domains was regulated by the peptide content (L/P ratio). Again, at L/P of 10 and after the first heating scan only a broad peak with very low intensity could be observed.

Figure 4.2-14C and **Figure 4.2-14D** exhibit the influence of $k_{9,a_{10}}$ -KLAL and $l_{11,k_{12}}$ -KLAL peptides, respectively. As revealed by CD spectroscopy, these two peptides actually form β -structures when mixed with DPPG vesicles at the L/P ratios used in DSC experiments. Both peptides decreased T_m by $\sim 1^\circ\text{C}$ at L/P of 200, whereas the peak position at the other L/P ratios was similar to free DPPG. The drop in the transition enthalpy was much more pronounced than in the case of KLA1 and k_{1,l_2} -KLAL, particularly at high peptide content (low L/P). Again, the transition was entirely abolished at L/P of 10 after the first heating scan.

Many attempts have been made to make general statements that correlate the type of interaction of proteins/peptides with lipid membranes and its influence on the measured DSC thermograms. For instance, Papahadjopoulos et al. (1975) classified the proteins into three groups; whether they show strong electrostatic binding, interact merely hydrophobically or exhibit both properties (Papahadjopoulos et al. 1975). Ivanova et al. (2003) used statistical

thermodynamic analysis to reveal the influence of peptide mixing on the heat capacity profiles of lipid membranes. Accordingly, they established four cases based on how favourable is the mixing of the peptide with the gel and fluid lipids (Ivanova et al. 2003).

The stabilization of lipid membranes and the subsequent increase in T_m is associated with the strong electrostatic binding of charged ligands, e.g. divalent cations (Garidel et al. 2000; Hauser and Shipley 1984), polyamines (Arouri 2004) and polylysine (Papahadjopoulos et al. 1975; Schwieger and Blume 2007), as well as to the preferential interaction with lipids in the gel phase (Ivanova et al. 2003). On the other hand, hydrophobic interactions with lipid membranes usually perturb the lipid chain packing, which may pronouncedly decrease the transition temperature, enthalpy and cooperativity (Papahadjopoulos et al. 1975). The solubilization of lipid vesicles by detergents (e.g. bile salts (Hildebrand et al. 2004; Hildebrand et al. 2002) and triton-X100 (Goni et al. 1986) was found to pronouncedly reduce the transition enthalpy with some decrease in the transition temperature and cooperativity. Additionally, high detergent concentrations could also completely abolish the transition, since mixed micelles or small aggregates are formed.

Due to the amphipathic nature of antimicrobial peptides, their net influence is a combination of one or more of the former phenomena. This includes electrostatic stabilization of the headgroups, disturbance of the bilayer hydrophobic core, peptide/lipid complex formation, lipid segregation, inducing membrane curvature, and possible membrane solubilization (Lohner and Prenner 1999). Nonetheless, the binding of some peptides may not alter the chain packing and transition of anionic membranes (Hunter et al. 2005). Again, the observed effect depends on the lipid properties (e.g. fluidity, headgroup, and acyl chain length) as well as on the peptide properties (e.g. size, secondary structure, and hydrophobic/polar ratio). Moreover, the peptide concentration (or lipid/peptide ratio) and the hydrophobic match/mismatch between the membrane and the peptide molecules play also a crucial role and can control the mode of action of the peptide (Ivanova et al. 2003; Jing et al. 2005; Liu et al. 2002; Lohner and Prenner 1999; Sevcsik et al. 2007).

In comparison to the other KLA peptides, the peptide with the highest helicity $k_{1,12}$ -KLAL showed a strong electrostatic interaction with DPPG vesicles, as it stabilized the DPPG bilayer and induced domains, particularly at high L/P ratios. The increase in T_m could be due to the neutralization of the PG headgroup by the cationic peptide, which reduced the repulsion between the headgroups and stabilized the bilayer (Abuja et al. 2004; Andrushchenko et al. 2007; Schwieger and Blume 2007). The splitting of the transition peak of DPPG was most probably due to the formation of peptide-poor domains ($T \leq T_m$) and peptide-rich domains (T

> T_m) (Abuja et al. 2004; Jing et al. 2005; Lohner and Prenner 1999; Seto et al. 2007). The stabilization of saturated PG membranes and the domain formation were also observed with other cationic ligands, e.g. the polyamines spermine and spermidine (Arouri 2004) as well as poly(L-lysines) (Schwieger and Blume 2007).

KLA1 and more considerably l_{11},k_{12} -KLAL and $k_{9,a_{10}}$ -KLAL destabilized the DPPG bilayer decreasing T_m at high L/P ratio of 200, and the transition enthalpy and cooperativity upon increasing the peptide content (L/P of 40 and 20). The down-shift in T_m and the reduction in the transition enthalpy and cooperativity are common phenomena with antimicrobial peptides. This behaviour is primarily due to the deep burial of the peptide hydrophobic moieties into the bilayer core and to the consequent perturbation of the acyl chain packing (Abrunhosa et al. 2005; Adao et al. 2008; Andrushchenko et al. 2007; Prenner et al. 1999; Seto et al. 2007; Thennarasu et al. 2005). Additionally, it can be due to a peptide-induced fluidization of the gel-state lipids in the vicinity of the peptides and defects (Oliynyk et al. 2008; Oliynyk et al. 2007) as well as to membrane thinning and increasing local membrane curvature (Abrunhosa et al. 2005; Adao et al. 2008; Hallock et al. 2003; Powers et al. 2005; Willumeit et al. 2005). The effect of the peptides was enhanced after the first heating scan. Therefore, we propose that heating up the complex through the lipid phase transition enhanced the peptide-lipid interaction and maximized the peptide burial into the membrane and the consequent perturbations of the lipid chain packing.

At L/P of 10 and after the first heating scan, KLA peptides entirely abolished the main transition of DPPG leaving a very broad small transition centred $\sim 43 - 45^\circ\text{C}$. Similar peaks at elevated temperatures were also observed in clavanin A-DPPC mixtures and correlated with the formation of microdomain (suprastructures) in which the peptide aggregates confined the lipid molecules in the gel state (van Kan et al. 2003). The disappearance of the main transition peak was most probably due to the massive perturbations of the membrane at high peptide concentrations. In addition, and as shown by the DLS experiments (see above), some KLA peptides might have partially solubilised the lipid vesicles. The detergent-like action was observed also with other antimicrobial peptides, where discoidal peptide-lipid aggregates were formed (Atkinson and Small 1986; Dufourcq et al. 1986; Lohner and Prenner 1999; Lohner et al. 1999; Sevcsik et al. 2007).

As discussed before (see above), KLA1 and k_{1,l_2} -KLAL formed α -helices in DPPG suspension at the studied L/P range (200 to 10) in the DSC experiments. However, both peptides showed an irreversible α -helix to β -sheet transformation upon heating them to high temperatures. $k_{9,a_{10}}$ -KLAL and l_{11},k_{12} -KLAL were mainly helical at L/P of 200, whereas they

adopted β -structures at lower L/P ratios (40 to 10). This indicates that after the first heating scan, and particularly at L/P of 40 to 10, all KLA peptides are β -structures. However, further experiments are required to determine if there are structural differences between the β -structured KLA peptides.

It appears as if the KLA peptides with the high helical propensity were much less perturbing than the peptides with the low helical propensity and the β -structured peptides, which obviously were buried deeper in the membrane as they substantially reduced the transition enthalpy.

The passive translocation of cationic peptides across highly negatively charged membranes is not common, yet, this capacity has been reported for some peptides like penetratin (Binder and Lindblom 2003), which adopts a hairpin conformation (Binder and Lindblom 2004). To clarify whether KLA1 peptide can cross the DPPG bilayer we carried out comparative experiments between normal premixed samples, where KLA1 was added to the already formed vesicles, and preloaded vesicles that were formed after adding the peptide. During the phase transition, the lipid vesicles become leaky and this allows the redistribution of the peptide and its entry to the interior of the vesicles. If the peptide cannot enter the vesicles and the vesicles remain intact, the former preparation (premixed) should have the peptide in the bulk interacting merely with outer leaflet and the latter (preloaded) should have the peptide on both sides interacting with the entire lipid in the system.

As one observes from **Figure 4.2-15**, the premixed vesicles were more perturbed by the peptide than the preloaded vesicles. The first and second DSC heating scans of the preloaded vesicles were almost identical. However, the second heating scan of the premixed vesicles was considerably different from the first heating scan, which could point out to some limited translocation of the KLA1 peptide across the DPPG bilayer during the phase transition. In both mixtures, the subsequent heating scans were similar to the second one (data not shown). The second and subsequent heating scans of the premixed vesicles did not resemble or come closer to that of the preloaded vesicles. Due to the significant differences between the DSC curves of both mixtures, we conclude that KLA1 peptide cannot freely penetrate DPPG vesicles. The local peptide concentration in premixed vesicles (L/P was ~ 10 on the outer leaflet, as the peptide did not penetrate the DPPG vesicles) was almost twice as high as that in preloaded vesicles (L/P is 20), hence, the premixed vesicles were much more perturbed by the peptide. Therefore, we firmly emphasize the importance of the local peptide concentration in determining the peptide mode of action.

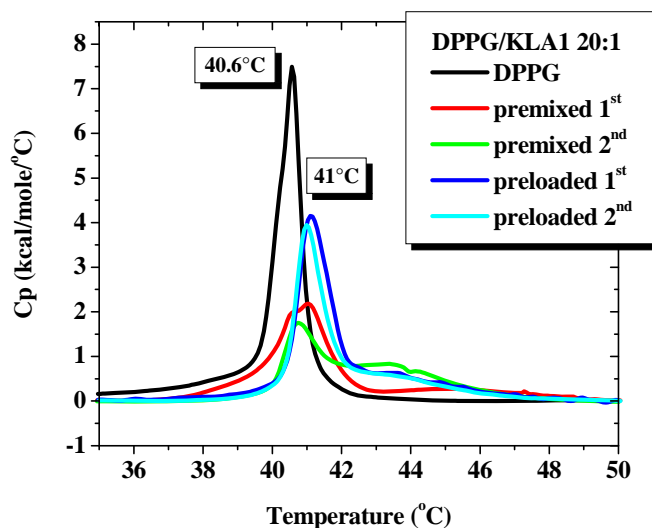


Figure 4.2-15 First and second heating DSC curves of a premixed and a preloaded DPPG/KLA1 (2 mM/100 μ M) 20:1 mixture. The samples were prepared in buffer (10 mM Tris, 154 mM NaCl, pH 7.4).

4.2.9 Fourier Transform Infrared (FT-IR)

For interactions of peptides with lipids, FT-IR provides invaluable insights into the interaction at the molecular and submolecular levels. This includes the secondary structure adopted by the peptide and the peptide-induced changes in the acyl chain packing, the thermotropic transitions, and the hydration state and hydrogen bonding of the carbonyl and phosphate groups of the lipid (Mantsch and McElhaney 1991; Tamm and Tatulian 1997). The peptide and lipid samples used in techniques like DSC and CD spectroscopy are prepared in excess water, whereas, in FT-IR experiments the samples are applied as a concentrated suspension. The complementary and consistent nature of the information provided with DSC and FT-IR techniques was demonstrated many times in literature (e.g. (Brauner and Mendelsohn 1986)). The comparison between the obtained results is of great importance to inspect the influence of the preparation procedure, lipid form, and peptide concentration regime on the behaviour of lipids and peptides.

We studied the interaction of KLA peptides with perdeuterated DPPG (DPPG- d_{62}) multilamellar bilayers. We used perdeuterated DPPG instead of normal DPPG since we also performed experiments with DPPG- d_{62} -containing mixed membranes, and this helped us to monitor, separately, the two lipid components in mixed membranes. However, the results of the mixed membranes will not be discussed here.

Figure 4.2-16 illustrates the amide I bands of 10 mM KLA1 in D_2O and their second derivative through the heating phase from 20 to 76°C and the subsequent cooling phase back

to 20°C. The amide I bands at 1611 and 1682 cm^{-1} show that KLA1 assumed antiparallel β -sheets in Tris buffer (Tamm and Tatulian 1997). In fact, the amide I at this very low wavenumber proposes peptide aggregates rather than normal β -structures (Tamm and Tatulian 1997; Zandomeneghi et al. 2004). The broad amide I band centred $\sim 1644 \text{ cm}^{-1}$ could be related to the unordered deuterated KLA1 peptide, However, contributions from a helical KLA1 structure as well as from the bending modes (δ) of H_2O , which could not be totally eliminated by the H/D exchange, cannot be ruled out (Tamm and Tatulian 1997).

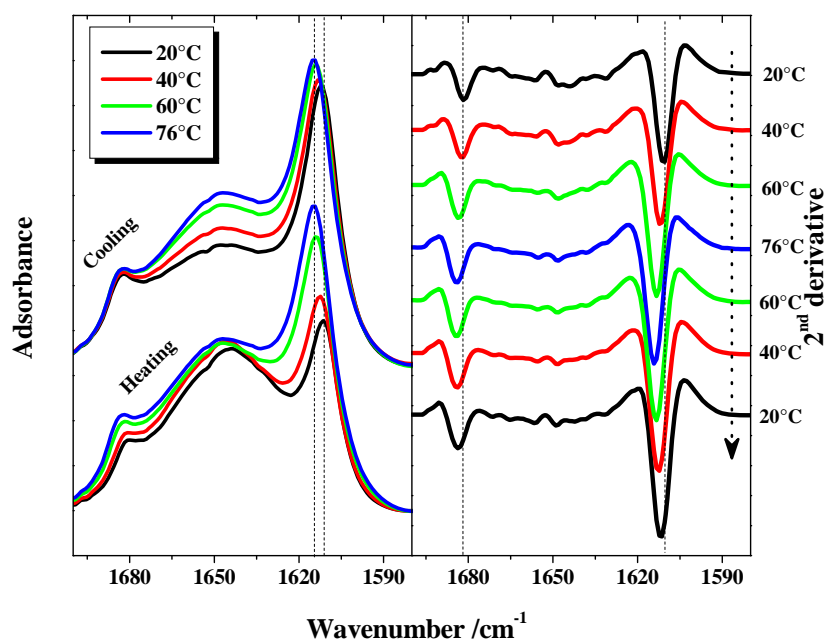


Figure 4.2-16 Amide I vibrational band (left) and its second derivative (right) of 10 mM KLA1 in D_2O (100 mM NaCl) at various temperatures through the heating phase from 20°C to 76°C and the cooling back to 20°C.

Heating the peptide from 20 to 76°C caused a gradual increase in the intensity of the amide I bands at 1611 and 1682 cm^{-1} together with their up-shift to 1614 and 1684 cm^{-1} , respectively. This increase in the intensity could indicate a thermal-induced β -sheet formation/aggregation of the peptide, a phenomenon that agrees with our CD experiments. The band at $\sim 1644 \text{ cm}^{-1}$ was shifted to $\sim 1647 \text{ cm}^{-1}$, which could suggest some structural changes induced by increasing temperature. The position of the peaks was only partially recovery by cooling back the peptide from 76 to 20°C.

A similar experiment was performed with DPPG- d_{62} /KLA1 6:1 mixture and the obtained amide I bands and their second derivative are shown in **Figure 4.2-17**. As a result of the interaction with DPPG- d_{62} and as clarified with the second derivative curves, KLA1

showed the coexistence of two populations of antiparallel β -sheet structures exhibited by the amide I bands at 1611 and 1681 cm^{-1} as well as at 1621 and 1692 cm^{-1} , respectively. A similar observation was reported in literature elsewhere (Dieudonne et al. 1998). Upon heating the peptide, the intensity ratio of the two bands changed, namely in favour of the band at 1621 cm^{-1} , and recovered with cooling down the sample, nonetheless, the position of the peaks remained unaltered. We anticipate that the peak at 1611 cm^{-1} represents the free KLA1 and the one at 1621 cm^{-1} belongs to the DPPG- d_{62} -bound peptide. We also anticipate that increasing temperature above T_m , which fluidized the membrane, increased the fraction of the bound peptide, whereas cooling the sample caused the peptide to be squeezed out from the membrane. This assumption agrees well with the domain formation observed from the CD_2 stretching modes of DPPG- d_{62} (discussed later). A similar phenomenon was reported for other antimicrobial peptides (Lewis et al. 2003; Lewis et al. 1999).

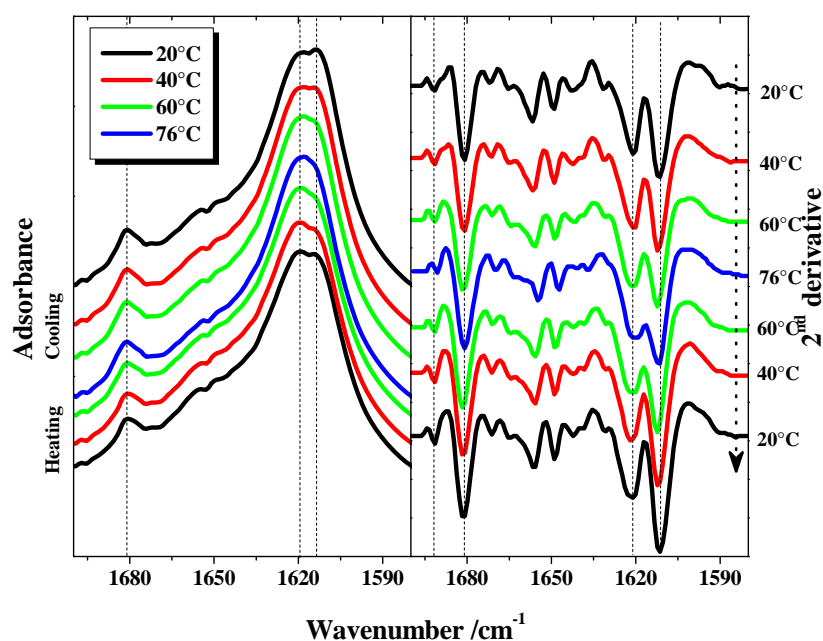


Figure 4.2-17 Amide I vibrational band (left) and its second derivative (right) of 10 mM KLA1 premixed with 60 mM DPPG- d_{62} ($L/P = 6$) in D_2O (100 mM NaCl) at various temperatures through the heating phase from 20°C to 76°C and the cooling back to 20°C.

In H_2O and using 10 mM peptide, all KLA peptides (KLA1, $k_{9,a10}$ -KLAL, $k_{1,l2}$ -KLAL, $l_{11,k12}$ -KLAL) adopted comparable antiparallel β -sheets as revealed by the amide I bands at 1615 - 1625 cm^{-1} and at $\sim 1692 \text{ cm}^{-1}$. Due to the masking bending modes (δ) of H_2O , no well-resolved peaks could be obtained and, therefore, we refrained from any further analysis of those amide I bands.

The CH₂ antisymmetric and symmetric stretching modes ($\nu_{\text{as}}(\text{CH}_2)$ at $\sim 2929 \text{ cm}^{-1}$ and $\nu_{\text{s}}(\text{CH}_2)$ at $\sim 2850 \text{ cm}^{-1}$, respectively) reflect the conformational state of the lipid acyl chains. Therefore, the $\nu(\text{CH}_2)$ is commonly used as a potent indicator for the lipid chain packing, however, qualitatively (Mendelsohn and Flach 2002), whereas its temperature dependence serves as to a tool to follow the *trans/gauche* ratio and to determine the phase transition temperature. The transition temperature determined with DSC and IR should be consistent (Brauner and Mendelsohn 1986). At low temperature in the gel phase, the acyl chains adopt an all-*trans* conformation. At the phase transition to L _{α} , the melting of the acyl chains leads to the progressive formation of the *gauche* conformers that is accompanied by the increase in $\nu(\text{CH}_2)$ vibrational frequencies. The phase transition of deuterated lipids takes place at lower temperatures than the “undeuterated” lipids. Due to the vibrational isotope effects the corresponding $\nu_{\text{as}}(\text{CD}_2)$ and $\nu_{\text{s}}(\text{CD}_2)$ are found at lower wavenumbers, namely at ~ 2195 and $\sim 2090 \text{ cm}^{-1}$, respectively (Mantsch and McElhaney 1991; Schwieger and Blume 2007; Tamm and Tatulian 1997; Tuchtenhagen et al. 1994).

The temperature dependence of $\nu_{\text{as}}(\text{CD}_2)$ of DPPG-d₆₂ before and after adding KLA peptides is displayed in **Figure 4.2-18**. The main phase transition temperature (T_m) of DPPG-d₆₂ was $\sim 37^\circ\text{C}$. KLA peptides strongly stabilized DPPG-d₆₂ bilayer and increased its T_m . The membrane stabilization was a consequence of the electrostatic binding of the cationic peptides to the anionic bilayer, which reduced the repulsion between the PG headgroups and maximized van der Waals interactions between the hydrocarbon chains. The peptides k_{9,a10}-KLAL, k_{1,l2}-KLAL and l_{11,k12}-KLAL increased T_m by 5, 6 and 7.5°C, respectively, whereas they barely altered the lipid chain packing. On the other hand, KLA1 induced the formation of two domains; a peptide-poor domain with $T_m \sim 38^\circ\text{C}$ and a peptide-enriched domain with $T_m \sim 67^\circ\text{C}$. Moreover, KLA1 noticeably reduced the CD₂ stretching vibrations to lower wavenumbers suggesting that the peptide binding enhanced the lipid chain packing in the membrane. Some structural differences might exist between the β -structured KAL peptides, which could be the reason for their different influence upon DPPG-d₆₂ bilayers. However, further investigations are required to confirm this notion.

The DSC thermograms demonstrated that the peptides at L/P of 10 highly disturbed the DPPG bilayer and induced a small broad transition at a temperature higher than T_m , which suggested some peptide-DPPG suprastructures. Interestingly, the IR spectra revealed only the electrostatic character of the interaction between KLA peptides and DPPG-d₆₂ which increased the transition temperature of the lipid membrane. This discrepancy between the observations obtained with DSC and FT-IR can be linked to the dissimilarities between both

techniques in the lipid form, peptide structure, preparation procedure, and particularly the used concentrations of the lipids and peptides.

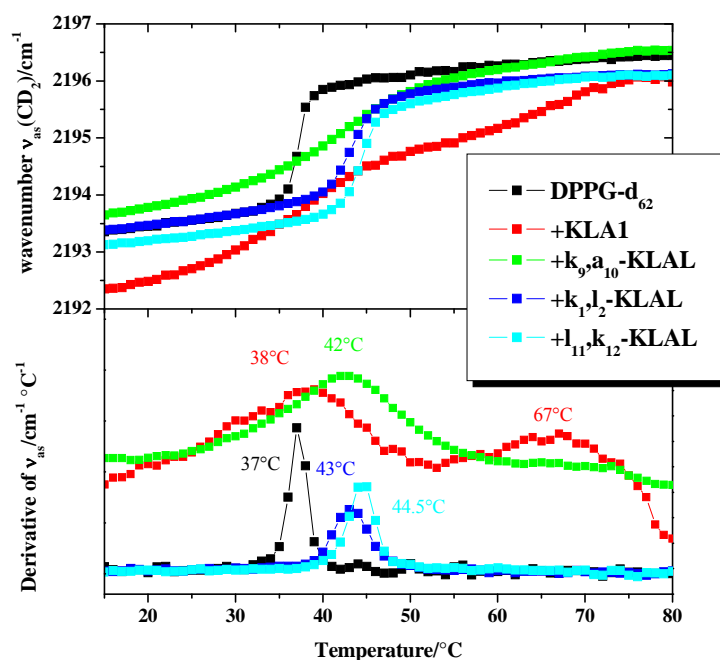


Figure 4.2-18 (Top) Temperature dependence of the wavenumber of the antisymmetric CD_2 -stretching band of 60 mM DPPG-d_{62} without and with 14.3 mol% KLA peptides ($L/P = 6$). The samples were prepared in H_2O (100 mM NaCl). **(Bottom)** First derivative of the curves shown in the top diagram.

The headgroup vibrations of phospholipids are represented in the IR spectra by the carbonyl band $\nu(\text{CO})$ at $\sim 1735 \text{ cm}^{-1}$ and the phosphate stretching modes, namely the antisymmetric $\nu_{\text{as}}(\text{PO}_2^-)$ at $\sim 1228 \text{ cm}^{-1}$ and the symmetric $\nu_{\text{s}}(\text{PO}_2^-)$ at $\sim 1085 \text{ cm}^{-1}$. The properties of those bands are highly sensitive to the hydration state of the membrane headgroup region as well as to the interaction/hydrogen bonding with the headgroup (Blume et al. 1988). The stretching modes of the phosphate group $\nu(\text{PO}_2^-)$ of DPPG-d_{62} were barely altered after the addition of KLA peptides.

Figure 4.2-19 displays the carbonyl band of free DPPG-d_{62} and of KLA1bound DPPG-d_{62} at various temperatures. The carbonyl band is essentially a superposition of two underlying bands separated by $\sim 15 \text{ cm}^{-1}$, which represent the hydrated and non-hydrated carbonyl groups in the lipid membrane (Blume et al. 1988).

To get further insights, we resolved the different carbonyl bands into their components, whose exact position and fraction is shown in **Figure 4.2-19**. To fit the curves, the Gaussians function was applied and the peak positions reported by Blume et al. (1988)

were used as a starting point. The peaks at ~ 1741 and ~ 1729 cm^{-1} of free DPPG-d₆₂ belonged to the non-hydrated and hydrated carbonyl groups, respectively.

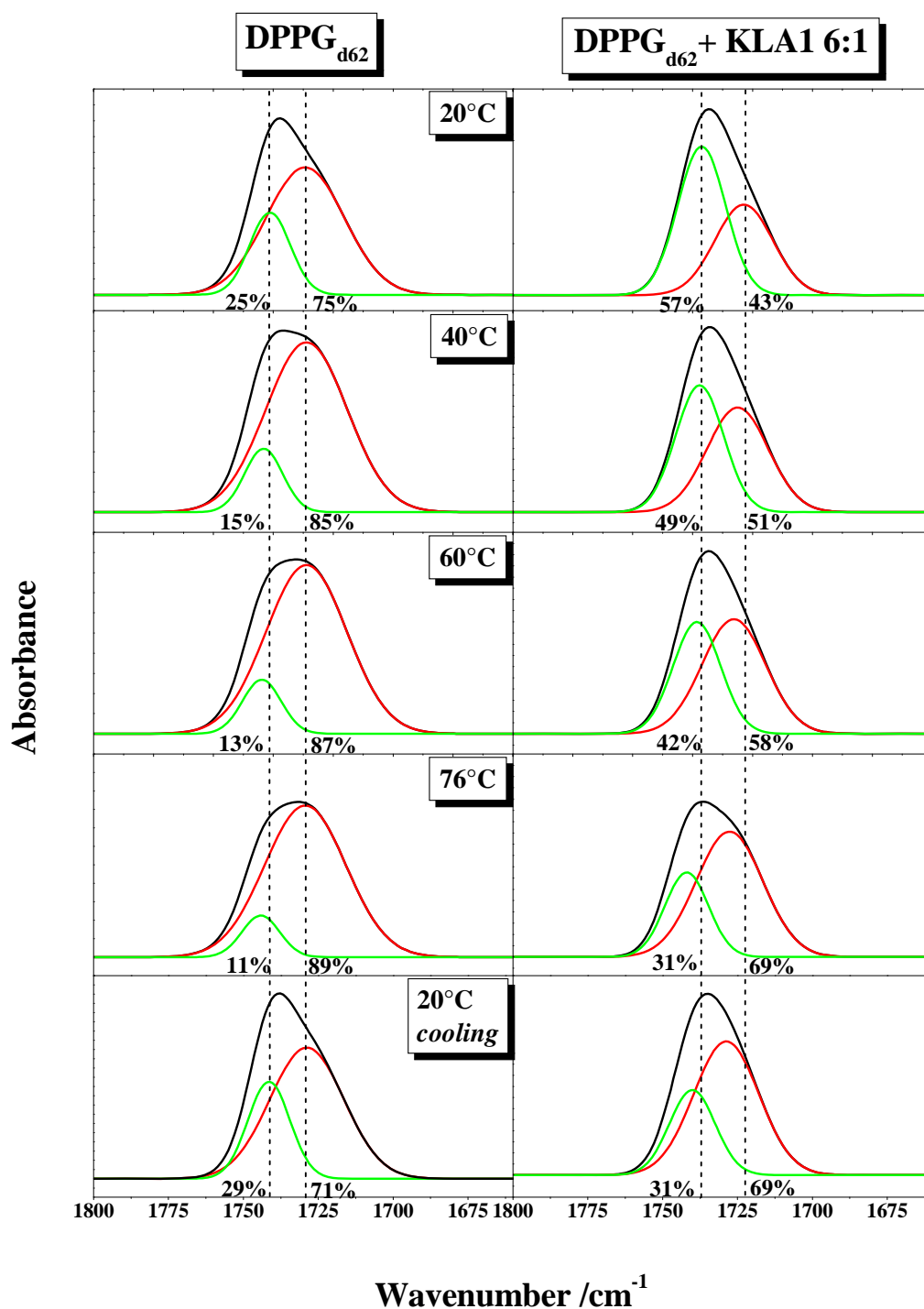


Figure 4.2-19 Carbonyl stretching vibrational bands ($\nu(\text{CO})$) of 60 mM DPPG-d₆₂ (left) and of 60 mM/ 10 mM DPPG-d₆₂/KLA1 (L/P 6:1) complex (right) in D₂O (100 mM NaCl) through the heating phase from 20 and 76°C and the cooling back to 20°C. The experimental bands (black lines) were resolved into two Gaussians representing the hydrated (red lines) and the non-hydrated states (green lines). The relative integral of each peak is shown underneath it as a percentage, whereas the original peaks positions are illustrated with dotted lines.

At 20°C, 75% of the carbonyl groups in DPPG-d₆₂ were hydrated. Heating the DPPG-d₆₂ sample through the L_β to L_α transition ~ 37°C enhanced the hydration state of the headgroups from 75% at 20°C to 85% at 40°C and reached 89% at 76°C. This increase in the hydration state of the headgroup region is due to the increase in the molecular area of the phospholipids, which takes place during the phase transition and allows more water to interact with the carbonyl groups (Blume et al. 1988). The original hydration state was almost entirely recovered after the cooling back from 76 to 20°C.

The interaction of KLA1 with DPPG-d₆₂ (L/P = 6) at 20°C pronouncedly reduced the hydration of the lipid headgroup from 75% to 43%. The bands representing the non-hydrated and hydrated carbonyl groups were down-shifted to ~ 1737 and ~ 1723 cm⁻¹, respectively. The reduced hydration state could be interpreted by the release of water molecules from the bilayer surface upon the peptide binding. This is in agreement with our ITC experiments, which showed that the interaction of KLA peptides with lipid vesicles was mostly entropy driven due to the release of water molecules (see below). On the other side, the down-shift of both carbonyl bands was most probably due to the hydrogen bonding between KLA1 and the carbonyl groups.

As shown in **Figure 4.2-18**, the DPPG-d₆₂/KLA1 complex underwent two broad transitions at ~ 38 and ~ 67°C. This explains the gradual increase in the hydration state of the carbonyl groups in the complex from 43% at 20°C to 69% at 76°C, whereas the increase in the hydration state of the headgroup of free DPPG-d₆₂ occurred mainly at the lipid phase transition, i.e. at 37°C.

The simulation indicates that cooling the complex from 76 to 20°C did not alter the hydration state of the DPPG-d₆₂ headgroups that remained at 69%. However, the shape of the original carbonyl band (black curve) of the complex after the cooling to 20°C resembled more the initial bands at lower temperatures. This would indicate that the initial hydration state of the complex was recovered after the cooling to 20°C. This shows that the model we used to fit the carbonyl bands has limitations.

4.2.10 Isothermal Titration Calorimetry (ITC)

Isothermal titration calorimetry has been intensively used to get insights into the thermodynamics of the interactions between membrane-active peptides and lipid membranes. In addition to quantifying the binding/adsorption/partitioning parameters, ITC is appropriate to separately observe other co-occurring secondary processes, for e.g. the conformational changes of the peptides (Wieprecht et al. 1999a, 2000a; Wieprecht et al. 2002) and peptide-

induced pore formation (Wenk and Seelig 1998; Wieprecht et al. 2000b). ITC can be also used to follow the translocation across the lipid membrane (Binder and Lindblom 2003; Tsamaloukas et al. 2007) and membrane solubilization by peptides (Heerklotz and Seelig 2007) as well as by detergents (Garidel et al. 2007; Heerklotz and Seelig 2000; Hildebrand et al. 2004; Hildebrand et al. 2002; Keller et al. 2006).

We carried out calorimetric titrations to characterize the interaction of KLA peptides with various lipid vesicles. Additionally, we were interested to elucidate the influence of the lipid fluidity, temperature, salt concentration, and surface charge density on the binding profiles of the peptides. The titration curves were analyzed using the “one-binding-site” model provided by ORIGIN[®] software in order to determine the apparent binding constant (K_{app}), the binding enthalpy (ΔH°) and the lipid/peptide binding stoichiometry (N). The standard free energy (ΔG°) and entropy (ΔS°) of the binding were calculated using the standard equations $\Delta G^\circ = -RT \ln K_{app}$ and $\Delta S^\circ = (\Delta H^\circ - \Delta G^\circ)/T$, respectively. In this model, and when titrating lipid vesicles to peptides, the lipid molecules are treated as ligands and the peptide is assumed to have n number of independent and equivalent binding sites.

The surface partitioning model is also commonly used to analyze the titration data and to derive the intrinsic binding factors (Schote et al. 2002). For interactions of charged peptides with charged/uncharged lipid membranes, the Gouy-Chapman theory is employed to correct the enhanced/reduced surface concentration of the peptide in comparison to the bulk concentration (Breukink et al. 2000; Bringezu et al. 2007b; Seelig 2004; Wen et al. 2007; Wieprecht et al. 2002; Wieprecht and Seelig 2002). However, due to the substantial amounts of salt and buffer present in the solution that screen the surface charge of the interacting molecules, the influence of the electrostatic attraction/repulsion is minimized so that corrections due to their effects are small (Cevc 1990; Langner and Kubica 1999). Our main goal is to describe the ITC curves numerically for comparison purposes without the over-interpretation of the obtained values. Due to the complexity of our system, it is practically impossible to resolve the different sub-processes (e.g. binding, partitioning, conformational changes, pore formation, vesicles micellization, aggregation ...), which could take place concurrently during the titration. Therefore, we believe that the use of the one-binding-site model, which indeed describes our ITC curves fairly well, to determine the apparent thermodynamic properties of the whole interaction process is sufficient. The one-binding-site model was also adequate to describe the binding isotherms in similar systems (Abraham et al. 2005a, b; Andrushchenko et al. 2008; Goncalves et al. 2005; Zhang and Rowe 1994).

The experiments presented below were performed by the titration of the lipid vesicles (typically 500 μM) into the peptide solution (typically 5 - 10 μM) in the reaction cell. The dilution enthalpy of 100 nm extruded lipid vesicles into 10 mM Tris buffer (154 mM NaCl, pH 7.4) was 250 – 350 cal mol⁻¹ at 15°C. According to the CD experiments discussed above and since the ITC experiments were carried out at relatively low temperatures (5 – 35°C) and using low peptide concentrations in the cell, it was expected that the KLA peptides would undergo a random-coil to α -helix transformation upon binding to lipid vesicles. It was also expected that at the beginning of the titration (low L/P ratio) the peptides with the high helical propensity, i.e. KLA1 and k_{1,l2}-KLAL, would stay helical, whereas the peptides with the lower helical propensity, i.e. l_{11,k12}-KLAL and k_{9,a10}-KLAL, might form β -structures or aggregates.

4.2.10.1 Interactions of KLA peptides with DPPG LUV

The binding isotherms of the four peptides to DPPG extruded LUV (100 nm diameter) are illustrated in **Figure 4.2-20** and the thermodynamic parameters are summarized in **Table 4.2-4**. The interactions were entropy driven, with favourable positive $T\Delta S^\circ$, compensated by a moderate endothermic contribution with unfavourable positive ΔH° . Studies of similar systems in literature revealed mostly entropy driven interactions (Abraham et al. 2005a; Andrushchenko et al. 2008; Bringezu et al. 2007b; Seelig 2004; Wen et al. 2007). However, enthalpy driven interactions were also encountered (Wieprecht et al. 2000b). The affinity of KLA peptides correlated with their helical propensity (k_{1,l2}-KLAL > KLA1 > k_{9,a10}-KLAL \geq l_{11,k12}-KLAL, see **Table 4.1-2**), whereas the decrease in K_{app} was almost entirely of entropic origin. As shown in **Table 4.2-4**, reducing the peptide helicity from 74 to 47% led to a decrease in K_{app} towards DPPG of around one order of magnitude (at 15°C and 154 mM NaCl). For the peptides k_{1,l2}-KLAL, KLA1 and l_{11,k12}-KLAL, the favourable $T\Delta S^\circ$ decreased with the helicity while the endothermic ΔH° increased. k_{9,a10}-KLAL showed the lowest K_{app} , ΔH° and $T\Delta S^\circ$ values among all KLA peptides.

For peptide-lipid interactions, it was found that 30 to 60% of ΔG° comes from the exothermic membrane-induced conformational changes of peptides, e.g. from random coil to α -helix (Bhunia et al. 2007; Wieprecht et al. 1999a, 2000a, b; Wieprecht et al. 2002). Therefore, the enhanced helicity increases the exothermic contribution and improves the peptide affinity to the membrane. Besides, a better binding to the lipid membrane is

associated with the release of more water molecules which increases the favourable entropic part. It is expected that this phenomenon would also apply for KLA peptides, however, their interactions with DPPG bilayers are associated with substantial endothermic events.

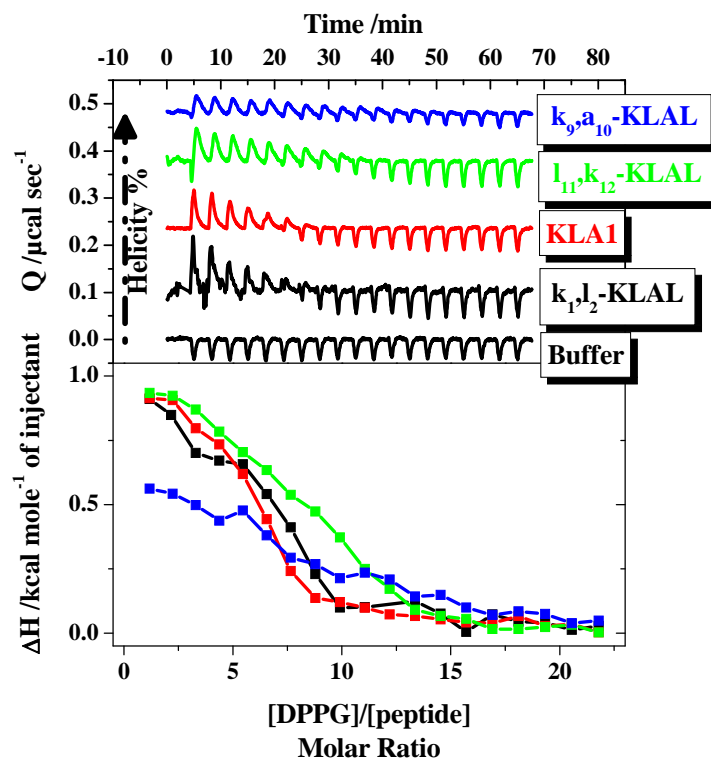


Figure 4.2-20 The experimental power signals (top) and the integrated peaks as a function of DPPG/peptide ratio (bottom) of the titration of DPPG LUV (500 μM) in the syringe into KLA peptides (5 μM) and buffer in the reaction cell at 15°C. The samples were prepared in buffer (10 mM Tris, 154 mM NaCl, pH 7.4).

Driving forces for binding can be hydrogen bonding and electrostatic, hydrophobic and van der Waals forces. However, it is difficult to disentangle the separate contributions to the thermodynamics of binding processes. The binding processes of our peptides are moderately endothermic and mainly driven by a large entropy gain. The differences in the thermodynamic profiles of the peptides may come principally from their varying helical propensity, since their sequence and other properties are comparable. The entropic part is due to the increase in the rotational and translational degrees of freedom of water molecules upon the desolvation of the hydrophobic residues of the interacting molecules. Such behaviour is explained in literature by the classical hydrophobic effects (White and Wimley 1998).

Table 4.2-4 The thermodynamic parameters of the interaction of KLA peptides with lipid vesicles at different conditions. The helicity of the peptides is as following: k_{1,12}-KLAL 74%, KLA1 54%, l_{11,k12}-KLAL 47%, and k_{9,a10}-KLAL 48%. The helicity was determined in POPG SUV suspension using 10 μM peptide (see Table 4.1-2).

Peptide	Lipid	[NaCl] (mM)	T (°C)	N	K _{app} x10 ⁻⁵ (M ⁻¹)	ΔH° (kcal mol ⁻¹)	TΔS° (kcal mol ⁻¹)	ΔG° (kcal mol ⁻¹)
k _{1,12} -KLAL	DPPG	154	15	7.6 ± 0.1	11.6 ± 2.3	0.81 ± 0.02	8.80 ± 0.09	-7.99 ± 0.10
KLA1*	DPPG	154	15	6.4 ± 0.1	8.8 ± 1.6	0.91 ± 0.02	8.75 ± 0.07	-7.84 ± 0.10
l _{11,k12} -KLAL	DPPG	154	15	8.5 ± 0.2	3.6 ± 0.6	0.97 ± 0.03	8.28 ± 0.06	-7.31 ± 0.09
k _{9,a10} -KLAL	DPPG	154	15	9.1 ± 0.5	2.6 ± 0.4	0.78 ± 0.07	7.91 ± 0.04	-7.13 ± 0.09
k _{1,12} -KLAL	DPPG/DPPC 3:1	154	15	16.6 (12.5) ± 0.3	6.3 ± 2.1	0.81 ± 0.02	8.45 ± 0.14	-7.64 ± 0.16
KLA1	DPPG/DPPC 3:1	154	15	11.4 (8.6) ± 0.1	5.7 ± 0.8	0.58 ± 0.01	8.16 ± 0.06	-7.59 ± 0.07
l_{11,k12}-KLAL	DPPG/DPPC 3:1	154	15	15.3 (11.5) ± 1.0	1.0 ± 0.5	1.03 ± 0.09	7.61 ± 0.15	-6.58 ± 0.25
k _{9,a10} -KLAL	DPPG/DPPC 3:1	154	15	14.6 (11.0) ± 0.5	2.5 ± 1.0	0.51 ± 0.02	7.63 ± 0.16	-7.12 ± 0.18
k _{1,12} -KLAL	DPPG/DPPE 3:1	154	15	10.3 (7.7) ± 0.2	7.4 ± 2.6	1.16 ± 0.04	8.89 ± 0.14	-7.73 ± 0.17
KLA1	DPPG/DPPE 3:1	154	15	9.0 (6.8) ± 0.3	5.3 ± 1.4	0.66 ± 0.03	8.20 ± 0.11	-7.54 ± 0.14
k_{9,a10}-KLAL	DPPG/DPPE 3:1	154	15	12.9 (9.7) ± 0.9	3.5 ± 2.5	0.47 ± 0.05	7.77 ± 0.27	-7.30 ± 0.31
KLA1	DPPG	154	5	11.7 ± 0.3	3.9 ± 1.0	0.66 ± 0.02	7.77 ± 0.10	-7.11 ± 0.13
KLA1	DPPG	154	10	9.6 ± 0.1	9.9 ± 1.6	0.84 ± 0.01	8.60 ± 0.07	-7.76 ± 0.08
KLA1*	DPPG	154	15	6.4 ± 0.1	8.8 ± 1.6	0.91 ± 0.02	8.75 ± 0.07	-7.84 ± 0.10
KLA1	DPPG	154	20	5.6 ± 0.1	6.3 ± 0.8	1.02 ± 0.02	8.79 ± 0.05	-7.77 ± 0.07
KLA1	DPPG	154	25	3.1 ± 0.1	2.9 ± 0.5	1.74 ± 0.10	9.18 ± 0.01	-7.44 ± 0.09
KLA1	DPPG	154	30	3.2 ± 1.1	6.3 ± 12.0	1.17 ± 0.50	9.22 ± 0.14	-8.04 ± 0.64
KLA1	DPPG	154	35	3.5 ± 0.4	37.1 ± 60.0	4.81 ± 0.70	14.07 ± 0.11	-9.26 ± 0.59
KLA1*	DPPG	154	15	6.4 ± 0.1	8.8 ± 1.6	0.91 ± 0.02	8.75 ± 0.07	-7.84 ± 0.10
KLA1	DPPG	300	15	8.8 ± 0.3	2.8 ± 0.6	0.58 ± 0.02	7.76 ± 0.09	-7.18 ± 0.11
KLA1	DPPG	500	15	5.5 ± 0.5	1.7 ± 0.7	0.37 ± 0.05	7.27 ± 0.14	-6.90 ± 0.18
KLA1	POPG	154	5	4.0 ± 0.1	36.0 ± 21.0	2.71 ± 0.13	11.05 ± 0.13	-8.34 ± 0.25
KLA1	POPG	154	15	4.2 ± 0.1	88.1 ± 100.0	1.71 ± 0.09	10.87 ± 0.34	-9.15 ± 0.43
KLA1^a	POPG	154	25	3.3 ± 0.2	20.5 ± 0.0	0.96 ± 0.07	9.57 ± 0.07	-8.61 ± 0.00
KLA1	POPG	154	50	-	-	-0.97	-	-

* Rows were repeated to ease comparison. (N) Shows N per DPPG molecules. ^aThe K_{app} was fixed to allow a better determination of the other parameters. The values in the rows marked bold are inaccurate due to low reaction enthalpy or poor curve fitting of the corresponding ITC isotherms.

Resolving the underlying enthalpy-associated events that take place during the titration is difficult, since what is measured is the net enthalpy change of all the exothermic and endothermic processes. Besides the noncovalent bonding and membrane partitioning (Hoyrup et al. 2001), the helical structuring of KLA1 peptides is an exothermic major driving force for the interaction (Bhunja et al. 2007; Wieprecht et al. 1999a, 2000a, b; Wieprecht et al. 2002). However, the possible formation of β -structures (see CD and IR spectra) can also increase the exothermic contribution. The profound membrane perturbation by the insertion of the peptides, which was seen with DSC, is endothermic since work must be applied to separate the lipid molecules. Therefore, the thermodynamic profile of the interaction with lipid membranes is sensitive to the hydrocarbon chain packing, i.e. the interaction with well packed lipid bilayers is associated with a higher endothermic ΔH° (Seelig 2004; Wieprecht et al. 2000a; Wieprecht et al. 2000c; Wieprecht et al. 2002). Moreover, the peptide induced lipid phase transition (see DSC experiments), which would be endothermic, have a substantial contribution (Wieprecht and Seelig 2002). Processes including vesicles aggregation and solubilization (Garidel et al. 2007), which we observed with the DLS titrations, as well as possible peptide translocation across the bilayer (Binder and Lindblom 2003; Heerklotz and Seelig 2007) can also participate to the net ΔH° .

In conclusion, the endothermic nature of the binding processes of KLA peptides to DPPG vesicles is, most probably, mainly due the considerable distortion of the lipid chain packing and the deep burial of the peptides in the lipid membrane, an assumption which strongly concurs with our DSC experiments. This is in addition to the endothermic peptide induced phase transition in DPPG bilayers (discussed later) as well as to the desolvation energy, which is evident by the high favourable entropy.

The stoichiometry of the binding (N) between DPPG and the peptides, obtained from the employed fit, can be used to estimate the extent of the molecular interactions, the integrity of the lipid vesicles and the ability of the peptides to penetrate the lipid vesicles. In contrast to highly curved SUV, where the outer leaflet contains 60% of the lipid molecules, the lipids in LUV are equally distributed in both leaflets. Our peptides have a nominal charge of $\sim +6$ due to 5 Lys residues and an uncapped N-terminus that is partially charged at neutral pH, whereas the C-terminus was amidated. Although the effective charge could be lower than the nominal charged as reported for some other peptides (Binder and Lindblom 2003; Goncalves et al. 2005; Wen et al. 2007), our stoichiometry values supported our assumption that the effective charge of KLA peptides is close the nominal one.

Since the interaction with DPPG is electrostatically driven, a DPPG/peptide stoichiometry of 12 would indicate that the peptide binds exclusively to the outer leaflet of the lipid vesicles. On the other hand, a DPPG/peptide stoichiometry of 6 would indicate that the peptides can cross the lipid bilayer and interact with the inner leaflet of the vesicles as well. Those two ideal cases were observed in ITC experiments performed to study the electrostatic interaction between short polyamines and anionic lipids ((Arouri 2004) and unpublished results). However, due to the complex nature of interactions with peptides, the stoichiometry can still vary depending on the experimental conditions, such as charge screening, steric hindrance, multilamellar vesicles, membrane fluidity and integrity, and the formation of lipid-peptide suprastructures.

The stoichiometry values are shown in **Table 4.2-4**. Interestingly, at 15°C the stoichiometry of the peptides with the higher helical propensity (KLA1 and k_{1,l_2} -KLAL) is ~ 7 , which is close to the required N for the full coverage of both leaflets, i.e. 6. This indicates the ability of the two peptides to efficiently penetrate DPPG vesicles in the gel phase. On the other hand, the permeabilization power of $k_{9,a_{10}}$ -KLAL and $l_{11,k_{12}}$ -KLAL is substantially lower as exhibited by their higher N (~ 9). The stoichiometry values of interactions with lipid vesicles, particularly of antimicrobial peptides, are not strictly reproducible as in the case of proteins (Arouri et al. 2007). Therefore, the N values exhibited formerly are averages of broader stoichiometry ranges.

4.2.10.2 Interactions of KLA peptides with DPPG/DPPC and DPPG/DPPE mixed LUV

The influence of the surface charge density of lipid vesicles on the binding and on the thermodynamic profiles of KLA peptides was also inspected. Diluting the surface charge of DPPG bilayers was achieved via the mixing with the zwitterionic lipids DPPC and DPPE.

Figure 4.2-21 illustrates the ITC curves of the interaction of KLA1 with DPPG, DPPC, and DPPE as well as with the mixed membranes DPPG/DPPC and DPPG/DPPE with varying molar ratios. The binding affinity was highly dependent on the negative charge content of the bilayer. Reducing the DPPG fraction by 50% in both mixed systems almost abolished the binding enthalpy. This phenomenon has been repeatedly reported in literature (Wieprecht et al. 2000b).

The KLA peptides do interact modestly with uncharged lipids, as have been shown with other techniques and as reported in literature (Dathe et al. 1996; Dathe et al. 1997). However, the interactions were not detectable by ITC. This could be due to a weak binding or that the binding is associated with small ΔH° .

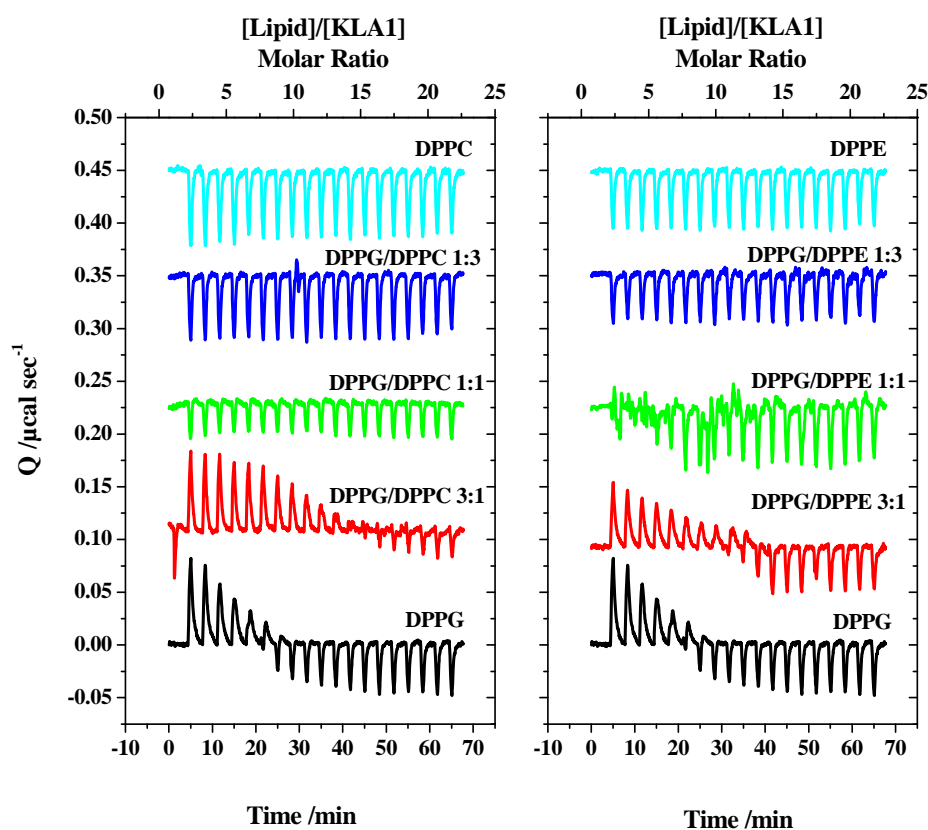


Figure 4.2-21 The experimental power signals of the binding of KLA1 (5 μM) to DPPG/DPPC (left) and DPPG/DPPE (right) LUV mixed vesicles (total lipid concentration 500 μM) as well as to the single components (500 μM) at 15°C. The samples were prepared in buffer (10 mM Tris, 154 mM NaCl, pH 7.4).

The thermodynamic profiles of the interactions with DPPG/DPPC 3:1 and DPPG/DPPE 3:1 mixed membranes are presented in **Table 4.2-4**. In principle and since the interaction of the peptides is of electrostatic origin, reducing the DPPG fraction should weaken the binding. However, the decrease in the surface charge density might give the peptide the opportunity to pack better on the vesicle surface (Schwieger and Blume 2007) and to sink deeper in the membrane (Wen et al. 2007). The binding affinities and energies obtained for DPPG/DPPC 3:1 and DPPG/DPPE 3:1 were comparable, however, slightly lower than DPPG. Again, the proportionality between the helical propensity and the binding affinity was also observed in both mixed systems.

The N values are listed in **Table 4.2-4** as ratios of total lipid/peptide and, in parenthesis, DPPG/peptide. In the case of DPPG/DPPC 3:1, the N for the peptides $k_{1,2}$ -KLAL, $k_{9,a_{10}}$ -KLAL and $l_{11,k_{12}}$ -KLAL as total lipid/peptide was ~ 16 (~ 12 as DPPG/peptide), indicating the full coverage and charge saturation of the outer leaflet of the lipid vesicles. However, KLA1, the peptide with a slightly lower hydrophobicity, showed a

lower N of ~ 11.4 (8.6), which indicates the ability of the peptide to partially penetrate DPPG/DPPC 3:1 membrane. This different effect showed by KLA1 could be due to the tryptophan residue, which has a preference for the interfacial region of the membrane.

The stoichiometries obtained with DPPG/DPPE 3:1 mixed bilayers were lower than that observed with DPPG/DPPC 3:1. This indicates that the incorporation of PE barely influences the penetrability of the vesicles, which was comparable to DPPG. In contrast, the incorporation of PC molecules in the membrane renders the vesicles more intact and hampers the translocation of KLA peptides. The good agreement between the nominal charge of the peptides and the experimentally determined N values confirms again that the interaction with pure DPPG as well as with both mixed systems is of electrostatic origin.

4.2.10.3 Influence of salt concentration

Due to the charge screening effects of salt ions, inspecting the influence of the ionic strength on biomolecular interactions is a common procedure to validate the electrostatic contribution to the binding process. For electrostatically driven associations, a substantial inverse-dependence of the binding affinity on salt concentration was established, which was predominately of entropic origin (Binder and Lindblom 2003; Klocek and Seelig 2008; Lundback and Hard 1996; Zhang and Rowe 1994). In fact, the interaction of charged peptides with the uncharged POPC was found to be weaker at higher salt concentrations (Kandasamy and Larson 2006). On the other hand, peptide-protein interactions of hydrophobic origin were barely affected by increasing the salt concentration (Arouri et al. 2007). The influence of the salt concentration on peptide-membrane interactions is an intermediate case. In comparison to 140 mM NaCl, the use of buffer without salt enhanced the binding affinity of dicynthaurin (ala) monomer to POPG and increased the exothermic ΔH° , whereas $T\Delta S^\circ$ was slightly reduced (Wen et al. 2007).

In case of anionic lipids one should take into consideration the influence of the salt concentration on the lipid chain packing and phase transition. The use of no salt led to a complex phase transition in DMPG, whereas one single, highly cooperative transition peak was found upon using 100 to 500 mM NaCl. Additionally, increasing the salt concentration shifted the T_m to a higher temperature. Interestingly, a highly concentrated dispersion (10 mM) of DPPG showed one highly cooperative phase transition in distilled water without salt (pH ~ 7.5) (Schneider et al. 1999).

We performed some ITC titrations of DPPG LUV suspension into KLA1 at 15°C using 154, 300, 500 and 1000 mM NaCl. The comparison of the recorded isotherms (see **Figure 4.2-22 (left)**) shows the strong influence the salt concentration had on the reaction enthalpy, since no binding could be detected at 1000 mM NaCl. The effect of varying the NaCl concentration on the binding parameters is presented in **Figure 4.2-22 (right)** and the numerical values are listed in **Table 4.2-4**. Increasing the NaCl concentration efficiently reduced K_{app} , the endothermic ΔH° , and $T\Delta S^\circ$. N was increased to 8.8 upon the use of 300 mM NaCl, which could be explained by the reduced binding affinity. At 500 mM NaCl, N was decreased to 5.5. This could be due to some membrane perturbations induced by the high salt concentration, which enhanced the permeability of the vesicles. Actually, we cannot rule out that the high salt concentration might have induced some changes in the structure of the peptide, which would change their thermodynamic profiles.

By fitting the salt concentration dependence of the experimental ΔH° , one could anticipate that the use of a salt-free solution will be associated with a maximum ΔH° of 1.1 kcal mol⁻¹, whereas the addition of ~ 727 mM NaCl will totally abolish the enthalpic contribution.

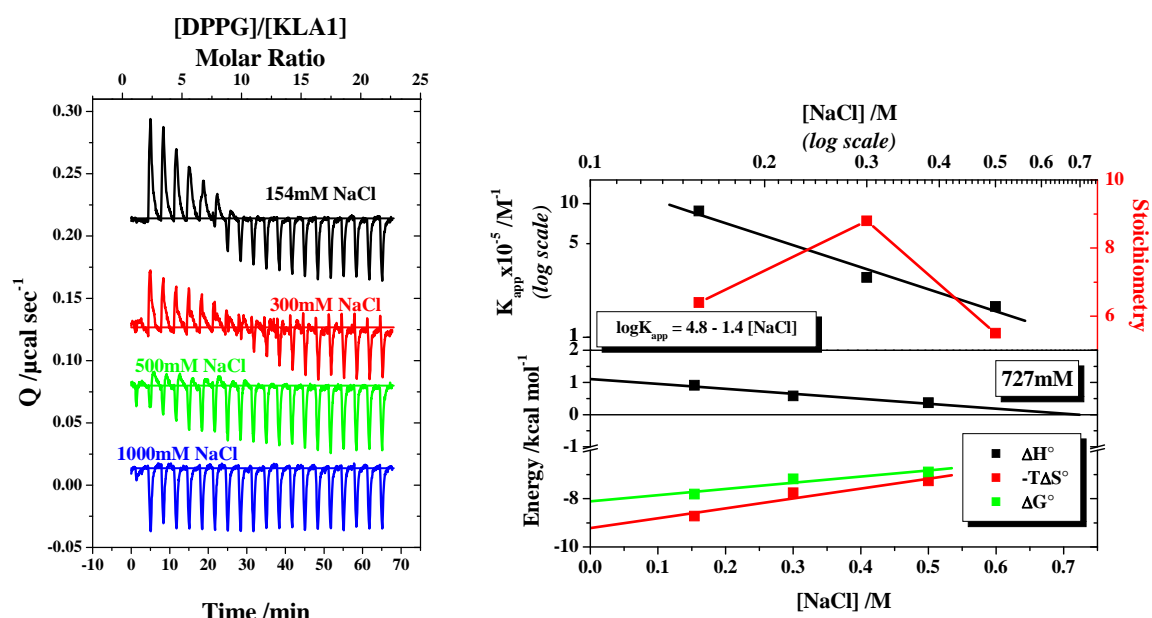


Figure 4.2-22 (Left) The experimental power signals of the binding of KLA1 (5 μM) to DPPG LUV (500 μM) at different NaCl concentrations (154 to 1000 mM) at 15°C. The samples were prepared in buffer (10 mM Tris, 154 mM NaCl, pH 7.4). **(Right)** The salt concentration dependence of the binding parameters of KLA1 to DPPG LUV at 15°C. The linear dependence of K_{app} on NaCl concentration was linearly fitted to determine K_T , the binding constant at 1M NaCl. ΔH° becomes zero at ~ 727 mM NaCl.

According to the equation $\log K = \log K_T - z \log [\text{Na}^+]$, plotting the experimental $\log K_{\text{app}}$ as a function of $\log [\text{Na}^+]$ should be linear. The slope z is the amount of Na^+ released upon the binding to one DPPG molecule, whereas the Y-intercept represents $\log K_T$. K_T is the binding constant at 1 M Na^+ concentration; commonly known as K_{nonionic} , since at this salt concentration the electrostatic binding is highly reduced (Klocek and Seelig 2008; Record et al. 1978). We do not consider in our calculations the ions coming from the DPPG and peptide samples, since their amount is negligible in comparison to the salt concentration in buffer. The binding to one DPPG molecule releases in average 1.4 Na^+ ions, whereas the nonionic binding constant K_T is $6.3 \times 10^4 \text{ M}^{-1}$. This analysis of the influence of NaCl concentration points again to the importance of the electrostatic attraction for driving the binding of KLA peptides to negatively charged lipid vesicles.

4.2.10.4 Influence of temperature

To further characterize the interaction of KLA1 with DPPG vesicles, we carried out ITC titrations over the temperature range of 5 - 50°C. The binding isotherms in the range of 5-25°C are presented in **Figure 4.2-23 (left)** and show that with increasing the temperature, the reaction enthalpy is enhanced and the saturation occurs at lower DPPG/KLA1 molar ratios (discussed later).

Interesting ITC isotherms were obtained at 30 and 35°C (**Figure 4.2-23 (right)**). They show an endothermic process at low DPPG/KLA1 molar ratios, which disappears at a molar ratio of ~ 6 until another exothermic event starts above the DPPG/KLA1 molar ratio of ~ 12 . The T_m of free DPPG is $\sim 41^\circ\text{C}$. The DSC thermograms showed that the addition of KLA1 broadened the transition and shifted it to about 35°C at L/P of 10. We propose that at temperatures $\geq 30^\circ\text{C}$ and during the first part of the titration, a peptide-induced gel to fluid phase transition of DPPG takes place (endothermic) due to the presence of excess KLA1. The further titration of DPPG vesicles will continuously cause peptide redistribution which will decrease the peptide surface concentration. Eventually, above the molar ratio of 12 (equimolar peptide-lipid charge ratio) this phenomenon will be reversed, and this is accompanied by the release of heat. Increasing the temperature from 30 to 35°C enhances the endothermic peptide-induced phase transition and consequently the exothermic event at the end of the titration. This behaviour does not appear for the interaction with fluid DPPG at 50°C (**Figure 4.2-23 (right)**) where a barely detectable enthalpy change is seen. This supports our

interpretation of this phenomenon, which is also discussed by Wieprecht et al. (2002) (Wieprecht and Seelig 2002).

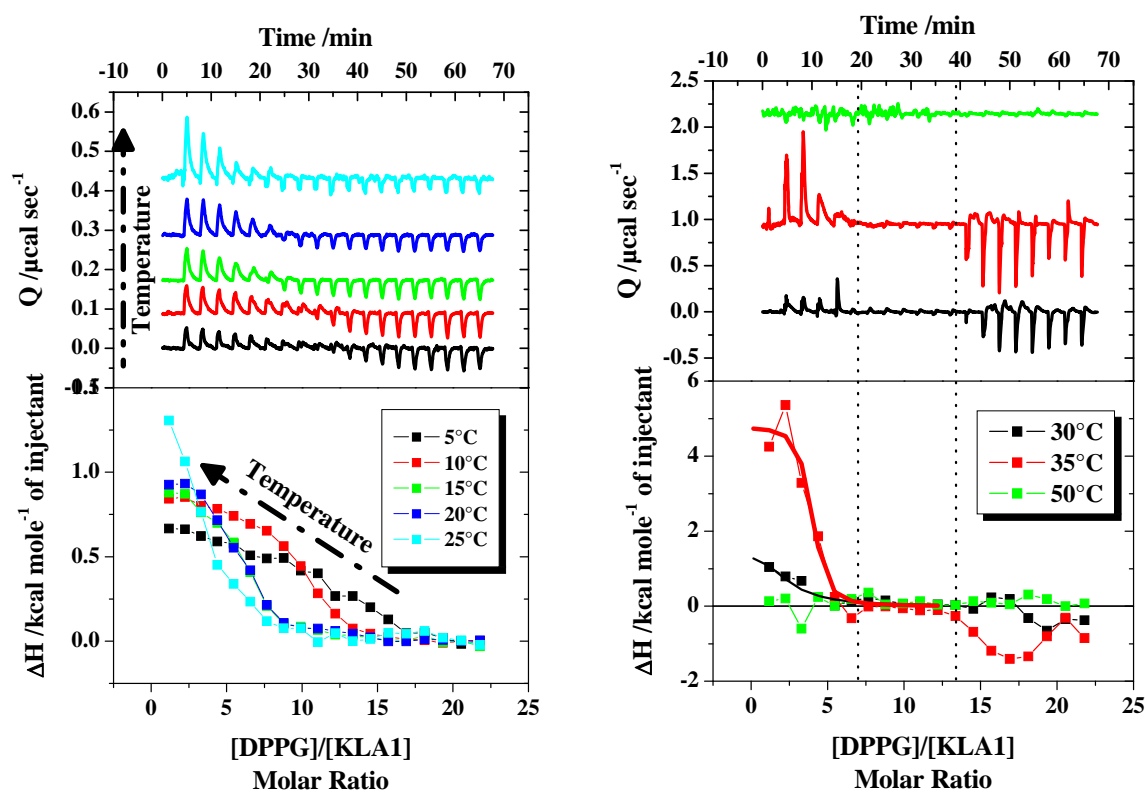


Figure 4.2-23 The experimental power signals (top) and the integrated peaks as a function of DPPG/KLA1 ratio (bottom) of the titration of DPPG LUV (500 μM) in the syringe into KLA1 peptide (5 μM) in the reaction cell at temperatures of 5 to 25°C (left) and of 30 to 50°C (right) The samples were prepared in buffer (10 mM Tris, 154 mM NaCl, pH 7.4).

The temperature dependence of the binding parameters, which were acquired by fitting the 5 - 25°C isotherms as well as the first endothermic part of the 30 and 35°C curves, are displayed in **Figure 4.2-24** and listed in **Table 4.2-4**. The binding affinity showed a maximum at 10°C, a phenomenon that was observed with other systems (Arouri et al. 2007; Klocek and Seelig 2008). In our case, this could be not due to a reduced binding affinity at 5°C but rather to the fitting of the less steep isotherm at 5°C. K_{app} was slightly reduced at high temperature, i.e. from $9.9 \times 10^5 \text{ M}^{-1}$ at 10°C to $2.9 \times 10^5 \text{ M}^{-1}$ at 25°C. The unfavourable ΔH° and the favourable $T\Delta S^\circ$ of the binding process were slightly increased by increasing the temperature, yet, ΔG° remained unaltered due to the known enthalpy-entropy compensation.

In protein associations, a linear correlation between ΔH° and $T\Delta S^\circ$ indicates that the interaction is accompanied by substantial hydrophobic effects (Arouri et al. 2007; Blokzijl

and Engberts 1993). In our case, this correlation is not linear (data not shown) which exhibits that the former assumption does not apply for such interactions.

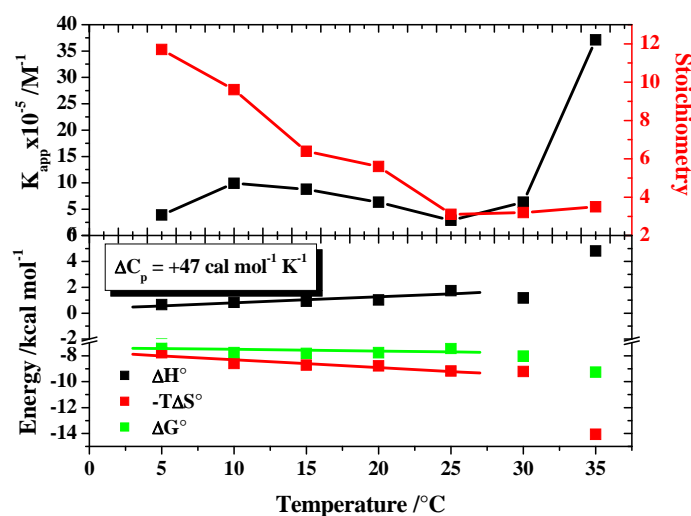


Figure 4.2-24 The temperature dependence of the binding parameters K_{app} , N , ΔH° , $-T\Delta S^\circ$ and ΔG° of KLA1 to DPPG LUV. The linear temperature dependence of ΔH° was linearly fitted to determine the change in specific heat capacity ΔC_p .

The slope of the temperature dependence of ΔH° can be used to anticipate the change in specific heat capacity (ΔC_p), assuming a temperature-independent ΔC_p . A ΔC_p value of $+47 \text{ cal mol}^{-1} \text{ K}^{-1}$ was determined. A positive ΔC_p is unusual in peptide-lipid interactions (Wieprecht et al. 1999b). On the other side, the binding of KLA1 to POPG exhibits a negative ΔC_p (discussed later). Though it remains difficult to explain the origin of the positive ΔC_p , it is obvious that it is related to some processes that takes place only with DPPG in the gel phase. We anticipate that it is due to the temperature enhanced perturbation and fluidization of the lipid hydrocarbon chains.

The change in the binding stoichiometry can be utilized to predict the intactness/permeability of the DPPG lipid vesicles over the studied temperature range. At 5°C , a stoichiometry of ~ 12 reveals that the peptide interacts merely with the outer leaflet of the bilayer. Increasing the temperature enhances the permeability of the vesicles, as exhibited by the decrease in the stoichiometry. The enhanced permeability upon increasing temperature ($T < T_m$) is correlated to the reduced lipid chain packing and the formation of defects due the expansion of the membrane. N is ~ 6 at 15 and 20°C , which shows the full peptide coverage of both leaflets. However, N becomes ~ 3 at 25, 30 and 35°C . This could be justified by the formation of some suprastructures of KLA1 with the fluidized DPPG at those temperatures. In

similar systems, temperature was reported to ease and accelerate the translocation across lipid membranes (Keller et al. 2006; Wieprecht et al. 2000c).

4.2.10.5 Interactions of KLA peptides with POPG LUV

For comparison purposes, we characterized the interaction of KLA1 with the fluid POPG vesicles at 5, 15, 25, and 50°C. The binding curves are presented in **Figure 4.2-25 (left)**. The binding was endothermic at 5, 15, and 25°C and became exothermic at 50°C. Moreover, the ITC isotherms displayed a minimum, after which ΔH° came back to values near the dilution enthalpy of the lipid vesicles. The position of the minimum was shifted to lower POPG/KLA1 molar ratios with raising the temperature, namely from ~ 11 at 5°C to ~ 4.4 at 50°C. This phenomenon has been reported and discussed before for various systems ((Binder and Lindblom 2003; Schwieger 2008) and references therein), yet, it is still not well understood. One could speculate that the minimum represents the point at which the peptide in the cell was totally bound to the lipid vesicles. Upon the addition of further vesicles, no more binding will take place (no free peptides available) but rather a redistribution of the bound peptides, which is associated with a net enthalpy change of around zero. The temperature would enhance the permeability of POPG vesicles, which would increase the number of lipid molecules available for the peptide. Therefore, the observed minimum would be shifted to lower lipid to peptide ratios. Another possibility might be that the minimum was the onset of a reversal of some membrane perturbation effects upon introducing excess lipids to the reaction cell that would decrease the local peptide concentration on the lipid membrane. It is also possible that at the minimum, a sudden aggregation process started upon reaching a certain critical concentration of vesicles in the cell.

The results of fitting the first part of the isotherm are exhibited in **Figure 4.2-25 (right)** and listed in **Table 4.2-4**. At 5, 15, and 25°C and similarly to DPPG, the interaction of KLA1 with POPG was also associated with unfavourable ΔH° and favourable $T\Delta S^\circ$. However, the binding affinity (K_{app}) towards POPG was always tenfold higher than the affinity towards DPPG at the respective temperature. Interestingly and in contrast to the case of DPPG, increasing the temperature reduced the endothermic ΔH° and also $T\Delta S^\circ$ ($\Delta H^\circ \approx 0$ at 37°C), which led to a negative ΔC_p of $-81 \text{ cal mol}^{-1} \text{ K}^{-1}$, meanwhile ΔG° was barely influenced. The negative ΔC_p is a characteristic of the classical and non-classical hydrophobic effects (Seelig and Ganz 1991; White and Wimley 1998). The N values obtained from the first part of the binding curves of POPG were similar to that achieved with DPPG at

temperatures $\geq 25^\circ\text{C}$. This indicates again the possibility of the formation of some suprastructures of KLA peptides with fluid PG, with a lipid to peptide molar ratio of 3 to 4. Up to now, there are still inadequate data to explain these phenomena and, therefore, our theory remains mere speculations.

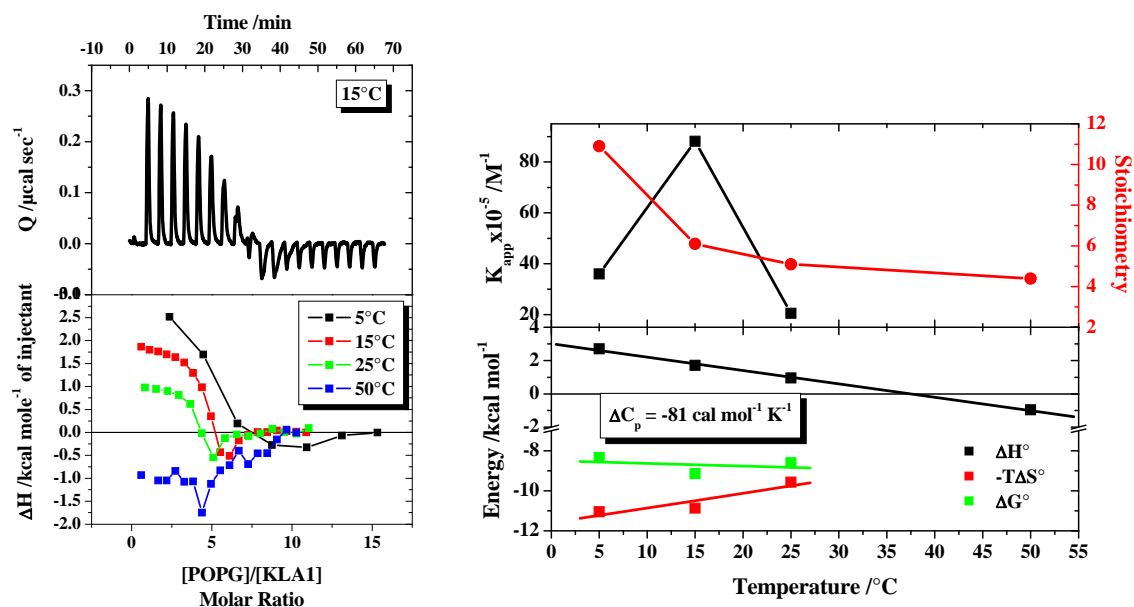


Figure 4.2-25 (Left) The experimental power signal at 15°C (top) and the integrated peaks as a function of POPG/KLA1 ratio at 5 to 50°C (bottom) of the interaction of KLA1 (5 – 10 μM) with POPG LUV (0.5 - 1 mM). The samples were prepared in buffer (10 mM Tris, 154 mM NaCl, pH 7.4). (Right) The temperature dependence of the binding parameters K_{app} , N , ΔH° , $-\Delta S^\circ$ and ΔG° of KLA1 to POPG LUV. The linear temperature dependence of ΔH° was linearly fitted to determine the change in specific heat capacity ΔC_p .

4.3 Summary

So far, the role of the secondary structure and helical propensity of cationic antimicrobial peptides in their antimicrobial activity and bacterial selectivity as well as their action on model lipid membranes is still not well understood. We utilized several biophysical techniques to explore the interaction of KLA peptides with different helical propensities with various lipid mono-, bi-, and multilayers. We mainly investigated the interaction of the peptides with PG, PE and PG/PE membranes as models for the cytoplasmic bacterial membrane as well as with PC as a model for the outer leaflet of mammalian membranes.

The experiments were carried out under different conditions (e.g. temperature, salt concentration, surface charge density, lipid fluidity and headgroup, peptide concentration, lipid/peptide ratio...) to inspect the impact of the peptides on lipid membranes (e.g. aggregation, solubilization, pore formation...), to check the influence of membrane components on the peptide behaviour (e.g. secondary structure), and to examine the role of the peptide conformation.

Despite the fact that real membranes are fluid in nature, the design of some experiments (for instance DSC and FT-IR) necessitated the use of gel-state lipids. The same model membranes were also investigated using other techniques, mainly ITC and DLS. For comparison purposes, we also carried out experiments with fluid lipids. Although the gel-state lipids are a poor choice for mimicking real membranes, the results of the experiments with gel-state lipids can still be used to give insights into the binding processes.

The cationic KLA peptides show a pronounced affinity towards anionic monolayers and bilayers as compared to the uncharged ones. Though the peptides do interact modestly with the zwitterionic PC and PE, their influence is undetectable with some of the used techniques. The effects of the peptides on lipid membranes are modulated by the peptide conformation, the membrane itself, and the experimental conditions.

Our observations and the results reported before (Dathe et al. 1996; Kerth et al. 2004; Krause et al. 1995) show the flexibility of KLA peptides in adopting various conformations depending upon the surrounding medium, temperature, lipid/peptide ratio, membrane composition, lipid form, and preparation procedure.

The KLA peptides in the helical conformation bind stronger to lipid membranes, have a higher aggregation power, and are capable of forming pores (unpublished BLM data support this notion). Those effects are enhanced with peptide helicity and surface charge density of

the membrane. The β -structured peptides highly perturb membranes and may render the vesicles leaky, although they cannot form structural pores. In addition, they can micellize lipid membranes.

The peptides with the lower helical propensity have a higher tendency to form β -structures, however, further experiments are required to estimate whether there are structural differences between β -structured KLA peptides. This will assist us to interpret their actions.

We propose both the toroidal pore and the peptide-induced membrane micellization as antimicrobial mechanisms for KLA peptides. However, the antimicrobial studies indicate that the helical peptide is the active form and, consequently, the pore formation as the prime mechanism. Nonetheless, we firmly emphasize the importance of local peptide concentration in determining the peptide mode of action.

5 RRWRF peptides

5.1 Introduction

Among all classes of antimicrobial peptides, the small peptides rich in arginine (R) and tryptophan (W) are of great interest due to their relatively high potency, broad range of activities and selectivity as well as to their small size and, consequently, low cost (Chan et al. 2006). Some examples presented in literature with pronounced antimicrobial activity are lactoferricin-derived hexapeptide (Tomita et al. 1994), truncated analogues of indolicidin (Staubitz et al. 2001), and hexapeptides derived from tritrypticin (Nagpal et al. 1999) as well others (Chan et al. 2006; Muta et al. 1990; Nakamura et al. 1988; Strom et al. 2003; Strom et al. 2002). In these peptides, R provides the positive charge and the capacity for hydrogen bonding, while the hydrophobic bulky amino acid W has a preference for the interfacial region of the bilayer allowing a deeper burial in the membrane. Moreover, the tryptophan anchors the peptides into the bilayer hydrophobic core and prolongs their attachment to the membrane (Appelt et al. 2005a; Chan et al. 2006). The relevancy of R and the aromatic residues for the activity was proven. The substitution of W by the less hydrophobic phenylalanine (F) in lactoferricin peptide reduced the activity, whereas the substitution by more hydrophobic residues enhanced the antibacterial activity (Haug et al. 2001). On the other side, replacing R with lysine (K) suppressed the activity in some peptides (Kang et al. 1996), whereas in other peptides the activity was barely altered (Staubitz et al. 2001).

The peptide Ac-RW (Ac-RRWRF-NH₂) is a linear synthetic hexapeptide obtained from screening a synthetic combinatorial library (Blondelle et al. 1995). The amphipathic structure of Ac-RW is illustrated in **Figure 5.1-1**. The peptide showed a broad spectrum antimicrobial activity but modest effects on eukaryotic cells (Blondelle and Houghten 1996; Blondelle et al. 1995). The substitution of R by K and of W by tyrosine (Y) reduced the antimicrobial activity (Dathe et al. 2004).

C-RW peptide was introduced by Dathe and co-workers through a head-to-tail cyclization of the linear sequence, i.e. Ac-RW (Dathe et al. 2004; Wessolowski et al. 2004). As exhibited in **Table 5.1-1**, the cyclization enhanced the antimicrobial activity towards *E. coli* and *B. subtilis*. However, the haemolytic activity was also enhanced (~ 3.3 times). The activity patterns of C-RW indicated a potent and selective antimicrobial peptide.

The activity of C-RW towards wall-deficient L-form bacteria was distinctly lower than the wild type (Junkes et al. 2008). This suggests the importance of the bacterial outer membrane for the antimicrobial effect, since the outer membrane possibly enhances the

accessibility of the inner membrane to the peptides, for instance through the “self promoted uptake” mechanism (Hancock and Chapple 1999).

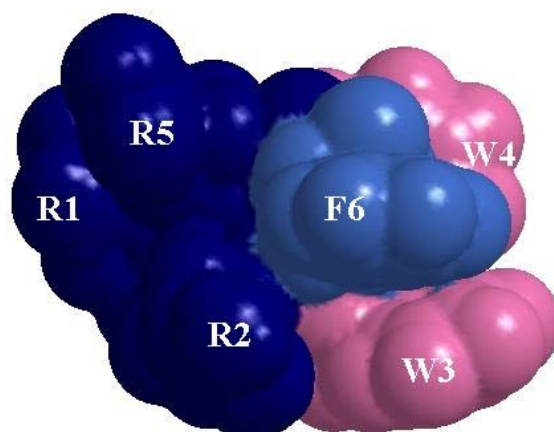


Figure 5.1-1 View of the amphipathic structure of Ac-RW, where the arginine (R) residues are oriented in one direction and the aromatic amino acids tryptophan (W) and phenylalanine (P) are aligned in the opposite direction.

The permeabilization of the bacterial membranes correlated well with the antimicrobial activity. However, substantial permeabilization of the inner and outer membranes was only achieved at concentrations 3-8 times higher than the MIC of the peptides. This supports the notion of the involvement of other mechanisms, besides membrane permeabilization, in the bacteriostatic and bactericidal action of the peptides (Junkes et al. 2008).

Table 5.1-1 The biological and bilayer permeabilizing activities and hydrophobic parameters of Ac-RW and C-RW peptides. Adapted from refs. (Dathe et al. 2004; Wessolowski et al. 2004)

Biological activities	Ac-RW	C-RW	Ratio Ac-RW/C-RW
<i>E. coli</i> (MIC) / μg	>100	6.3	>16
<i>B. subtilis</i> (MIC) / μg	25	3.1	8
Erythrocyte lysis (%)	7.3	24.4	0.3
Permeabilizing activities (EC_{25}) / μmol			
POPC	4	1	4.0
POPC/POPG 3:1	40	15	3.7
POPC/POPG 1:1	160	40	4.0
POPC/POPG 1:3	25	24	1.0
POPG	6.5	7.5	0.9
POPE/POPG 1:3	84.2	19.4	4.3
POPC/cholesterol 3:1	44.2	7.6	5.8
Hydrophobic parameter* (t_R /min)	15.2	15.9	0.96

* For the definition of the hydrophobicity parameter and the method for its determination by RP-HPLC see for instance (Kaliszan 1998).

The introduction of D-amino acids slightly reduced the activity of the peptides (Dathe et al. 2004; Wessolowski et al. 2004). The scrambling of the primary sequence of C-RW was found to have only a small influence on the activity and amphipathicity of the peptide, which

indicates the importance of the global properties of the peptide and the irrelevancy of the exact peptidic sequence (Appelt et al. 2008).

As expected, the binding of the peptides to lipid membranes was electrostatic-driven and was enhanced upon increasing the surface charge density. C-RW showed a higher affinity towards charged vesicles which was explained by the increased charge density in the peptide. On the other side, the clustering of the aromatic residues in C-RW maximized the hydrophobic interactions with POPC as compared to the linear analogue (Dathe et al. 2004). The latter notion is supported by the enhanced hydrophobicity parameter of C-RW as compared to Ac-RW, which were derived from the t_R -values determined by RP-HPLC (**Table 5.1-1**) (Wessolowski et al. 2004). The peptides were located next to the headgroup region in the membrane, whereas the absence of the net negative charge in POPC allowed a deeper burial of the peptides in the membrane hydrophobic core. The position of the linear and cyclic peptides in lipid membranes was comparable (Dathe et al. 2004).

As demonstrated in **Table 5.1-1**, the linear peptide showed comparable dye release activities on POPC and POPG vesicles, however, its activity was lower towards mixed membranes, being minimal with POPG/POPC 1:1. The cyclization pronouncedly enhanced the permeabilization of neutral and moderately charged bilayers, whereas the effect on highly charged bilayers was barely altered. POPG/POPE 3:1 vesicles were more resistant to the permeabilization of Ac-RW as compared to POPG/POPC 3:1. The incorporation of cholesterol in POPC bilayers reduced the permeabilizing efficiency of the peptides.

C-RW exhibited slightly slower permeabilization kinetics, a behaviour that was explained by the bulky and constrained nature of the peptide. The bilayer permeabilization was described to be determined by two components; an electrostatic binding, which was pronouncedly enhanced upon increasing the membrane surface charge density, and the permeabilizing efficiency controlled by the extent of the hydrophobic interaction (Dathe et al. 2004).

The pronounced activity towards highly charged vesicles could be due to the higher accumulation of the peptides, which neutralized the surface charge and relieved the tension in the outer leaflet. On the other hand, the effective disruption of neutral membranes was possible because of the deeper insertion of the aromatic side chains of the peptides in the membrane. The relatively reduced activity towards POPG/POPC 1:1 could be correlated with the lower accumulation of the peptides as compared to POPG, whereas the surface charge hinders the deeper burial of the peptide hydrophobic face in the membrane as compared to POPC (Dathe et al. 2004).

The CD (Dathe et al. 2004) and NMR (Jing et al. 2003) data showed the flexibility of Ac-RW in solution which was reduced upon approaching the membrane. C-RW displayed a more ordered structure in solution and even a more well-defined structure in the vesicles bound state (Appelt et al. 2005b; Dathe et al. 2004). Both Ac-RW and C-RW assume an amphipathic structure when bound to a detergent micelle or to a lipid bilayer. The arginine residues and the tryptophan and phenylalanine side chains of Ac-RW are arranged on opposite sides of the backbone (Jing et al. 2003). In the conformationally constrained C-RW, the cyclic backbone leads to the charged side chains being oriented to one side to form the hydrophilic face and a cluster of the aromatic side chains to the opposite hydrophobic part (Appelt et al. 2005a; Appelt et al. 2005b). This arrangement allows a simultaneous electrostatic interaction of the arginine side chains with the lipid polar/charged headgroup and an insertion of the aromatic rings into the hydrophobic core of the membrane (Appelt et al. 2005a; Dathe et al. 2004). The structures of the C-RW were nearly identical in neutral and charged micelles, where the peptide formed a combination of two β -turns and was oriented almost parallel to the membrane surface (Appelt et al. 2005b). The structures of both peptides in uncharged and charged micelles are illustrated in [Figure 5.1-2](#).

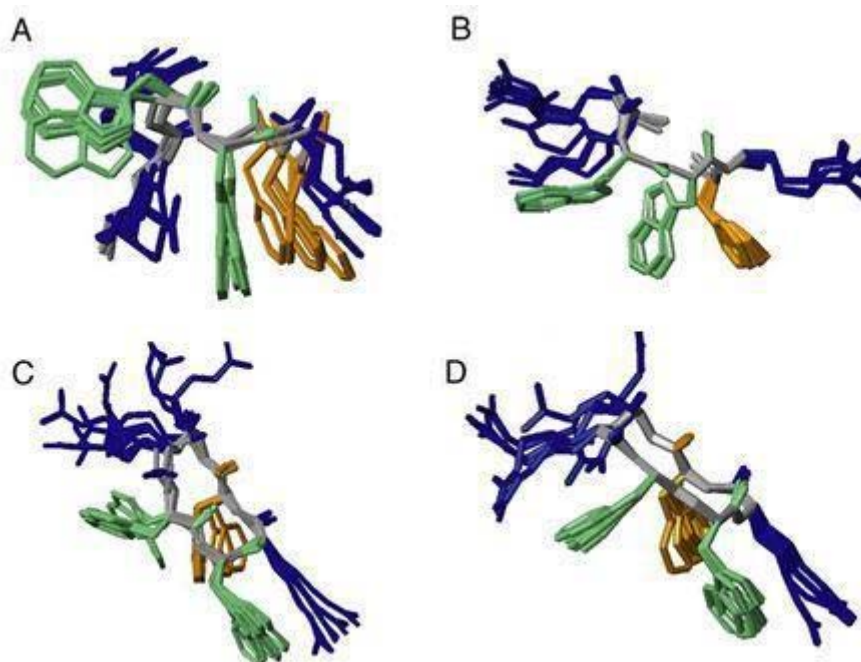


Figure 5.1-2 (A and B) Ac-RW peptide in the presence of DPC and SDS micelles, respectively. (C and D) C-RW peptide in the presence of DPC and SDS micelles, respectively. The structures were determined by means of NMR (Appelt et al. 2005b; Jing et al. 2003). Tryptophan residues are highlighted in pale-green, Phenylalanine is shown in orange, and Arginine residues are presented in blue colour. Adapted from ref. (Chan et al. 2006)

5.2 Results and discussion

5.2.1 Dynamic Light Scattering (DLS)

We performed DLS measurements to answer the question whether the peptides can solubilise or fuse lipid vesicles as well as to examine their aggregation power. The experiments were carried out by titrating extruded DPPG or DPPC LUV (~ 50 nm radius) into the peptide solution in the cuvette. The radius of the lipid vesicles was determined prior to each titration. As shown in **Figure 5.2-1 (left)**, both peptides exhibited a comparable aggregation of DPPG vesicles at low L/P. At L/P of 12, the aggregation capacity of the peptides was exceeded and, therefore, the lipid-peptide aggregates started to dissociate. The further addition of DPPG vesicles caused the aggregates to dissociate completely. The size distribution at L/P of 188 was very similar to that of free DPPG before the titration. This suggests that the DPPG vesicles were not disrupted by the peptides. Comparably, the size of DPPC vesicles was barely affected by the peptides, as indicated by the size distribution at low L/P (see **Figure 5.2-1 (right)**).

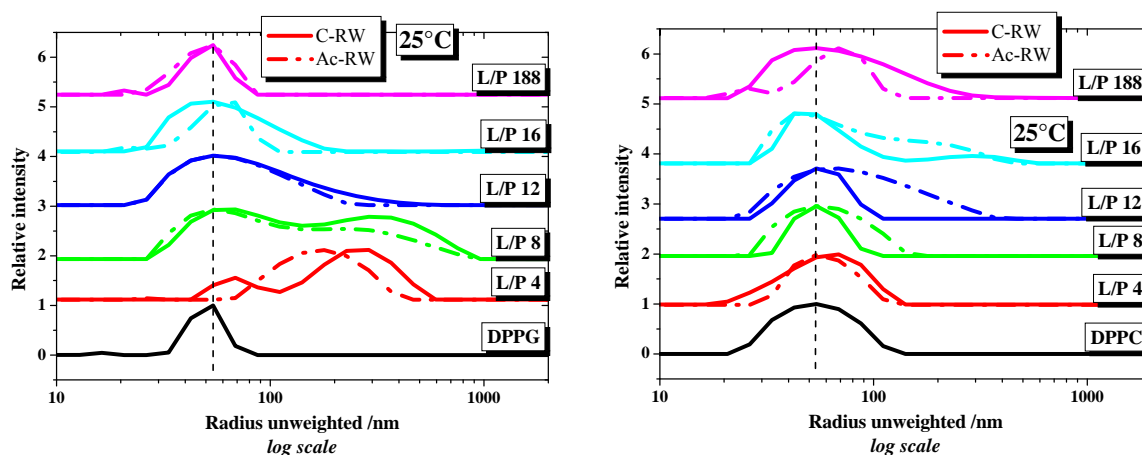


Figure 5.2-1 Unweighted distribution of hydrodynamic radii obtained from DLS measurements of DPPG (left) and DPPC (right) vesicles (1 mM, ~ 50 nm radius) before and after the multi-step addition to Ac-RW and C-RW solutions (500 μ l, 5 μ M) at 25°C. The samples were prepared in buffer (10 mM Tris, 154 mM NaCl, pH 7.4).

5.2.2 Differential Scanning Calorimetry (DSC)

Differential scanning calorimetry was utilized to inspect the influence of Ac-RW and C-RW on the thermotropic phase transitions of the anionic lipids DPPG, DMPA, DPPS, and TMCL as well as of the zwitterionic lipids DMPC and DPPE. These experiments were performed to clarify the specificity of the peptides towards negatively charged phospholipids. Ac-RW (N-terminus acetylated and C-terminus amidated) and C-RW have a nominal net

charge of +3 at neutral pH. Therefore, a much higher selectivity of the peptides towards negatively charged lipids over uncharged ones was anticipated due to the electrostatic attraction.

5.2.2.1 DSC of single-component lipid membranes

Figure 5.2-2 shows the DSC curves of the second heating scan of free DMPC, DPPG, and DPPE vesicles and of the same lipid vesicles after the addition of 4.8 mol% of the peptides Ac-RW and C-RW. The first heating scans (not shown) were always slightly different from the subsequent scans. This is caused by the fact that the peptides were added to the outside of the vesicles at room temperature and that heating the lipids through the phase transition enhanced the peptide translocation to the inner side.

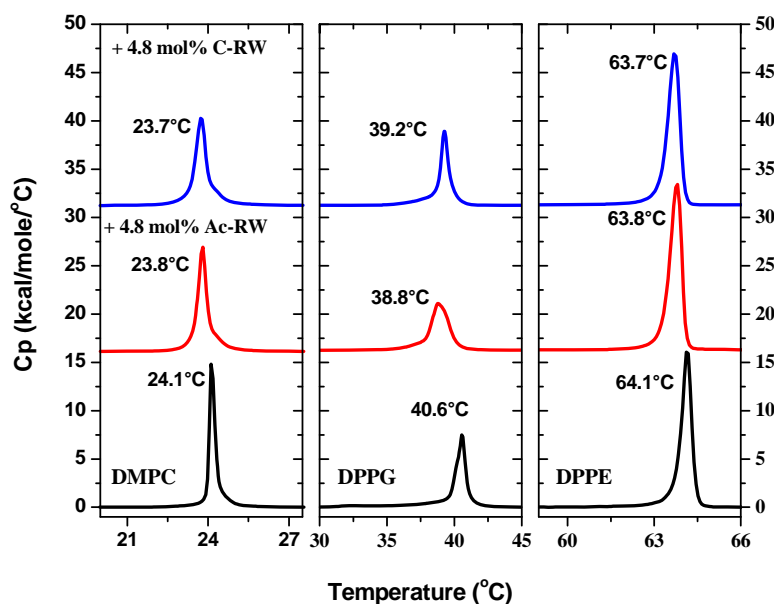


Figure 5.2-2 DSC curves of DMPC, DPPG, and DPPE LUV (lipid concentration 1 – 2 mM) with and without added peptides Ac-RW and C-RW (L/P 20:1). The samples were prepared in buffer (10 mM Tris, 154 mM NaCl, pH 7.4).

The peptides shifted the main phase transition temperature (T_m) of DPPG vesicles to slightly lower values, whereas their effect on DMPC and DPPE was modest. ITC, DSC and fluorescence quenching experiments carried out before with PC, PG and PG/PC mixtures had already shown the clear preference of peptides binding to anionic vesicles (Dathe et al. 2004; Jing et al. 2003; Rezansoff et al. 2005). The T_m of DPPG from the gel to the liquid crystalline L_α phase was detected $\sim 40.6^\circ\text{C}$, which agrees well with literature (Garidel and Blume 2000; Schwieger and Blume 2007). The T_m decreased by 1.8°C (38.8°C) and 1.4°C (39.2°C) upon

adding 4.8 mol% of Ac-RW and C-RW, respectively. The linear peptide destabilized DPPG bilayers slightly more than the cyclic peptide, whereas it increased the half-width of the DPPG phase transition pointing to a decrease in the transition cooperativity, as reported before (Jing et al. 2003). Marginal changes in cooperativity were found with C-RW. The slightly weaker influence of the cyclic peptide upon the negatively charged DPPG bilayer correlates well with the slightly reduced permeabilizing activity of C-RW towards POPG vesicles as compared to Ac-RW (see **Table 5.1-1**) (Dathe et al. 2004).

A comparison of the influence of 2.4 mol% C-RW on the thermotropic phase behaviour of the negatively charged phospholipids DPPG, DPPS, DMPA, and TMCL is demonstrated in **Figure 5.2-3**.

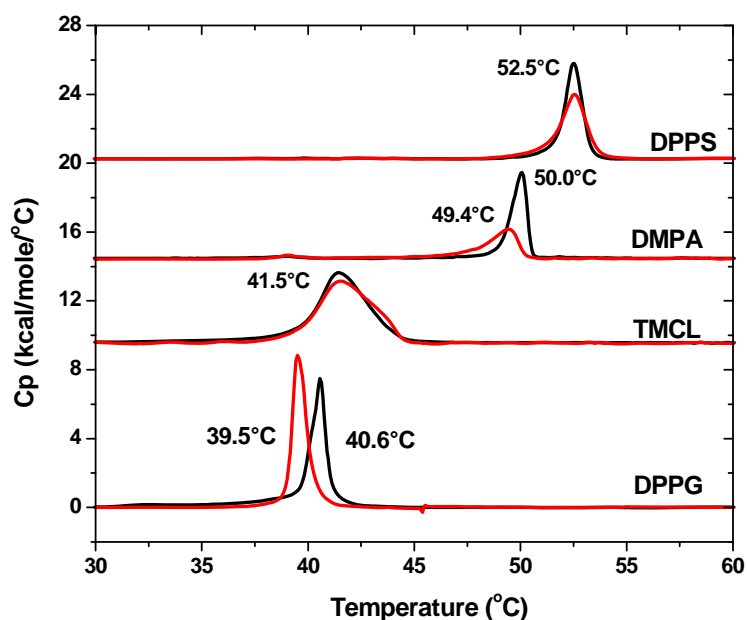


Figure 5.2-3 DSC curves of DPPS, DMPA, TMCL and DPPG LUV (lipid concentration 1 – 2 mM) before (black lines) and after the addition of 2.4 mol% C-RW (red lines) (L/P 40:1). The samples were prepared in buffer (10 mM Tris, 154 mM NaCl, pH 7.4).

The thermodynamic parameters of the DSC thermograms in **Figure 5.2-3** are listed in **Table 5.2-1**, namely the main transition temperature (T_m), the transition enthalpy (ΔH) and the half height width (HHW) as an indication of the transition cooperativity. Upon the addition of 2.4 mol% C-RW, the T_m of DPPG was decreased by 1.1°C (from 40.6 to 39.5°C), however ΔH and HHW remained almost unaltered.

The T_m of DMPA, whose negative headgroup charge is more exposed to the surrounding than that of other lipids, was also down-shifted by 0.7°C (from 50.1 to 49.4°C) upon the interaction with the peptide, whereas the transition enthalpy and cooperativity were

considerably reduced (see **Table 5.2-1**). These changes in the transition of DMPA could be due to the well-known sensitivity of PA bilayers to the surrounding medium rather than to a specific interaction with our peptides.

Table 5.2-1 The thermodynamic parameters of the DSC thermograms presented in **Figure 5.2-3** of DPPG, TMCL, DMPA and DPPS before and after the addition of 2.4 mol% C-RW.

Lipid	T_m (°C)	ΔH (kcal mol ⁻¹)	HHW ^a (°C)
DPPG	40.6	8.8	0.8
DPPG + C-RW	39.5	8.4	0.7
Change	-1.1	-0.4	-0.1
TMCL	41.5	11.8	2.5
TMCL + C-RW	41.6	11.8	3.1
Change	+0.1	0.0	+0.6
DMPA	50.1	4.2	0.8
DMPA + C-RW	49.4	3.2	1.5
Change	-0.7	-1.0	+0.7
DPPS	52.5	5.3	0.9
DPPS + C-RW	52.5	5.0	1.3
Change	0.0	-0.3	+0.4

^a HHW is the half height width.

Unexpectedly, the T_m and ΔH of the main transition of DPPS and TMCL were barely influenced by C-RW, whereas the cooperativity of the transition (i.e. HHW) was moderately decreased. From the DSC thermograms, a clear preference of C-RW towards DPPG as compared to the other negatively charged phospholipids DPPS and TMCL was concluded. This notion assumes a strong correlation between the peptide binding and the observed influence on the lipid phase transition. So far, it remains unclear why C-RW prefers PG over other negatively charged phospholipids. It can only be speculated that this was due to possible hydrogen bonding between the peptides and the glycerol headgroup of DPPG or due to steric effects since the size of the lipid headgroups varies, however, further investigations are required to support those notions. The effect of the zeta potential of acidic lipid vesicles on their affinity towards cationic peptides cannot be ruled out (Matsuzaki et al. 1991). In addition, the fact that DPPG has the lowest transition temperature among the investigated anionic lipids should not be overlooked. The more selective interaction of antimicrobial peptides with PG over PS and PA (Jing et al. 2005) as well as the discriminative binding to certain lipid headgroups (Choung et al. 1988; Lohner and Prenner 1999; Matsuyama and Natori 1990) was already proposed in other studies.

Despite the similarities between the chemical structure of DPPG and TMCL, they do interact differently with C-RW. This discrepancy between CL and PG molecules was reported before and referred to the relative rigidity and inefficient penetrability of CL membranes (Lewis et al. 2007). The possibility of the formation of cyclic intramolecular hydrogen-

bonded structures in the headgroup region of CL may also play a role (Kates et al. 1993). Furthermore, the reduced structural flexibility of the constrained C-RW hampers its deeper burial in lipid membranes, particularly, the rigid ones.

For pure electrostatic binding to PG headgroup one would expect an increase in T_m (Schwieger and Blume 2007). On the other hand, mere peptide interactions with the hydrophobic region of membranes as well as perturbing the lipid chains often exhibit a large reduction in the transition temperature and enthalpy (Lohner and Prenner 1999). The observed decrease in T_m suggests that the net effect on DPPG is primarily due to the perturbing effects on the lipid chains which overcompensates the electrostatic effect of the interaction with the headgroups.

Both Ac-RW and C-RW assume an amphipathic structure when bound to lipid membranes, which allows a simultaneous electrostatic interaction of the arginine side chains with the lipid polar/charged headgroup and an insertion of the aromatic rings into the hydrophobic core of the membrane (Appelt et al. 2005a; Dathe et al. 2004; Jing et al. 2003). Thus, the destabilization induced by the peptides can be related to the perturbation of the chain packing in the DPPG bilayer by the aromatic rings of the peptides. The activity of the peptides was shown to be directly correlated to how deeply the hydrophobic residues were buried in the membrane core (Dathe et al. 2004). For instance, the distance between the tryptophan residues of C-RW and Ac-RW and the centre of the POPC bilayer was determined to range between 9.4 to 12.4 Å, whereas their distance to the centre of the POPG/POPC 1:3 bilayer was much larger, namely 15.2 to 15.6 Å. This concurs well with the bilayer permeabilizing activity of the peptides which was 10 to 15 times higher towards POPC as compared to POPG/POPC 1:3 vesicles (Dathe et al. 2004).

The DSC peaks of DPPG were single peaks with no shoulders indicating a uniform distribution of the peptides at the interface of DPPG vesicles. Moreover, this observation suggests that the peptides can enter the DPPG vesicles, particularly when the lipid bilayers are in their fluid state, and, consequently, interact with the inner leaflet of the bilayer as well. This is not unrealistic as translocation across highly negatively charged lipid bilayers has recently been suggested for the cationic peptide penetratin (Binder and Lindblom 2003). The evidence from the DSC data for this translocation is that the first scan was always different from the subsequent heating scans. To prove this translocation we also performed DSC scans with DPPG vesicles preloaded with the peptides (the peptides existed from the beginning inside and outside the vesicles). Only small differences were observed between the DSC curves

obtained with preloaded DPPG vesicles and with the results of the former experiments (data not shown).

A quantitative description of the destabilization of DPPG vesicles by the peptides is demonstrated in **Figure 5.2-4**. A higher peptide-to-DPPG molar ratio leads to a stronger reduction, however, non-linear, of the T_m with Ac-RW being slightly more efficient than C-RW. The transition enthalpy and the cooperativity remained almost unaffected over the entire tested molar ratio range. An unaltered transition enthalpy for Ac-RW was also reported by Jing et al. (2003) (Jing et al. 2003). We propose that the DPPG vesicles remained intact up to 9.1 mol% peptides. Our DLS data, which show neither solubilization nor fusion of DPPG and DPPC vesicles after peptide binding, support this assumption (see above).

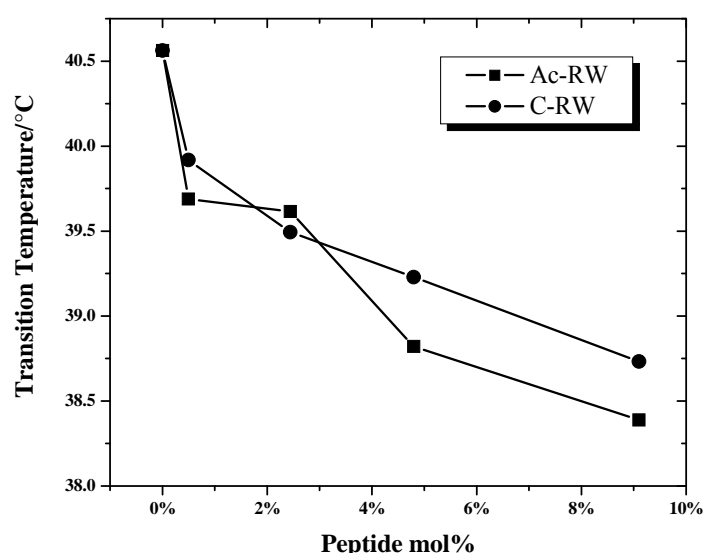


Figure 5.2-4 Transition temperature of DPPG (1 – 2 mM) as a function of peptide concentration.

5.2.2.2 DSC of two-component lipid membranes

The study of the interaction of the peptides with DPPG/DMPC and DPPG/DPPE mixed vesicles was performed to examine the effect of the surface charge density of the vesicles on peptide binding as well as to check whether there are differences between the two zwitterionic phospholipids PC and PE mixed with PG.

The design of the experiments necessitated the use of phospholipids with different acyl chain lengths (C14 and C16). However, this should not have any influence on our results since our peptides due to their amphipathic nature interact mainly with the headgroup region and do not penetrate deeply into the lipid bilayer. Furthermore, under our experimental conditions, PG/PC and PG/PE mixtures of saturated phospholipids with an acyl chain length

difference of two methylene units are completely miscible and form homogeneous bilayers in both gel and liquid-crystalline phases (Garidel and Blume 2000; Garidel et al. 1997b).

Figure 5.2-5 shows the DSC curves of DPPG/DMPC vesicles premixed with 6.3 mol% of the peptides. The phase transition of DPPG/DMPC lipid mixtures was shifted to a lower temperature upon premixing with the peptides (destabilization) without an indication of any demixing. Both Ac-RW and C-RW appeared to have a similar impact on the mixed vesicles. The decrease of the transition temperature is somewhat more pronounced in the mixtures than for the pure lipid vesicles, as long as there is sufficient DPPG in the vesicles to ensure adequate accumulation of the peptides at the bilayer interface due to the electrostatic effects. As stated above, this phenomenon is caused upon distorting the lipid chain packing by the hydrophobic side chains of the peptides.

The permeabilization experiments with unsaturated PC/PG mixtures by Dathe et al. (2004) (Dathe et al. 2004) showed that the activity of the peptides changes with modifying the PG content of the mixed bilayer (see above). The DSC curves in **Figure 5.2-5** just show a down-shift of T_m but the slight differences of the effects caused by Ac-RW and C-RW, respectively, cannot be interpreted. Likewise, the discrepancies observed for different lipid compositions were not significant enough.

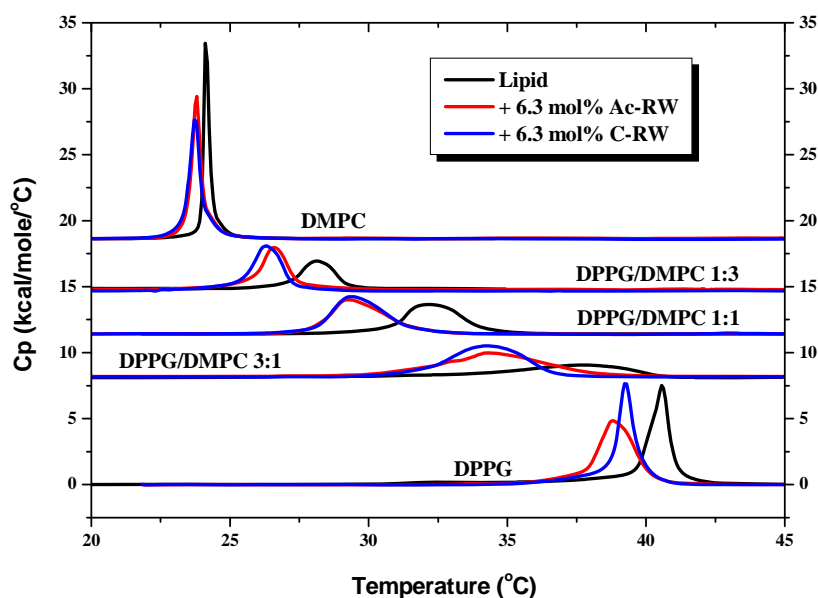


Figure 5.2-5 DSC curves of **DPPG/DMPC** mixtures (total lipid concentration 1 – 2 mM) without and with added peptides Ac-RW and C-RW (L/P 15:1). The samples were prepared in buffer (10 mM Tris, 154 mM NaCl, pH 7.4).

Vesicles composed of PG and PC with various ratios are commonly used to study the effect of electrostatics, i.e. surface charge density, on the binding of cationic peptides. In spite

of the fact that prokaryotic membranes contain no PC but rather a high amount of the zwitterionic PE in their membranes, particularly the Gram-negative bacteria, it is common that PG/PC mixtures are used as a model system for bacterial membranes. This is because PC vesicles are more stable, easier to prepare and to handle, and that PC is zwitterionic similarly to PE. However, the two headgroups of PC and PE, respectively, have a different size and PE has the additional possibility to function as a hydrogen bond donor. Therefore, the binding characteristics of peptides to PG/PE bilayers might be different.

To mimic the composition of a bacterial membrane, we used DPPG/DPPE mixtures to test whether the nature of the zwitterionic phospholipid has any influence on the properties of the membranes after peptide binding. We used DPPE instead of DMPE to ensure a sufficient separation of T_m of the individual lipids and a wide range of transition temperatures of the mixed lipid system. The phase diagrams of different PG/PE mixtures have been studied before and indicated complete although non-ideal miscibility in both phases indicating a preference for the formation of mixed PG-PE pairs (Garidel and Blume 2000). This miscibility could be confirmed for our DPPG/DPPE mixtures as only one broad transition peak was observed for all mixtures without added peptide (see **Figure 5.2-6**).

As evident in **Figure 5.2-6**, the addition of Ac-RW and C-RW to DPPG/DPPE mixtures led to the appearance of two well-separated peaks indicating lipid demixing with domain formation. The first peak at low temperature ($< 40^\circ\text{C}$) corresponds to a DPPG-rich domain, where the peptide is probably bound, and the second broad peak at a higher temperature belongs to a domain enriched in DPPE with the remaining amount of DPPG and possibly some peptide. The demixing behaviour was most pronounced for vesicles with the highest DPPG content, namely the DPPG/DPPE 3:1 mixture. When the DPPG fraction in the mixture was lowered, the first peak related to the DPPG-rich domain became smaller, because the amount of available and peptide-associated DPPG in the system decreased. However, the destabilization of the DPPG-domain increased due to the improved peptide-to-DPPG ratio. Simultaneously, the remaining DPPE-rich domain becomes increasingly depleted in DPPG and the transition temperature of the second peak becomes dominated by DPPE as the main component, i.e. the T_m gets closer to that of pure DPPE.

The position of the low temperature transition that belonged to the DPPG-rich domains was always lower than that for the pure DPPG without bound peptide. Taking the

data of **Figure 5.2-4**, one can anticipate that the low temperature peak is probably due to almost pure DPPG with a certain amount of bound peptide. In the case of the DPPG/DPPE 3:1 mixture, the peaks of DPPG-C-RW and DPPG-Ac-RW showed up at 39°C and 37.8°C, respectively. For a DPPG-C-RW complex having a T_m of 39°C, a peptide content of 6.8 mol% could be estimated using the peptide concentration dependent experiments (see **Figure 5.2-4**). Again, from **Figure 5.2-4**, a DPPG-Ac-RW complex with 9.1 mol% peptide content decreases the T_m of DPPG to 38.4°C. Since the T_m of DPPG-Ac-RW complex in DPPG/DPPE 3:1 was 37.8°C (**Figure 5.2-6**), an Ac-RW content of more than 9.1 mol% is required for this effect. These estimated numbers are the lower limits for the peptide content in the DPPG domain, since the remaining DPPE domain contains residual DPPG. Independent on the exact composition of DPPG-peptide domains, it is evident that Ac-RW leads to a slightly larger down-shift of the T_m of the DPPG domains than C-RW.

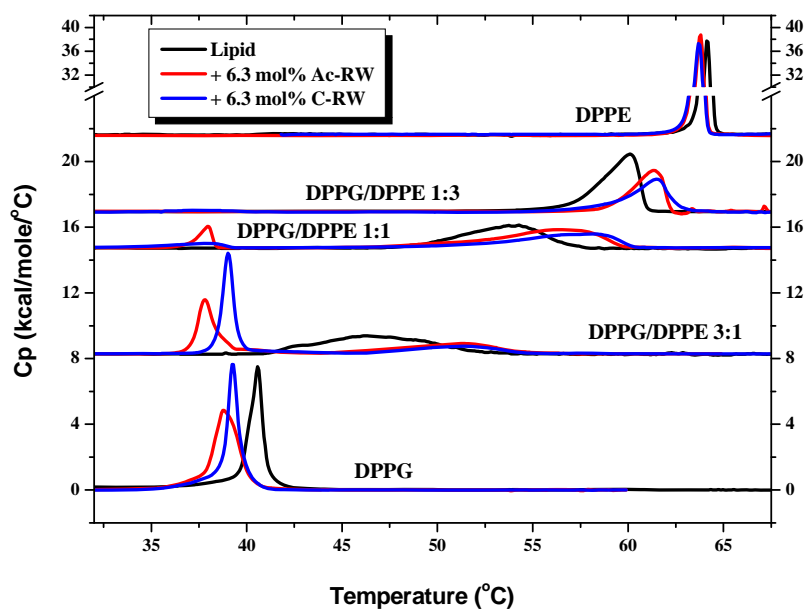


Figure 5.2-6 DSC curves of **DPPG/DPPE** mixtures (total lipid concentration 1 – 2 mM) without and with added peptides Ac-RW and C-RW (L/P 15:1). The samples were prepared in buffer (10 mM Tris, 154 mM NaCl, pH 7.4).

The DSC curves clearly indicate the following effect: in a DPPG/DPPE mixture with bound peptides, separate gel phase domains of almost pure DPPG with bound peptide and peptide-poor DPPE-enriched domains exist. Upon heating, the DPPG domains become liquid-crystalline, while DPPE stays in the gel phase until the transition temperature of almost pure DPPE is reached. When the complete mixture is in the liquid-crystalline phase this partial demixing might persist, though the DSC curves contain no information on this process. If

demixing in the liquid-crystalline phase induced by the peptides would indeed occur, this would create boundaries between domains of different composition. These boundaries would then serve as additional pathways for solutes to cross the membrane and would also destabilize the membrane. Consequently, in addition to the usual pore formation induced by the peptides, the formation of domain boundaries due to demixing in PG/PE bilayers induced by C-RW and Ac-RW would help creating defects. Comparable data for our system on the permeabilization of unsaturated lipid bilayers of PG and PE unfortunately do not exist. Therefore, the proposed demixing in the liquid-crystalline phase remains a hypothesis and needs to be proven.

The incorporation of cardiolipin in our model membrane brings us a step closer to the real phospholipid composition in most of the outer and cytoplasmic bacterial membranes (Lohner et al. 2008). Therefore, we additionally investigated TMCL-containing binary and ternary mixtures.

The DSC thermograms of TMCL/DPPG mixed membranes before and after the addition of 6.3 mol% Ac-RW and C-RW, respectively, are illustrated in **Figure 5.2-7**. TMCL showed a subtransition (T_{sub}) from lamellar subgel L'_C to gel L_β at $\sim 25.5^\circ\text{C}$ and an asymmetric main phase transition (T_m) to lamellar liquid crystalline L_α at $\sim 41.5^\circ\text{C}$ ($\Delta H \sim 13 \text{ kcal mol}^{-1}$ and HHW $\sim 2.5^\circ\text{C}$), which concurs with literature (Lewis et al. 2007). The interaction of C-RW with TMCL barely influenced its main transition, whereas a second smaller transition was observed at $\sim 21.5^\circ\text{C}$. Ac-RW down-shifted T_m of TMCL to $\sim 40^\circ\text{C}$ and induced a transition at $\sim 28.7^\circ\text{C}$. We believe that the transitions observed of the peptide-bound TMCL at ~ 21.5 and $\sim 28.7^\circ\text{C}$ were due to a destabilized and stabilized subgel L'_C structures, respectively. The modest influence of C-RW on TMCL vesicles could be due to the relative rigidity and poor penetrability of CL membranes (Lewis et al. 2007), whereas the flexibility of Ac-RW allowed a better interaction with the rigid TMCL bilayer and a deeper insertion in the membrane. This notion is supported by the observation that DPPG vesicles were more destabilized by Ac-RW as compared to C-RW (see above).

It was found that the major changes in the interfacial conformation and hydration take place during the L'_C/L_β transition (Lewis et al. 2007). Since our peptides interact preferentially with the lipid headgroup region, it is reasonable that they have a profound influence on TMCL subtransition.

The T_m of DPPG and TMCL was ~ 40.6 and 41.5°C , respectively. Interestingly, T_m of the binary mixture was $\sim 1.5^\circ\text{C}$ lower than ideally expected (**Figure 5.2-7**). This phenomenon

was reported before for PC/PE mixtures (Ipsen and Mouritsen 1988; Sugar and Monticelli 1985), and can be explained by the existence of partial demixing with lower azeotropic points.

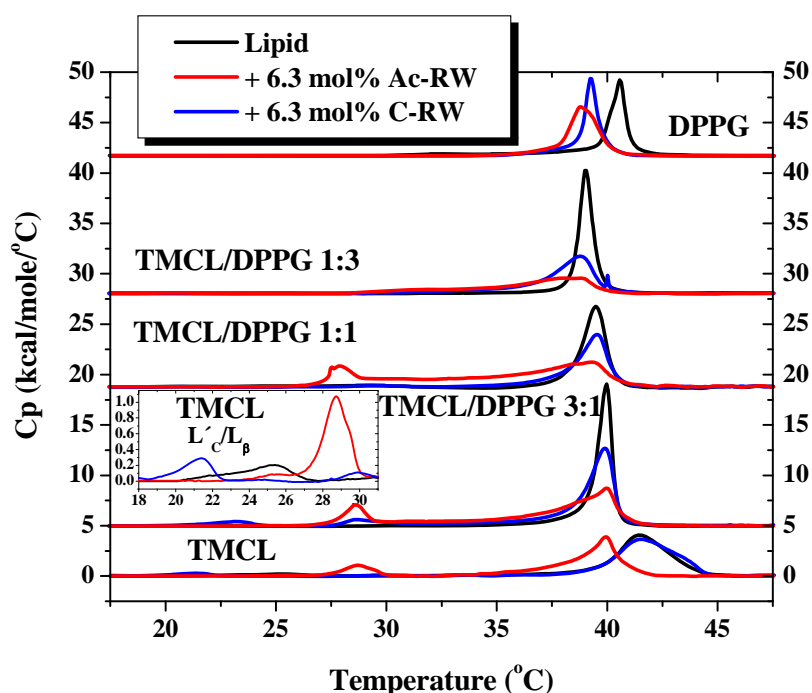


Figure 5.2-7 DSC curves of **TMCL/DPPG** mixtures (total lipid concentration 1 – 2 mM) without and with added peptides Ac-RW and C-RW (L/P 15). The samples were prepared in buffer (10 mM Tris, 154 mM NaCl, pH 7.4).

The binding of the peptides to TMCL/DPPG mixed bilayers substantially broadened the phase transition, whereas ΔH and T_m were modestly affected. The influence of Ac-RW was more pronounced than C-RW. We anticipate that the peptides induce some demixing in TMCL/DPPG membranes, yet, less efficiently in comparison to DPPG/DPPE mixtures. Our FT-IR data support this assumption (discussed later). Though no subtransition was observed with the free TMCL/DPPG mixtures, the subtransition of TMCL can be seen in the curves of peptide-bound TMCL/DPPG mixtures, particularly the ones with high TMCL content. This indicates that the peptides induce the formation of the L'_c phase of TMCL in the mixture, which evidences the peptide-induced demixing.

As shown in **Figure 5.2-8**, the peptides induced some demixing in TMCL/DPPE mixtures as well, as indicated by the appearance of the TMCL subtransition as well as by the up-shift of the main transition. C-RW reduced the width of the main phase transition which could be due to a stabilization of the mixed membrane, whereas Ac-RW pronouncedly

perturbed the lipid mixture and broadened the main phase transition, particularly of TMCL/DPPE 1:1.

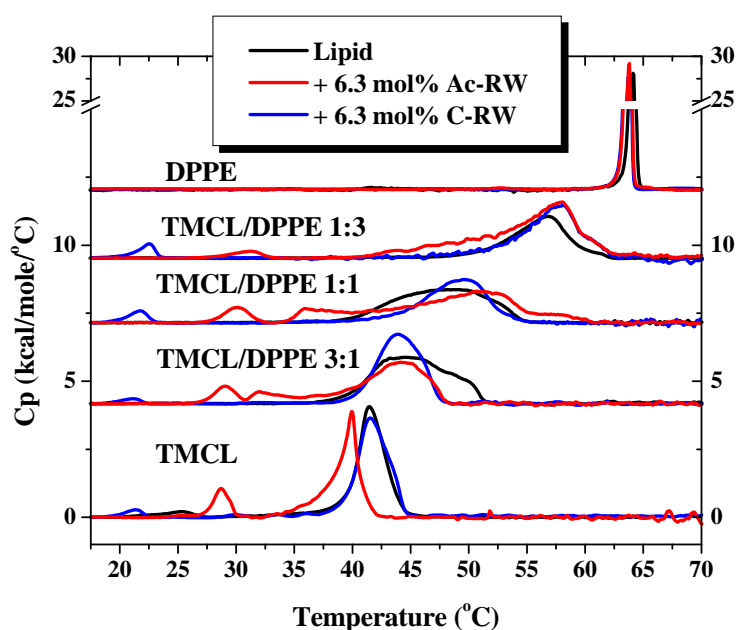


Figure 5.2-8 DSC curves of TMCL/DPPE mixtures (total lipid concentration 1 – 2 mM) without and with added peptides Ac-RW and C-RW (L/P 15:1). The samples were prepared in buffer (10 mM Tris, 154 mM NaCl, pH 7.4).

5.2.2.3 DSC of three-component lipid membranes

The influence of the peptides on DPPG/DPPE/TMCL 1:1:1 ternary mixed membrane is demonstrated in **Figure 5.2-9**, which shows the thermograms of the free mixture as well as after the addition of 6.3 mol% Ac-RW and C-RW, respectively. The ternary mixture showed one broad phase transition with T_m , ΔH and HHW of 45.2°C, 11.4 kcal mol⁻¹ and 8°C, respectively. The interaction with the peptides induced three major endothermic transitions; at 27.9, 35.3 and 48.1°C in case of Ac-RW and at 24.5, 32.8 and 46.7°C in case of C-RW. We anticipate that the lower-temperature transition was the subtransition of TMCL induced by the peptides, whereas the other two transitions belonged to peptide-DPPG-rich domains at $T < T_{\text{pure}}$ and DPPE-rich domains at $T > T_{\text{pure}}$, similar to what observed with DPPG/DPPE mixtures. Our results obtained with binary mixtures as well as the FT-IR experiments with ternary mixtures (discussed later) are in a good agreement with this interpretation. The sum of ΔH of the three transitions in case of C-RW was comparable to that of the free mixture, whereas Ac-RW highly reduced ΔH . This indicates a higher perturbation of the lipid chain packing by Ac-RW.

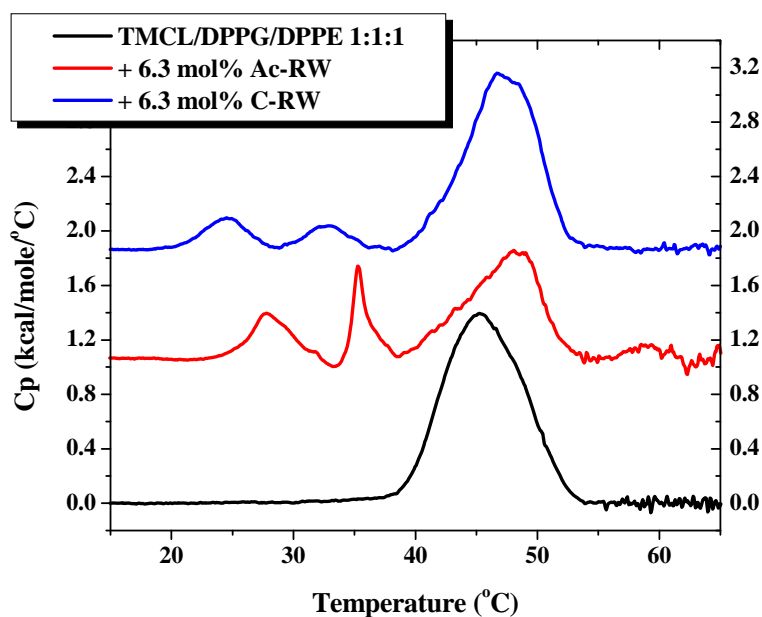


Figure 5.2-9 DSC curves of the ternary TMCL/DPPG/DPPE 1:1:1 mixture (total lipid concentration 1 – 2 mM) without and with added peptides Ac-RW and C-RW (L/P 15:1). The samples were prepared in buffer (10 mM Tris, 154 mM NaCl, pH 7.4).

5.2.3 Fourier Transform Infrared (FT-IR)

To verify the results obtained by DSC experiments, FT-IR-spectroscopy was used to examine the influence of the peptides on single component, binary and ternary multilamellar lipid films as well as to investigate the thermotropic transitions of the lipid-peptide mixtures. Here we were specifically interested in answering the question whether the peptides indeed induced demixing in DPPG/DPPE and DPPG/DPPE/TMCL mixtures, since FT-IR can serve as a tool to follow lipid demixing (Redfern and Gericke 2004). The complementary and consistent nature of the information provided with FT-IR and DSC was exhibited many times in literature, e.g. (Brauner and Mendelsohn 1986). To this end, we used lipid mixtures where one of the components contained perdeuterated acyl chains. This enabled the distinction of transitions of the individual components separately.

Because the frequencies of the symmetric and antisymmetric CH_2 stretching vibrations ($\nu_s(\text{CH}_2)$ at $\sim 2850 \text{ cm}^{-1}$ and $\nu_{\text{as}}(\text{CH}_2)$ at $\sim 2929 \text{ cm}^{-1}$, respectively) are sensitive to the conformation of the lipid acyl chains, they can be used to follow the changes in the *trans/gauche* ratio occurring at the lipid phase transition (Mantsch and McElhaney 1991; Schwieger and Blume 2007; Tuchtenhagen et al. 1994). The "melting" of the all-*trans* chains in the gel phase to the liquid phase, which is associated with an increase in the number of *gauche* conformers, is accompanied by an increase in the $\nu_s(\text{CH}_2)$ and $\nu_{\text{as}}(\text{CH}_2)$ vibrational

frequencies. For the lipids with the perdeuterated chains, the corresponding $\nu_s(\text{CD}_2)$ and $\nu_{\text{as}}(\text{CD}_2)$ vibrational frequencies are at lower wavenumber ($\sim 2090 \text{ cm}^{-1}$ and $\sim 2195 \text{ cm}^{-1}$, respectively) due to the vibrational isotope effect. In addition, the transition temperatures of lipids with perdeuterated chains are generally somewhat lower (Mantsch and McElhaney 1991). For instance, since the T_m of DPPG- $\text{d}_{62} \sim 37^\circ\text{C}$ is lower than the T_m of DPPG $\sim 40.6^\circ\text{C}$, the phase transition of the DPPG- d_{62} -containing lipid mixtures will take place at lower temperatures as compared to the DPPG-containing lipid mixtures with the same composition.

5.2.3.1 FT-IR of one-component lipid membranes

The temperature dependence of the wavenumber of the $\nu_{\text{as}}(\text{CD}_2)$ vibrational band in DPPG- d_{62} and DPPG- d_{62} /C-RW 6:1 (14.3 mol% C-RW) is displayed in **Figure 5.2-10**. The first derivative of the curves was calculated to detect more precisely the T_m of the lipids and lipid-peptide mixtures. The T_m of pure DPPG- d_{62} was $\sim 37^\circ\text{C}$ and decreased by $\sim 1.5^\circ\text{C}$ upon premixing with 14.3 mol% C-RW. The interaction of C-RW and DPPG- d_{62} induced a down-shift in the CD_2 stretching vibrations below T_m , whereas above T_m the CD_2 stretching vibrations remained unaltered. The slight down-shift in the stretching vibrations is usually explained by an increase in order of the acyl chains. However, the binding of C-RW into the hydrophobic core of the lipid membrane leads to a slight decrease in T_m , indicating a less ordered packing of the acyl chains of the lipid. Therefore, the decrease in wavenumber is probably due to other effects, which are unexplained at present but have been regularly observed upon binding of cationic peptides to negatively charged phospholipids. A probable explanation is the increase in interchain vibrational coupling caused by a reduction of rotational disorder of the chains after peptide binding (Schwieger 2008).

In order to gain analyzable information about the DPPG carbonyl groups as well as the secondary structure assumed by the peptides, we repeated the experiments in D_2O . The amide I and guanidinium, i.e. the charged end group of arginine ($-\text{CN}_3\text{H}_5^+$), vibrational bands of the free and DPPG- d_{62} bound peptide are shown in **Figure 5.2-11** and **Figure 5.2-12**, respectively. In case of the free peptides (**Figure 5.2-11**), the wavenumber of the asymmetric and symmetric stretching vibrations of guanidinium in D_2O was ~ 1608 and $\sim 1585 \text{ cm}^{-1}$, respectively, which agrees well with literature (Chirgadze et al. 1975; Tamm and Tatulian 1997). The electrostatic interaction and hydrogen bonding between the guanidyl groups of C-RW and Ac-RW and the PG headgroups shifted guanidyl bands to lower wavenumbers,

namely, by ~ 4.5 and $\sim 6 \text{ cm}^{-1}$, respectively. The higher down-shift observed with Ac-RW could be due to a stronger binding to the PG headgroups or to a different degree of hydration.

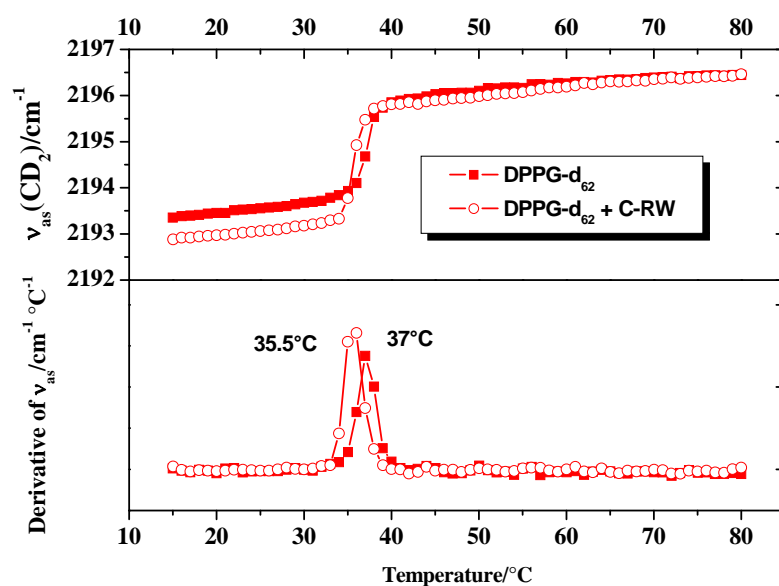


Figure 5.2-10 (Top) Temperature dependence of the wavenumber of the antisymmetric CD_2 -stretching band of 60 mM DPPG-d_{62} liposomes without and with 14.3 mol% C-RW (L/P 6:1). The samples were prepared in H_2O (100 mM NaCl). **(Bottom)** First derivate of the curves shown at the top.

The free linear peptide showed an amide I band at $\sim 1643 \text{ cm}^{-1}$ indicating an unstructured sequence (Goormaghtigh et al. 1994; Tamm and Tatulian 1997). The binding of Ac-RW to DPPG-d_{62} provoked the formation of β -structures as concluded from the amide I band $\sim 1631 \text{ cm}^{-1}$. The reported decrease in the flexibility of Ac-RW upon the binding to lipid membranes (Dathe et al. 2004; Jing et al. 2003) concurs with our IR spectra. On the other hand, the amide I peaks observed in the IR spectra of free C-RW at ~ 1630 and $\sim 1672 \text{ cm}^{-1}$ reflected the β -turn conformation observed in the NMR structure (Appelt et al. 2005b). In addition, the interaction with PG headgroups did not alter the Amide I bands of C-RW confirming its constrained structure.

The influence of temperature (heating from 20 to 76°C) on the guanidyl and amide I vibrational bands was modest, which could be due to changes in the hydration of the lipids. The bands recovered their original positions after cooling down the samples to 20°C .

The interaction of the peptides with DPPG-d_{62} highly reduced the hydration of the carbonyl groups (data not shown). This was due to the pronounced release of water molecules upon the binding of the peptides, which is in a good agreement with the high entropy change observed in the ITC titrations (see below). This is common for lipid-peptide interactions. The

hydrogen bonding between the peptides and the carbonyl groups down-shifted the carbonyl bands, which was more pronounced in the case of Ac-RW.

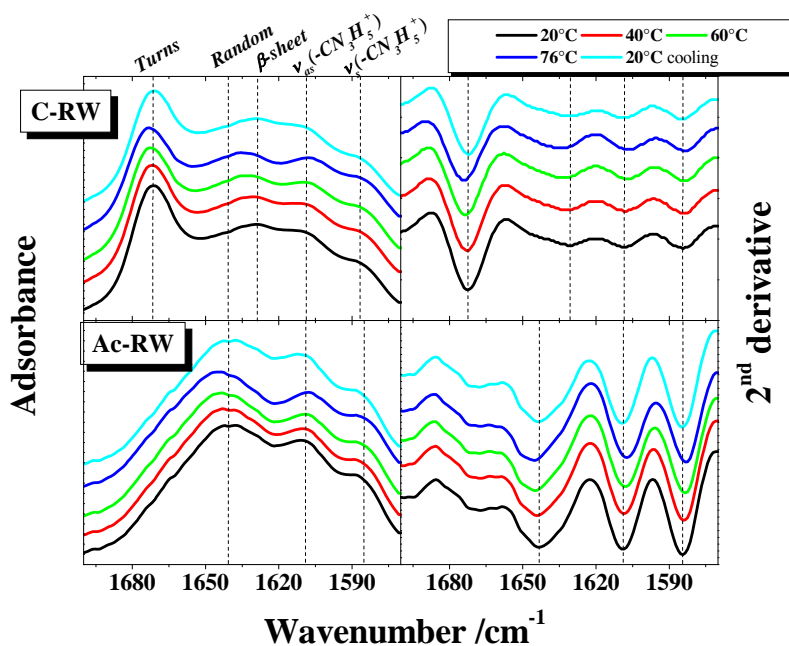


Figure 5.2-11 Amide I and guanidinium vibrational bands (left) and their second derivative (right) of 10 mM Ac-RW and C-RW, respectively, in D₂O (100 mM NaCl) at various temperatures through the heating phase from 20°C to 76°C and the cooling back to 20°C.

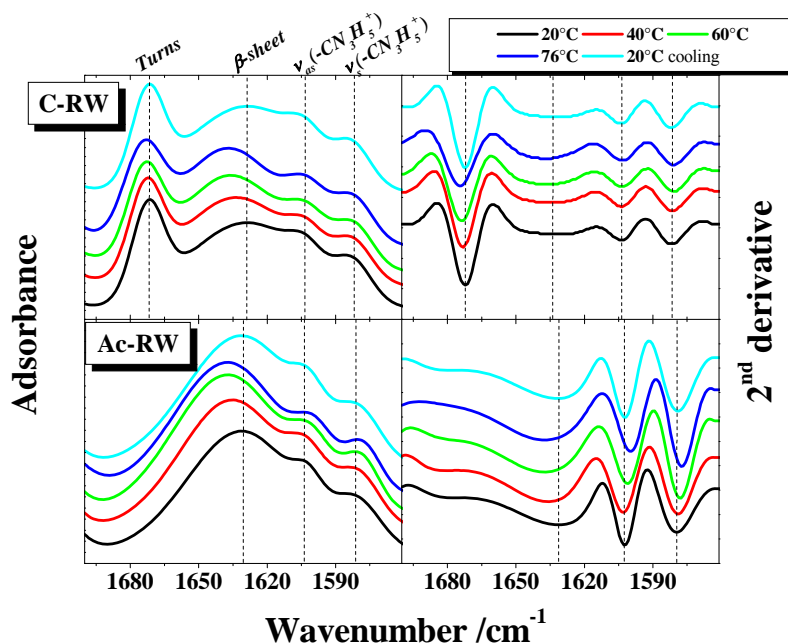


Figure 5.2-12 Amide I and guanidinium vibrational bands (left) and their second derivative (right) of 10 mM Ac-RW and C-RW peptides, respectively, premixed with 60 mM DPPG-d₆₂ (L/P 6:1) in D₂O (100 mM NaCl) at various temperatures through the heating phase from 20°C to 76°C and the cooling back to 20°C.

The incorporation of cardiolipin in our model membrane was necessary for a closer mimic of the real bacterial membranes. Therefore, we studied first the effect of C-RW on TMCL. **Figure 5.2-13** shows the temperature dependence of the CH_2 symmetric stretching and scissoring vibrations, i.e. $\nu_s(\text{CH}_2)$ and $\delta(\text{CH}_2)$, respectively, as well as the first derivative of $\nu_s(\text{CH}_2)$. The wavenumber of $\nu_s(\text{CH}_2)$ is determined by the *trans/gauche* content of the lipid hydrocarbon chains, whereas $\delta(\text{CH}_2)$ is sensitive to the lateral packing interactions between hydrocarbon chains (Lewis et al. 2007; Mantsch and McElhaney 1991; Tamm and Tatulian 1997).

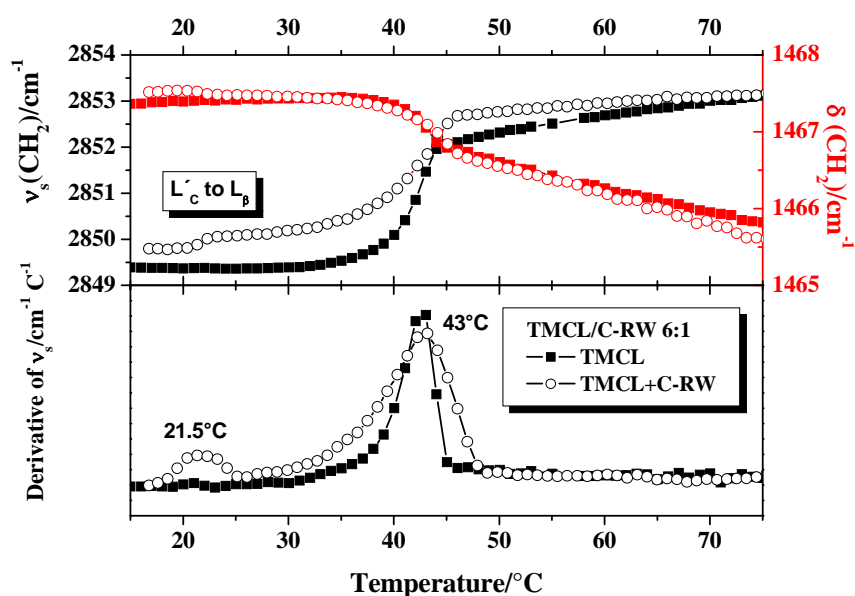


Figure 5.2-13 (Top) Temperature dependence of the wavenumber of the symmetric CH_2 -stretching band (left ordinate) and of the wavenumber of the CH_2 -scissoring band (right ordinate) of **TMCL** (60 mM) without (full symbols) and with 14.3 mol% added peptide C-RW (L/P 6:1) (open symbols). The samples were prepared in H_2O (100 mM NaCl). (Bottom) First derivative of the curves shown in the top diagram.

The chain melting (L_β/L_α transition) of free TMCL was at $\sim 43^\circ\text{C}$ and was accompanied by an increase in the wavenumber of $\nu_s(\text{CH}_2)$ and a moderate decrease in the wavenumber of $\delta(\text{CH}_2)$. However, no significant changes in the wavenumber of $\nu(\text{CH}_2)$ were observed during the L'_C/L_β transition ($\sim 25^\circ\text{C}$, see **Figure 5.2-7**), which is similar to what was reported by Lewis et al. (2007) (Lewis et al. 2007). The addition of 14.3 mol% C-RW did not alter the lipid chain packing or the main transition temperature of TMCL, however, a cooperative step-like increase in the wavenumber of $\nu_s(\text{CH}_2)$ was observed at $\sim 21.5^\circ\text{C}$, which suggests a peptide-induced formation of the L'_C phase at low temperatures. The wavenumber

of $\delta(\text{CH}_2)$ ($1465.5 - 1467.5 \text{ cm}^{-1}$) proposes that the hydrocarbon chains of free and bound TMCL were hexagonally arranged in the gel and liquid-crystalline phases.

5.2.3.2 FT-IR of two-component lipid membranes

The temperature dependence of the frequencies of the $\nu_{\text{as}}(\text{CD}_2)$ and $\nu_{\text{as}}(\text{CH}_2)$ vibrational bands in a DPPG- d_{62} /DMPC 1:1 lipid mixture and in DPPG- d_{62} /DMPC 1:1 premixed with 14.3 mol% C-RW is illustrated in **Figure 5.2-14**. The first derivative of the $\nu_{\text{as}}(\text{CD}_2)$ and $\nu_{\text{as}}(\text{CH}_2)$ bands of DPPG- d_{62} /DMPC lipid mixture, which represent DPPG- d_{62} and DMPC, respectively, showed a $T_m \sim 31^\circ\text{C}$.

The interaction of C-RW with DPPG- d_{62} /DMPC lipid mixture reduced the T_m to $\sim 29^\circ\text{C}$. The similar T_m observed for the individual lipids in DPPG- d_{62} /DMPC mixture with and without C-RW suggests the homogeneity of the lipid film in both cases and no peptide induced phase separation. These results are in accordance with our DSC data shown above. Again, below the phase transition a decrease of the $\nu_{\text{as}}(\text{CD}_2)$ as well as the $\nu_{\text{as}}(\text{CH}_2)$ vibrational bands is observed. Above the phase transition temperature, the wavenumber of the bands is not influenced by the binding of the peptide.

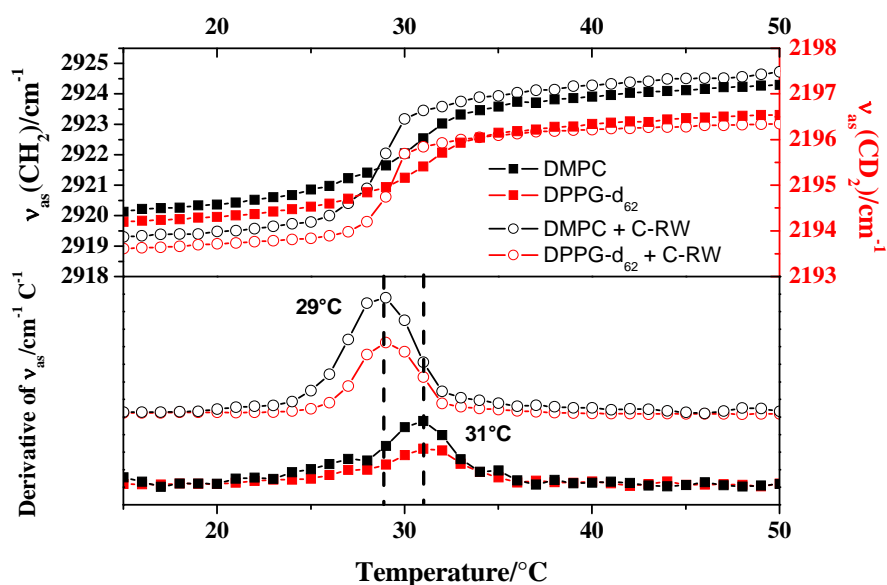


Figure 5.2-14 (Top) Temperature dependence of the wavenumber of the antisymmetric CH_2 -stretching band of DMPC (left ordinate) and of the wavenumber of the antisymmetric CD_2 -stretching band of DPPG- d_{62} (right ordinate) in a DPPG- d_{62} /DMPC 1:1 mixture (total lipid concentration 60 mM) without (full symbols) and with 14.3 mol% added peptide C-RW (L/P 6:1) (open symbols). The samples were prepared in H_2O (100 mM NaCl). **(Bottom)** First derivative of the curves shown in the top diagram.

A different phenomenon was observed from the IR spectra of DPPG-d₆₂ and DPPE in the (DPPG-d₆₂/DPPE 1:1)/C-RW 6:1 mixture (**Figure 5.2-15**). The DPPG-d₆₂/DPPE 1:1 mixture has a T_m of ~54.5°C, and the temperature dependence of the CH₂-band (DPPE) as well as the CD₂-band (DPPG-d₆₂) show the same transition temperature (see lower panel of **Figure 5.2-15**).

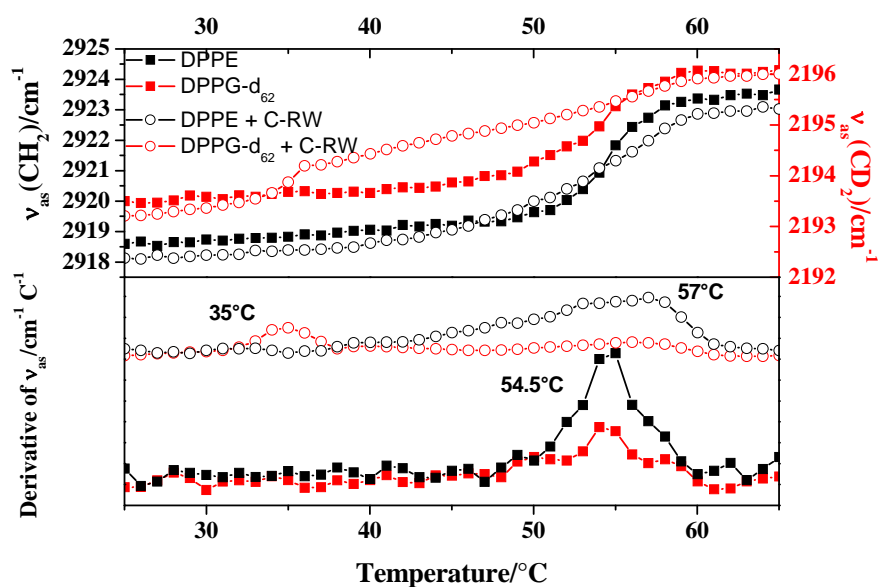


Figure 5.2-15 (Top) Temperature dependence of the wavenumber of the antisymmetric CH₂-stretching band of DPPE (left ordinate) and of the wavenumber of the antisymmetric CD₂-stretching band of DPPG-d₆₂ (right ordinate) in a DPPG-d₆₂/DPPE 1:1 mixture (total lipid concentration 60 mM) without (full symbols) and with 14.3 mol% added peptide C-RW (L/P 6:1) (open symbols). The samples were prepared in H₂O (100 mM NaCl). **(Bottom)** First derivative of the curves shown in the top diagram.

Upon the addition of C-RW, the wavenumber of the CH₂ vibrational band, which represents DPPE, showed a broad asymmetrical phase transition over a temperature range of 40 – 60°C, with a peak maximum ~ 57°C. In contrast, the wavenumber of the CD₂ band of DPPG-d₆₂ revealed a sharp transition ~ 35°C followed by a much wider transition at a higher temperature (40 – 60°C) (see lower panel of **Figure 5.2-15**). The presence of a phase transition ~ 35°C observed in the temperature dependence of the DPPG-d₆₂ band and its absence in the DPPE band supports the conclusion that demixing of the DPPG-d₆₂/DPPE lipid mixture together with the formation of a DPPG-d₆₂-C-RW complex has occurred. Again, the observations obtained by FT-IR agree well with the DSC results presented above. In the case of the DPPG-d₆₂/DPPE lipid mixture a slight overall decrease in the wavenumber of the CH₂ as well as the CD₂ stretching vibrational bands is observed, in the gel and somewhat less also at high temperature in the liquid-crystalline phase of the bilayers. The usual interpretation that

this is due to an increase in chain order does not hold, because then an overall increase in the transition temperature should occur. The suggestion presented above is probably also valid here, i.e. the decrease in wavenumber is due to increased vibrational interchain coupling, because the rotational disorder is reduced by the peptide binding (Schwieger 2008).

The influence of C-RW on TMCL/DPPE-d₆₂ 1:1 mixture is shown in **Figure 5.2-16**. Both lipids in the free mixture underwent the L_β/L_α phase transition at the same temperature ~ 50.5°C, which indicates the homogeneity of the lipid mixture. The addition of 14.3 mol% C-RW destabilized the mixture where T_m was decreased to ~ 49°C. Furthermore, the peptide caused a cooperative increase in the wavenumber of ν_s(CH₂) of TMCL at ~ 23°C, whereas no such changes were seen in the wavenumber of ν_s(CD₂) of DPPE-d₆₂. This could be due to a peptide induced subtransition of TMCL, which would indicate the formation of TMCL domains in the mixture.

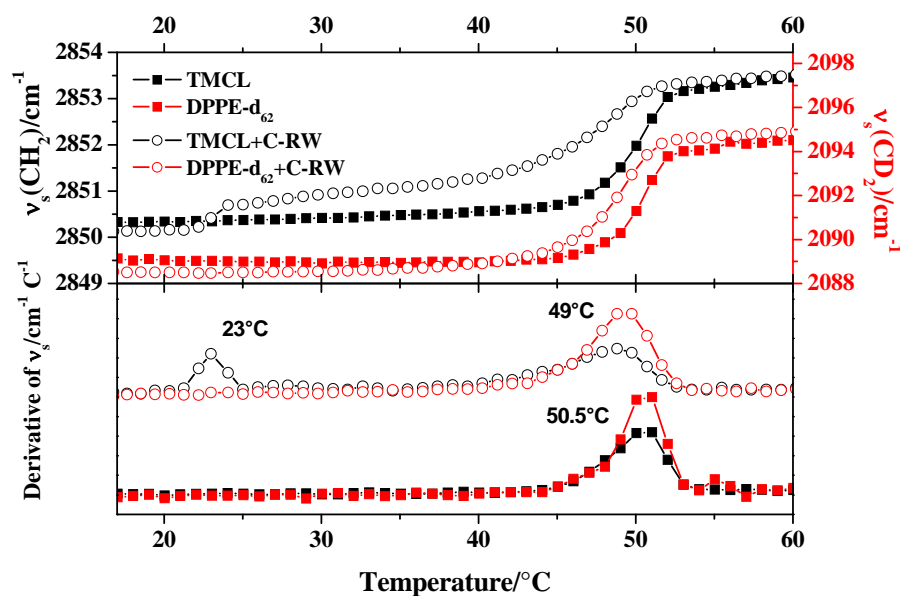


Figure 5.2-16 (Top) Temperature dependence of the wavenumber of the symmetric CH₂-stretching band of TMCL (left ordinate) and of the wavenumber of the symmetric CD₂-stretching band of DPPE-d₆₂ (right ordinate) in a TMCL/DPPE-d₆₂ 1:1 mixture (total lipid concentration 60 mM) without (full symbols) and with 14.3 mol% added peptide C-RW (L/P 6:1) (open symbols). The samples were prepared in H₂O (100 mM NaCl). **(Bottom)** First derivative of the curves shown in the top diagram.

TMCL/DPPG-d₆₂ 1:1 mixture showed a T_m at ~ 41°C (**Figure 5.2-17**). The addition of 14.3 mol% C-RW induced some demixing, as indicated by the slight cooperative increase in the wavenumber of ν_s(CD₂) of DPPG-d₆₂ at ~ 28°C and the up-shift in T_m of the TMCL-enriched domains to ~ 42°C. The demixing was not pronounced, since the increase in the wavenumber of stretching vibrations during the chain melting was not broadened. No

subtransition was detected in both TMCL/DPPG-d₆₂ 1:1 mixtures and this is in accordance with the DSC data.

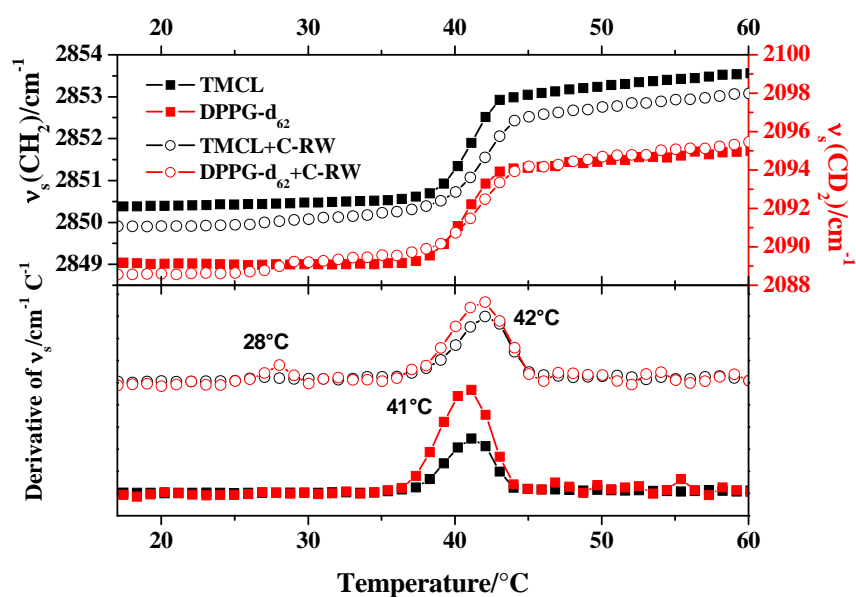


Figure 5.2-17 (Top) Temperature dependence of the wavenumber of the symmetric CH₂-stretching band of TMCL (left ordinate) and of the wavenumber of the symmetric CD₂-stretching band of DPPG-d₆₂ (right ordinate) in a TMCL/DPPG-d₆₂ 1:1 mixture (total lipid concentration 60 mM) without (full symbols) and with 14.3 mol% added peptide C-RW (L/P 6:1) (open symbols). The samples were prepared in H₂O (100 mM NaCl). **(Bottom)** First derivative of the curves shown in the top diagram.

DPPG and TMCL have a similar phase transition temperature. In addition, the subtransition of TMCL and the chain melting of the peptide-bound DPPG occur at the same temperature range. In an attempt to disentangle this overlapping, which was necessary for studying ternary mixtures, we investigated binary and ternary mixed membranes that contained undeuterated and perdeuterated DMPG instead of their DPPG analogues, since DMPG melts at a much lower temperature (T_m of DMPG and DMPG-d₅₄ is ~ 24 and ~ 20°C, respectively). This might also be useful to check the influence of the acyl chain length of lipids.

Figure 5.2-18 shows the results obtained with TMCL/DMPG-d₅₄ 1:1. In the lipid mixtures with and without peptide, the phase transition of DMPG-d₅₄ started at a slightly lower temperature than TMCL. This is because pure DMPG-d₅₄ has a T_m significantly lower than the T_m of pure TMCL. The addition of 14.3 mol% C-RW caused a moderate lipid demixing. Again, the DMPG-d₅₄-C-RW complex formation is evident by the broadened phase transition of DMPG-d₅₄, which started at ~ 18.5°C, whereas the T_m of the DMPG-d₅₄-depleted

lipid mixture was increased by 1 – 2°C. No subtransition was detected in the TMCL/DMPG-d₅₄ 1:1 mixtures, comparable to what is observed with TMCL/DPPG mixtures.

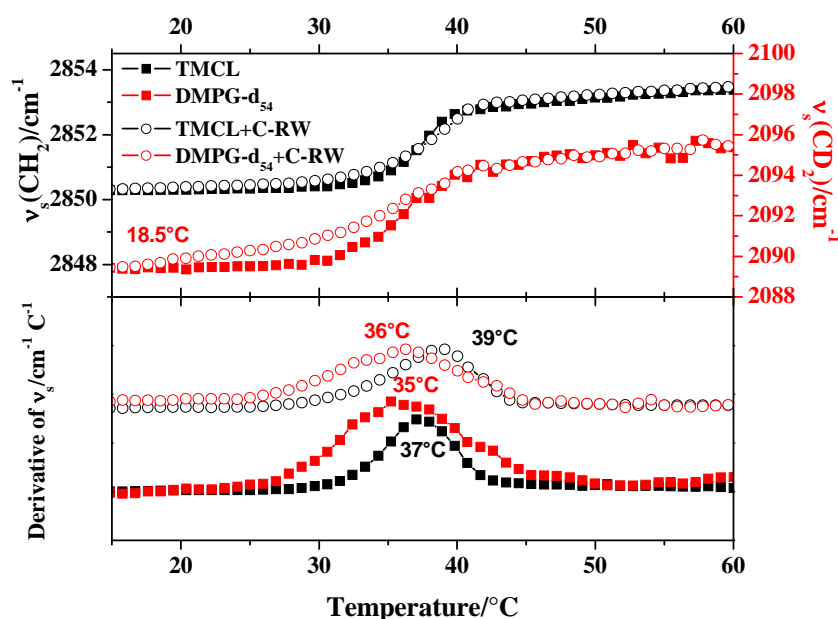


Figure 5.2-18 (Top) Temperature dependence of the wavenumber of the symmetric CH₂-stretching band of TMCL (left ordinate) and of the wavenumber of the symmetric CD₂-stretching band of DMPG-d₅₄ (right ordinate) in a TMCL/DMPG-d₅₄ 1:1 mixture (total lipid concentration 60 mM) without (full symbols) and with 14.3 mol% added peptide C-RW (L/P 6:1) (open symbols). The samples were prepared in H₂O (100 mM NaCl). **(Bottom)** First derivative of the curves shown in the top diagram.

5.2.3.3 FT-IR of three-component lipid membranes

Investigating the effects of C-RW on TMCL/DPPG/DPPE and TMCL/DMPG/DPPE mixtures with FT-IR helps us to monitor the individual components in the ternary model membrane. The experiment was performed twice for each mixture, one time using a mixture of DPPE-d₆₂, TMCL and either DPPG or DMPG, and the other time using a mixture of DPPE, TMCL and either DPPG-d₆₂ or DMPG-d₅₄.

Figure 5.2-19 illustrates the temperature dependence of the frequencies of $\nu_s(\text{CH}_2)$ and $\nu_s(\text{CD}_2)$ in the TMCL/DPPG/DPPE-d₆₂ 1:1:1 system, which represent the change in chain order of TMCL/DPPG and DPPE-d₆₂, respectively. The three components in the pure mixture show a uniform T_m at ~ 47°C. After the addition of the peptide, TMCL/DPPG mixture shows two phase transitions at ~ 27 and ~ 48°C, whereas DPPE-d₆₂ undergoes only one phase transition at ~ 48°C. We anticipate that the lower temperature transition (~ 27°C) belongs to the peptide-bound DPPG and, possibly, to the peptide-induced subtransition of TMCL, whereas the transition at ~ 48°C is, most probably, of the DPPE-enriched lipid mixture.

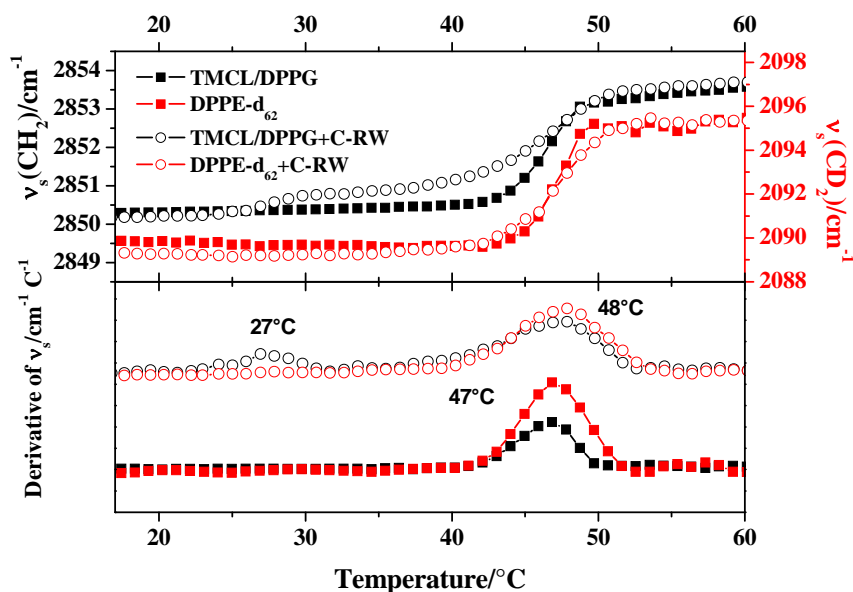


Figure 5.2-19 (Top) Temperature dependence of the wavenumber of the symmetric CH_2 -stretching band of TMCL/DPPG 1:1 mixture (left ordinate) and of the wavenumber of the symmetric CD_2 -stretching band of DPPE- d_{62} (right ordinate) in a TMCL/DPPG/DPPE- d_{62} 1:1:1 ternary mixture (total lipid concentration) without (full symbols) and with 14.3 mol% added peptide C-RW (L/P 6:1) (open symbols). The samples were prepared in H_2O (100 mM NaCl). (Bottom) First derivative of the curves shown in the top diagram.

To follow the change in DPPG chain order separately, we inspected TMCL/DPPE/DPPG- d_{62} 1:1:1 lipid mixture (**Figure 5.2-20**). In this case, $\nu_s(\text{CH}_2)$ and $\nu_s(\text{CD}_2)$ represent the chain order of TMCL/DPPE and DPPG- d_{62} , respectively. The T_m of the ternary mixture without peptide is $\sim 48.5^\circ\text{C}$. The addition of C-RW increases T_m of the mixture to $\sim 51^\circ\text{C}$ and slightly broadens the chain melting, which starts at $\sim 24.5^\circ\text{C}$. This again indicates some demixing of the lipid components in the mixture.

In the following mixtures, DPPG was replaced with DMPG which has a lower T_m . **Figure 5.2-21** illustrates the temperature dependence of the frequencies of $\nu_s(\text{CH}_2)$ and $\nu_s(\text{CD}_2)$ in the TMCL/DMPG/DPPE- d_{62} 1:1:1 system. The addition of C-RW induces a demixing in the TMCL/DMPG/DPPE- d_{62} 1:1:1 mixture, which is more pronounced than what is observed with TMCL/DPPG/DPPE- d_{62} 1:1:1 mixture (see **Figure 5.2-19**). Again, the demixing is evident by the cooperative transition at $T < T_m$ and the up-shift and broadening of the chain melting at $T > T_m$. The influence of the peptide on TMCL/DPPE/DMPG- d_{54} 1:1:1 is shown in **Figure 5.2-22**. The C-RW peptide segregates DMPG- d_{54} in the mixture inducing an extensive lipid demixing. The peptide bound DMPG- d_{54} melted at $\sim 18^\circ\text{C}$. Interestingly, the subtransition of TMCL is not observed, which can be due to the lower T_m of DMPG- d_{54} .

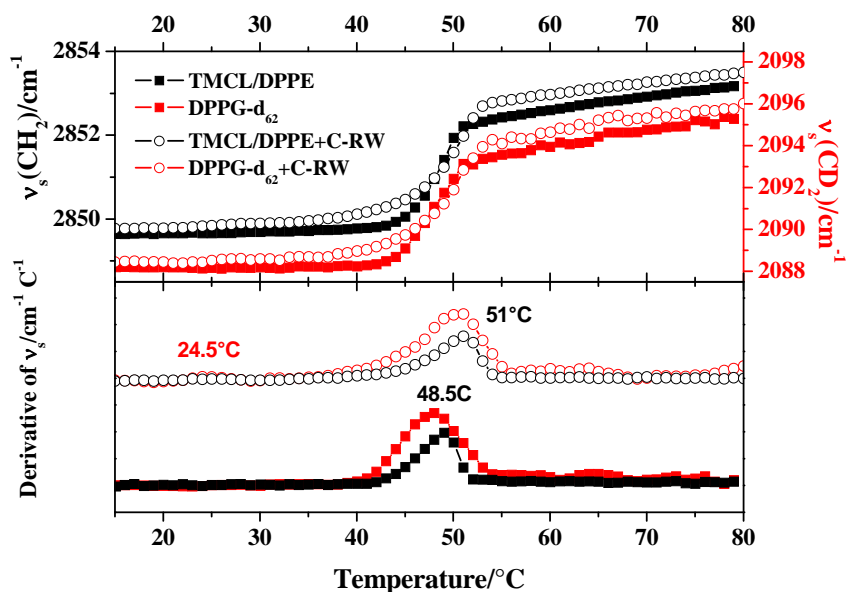


Figure 5.2-20 (Top) Temperature dependence of the wavenumber of the symmetric CH_2 -stretching band of TMCL/DPPE 1:1 mixture (left ordinate) and of the wavenumber of the symmetric CD_2 -stretching band of DPPG- d_{62} (right ordinate) in a TMCL/DPPE/DPPG- d_{62} 1:1:1 ternary mixture (total lipid concentration 60 mM) without (full symbols) and with 14.3 mol% added peptide C-RW (L/P 6:1) (open symbols). The samples were prepared in H_2O (100 mM NaCl). (Bottom) First derivative of the curves shown in the top diagram.

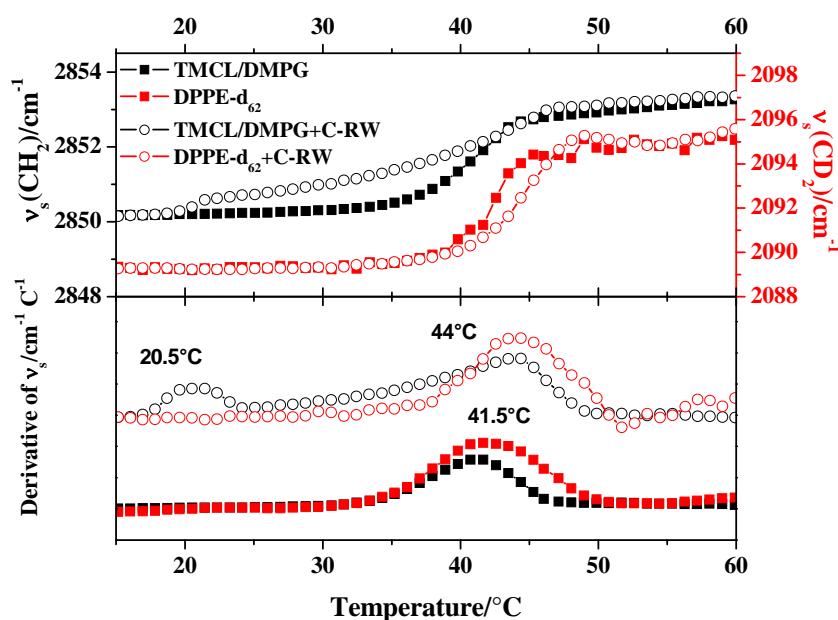


Figure 5.2-21 (Top) Temperature dependence of the wavenumber of the symmetric CH_2 -stretching band of TMCL/DMPG 1:1 mixture (left ordinate) and of the wavenumber of the symmetric CD_2 -stretching band of DPPE- d_{62} (right ordinate) in a TMCL/DMPG/DPPE- d_{62} 1:1:1 ternary mixture (total lipid concentration 60 mM) without (full symbols) and with 14.3 mol% added peptide C-RW (L/P 6:1) (open symbols). The samples were prepared in H_2O (100 mM NaCl). (Bottom) First derivative of the curves shown in the top diagram.

The more pronounced demixing that is observed with DMPG-containing mixtures as compared to DPPG-containing mixtures can be due to the lower T_m of DMPG or to the difference in the length of the acyl chains of the two lipids.

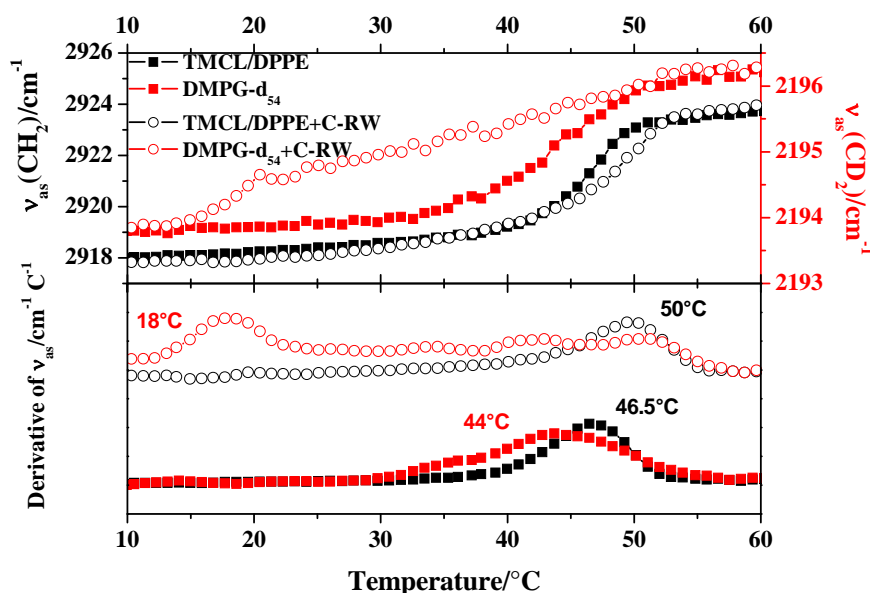


Figure 5.2-22 (Top) Temperature dependence of the wavenumber of the antisymmetric CH₂-stretching band of TMCL/DPPE 1:1 mixture (left ordinate) and of the wavenumber of the antisymmetric CD₂-stretching band of DMPG-d₅₄ (right ordinate) in a TMCL/DPPE/DMPG-d₅₄ 1:1:1 ternary mixture (total lipid concentration 60 mM) without (full symbols) and with 14.3 mol% added peptide C-RW (L/P 6:1) (open symbols). The samples were prepared in H₂O (100 mM NaCl). (Bottom) First derivative of the curves shown in the top diagram.

5.2.3.4 FT-IR of DPPG-d₆₂/POPE 1:1 mixture

Carrying out DSC and FT-IR experiments with unsaturated lipids is hampered by their very low T_m . In order to answer the question whether our peptides can induce lipid demixing in membranes that contain unsaturated lipids, we investigated the influence of C-RW on a DPPG-d₆₂/POPE lipid mixture by means of FT-IR. The temperature dependence of the CH₂ and CD₂ stretching vibrations of the mixture before and after the addition of 14.3 mol% C-RW are presented in **Figure 5.2-23**. Even though the majority of chain melting of the free lipid mixture takes place at $\sim 30.5^\circ\text{C}$, gradual *trans/gauche* conformational changes occur over a much wider temperature range (12 – 42°C). However, this temperature range obviously exceeds T_m of the single components POPE and DPPG-d₆₂, which is ~ 25 and $\sim 37^\circ\text{C}$, respectively. Further experiments are necessary to explain this behaviour. The interaction with C-RW decreases T_m of the mixture to $\sim 26^\circ\text{C}$ (**Figure 5.2-23**). The decrease in T_m points out

to a substantial destabilization of the lipid mixture, where the shoulder on the high temperature side suggests a moderate segregation of DPPG-d₆₂.

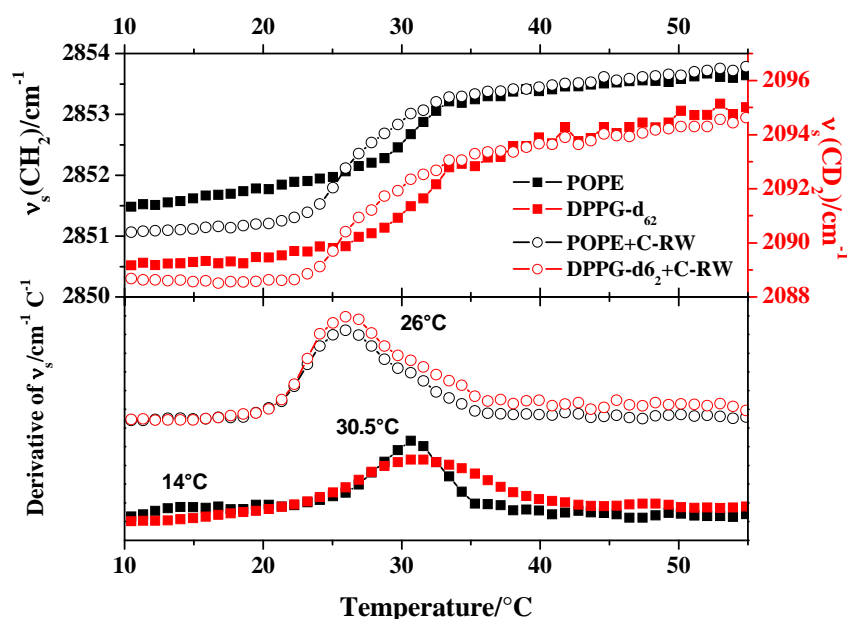


Figure 5.2-23 (Top) Temperature dependence of the wavenumber of the symmetric CH₂-stretching band of POPE (left ordinate) and of the wavenumber of the symmetric CD₂-stretching band of DPPG-d₆₂ (right ordinate) in a DPPG-d₆₂/POPE 1:1 mixture (total lipid concentration 60 mM) without (full symbols) and with 14.3 mol% added peptide C-RW (L/P 6:1) (open symbols). The samples were prepared in H₂O (100 mM NaCl). **(Bottom)** First derivative of the curves shown in the top diagram.

Those results are in accordance with our assumption, as we indeed do not expect an extensive lipid demixing as observed with the saturated lipid mixtures. This is due to the fluid nature of POPE as compared to DPPE. However, the mixture of the saturated gel-state DPPG and the unsaturated fluid POPE was not entirely homogeneous, a phenomenon that was observed with comparable mixtures (Lupi et al. 2008). We anticipate that the phase separation in fluid mixtures might still occur but is probably on a much smaller scale and therefore difficult to prove.

5.2.4 Isothermal Titration Calorimetry (ITC)

ITC was utilized before to study the interaction of Ac-RW and C-RW with fluid lipid membranes. The reported association constant of the binding of Ac-RW to POPG and POPC LUV was 2.1×10^5 and $6.7 \times 10^4 \text{ M}^{-1}$, respectively (Jing et al. 2003). The cyclization improved the affinity of the peptide towards charged and uncharged vesicles (Dathe et al. 2004).

We carried out calorimetric titrations to characterize the interaction of Ac-RW and C-RW peptides with DPPG and DPPG containing vesicles. The main aim was to seek possible

differences between the thermodynamic profiles of the peptides, which could explain the discrepancy in their behaviour. The influence of temperature, salt concentration, surface charge density and the zwitterionic headgroup on the binding was also studied. The ITC isotherms were fitted using the “one-binding-site” model provided by the ORIGIN[®] software in order to determine the apparent binding constant (K_{app}), the binding enthalpy (ΔH°) and the lipid/peptide binding stoichiometry (N). The standard free energy (ΔG°) and entropy (ΔS°) of the binding were calculated using the standard equations $\Delta G^\circ = -RT \ln K_{app}$ and $\Delta S^\circ = (\Delta H^\circ - \Delta G^\circ)/T$, respectively.

5.2.4.1 Interactions with DPPG LUV

As shown in **Figure 5.2-24 (left)**, the experimental power signal, which resulted from titrating 5 mM DPPG LUV into 20 μ M Ac-RW solution in the reaction cell at 15°C, was exothermic with a complex biphasic shape. Interestingly, no such complex isotherm was observed in the ITC experiments carried out before with the fluid lipids POPG and POPC but rather step-like isotherms (Dathe et al. 2004; Jing et al. 2003). Despite the “almost” gradual decrease in the height of the experimental power signal of the titration peaks (**Figure 5.2-24 (left, top)**), the integrated peaks, which represent the reaction heat as a function of the DPPG/Ac-RW molar ratio, showed a different dependence (**Figure 5.2-24 (left, bottom)**). This is because the spacing between some of the injections was not long enough for the power signal to return to the baseline, which was due to the occurrence of some slow processes. In addition, many exothermic peaks were followed by a small endothermic peak. This decreased the value of the exothermic enthalpy per injection after the integration of the whole peak.

Isotherms with a comparable biphasic shape were reported before in literature for interactions of other antimicrobial peptides with fluid membranes and were correlated to reversible pore formation/pore disintegration processes (Wenk and Seelig 1998; Wieprecht et al. 2000b). The biphasic ITC isotherm was explained as a superposition of two co-occurring processes; an exothermic binding coupled to an endothermic pore formation until a critical L/P ratio was exceeded, thereafter, an exothermic pore disintegration took place. Therefore, the enthalpy at the beginning of the titration was less exothermic than expected for pure binding, whereas beyond the threshold ratio the enthalpy became more exothermic than expected (Wieprecht and Seelig 2002).

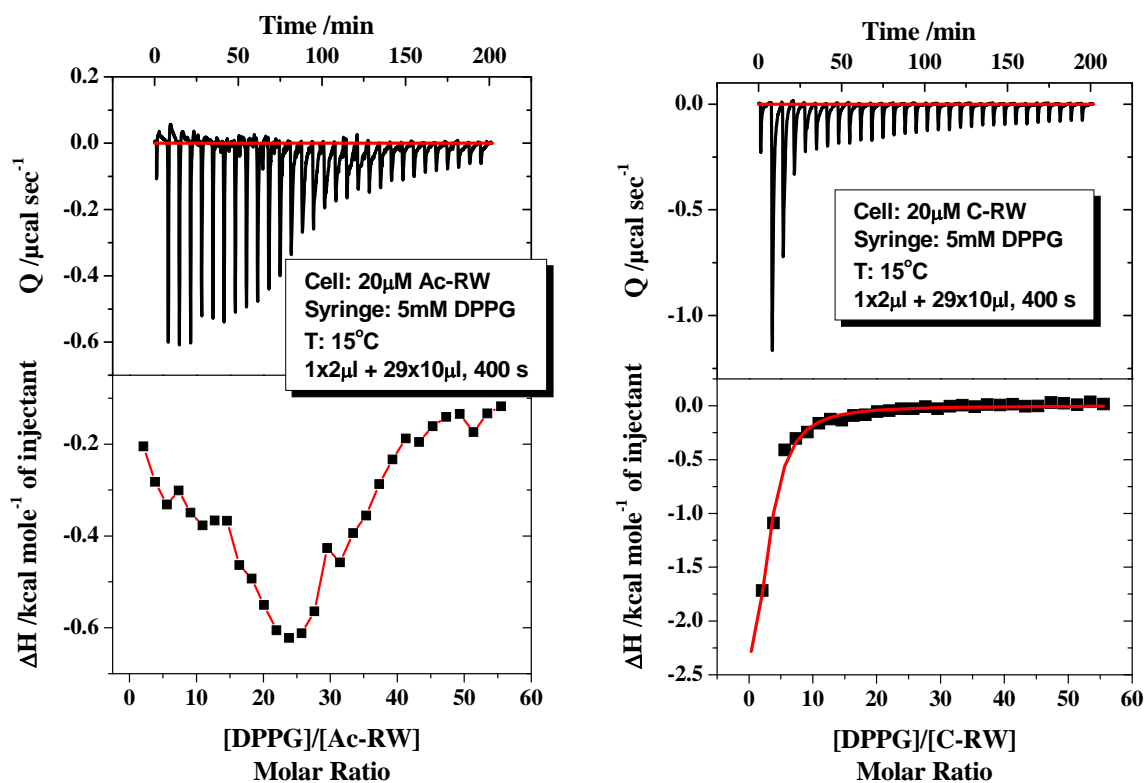


Figure 5.2-24 The experimental power signals (top) and the integrated peaks as a function of DPPG/peptide ratio (bottom) of the titration of DPPG LUV (5 mM) in the syringe into Ac-RW (left) and C-RW (right) peptide solutions (20 μM) in the reaction cell, respectively, at 15°C. The samples were prepared in buffer (10 mM Tris, 154 mM NaCl, pH 7.4).

Under the same conditions, a step-like binding isotherm was observed for the titration of DPPG LUV into C-RW (**Figure 5.2-24 (right)**). The binding parameters are presented in **Table 5.2-2**. The interaction of C-RW with DPPG was enthalpy and entropy driven, i.e. associated with a favourable negative ΔH° and a favourable positive ΔS° . Due to the constrained structure of C-RW, only modest peptide conformational changes were expected to take place after the binding to DPPG. As evident by our DSC and FT-IR experiments (see above), C-RW did not significantly perturb the hydrocarbon chain packing of DPPG molecules. Moreover, no significant peptide-induced phase transition “fluidization” of DPPG bilayers is expected to take place at 15°C. Therefore, we anticipate that the major source of the negative ΔH° was the hydrogen bonding and van der Waals interactions. On the other side, the favourable entropy was due the desolvation of the hydrophobic surfaces of the interacting molecules, i.e. the increase in the rotational and translational degrees of freedom of water molecules.

The stoichiometry of the interaction (N) of C-RW with DPPG, obtained from the employed fit, gives information about the penetrability of the lipid vesicles. The nominal

charge of C-RW is ~ 3 , therefore, N (L/P) of ~ 3 indicates that the peptide freely enters the lipid vesicles and interacts with all DPPG molecules in the system, i.e. inner and outer bilayer leaflets. On the other side, N of ~ 6 implies that the peptide is merely bound to the outer leaflet of the vesicle. However, due to the complex nature of the interaction, N values outside this range can still be observed.

As shown in **Table 5.2-2**, a DPPG/C-RW stoichiometry of ~ 3 is observed at the various temperatures and salt concentrations (see below). This suggests that the peptide freely translocates across the bilayer. The rapid entry of the peptides into DPPG vesicles without a significant membrane disruption is also deduced from the DSC measurements.

Table 5.2-2 The thermodynamic parameters of the interaction of C-RW with lipid vesicles at different conditions.

Peptide	Lipid	[NaCl] (mM)	T (°C)	N	$K_{app} \times 10^{-5} (M^{-1})$	$\Delta H^\circ (kcal mol^{-1})$	$T\Delta S^\circ (kcal mol^{-1})$	$\Delta G^\circ (kcal mol^{-1})$
C-RW	DPPG	154	15	2.32 \pm 0.41	0.32 \pm 0.07	-3.99 \pm 0.83	1.94 \pm 0.72	-5.93 \pm 0.11
C-RW	DPPG	154	25	2.99 \pm 0.02	8.47 \pm 1.55	-3.08 \pm 0.04	5.01 \pm 0.06	-8.08 \pm 0.10
C-RW	DPPG	300	25	2.67 \pm 0.07	6.46 \pm 2.80	-1.77 \pm 0.07	6.15 \pm 0.14	-7.92 \pm 0.21
C-RW	DPPG	500	25	3.09 \pm 0.06	30.40 \pm 19.00	-1.03 \pm 0.04	7.81 \pm 0.25	-8.84 \pm 0.29
C-RW	DPPG/DPPC 3:1	154	25	4.68 (3.5) \pm 0.08	5.25 \pm 2.40	-1.31 \pm 0.04	6.49 \pm 0.19	-7.80 \pm 0.22
C-RW	DPPG/DPPC 1:1	154	25	7.35 (3.7) \pm 0.27	0.50 \pm 0.16	-0.28 \pm 0.01	6.13 \pm 0.15	-6.40 \pm 0.16
C-RW	DPPG/DPPC 1:3	154	25	9.95 (2.5) \pm 21.00	0.03 \pm 0.08	-0.04 \pm 0.10	4.69 \pm 0.66	-4.73 \pm 0.76
C-RW	DPPG/DPPE 3:1	154	25	4.485 (3.4) \pm 0.20	1.30 \pm 0.56	-0.59 \pm 0.04	6.38 \pm 0.18	-6.97 \pm 0.21
C-RW	DPPG/DPPE 1:1	154	25	2.35 (1.2) \pm 2.30	0.13 \pm 0.17	-0.19 \pm 0.23	5.42 \pm 0.26	-5.62 \pm 0.49
C-RW	DPPG/DPPE 1:3	154	25	22.2 (5.6) \pm 0.75	0.88 \pm 0.49	-0.20 \pm 0.01	6.92 \pm 0.24	-7.13 \pm 0.25

(N) Shows the stoichiometry per DPPG molecules. The values in the rows marked bold are inaccurate due to low reaction enthalpy or poor curve fitting of the corresponding ITC isotherms.

5.2.4.2 Influence of temperature

Increasing the temperature from 15 to 25°C pronouncedly enhanced the binding affinity of C-RW towards DPPG, namely, from 3.2×10^4 to $8.5 \times 10^5 M^{-1}$. This increase in K_{app} was of entropic origin, where $T\Delta S^\circ$ increased from 1.94 to 5.01 kcal mol⁻¹, compensated by a decrease in ΔH° from -3.99 to -3.08 kcal mol⁻¹. This enhanced binding at a higher temperature was most probably due to the reduced lipid chain packing and the formation of defects in the membrane, which maximized the hydrophobic interactions as evident by the substantial increase in the entropy change. The decrease in ΔH° over temperature gave rise to a negative change in the specific heat (ΔC_p), which was a mark of the classical hydrophobic effects (White and Wimley 1998). The temperature range in which proper binding ITC curves could be obtained was limited; at $T < 15^\circ C$ the binding affinity became very low, whereas at $T > 25^\circ C$ the peptide induced an endothermic DPPG transition that masked the binding signal (see DSC and FT-IR data) (data not shown). Therefore, we have refrained from analyzing the temperature dependence of the binding parameters quantitatively. In comparison to our

results, the interaction of C-RW with POPC showed similar ΔG° but less favourable entropy and higher favourable enthalpy (Dathe et al. 2004).

5.2.4.3 Influence of salt concentration

To characterize the interaction further, we performed additional titrations at 25°C using higher salt concentrations, namely, 300 and 500 mM NaCl. This procedure has been commonly used to examine the electrostatic contribution to biomolecular associations. The binding affinity of hydrophobic interactions was barely affected by the ionic strength of the solution (Arouri et al. 2007), whereas the affinity of strongly electrostatic associations decreased substantially with increasing the salt concentration (Binder and Lindblom 2003; Klocek and Seelig 2008; Lundback and Hard 1996; Zhang and Rowe 1994).

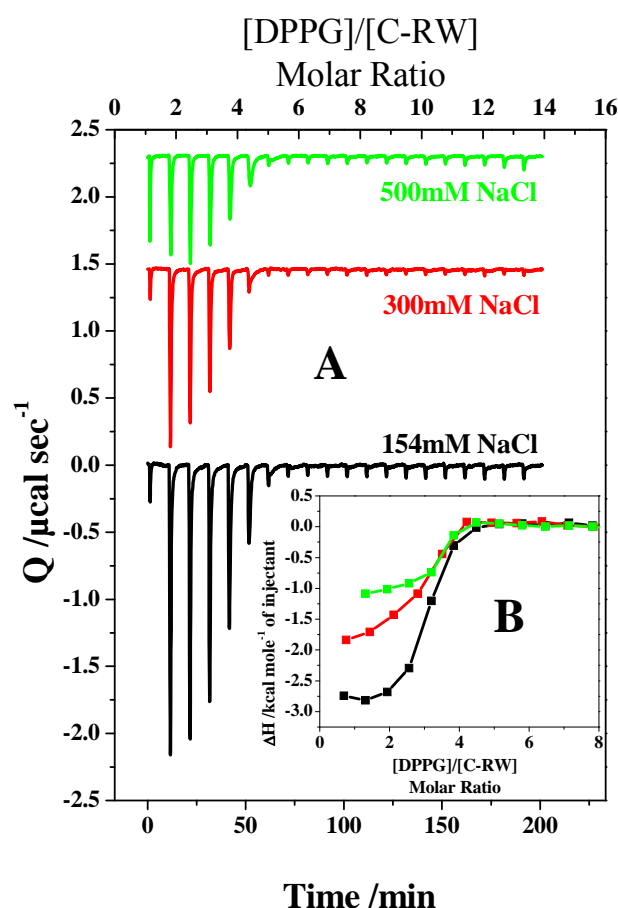


Figure 5.2-25 The experimental power signals (A) and the integrated peaks as a function of DPPG/C-RW ratio (B) of the titration of DPPG LUV (2.5 mM) in the syringe into C-RW peptide solution (40 μM) in the reaction cell at different NaCl concentrations (154 to 500 mM) at 25°C. The samples were prepared in buffer (10 mM Tris, 154 mM NaCl, pH 7.4).

The titration curves are displayed in **Figure 5.2-25** and the binding parameters are listed in **Table 5.2-2**. Increasing the NaCl concentration reduced ΔH° and increased ΔS° , whereas N , K_{app} and ΔG° were barely altered. This indicates that the charge screening effects reduced the electrostatic interaction between C-RW and DPPG headgroups, which allowed a deeper burial of the peptide hydrophobic groups in the lipid membrane and this enhanced the hydrophobic effects.

5.2.4.4 Interactions with DPPG/DPPC and DPPG/DPPE mixed LUV

In the DSC and FT-IR measurements, we observed a peptide-induced lipid demixing in DPPG/DPPE but not in DPPG/DMPC mixed bilayers (see above). Therefore, an important goal of this ITC study was to inspect the thermodynamic profiles of interactions with both mixed membranes, which could help us to explain this discrepancy. To this end, we carried out titrations of pure DPPC and DPPE as well as of DPPG/DPPC and DPPG/DPPE mixed vesicles into C-RW at 25°C and 154 mM NaCl. The experimental power signals are shown in **Figure 5.2-26**.

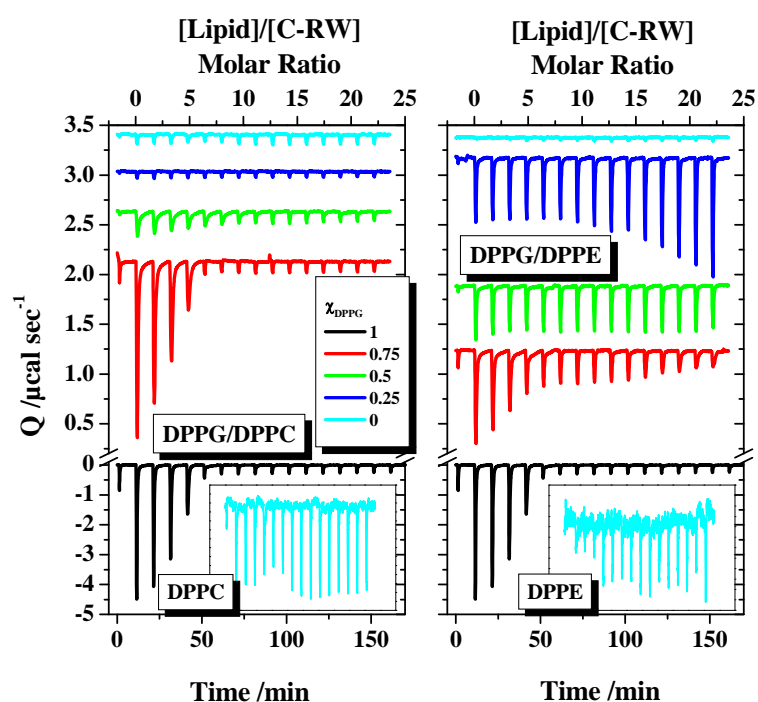


Figure 5.2-26 The experimental power signals of the titration of DPPG/DPPC and DPPG/DPPE mixed LUV (total lipid concentration 5 mM) as well as of the single components (5 mM) in the syringe into C-RW peptide solution (20 - 50 μ M) in the reaction cell at 25°C. The samples were prepared in buffer (10 mM Tris, 154 mM NaCl, pH 7.4).

No binding was detected with the uncharged vesicles. The interaction with DPPG/DPPC was exothermic where the binding affinity was reduced with decreasing the DPPG fraction, which is clearly due to the lower binding enthalpy. Interestingly, the binding curves of DPPG/DPPE bilayers were a superposition of two exothermic processes, a decaying one dependent on the DPPG fraction and a growing process dependent on the DPPE fraction. The latter process occurred only in DPPG/DPPE mixed vesicles since it was not observed with pure DPPE. The numerical values from the fitting of the isotherms are listed in **Table 5.2-2**. In consequence of the modest ΔH° associated with the binding to some of the mixtures, the values obtained for those mixtures were inaccurate.

The binding process of C-RW to DPPG/DPPE vesicles is exothermic. On the other hand, the peptide-induced demixing in DPPG/DPPE membranes is an endothermic process, since some work must be applied to segregate the lipid molecules. At the beginning of the titration and due to the low L/P ratio, i.e. excess peptide, the binding and demixing enthalpies per injection would be maximum. Therefore, the exothermic binding ΔH° would, at least partially, be compensated by the endothermic demixing ΔH° . The further additions of lipid vesicles to the cell would cause a reversal of the demixing, i.e. a mixing process, which would be exothermic. At the end of the titration, the sum of both exothermic enthalpies, i.e. binding and mixing, led to the higher-than-expected enthalpy per injection. The binding enthalpy increased with the DPPG fraction, whereas the mixing enthalpy increased with the DPPE fraction.

Indeed, ΔH° observed with DPPG/DPPE 3:1 and 1:1 was lower than that with DPPG/DPPC mixtures with the same DPPG content. As a result, ΔG° and K_{app} were also decreased. Therefore, we anticipate that the observed reduced binding affinity of C-RW towards DPPG/DPPE was primarily due to the former effects. On the other side, we suggest that the exothermic ITC isotherm observed with DPPG/DPPE 1:3 was mainly due the reversal of the demixing process. This phenomenon was associated with high favourable entropy, apparently, due to the increased rotational and translational degrees of freedom of the lipid molecules.

The demixing and mixing processes in DPPG/DPPE mixed bilayers, which are in the gel phase at 25°C, are not unrealistic at the time scale of the ITC experiment. The following equation, $\langle r^2 \rangle = 4Dt$, can be used to estimate the average distance that lipid molecules can travel in 600 s, which is the spacing between the ITC injections. $\langle r^2 \rangle$ is the mean square displacement in two dimensions from the origin to the point (x,y), D is the diffusion coefficient, and t is the time. D of gel-state lipids vary significantly in literature $10^{-16} - 10^{-9}$

$\text{cm}^2 \text{s}^{-1}$ (Hac et al. 2005). If D is $10^{-12} \text{cm}^2 \text{s}^{-1}$, then the average r will be $\sim 500 \text{nm}$, which is almost enough for the formation of lipid domains of $1 \mu\text{m}^2$ in size.

As shown in **Table 5.2-2**, the stoichiometries observed with DPPG/DPPC as well as with DPPG/DPPE 3:1 and 1:1 mixtures suggest that the peptide can freely cross the charged lipid bilayer as well as that the electrostatic attraction is the driving force for the interaction.

5.3 Summary

We studied the interaction of a linear and a cyclic R- and W-rich antimicrobial hexapeptide, Ac-RW and C-RW, respectively, with identical amino acid sequences with model lipid membranes.

The two cationic peptides interact preferentially with negatively charged lipid membranes, and their affinity is proportional to the surface charge density of the membrane. Our FI-IR spectra indicate that Ac-RW is unstructured in buffer and assumes a β -structure upon the interaction with DPPG, whereas free and DPPG-bound C-RW adopt a comparable β -structure, which can be explained by its constrained (rigid) nature. This agrees well with the results reported before (Appelt et al. 2005a; Appelt et al. 2005b; Dathe et al. 2004; Jing et al. 2003). Our DSC, ITC, and DLS experiments show a rapid entry of the peptides into DPPG vesicles without any indication of a significant vesicle disruption and thus a homogeneous distribution of the peptides in the outer and inner leaflets. This is in a good agreement with the finding that the peptides easily permeabilize bacterial membranes and vesicles bilayers (Dathe et al. 2004; Junkes et al. 2008; Rezansoff et al. 2005; Wessolowski et al. 2004). Due to the flexibility of the linear peptide, it perturbs the lipid chain packing more pronouncedly than C-RW and shows the ability to form ion channels (unpublished BLM data support this notion). This actually is in contrast to the enhanced antimicrobial activity and bacterial selectivity of C-RW as compared to Ac-RW (Dathe et al. 2004; Wessolowski et al. 2004). In addition, it was found that both peptides could readily penetrate bacterial membranes, however, at concentrations higher than their MIC (Junkes et al. 2008; Rezansoff et al. 2005). These observations evidence the involvement of other mechanisms in the antimicrobial activity of the peptides besides membrane permeabilization.

In mixed membranes, the electrostatic interaction with anionic components enhances the accumulation of the peptides on the bilayer surface. However, the bilayer-influencing activity strongly depends on the nature of the negatively charged head group and the amount and properties of the zwitterionic lipids. For DPPG/DMPC mixed vesicles, the addition of peptides decreases the phase transition temperature, however, no demixing is detected. On the other hand, the addition of both peptides induces a phase separation in DPPG/DPPE mixtures that results in the appearance of two phase transitions; the first one due to the transition of mainly peptide-bound DPPG and the second belonging to the DPPG-depleted DPPE-enriched lipid domain. This demixing phenomenon is proven by DSC, FT-IR and X-ray (X-ray data are not included in the thesis). **Figure 5.3-1** shows a cartoon illustrating the observed C-RW-induced demixing in PG/PE membranes. Less intensive peptide-induced phase segregation in

DPPG/DPPE mixtures was also observed before by Lohner et al. with other peptides (Lohner et al. 1997; Lohner and Prenner 1999; Lohner et al. 2008). The ITC titrations suggest the reversibility of the C-RW induced demixing in DPPG/DPPE mixed bilayers, where mixing can take place upon increasing the lipid/peptide ratio in the system.

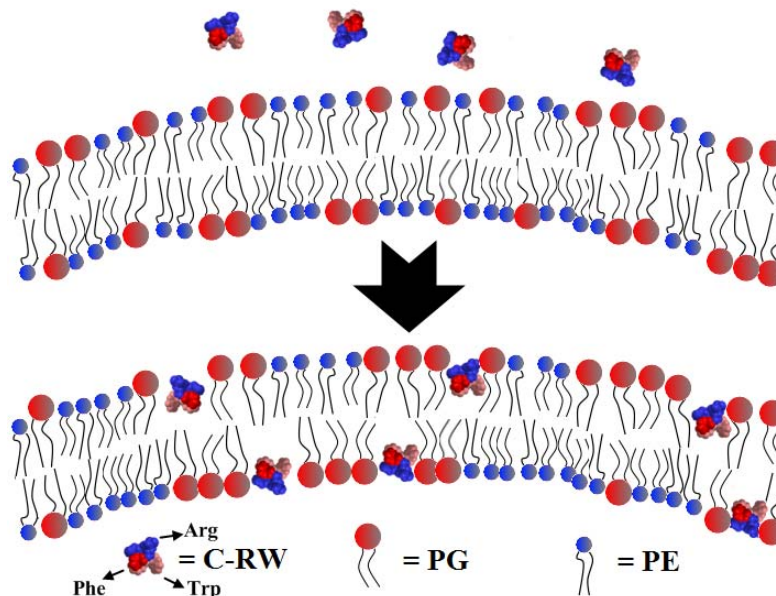


Figure 5.3-1 Cartoon illustrating the C-RW-induced demixing in a bilayer of mixed PG/PE, represented by red and blue balls, respectively. C-RW segregates PG from PE creating defects between the formed domains. The hydrophobic amino acids Trp and Phe of the peptide are somewhat buried in the membrane core while the arginine residues interact with the PG headgroup region.

The demixing was also observed in TMCL/DPPG/DPPE ternary mixture and, less pronouncedly, in DPPG/POPE, TMCL/DPPG, and TMCL/DPPE binary mixtures. The phase separation in fluid mixtures might still occur but is probably on a much smaller scale and therefore difficult to prove. We just want to mention the ongoing debate about the nature of "lipid rafts", which are small and dynamic and therefore difficult to visualize. Epanand and Epanand proposed that the presence of multiple cationic residues, a conformational flexibility and sufficient hydrophobicity could be a prerequisite for an antimicrobial agent to induce phase segregation of anionic lipids (Epanand and Epanand 2008).

Further experiments are required to explain the different effects of the peptides on the miscibility in DPPG/DMPC and DPPG/DPPE vesicles. Since the peptides did not show a substantial affinity towards pure DMPC and DPPE membranes, one possible interpretation of the observed effects could be that the interactions between PG and PE in the mixture are affected due to the preference of the peptides for PG. The addition of the peptides apparently breaks up the PG-PE pair formation (Garidel and Blume 2000; Murzyn et al. 2005) with the consequence of demixing.

This peptide-induced segregation of different types of lipids will change the lipid environment of the peptides as well as destabilize the membrane by introducing phase boundary defects between the lipid domains. In addition, the formation of PE rich domains might destabilize the bilayers because of the high negative curvature tendency of PE lipids, particularly the unsaturated ones. Thus, the induction of phase separation in PG-PE mixtures caused by the addition of the peptides may have important consequences for their biological function and their specificity towards bacterial membranes. As the cytoplasmic membranes of Gram-negative bacteria as well as the cytoplasmic membranes of some Gram-positive bacteria contain mainly PG and PE (Lohner et al. 2008), the possibility exists that the specificity of peptides for bacterial membranes may not rely exclusively on their higher negative surface charge but may additionally be enhanced by exploiting this mechanism of peptide induced phase separation. The correlation between the observed lipid demixing and the antimicrobial activity of the peptides needs, though, to be established. The results obtained here are valid for saturated phospholipids where the phase separation is detected by the formation of gel phase domains upon cooling. It has to be shown that the same effect occurs also in liquid-crystalline membranes. A comparable phenomenon on the interaction with fluid bilayers of mixed PG/PE and PE/CL has been reported for a flexible sequence random-polymer (Erand et al. 2008a), for some isomeric alpha/beta peptides (Erand et al. 2006) and for an oligo-acyl-lysine (OAK) (Erand et al. 2008b).

An important consequence of our results is that for studies of the interaction of antimicrobial peptides with model bacterial membranes, a PG-PC mixture is a poor choice. Because of the selective interactions, we found in our studies, it is advisable to study PG-PE membranes as a model system for bacterial membranes, particularly Gram-negative bacteria, despite the difficulty of obtaining stable vesicle systems. In our studies using DSC and FT-IR, the aspect of vesicle stability was of minor importance, because these techniques can also be used with large multilamellar liposomes. When applying fluorescence spectroscopy the problems are, however, more severe and it might be impossible to overcome them.

The proposal of the lipid demixing in PG-PE containing membranes as an additional mechanism of action of antimicrobial peptides emphasizes that the *in vivo* potency of membrane-active agents should not always be associated with a significant destruction of membranes. Therefore, the permeabilization experiments are not always the appropriate measure for valuing the antimicrobial action. Besides, the discrepancy between activity against cells and on model lipid membranes, which is reported often in literature, indicates an important role of the outer membrane.

6 The antimicrobial action on supported lipid bilayers

6.1 Supported lipid membranes

The vast majority of the biophysical experiments carried out to study the interaction of antimicrobial peptides with model lipid systems utilize micelles, monolayers, vesicles, and multilamellar films. So far, the use of supported lipid bilayers (SLB) is still limited due to technical issues (method complexity, time consuming procedure, membrane instability) and model restrictions (it is only possible to control the solution in one side, the effect of the solid support should be considered, the limited lipid species and lipid mixtures that can be used). Nonetheless, the two dimensional supported membranes in which the lipid mobility is constricted to two dimensions provide a potent tool to investigate lipid domains, intermembrane interactions, and membrane associated processes by means of surface sensitive microscopic and spectroscopic techniques (Jelinek and Kolusheva 2005; Richter et al. 2006; Tamm 2002; Tamm and McConnell 1985).

We utilized epifluorescence microscopy to study the morphological changes associated with the interaction of KLA and RRWWRF antimicrobial peptides with NBD-DPPE labelled lipid bilayers supported on quartz substrates. This provides information complementary to the previously discussed biophysical experiments carried out using lipid monolayers as well as unilamellar and multilamellar vesicles. To mimic the relevant biomembranes and in accordance with the former experiments, we investigated the influence of the peptides on supported membranes of POPG/POPC 1:1, POPG/POPE 1:1 and the individual components as well as *E. coli* lipid extract (67% PE, 23.2% PG, 9.8% cardiolipin).

It was necessary to seek protocols to efficiently produce supported bilayers of our lipids of interest. The stability, integrity, and reproducibility of the SLB had to be checked. The quality of the produced SLB was examined visually by epifluorescence and also by means of fluorescence recovery after photobleaching (FRAP) (Tamm and Kalb 1993). FRAP was used to determine the lateral diffusion coefficient of the NBD-DPPE labelled SLB, in order to check the fluidity and continuity of the membrane (see methods).

Supported planar membranes can be prepared by one of three methods (Tamm and Tatulian 1997): vesicle fusion (Brian and McConnell 1984), Langmuir Blodgett/Langmuir Schaefer (Tamm and McConnell 1985), or combined Langmuir Blodgett/vesicle fusion (Kalb

et al. 1992). The preparation of uncharged and moderately charged supported membranes is relatively uncomplicated. However, bacterial membranes are rich in negatively charged lipid components, particularly PG. Consequently, the incorporation of high amounts of PG in our model membranes became the main obstacle in producing supported membranes.

6.2 Vesicle fusion and Langmuir Blodgett/vesicle fusion techniques

The combined LB/VF technique failed to produce SLB of lipid preparations rich in POPG, as the first LB monolayer was highly instable towards buffer. In addition, no POPG supported bilayers could be obtained by the vesicle fusion method (without any additives), as the electrostatic repulsion between POPG vesicles and the negatively charged quartz substrate hampered proper adsorption of the anionic lipid vesicles. The utilization of divalent cations, particularly calcium, is common to aid the adsorption of lipid vesicles and the rupture to supported membranes (Barman et al. 2006; Kalb et al. 1992; Nollert et al. 1995; Richter et al. 2006). As illustrated in **Figure 6.2-1**, the POPG vesicles adsorbed to the quartz surface after the premixing with 1 mM Ca^{+2} , however, did not rupture and remained intact as proven visually and by FRAP experiments.

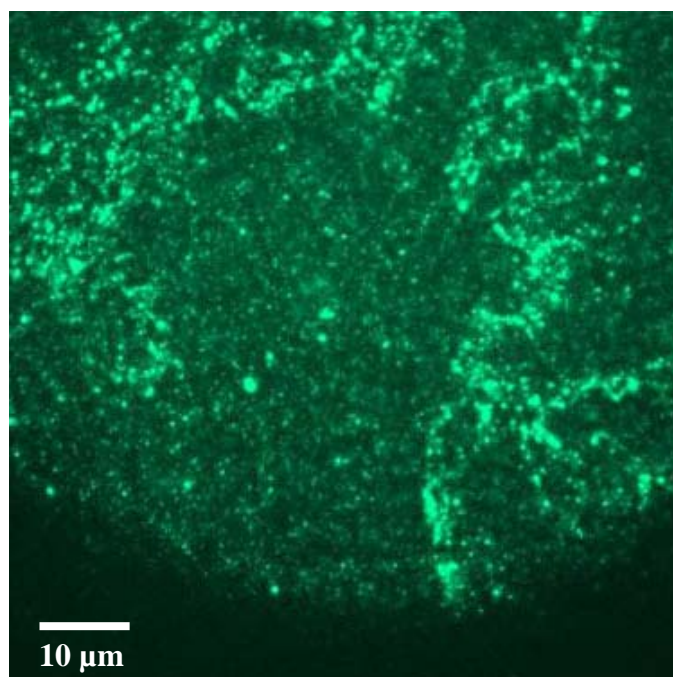


Figure 6.2-1 Epifluorescence image showing the aggregation of POPG LUV (NBD-DPPE 1 mol%) at the quartz substrate upon the premixing with 1 mM CaCl_2 . The addition of Ca^{+2} ions facilitated the adsorption of POPG vesicles to the acidic substrate but no supported membranes were formed.

The premixing with smaller (200 μM) Ca^{+2} concentrations was sufficient for the adsorption and fusion of POPG/POPC 1:3 vesicles and facilitated the formation of supported membranes (**Figure 6.2-2A**). After the injection of 1 μM C-RW peptide into the bulk buffer

(Figure 6.2-2B), which faces the distal monolayer of the SLB, one can clearly see agglomerated lipid structures in the bulk adjacent to the supported bilayer. It is not possible to determine the origin of the lipid structures, which can be the SLB itself, or lipid vesicles that could not be washed away after flushing with buffer, or both. Besides, it is expected that Ca^{+2} induces the aggregation and possibly the fusion of the PG containing lipid vesicles, which is already a known effect of divalent cations on acidic membranes (Ginsberg 1978; Leventis et al. 1986; Ohki 1984; Ohki and Ohshima 1985). This indicates that the effects of Ca^{+2} and the antimicrobial peptides are superimposed and cannot be separated.

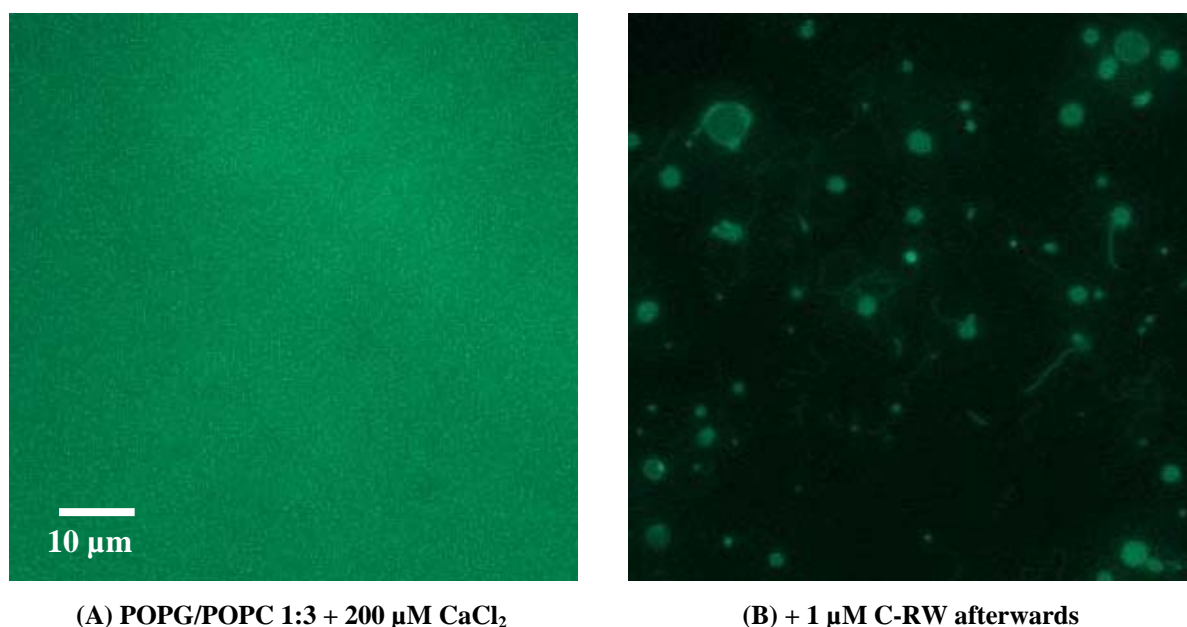


Figure 6.2-2 (A) SLB prepared by VF of POPG/POPC 1:3 LUV (NBD-DPPE 1 mol%) premixed with 200 μM CaCl_2 . (B) The SLB after the addition of 1 μM C-RW.

Interestingly, the premixing of 10 μM of the cationic C-RW (no Ca^{+2}) with POPG/POPC 1:3 and POPG/POPE 1:3 lipid vesicles, respectively, facilitates the adsorption and rupture of the vesicles and the formation of the supported membranes. Nonetheless, it is not possible to produce “control” supported bilayers by the VF technique without the use of the peptide or Ca^{+2} .

6.3 Langmuir Blodgett/Langmuir Schaefer technique

With the utilization of Langmuir Blodgett/Langmuir Schaefer (LB/LS) method, we could successfully prepare supported membranes rich in POPG without the need to use any fusogenic agents. The bilayers were produced using lipid monolayers whose surface pressure were maintained constant at 32 mN m^{-1} which is equivalent to the pressure inside bilayer membranes (Blume 1979; Tamm 2002).

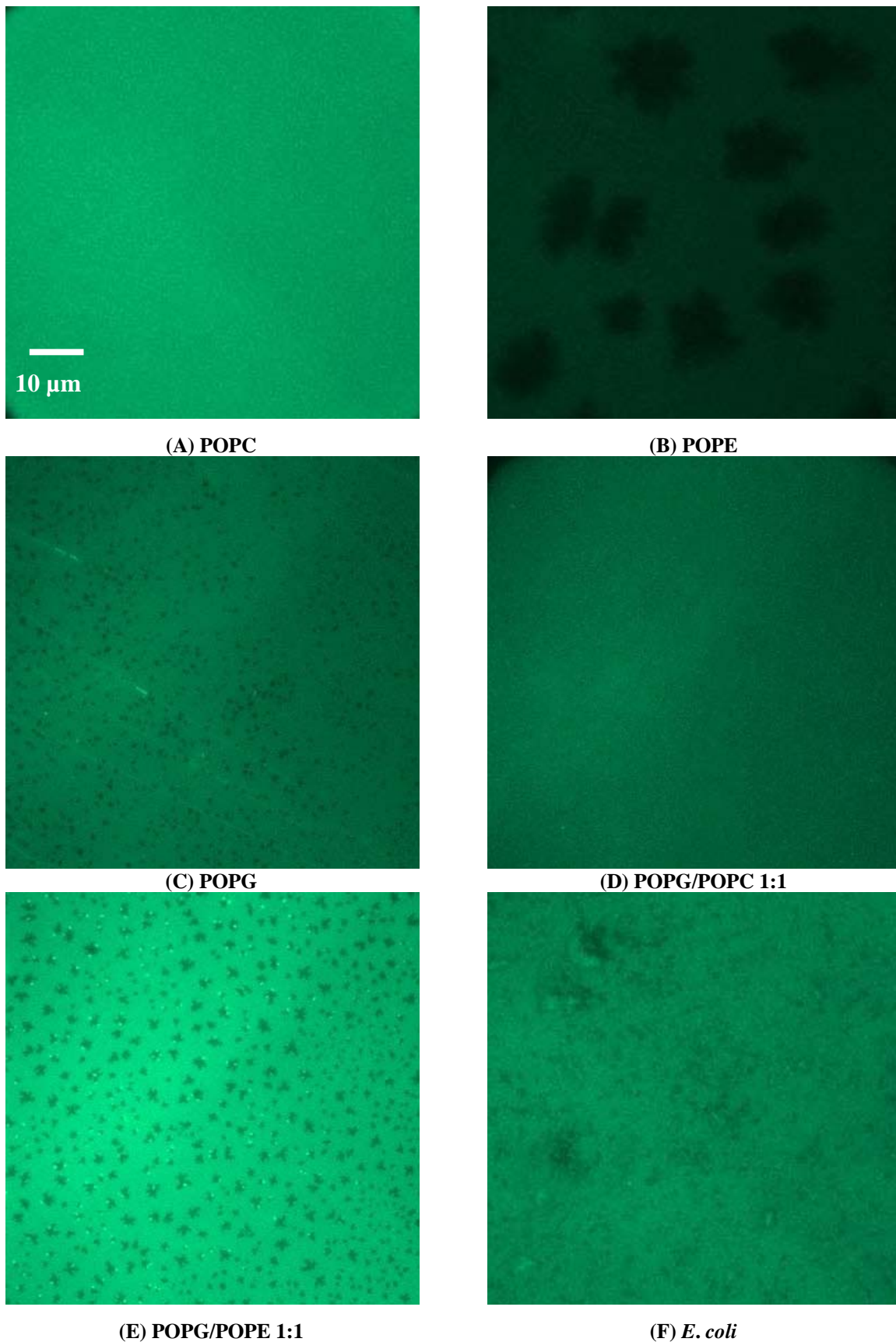


Figure 6.3-1 SLB prepared by LB/LS of the pure lipids POPC (A), POPE (B), POPG (C), POPG/POPC 1:1 (D), POPG/POPE 1:1 (E), and *E. coli* lipid extract (F). The lipid preparations were premixed with 0.75 mol% NBD-DPPE. The dark spots represent dye-depleted domains.

Figure 6.3-1A to F shows the epifluorescence images of the SLB of POPC, POPE, POPG, POPG/POPC 1:1, POPG/POPE 1:1, and *E. coli* lipid extract, respectively. The lipid preparations were premixed with 0.75 mol% NBD-DPPE, which is very miscible with fluid (disordered) membranes.

The SLB of POPC (**Figure 6.3-1A**) was uniformly bright due to the homogeneous distribution of the fluorescent dye in the bilayer. The epifluorescence image of POPE (**Figure 6.3-1B**), whose phase transition is around room temperature ($\sim 25^\circ\text{C}$, (Pozo Navas et al. 2005)), exhibited dye-depleted leaf-shaped lipid domains. We believe that the dark spots represent the POPE ordered phase, from which the fluorescent dye molecules were squeezed out. Dark domains are commonly observed in monolayers and bilayers of gel-state lipids (Bringezu et al. 2007a; Gidalevitz et al. 2003).

Interestingly, the epifluorescence image of the POPG (**Figure 6.3-1C**) shows small distributed dark domains. Due to the fluid nature of POPG and similar to POPC, it was expected that the structure of SLB of POPG would look similar to that of POPC. Furthermore, no such dark domains were obtained with POPG monolayers prepared by Langmuir Blodgett method but rather a bright epifluorescence image as observed with POPC SLB (data not shown). Therefore, we believe that the interaction of POPG supported bilayer with the quartz surface induced the formation of those ordered domains. Nonetheless, the possibility that some of the dark domains were due to bilayer imperfections cannot be ruled out.

The structure of the supported membranes of POPG/POPC 1:1 and POPG/POPE 1:1 lipid mixtures are depicted in **Figure 6.3-1D** and **Figure 6.3-1E**, respectively. Both bilayers showed the presence of small dark domains, which were expectedly much smaller in the case of the POPG/POPC 1:1 lipid mixture. The epifluorescence image of *E. coli* lipid extract (**Figure 6.3-1F**) shows a more complicated membrane structure, which is definitely associated with the complex composition of the lipid extract.

As shown in **Figure 6.3-2**, in some cases the fluorescent dye molecules tend to cluster at the boundaries between the ordered and disordered domains, a behaviour that is common for guest molecules in lipid membranes.

One of the most significant observations is the transmembrane domain coupling between both lipid leaflets of the supported membrane, i.e. both monolayers share the same ordered dye-depleted domains (see **Figure 6.3-1**). This phenomenon indicates the strong influence each lipid monolayer has on the other monolayer.

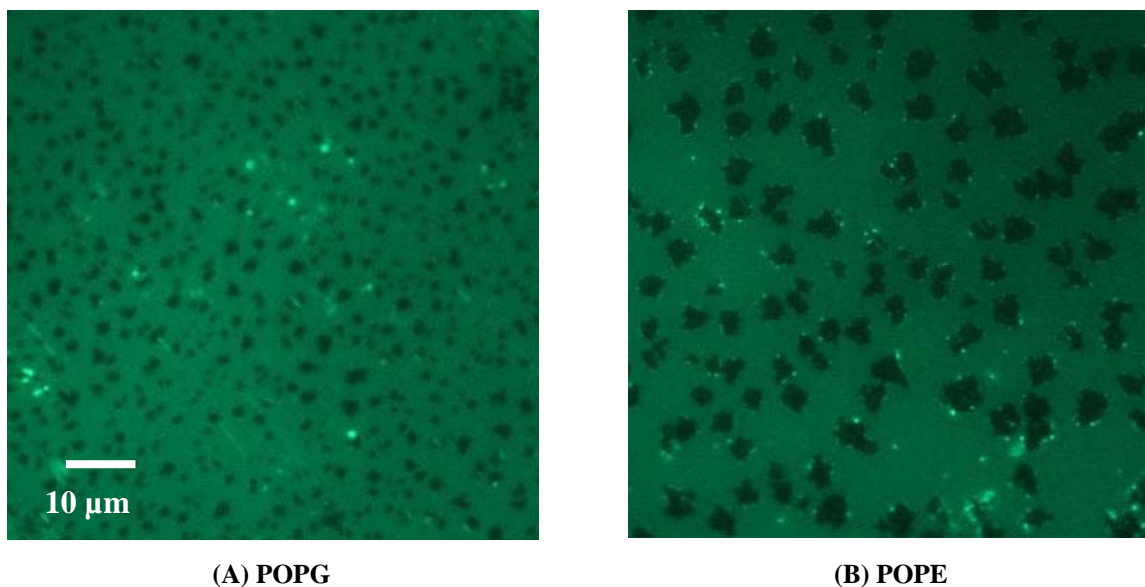


Figure 6.3-2 SLB prepared by LB/LS of POPG (A) and POPE (B). The figure shows the segregation of the dye molecules (NBD-DPPE 0.75 mol%) at the domains boundaries.

The uncoupling phenomenon was rarely observed. We present in **Figure 6.3-3** an epifluorescence image of POPG/POPE 1:1 SLB, where both lipid monolayers were uncoupled, where one can clearly see the separate domains of both leaflets. The transmembrane coupling was investigated for cholesterol rich lipid ordered domains in asymmetric SLB (Kießling et al. 2006; Wan et al. 2008). It was found that the cholesterol rich liquid ordered domains in one leaflet could induce lipid ordered domains in the opposite asymmetric leaflet when this leaflet was composed of certain lipid species.

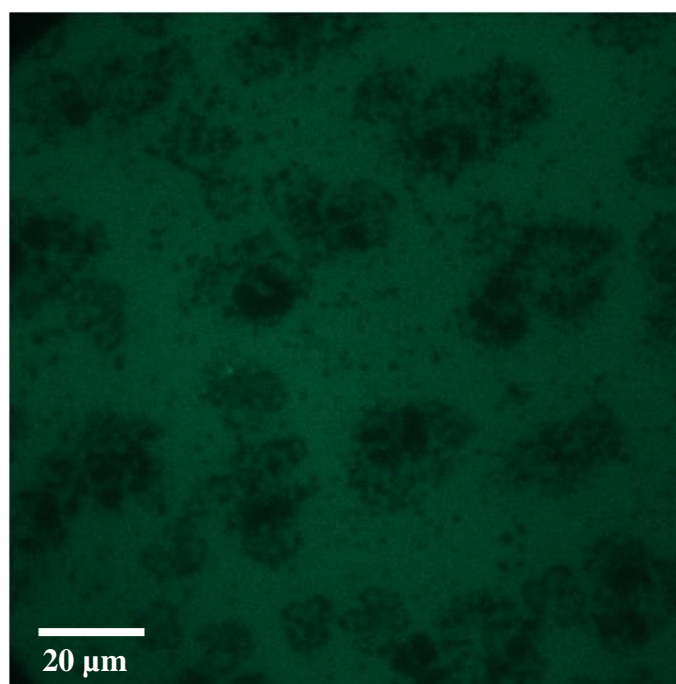


Figure 6.3-3 SLB prepared by LB/LS of POPG/POPE 1:1 (NBD-DPPE 0.75 mol%) showing the domains uncoupling between the two leaflets of the supported membrane.

The appearance of SLB is very sensitive to the preparation procedure and any small alteration in the preparation routine can cause drastic changes in the structure of the supported membrane, particularly the size, shape, and distribution of the ordered domains. Among the various parameters that should be controlled are the dye type and concentration as well as the technique used to prepare and deposit the lipid monolayers, such as the subphase used, monolayer starting pressure, compression speed, final pressure, the monolayer deposition speed, and times given for equilibration. Nevertheless, the appearance of certain supported bilayers can slightly vary from one preparation to another.

6.4 The interaction of RRWWRF peptides with SLB prepared by LB/LS

We investigated the effect of C-RW on various supported membranes and the morphological changes that accompanied the addition of the peptide into the buffer. The action of the peptide was rapid (within few minutes) and dependent on the peptide concentration and the PG fraction in the membrane.

Up to ~ 1 hour, C-RW did not show any influence on the SLB of the uncharged lipids POPC and POPE (data not shown).

As demonstrated in **Figure 6.4-1**, $1 \mu\text{M}$ C-RW triggered the formation of bright fibrils within minutes, which continued to grow in size and length over time. The fluorescent fibrils bulged out of the SLB plane into the bulk, whereas the brighter spot of the structure remained in focus and indicated where the fibril was attached to the supported membrane. Besides, the fibrils floating ends showed high flexibility as evident by their rapid Brownian movement in bulk (visible in the time dependent images). After ~ 1 hour, the length of some fibrils exceeded $100 \mu\text{m}$, whereas their width varied from 1 to $4 \mu\text{m}$.

Another interesting phenomenon was that peptide induced formation of pearl-chain instabilities (**Figure 6.4-1D**), where a chain of vesicles were connected to each other through small bilayer tubes. Such instabilities have been widely studied experimentally and are formed when a sudden tension is applied upon lipid membranes, for instance through laser tweezers, osmotic perturbations, bilayer asymmetry and anchoring of amphipathic molecules (Campelo and Hernandez-Machado 2007).

Increasing the concentration of C-RW to $4 \mu\text{M}$ strongly altered the effect of the peptide on POPG SLB (**Figure 6.4-2**). The action of the peptide became faster, while the fibrils did not grow but rather transformed into giant spherical structures “vesicles” (compare **Figure 6.4-2B** and **Figure 6.4-2C**). The diameter of some of the formed vesicles was larger than $6 \mu\text{m}$. In addition, several giant structures ruptured and flattened on the SLB distal

surface leaving patches of irregular structures, see **Figure 6.4-2D**, which can be easily distinguished from other places on the SLB where no patches were adsorbed to distal leaflet.

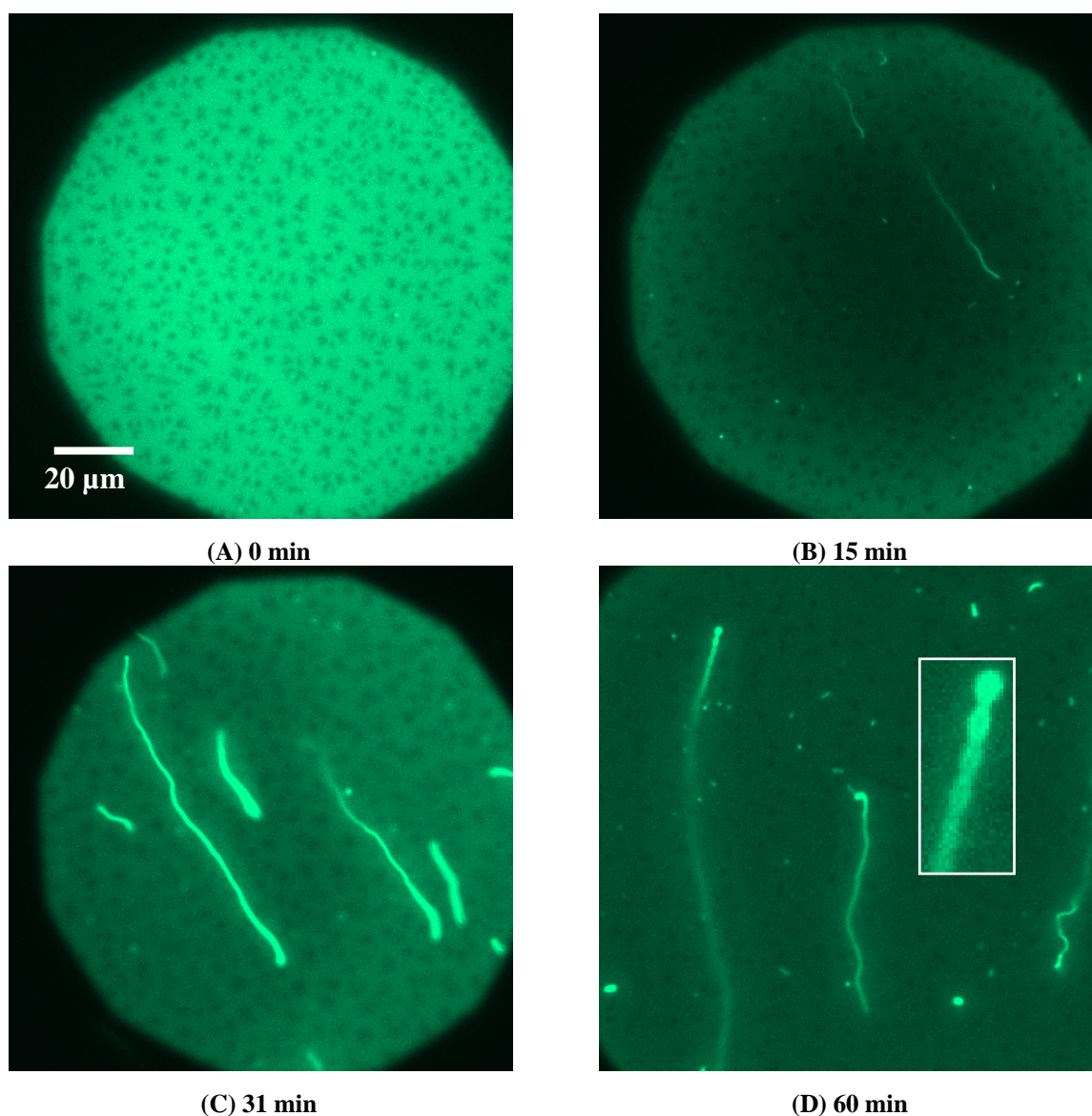


Figure 6.4-1 SLB prepared by LB/LS of POPG (NBD-DPPE 0.75 mol%). The figures illustrate the effect and morphological changes over time (0 to 60 min) of adding 1 μM C-RW into the buffer. The subsequent images became darker as compared to the control image due to the photobleaching effect. The inset in (D) is a magnification of the pearl-chain instability.

Comparable fibrillar structures were observed by Domanov et al. (2006) after the addition of some antimicrobial peptides to POPG/POPC 4:1 SLB. From additionally observing the behaviour of fluorescent labelled peptides, they found that the fibrils were composed of both lipids and amphipathic peptides. Moreover, they demonstrated that the fibrils were tubular structures formed of lipid bilayers rather than long cylindrical micelles made by single cylindrical lipid leaflet. Furthermore, Domanov et al. proposed two ways to relieve the increased lateral pressure profile across the lipid monolayer upon the binding of an

amphipathic peptide (**Figure 6.4-3**); 1) monolayer dilation and membrane thinning, and 2) the formation of protrusions which takes place at higher peptide concentrations (Domanov and Kinnunen 2006). It should be noted that the protrusion demonstrated in (**Figure 6.4-3**) is much smaller than what is observed experimentally.

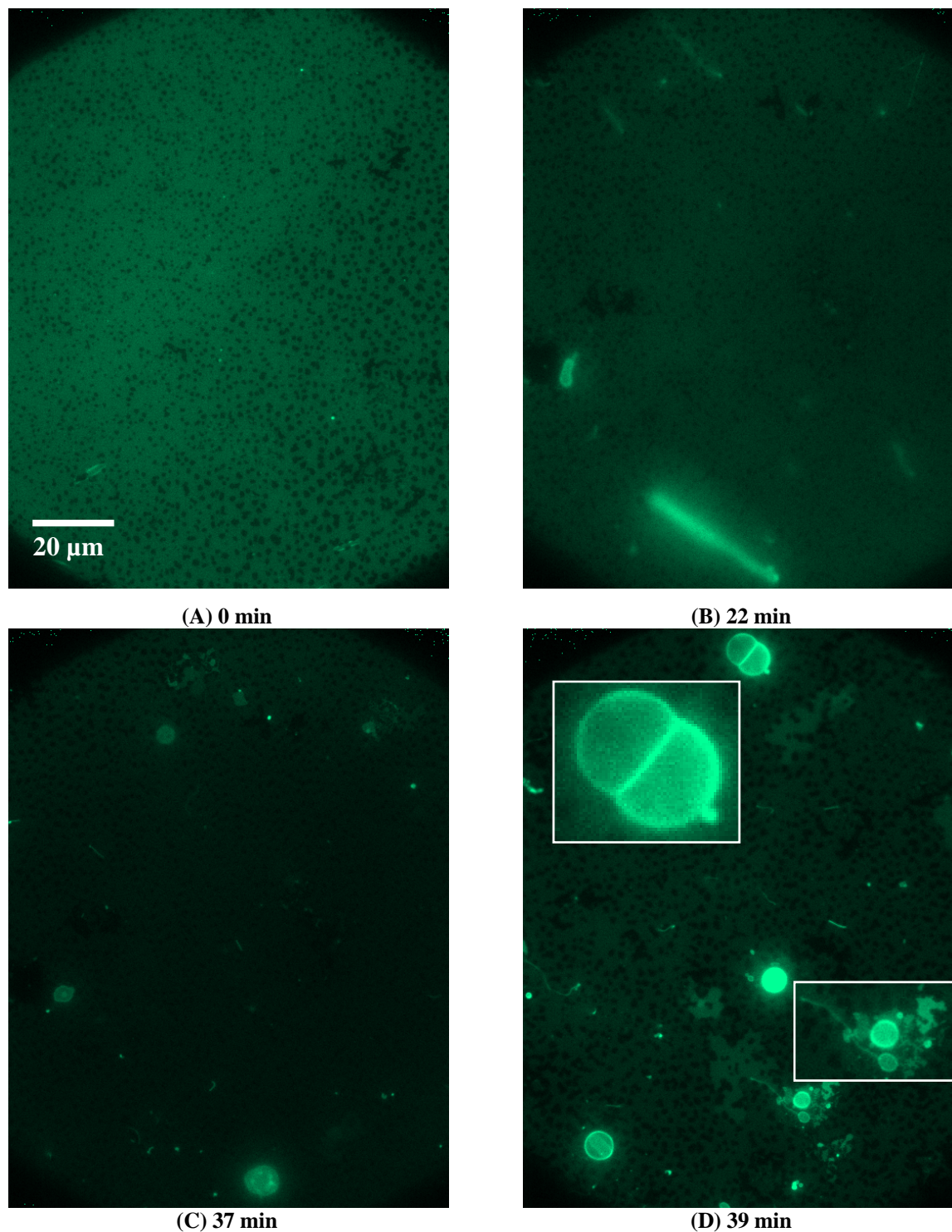


Figure 6.4-2 SLB prepared by LB/LS of POPG (NBD-DPPE 0.75 mol%). The figures illustrate the effect and morphological changes over time (0 to 39 min) of adding 4 μM C-RW into the buffer. The subsequent images became darker as compared to the control image due to the photobleaching effect. The insets in (D) are magnifications of some structures in the image.

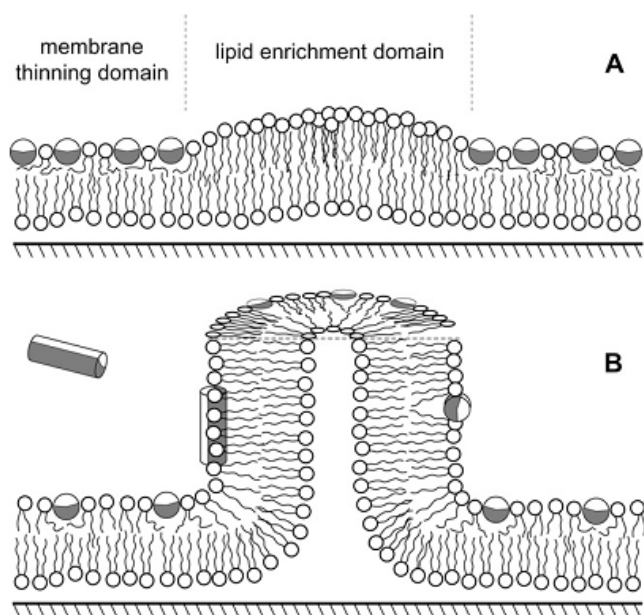


Figure 6.4-3 A proposed mechanism for the tubular outgrowth from SLB induced by the binding of amphipathic helical peptides. The α -helical peptides are represented by cylinders with their hydrophobic sides shaded gray. (A) Lipid segregation and membrane thinning induced at low peptide concentration. (B) The formation of fibrils that consists of lipids and peptides at high peptide concentration. Adapted from ref. (Domanov and Kinnunen 2006)

C-RW-induced morphological alterations in the SLB of POPG/POPC 1:1 and POPG/POPE 1:1 lipid mixtures, which were somewhat different from that induced in pure POPG. As shown in **Figure 6.4-4**, 1 μM C-RW provoked the formation of numerous small fibrils in POPG/POPC 1:1 SLB of few micrometers in length and $< 1 \mu\text{m}$ in width. The fibrils remained small and did not grow as in the case of pure POPG, whereas some fibrils transformed into a more spherical geometries.

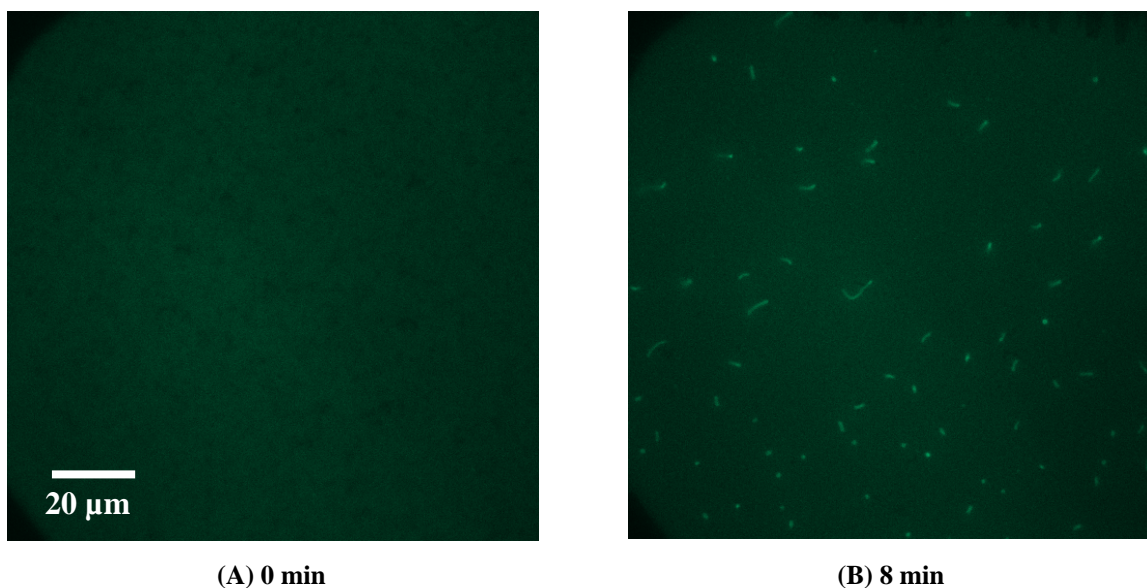


Figure 6.4-4 SLB prepared by LB/LS of POPG/POPC 1:1 (NBD-DPPE 0.75 mol%) before (A) and 8 min after the addition of 1 μM C-RW into the buffer (B).

Increasing the C-RW concentration to 4 μM (**Figure 6.4-5**) enhanced the formation of small fibrils. In **Figure 6.4-5C**, one can observe the detached fibrils from the membrane surface floating in the bulk adjacent to the SLB. Over time, the fibrils merged to produce giant spherical structures a few micrometers in diameter (**Figure 6.4-5D**).

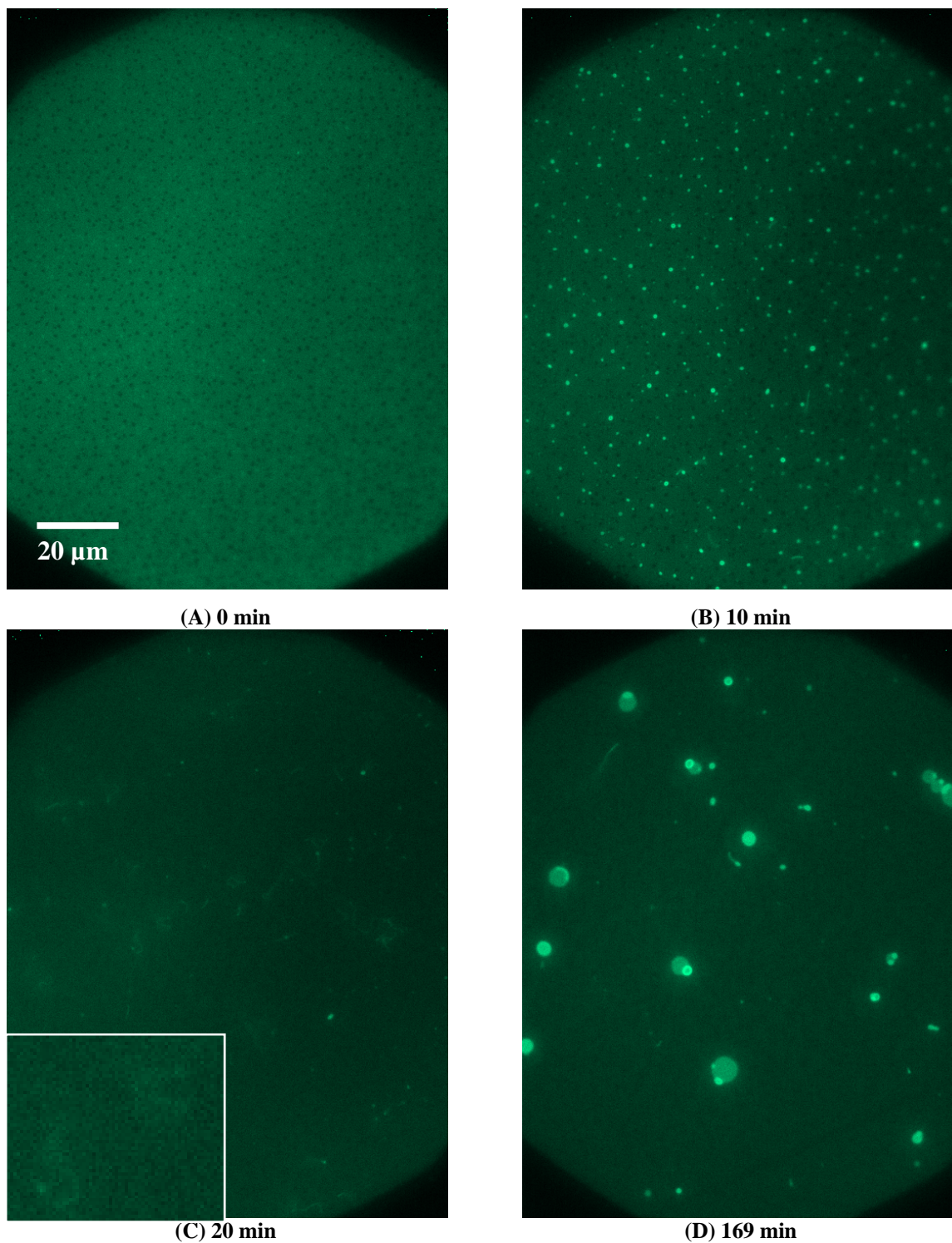


Figure 6.4-5 SLB prepared by LB/LS of POPG/POPC 1:1 (NBD-DPPE 0.75 mol%). The figures illustrate the effect and morphological changes over time (0 to 169 min) of adding 4 μM C-RW into the buffer. The inset in (C) is a magnification of some structures in the image.

Interestingly, the C-RW peptide caused the ordered-domains in the SLB of POPG/POPC 1:1 to disappear. This is most probably due to the fluidizing effects the peptide has upon its insertion into the membrane headgroup-acyl chains interface region, which is in a good agreement with the results of the other techniques.

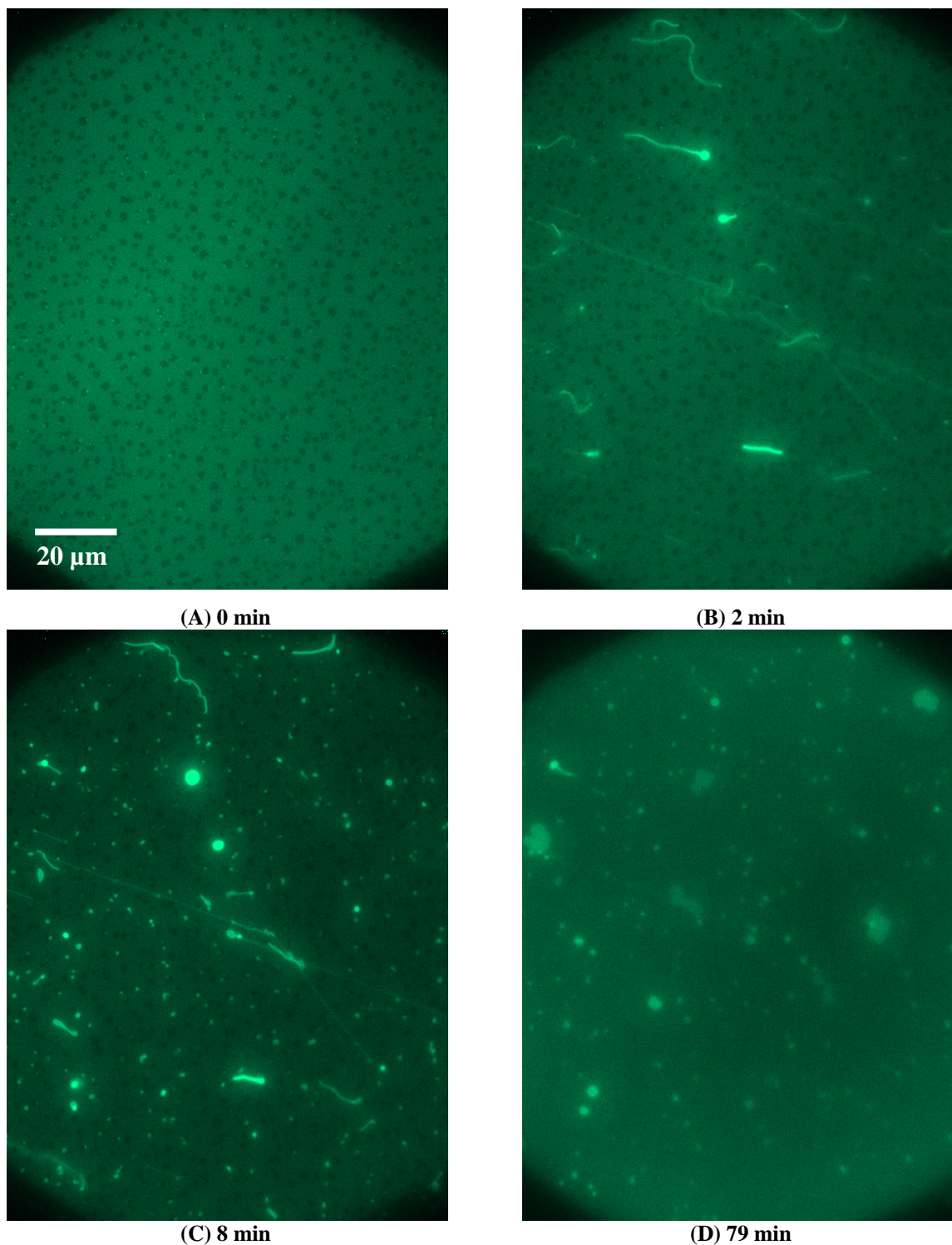


Figure 6.4-6 SLB prepared by LB/LS of POPG/POPE 1:1 (NBD-DPPE 0.75 mol%). The figures illustrate the effect and morphological changes over time (0 to 79 min) of adding 4 μM C-RW into the buffer.

The interaction of C-RW with POPG/POPE 1:1 caused the growth of mid-size fibrils (**Figure 6.4-6**), i.e. smaller than in the case of POPG but larger than that in POPG/POPC 1:1 SLB. The fibrils showed morphological changes over time into bulkier structures, where some structures ruptured and flattened on the SLB distal surface leaving patches on the supported membrane. Similar to what was observed in the SLB of POPG/POPC 1:1, C-RW fluidized the ordered domains in the SLB of POPG/POPE 1:1 that disappeared over time (see **Figure 6.4-6**).

To investigate the antimicrobial action of the peptides on membranes with compositions resembling a natural membrane, we performed the experiments on SLB of *E. coli* lipid extract (**Figure 6.4-7**). The effect of C-RW on *E. coli* SLB was comparable to model supported membranes, yet, slower and less massive. This could be explained by the low PG content in the *E. coli* lipid extract.

It can be clearly seen in **Figure 6.4-5B** and **Figure 6.4-6C** that the origin of the structures bulging out from the supported bilayers was frequently close to the boundaries of the ordered-lipid domains. This may explain why less fibrils were formed in POPG and POPG/POPE 1:1 SLB as compared to POPG/POPC 1:1 and *E. coli* SLB, since the ordered domains in the former SLB were larger and less frequent in comparison to the latter SLB.

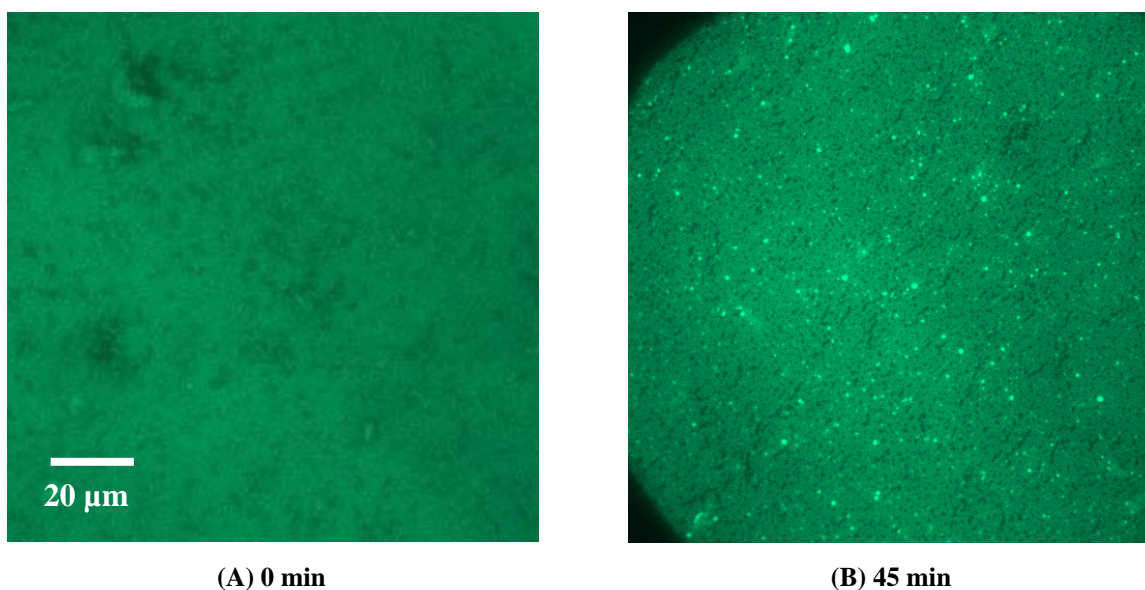


Figure 6.4-7 SLB prepared by LB/LS of *E. coli* lipid extract (NBD-DPPE 0.75 mol%) before (A) and 45 min after the addition of 1.2 μM C-RW into the buffer (B). The difference in brightness between both images is due to the gray scaling applied upon processing both pictures.

We also carried out experiments to see the effect of the linear peptide Ac-RW on the aforementioned supported membranes. Ac-RW showed a comparable behaviour to the cyclic peptide C-RW (data not shown).

6.5 The interaction of KLA peptides with SLB prepared by LB/LS

We also investigated the influence of KLA1 peptide on the supported membranes of the different lipids.

The interaction of KLA1 with the uncharged SLB of POPC (**Figure 6.5-1A**) and POPE (**Figure 6.5-1B**) slowly induced the formation of structural protrusions. However, the effect on POPE was much weaker, apparently due to its higher chain packing as compared to POPC.

Our calorimetric and spectroscopic experiments revealed indeed the more disturbing effects KLA peptides have on PC membranes as compared to PE membranes (data not shown).

As shown in **Figure 6.5-2**, the influence of KLA1 on POPG SLB was drastically different from that of C-RW. Whereas the action of KLA1 was faster, no long fibrils were formed but rather small local protrusions. The induced protrusions did not coalesce into giant vesicular structures, on the contrary, many protrusions disappeared over time by either budding out of the SLB completely or fusing back to the SLB.

The action of KLA1 on POPG/POPC 1:1 SLB (**Figure 6.5-3**) was comparable to that of POPG, however, some of the protrusions did form larger structures over time.

On the other side, the protrusions formed in POPG/POPE 1:1 (**Figure 6.5-4**) were larger and mostly originated from the boundaries of the ordered domains. Interestingly, the protrusion acquired irregular shapes similar to that of the ordered domains.

The influence of KLA1 on SLB of *E. coli* lipid extract (**Figure 6.5-5**) was relatively weak as compared to the other model SLB. Again, this can be explained by the lower charge content of the *E. coli* membrane.

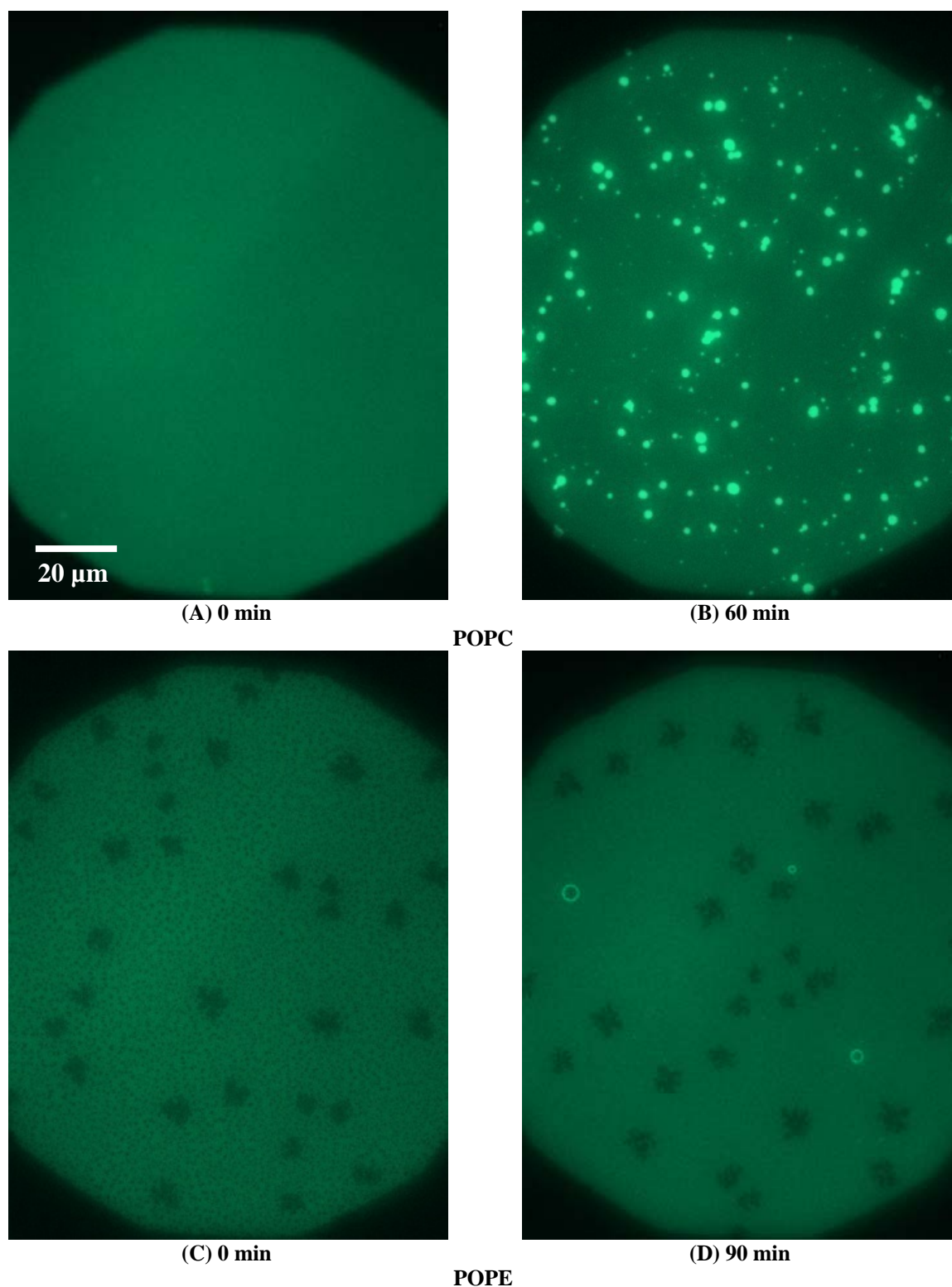


Figure 6.5-1 SLB prepared by LB/LS of POPC (left) and POPE (right) (NBD-DPPE 0.75 mol%) before (A and C, respectively) as well as 60 and 90 min after the addition of 4 μM KLA1 into the buffer (B and D, respectively).

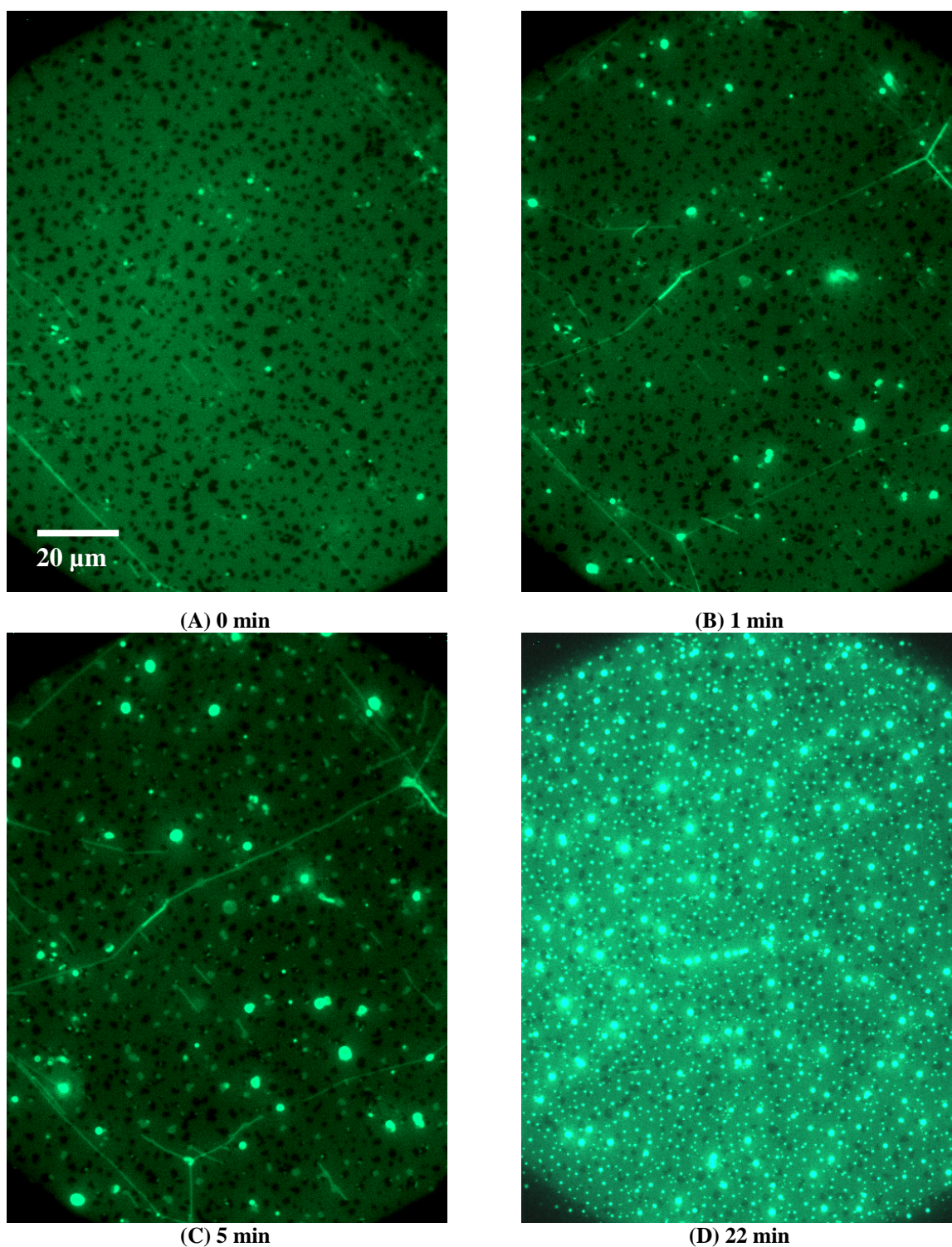


Figure 6.5-2 SLB prepared by LB/LS of POPG (NBD-DPPE 0.75 mol%). The figures illustrate the effect and morphological changes over time (0 to 22 min) of adding 4 μM KLA1 into the buffer. The bright lines in the SLB shown in (B) and (C) are most probably membrane deformations that were formed, initially, during the peptide injection process.

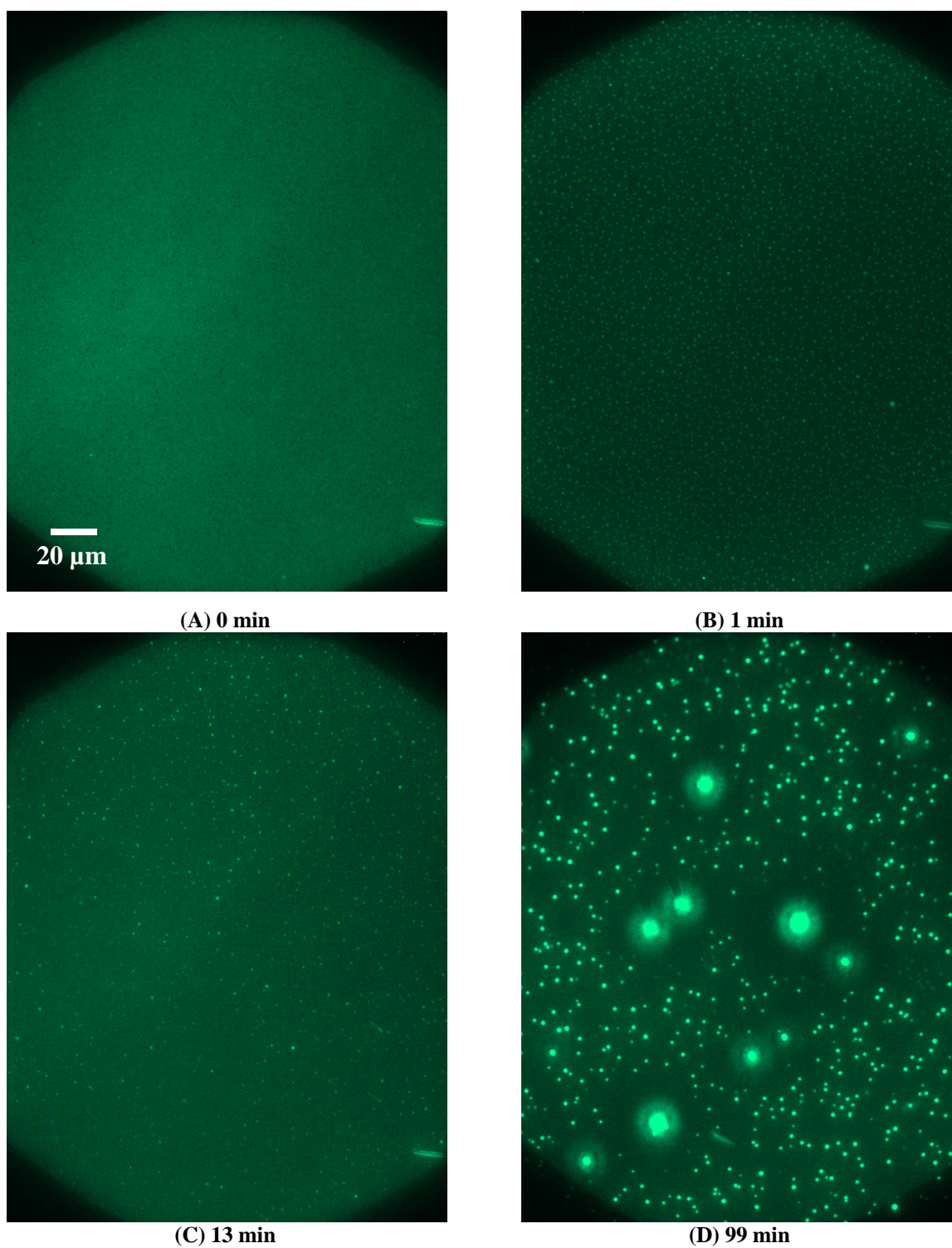


Figure 6.5-3 SLB prepared by LB/LS of POPG/POPC 1:1 (NBD-DPPE 0.75 mol%). The figures illustrate the effect and morphological changes over time (0 to 99 min) of adding 4 μ M KLA1 into the buffer.

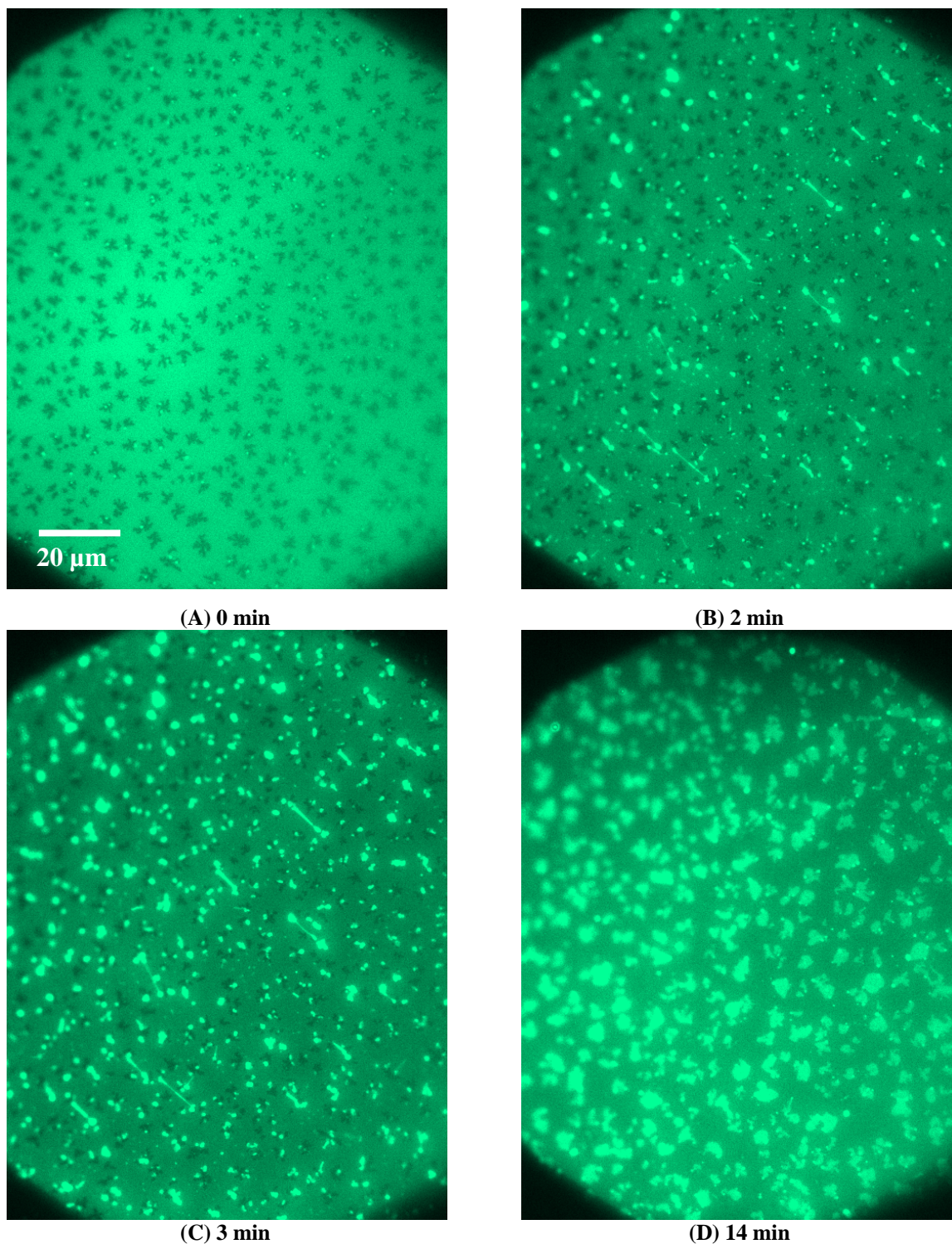


Figure 6.5-4 SLB prepared by LB/LS of POPG/POPE 1:1 (NBD-DPPE 0.75 mol%). The figures illustrate the effect and morphological changes over time (0 to 14 min) of adding 4 μM KLA1 into the buffer.

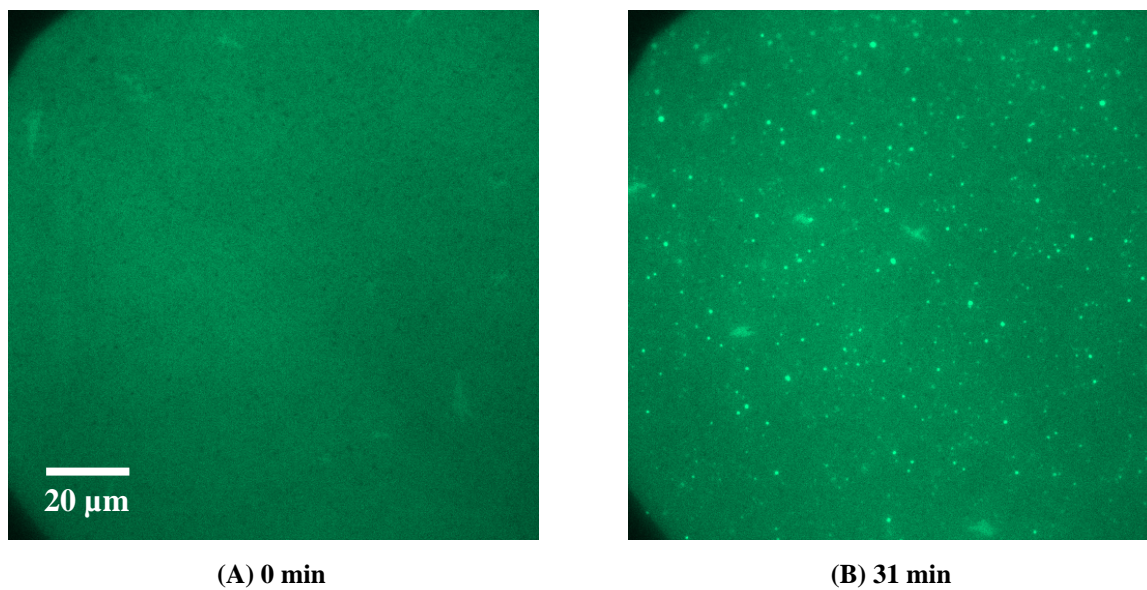


Figure 6.5-5 SLB prepared by LB/LS of *E. coli* lipid extract (NBD-DPPE 0.75 mol%) before (A) and 31 min after the addition of 5 μ M KLA1 into the buffer (B).

6.6 Summary

We investigated using epifluorescence microscopy the action of the antimicrobial peptides C-RW and KLA1 on biologically relevant lipid membranes supported on quartz. Furthermore, we demonstrated the surface structure of supported bilayers composed of POPG and of POPG rich lipid mixtures. Due to the high PG content in our model membranes, the Langmuir Blodgett/Langmuir Schaefer technique was the only possible method to prepare SLB without the necessity to utilize fusogenic agents such as Ca^{+2} . To our knowledge, such supported membranes have not been reported before in literature. The action of the membrane active peptides C-RW and KLA1 was quick (few minutes) and driven by electrostatic binding to the PG headgroup. The peptides triggered the formation of lipid protrusions that bulged out of the SLB. The protrusions seemed to grow particularly from the domain boundaries and membrane defects. Whereas C-RW facilitated the formation of long fibrils, KLA1 induced smaller membrane structures. Besides, long fibrils tended to restructure into spherical structures over time. The small differences in the behaviour of C-RW and KLA1 are most probably due to their different mode of action; C-RW is smaller and interacts preferentially with the membrane interfacial region, whereas KLA1 is buried deeper in the membrane hydrophobic core. Generally, the peptide-induced structures and the morphological changes that take place are controlled by many factors, such as 1) shape and size of the peptide, 2) peptide concentration, 3) membrane composition, 4) surface charge density, and 5) geometry of the lipid components, which could favour positive or negative curvatures.

Based on the comparable behaviour shown by the different peptides, it is obvious that the lipid protrusions and the morphological changes that occur in supported membranes are a common effect for all amphipathic structures. However, the biological relevancy of this phenomenon should be investigated further.

7 Conclusions

Several biophysical techniques, e.g. DSC, ITC, DLS and FT-IR spectroscopy, were utilized to investigate the interaction of KLA peptides with different helical propensities as well as of a linear and a cyclic arginine- and tryptophan-rich antimicrobial hexapeptide with identical amino acid sequences (Ac-RW and C-RW, respectively) with various model lipid membranes of different composition. The main findings are as follows:

KLA peptides

- The effect of the peptides on lipid membranes is modulated by the peptide conformation, the membrane properties, and the experimental conditions.
- KLA peptides can adopt various conformations depending upon the surrounding medium, temperature, lipid/peptide ratio, membrane composition, and the aggregation form.
- The KLA peptides in the helical conformation bind stronger to lipid membranes, induce higher vesicle aggregation, and are capable of forming pores. Those effects are enhanced with peptide helicity and membrane surface charge density.
- The peptides that tend to form a β -sheet structure highly perturb membranes and may render lipid vesicles leaky, although they cannot form structural pores. In addition, they can micellize lipid membranes.

Ac-RW and C-RW peptides

- Ac-RW is unstructured in buffer, whereas it assumes a β -structure upon the interaction with DPPG. Free and DPPG-bound C-RW adopt comparable β -sheet structures.
- The peptides enter anionic vesicles rapidly without an indication of a significant vesicle disruption.
- Ac-RW perturbs the lipid chain packing more pronouncedly than C-RW and shows the ability to form pores.
- The peptides decrease the phase transition temperature in DPPG and DPPG/DMPC vesicles, however, no demixing or domain formation is detected.
- The peptides induce a phase separation in DPPG/DPPE mixtures and the formation of two domains, a peptide-bound DPPG domain and a DPPG-depleted DPPE domain.
- The demixing was also observed in a TMCL/DPPG/DPPE ternary mixture and, less pronouncedly, in DPPG/POPE, TMCL/DPPG, and TMCL/DPPE binary mixtures.

In addition, epifluorescence microscopy was used to monitor the action of the antimicrobial peptides C-RW and KLA1 on supported lipid bilayers (SLB). The main observations are:

- Due to the high PG content in our model membranes, the Langmuir Blodgett/Langmuir Schaefer technique is the only possible method to prepare SLB.
- The action of the membrane active peptides C-RW and KLA1 is quick (few minutes) and driven by the electrostatic binding to the PG headgroup.
- The peptides trigger the formation of lipid protrusions that bulge out of the SLB. The protrusions seem to grow particularly from the domain boundaries and membrane defects.
- C-RW facilitates the formation of long lipid fibrils, which tend to restructure into spherical structures over time. On the other side, KLA1 induces smaller membrane protrusions as compared to C-RW.
- The peptide-induced structures and the morphological changes that take place are controlled by many factors, such as 1) shape and size of the peptide, 2) peptide concentration, 3) membrane composition, 4) surface charge density, and 5) form factor of the lipid components, which could favour a positive or a negative membrane curvature.

8 Zusammenfassung

Um die Wechselwirkung von zu unterschiedlicher Helizität neigenden amphipathischen KLA-Peptiden und einem linearen bzw. einem zyklischen arginin- und tryptophanreichen antimikrobiellen Hexapeptid mit identischen Aminosäuresequenzen (Ac-RW bzw. C-RW) mit verschiedenen Modell-Lipidmembranen unterschiedlicher Lipidzusammensetzung zu untersuchen, wurden verschiedene biophysikalische Methoden wie z.B. DSC, ITC, DLS und FT-IR-Spektroskopie eingesetzt. Folgende Ergebnisse werden erzielt:

KLA-Peptide

- Der Einfluss der Peptide auf die Lipidmembranen wird durch die Peptid-Konformation, die Membraneigenschaften und die experimentellen Bedingungen beeinflusst.
- KLA-Peptide können verschiedene Konformationen bilden, abhängig von dem umgebenden Medium, der Temperatur, dem Lipid/Peptid-Verhältnis, der Membranzusammensetzung und der Aggregationsform.
- Die KLA-Peptide in der α -helikalen Konformation binden stärker an Lipidmembranen, zeigen eine höhere Aggregationstendenz und können damit auch Poren bilden. Diese Effekte werden mit der Peptid-Helizität und Oberflächenladungsdichte der Membran erhöht.
- Die Peptide, die zur Bildung einer β -Faltblattstruktur neigen, stören die Membranen stark und können Lipidvesikel undicht machen, obwohl sie keine strukturellen Poren bilden können. Zusätzlich können sie die Lipidmembranen mizellisieren.

Ac-RW- und C-RW-Peptide

- Ac-RW ist in Pufferlösung unstrukturiert. Die Bindung an DPPG erfolgt als β -Faltblattstruktur. Freies und DPPG-gebundenes C-RW bilden vergleichbare β -Faltblattstrukturen.
- Die Peptide dringen schnell in anionische Vesikel ohne deren Zerstörung ein.
- Ac-RW stört die Packung der Lipidketten in stärkerem Maße als C-RW und zeigt die Fähigkeit Poren zu bilden.

- Die Peptide senken die Phasenumwandlungstemperatur von DPPG- und DPPG/DMPC- Vesikeln ab, es wird jedoch keine Entmischung oder Bildung von Domänen beobachtet.
- Die Peptide verursachen eine Phasentrennung in DPPG/DPPE-Mischungen und die Bildung von zwei Domänen, eine DPPG-Domäne mit gebundenem Peptid und eine DPPG-arme DPPE-Domäne.
- Die Entmischung wurde auch in einer ternären Mischung aus TMCL/DPPG/DPPE beobachtet, jedoch weniger in binären Mischungen von DPPG/POPE, TMCL/DPPG und TMCL/DPPE.

Es wurde außerdem mit Epifluoreszenzmikroskopie der Einfluss der antibiotischen Peptide C-RW und KLA1 auf festkörperunterstützte Lipiddoppelschichten (supported lipid bilayers „SLB“) untersucht. Die Hauptergebnisse sind:

- Wegen des hohen PG-Gehalts in unseren Modellmembranen ist die Langmuir-Blodgett/Langmuir-Schäfer-Technik die einzige mögliche Methode, um SLBs herzustellen.
- Die Wirkung der membranaktiven Peptide C-RW und KLA1 setzt schnell ein (wenige Minuten) und wird durch elektrostatische Bindung an die PG-Kopfgruppe getrieben.
- Die Peptide verursachen die Bildung von Lipidprotrusionen, die aus dem SLB herauswachsen. Die Protrusionen scheinen besonders von Domänengrenzen und von Membrandefekten ausgehend zu wachsen.
- C-RW erleichtert die Bildung von langen Lipidschläuchen, die dazu neigen sich über eine gewisse Zeit in kugelförmige Strukturen umzuwandeln. KLA1 verursacht kleinere Membranprotrusionen im Vergleich zu C-RW.
- Die peptidinduzierten Strukturen und die morphologischen Änderungen werden durch viele Faktoren gesteuert, wie 1) Form und Größe des Peptids, 2) Peptidkonzentration, 3) Membranzusammensetzung, 4) Oberflächenladungsdichte und 5) den Formfaktor der Lipidmoleküle, der zu einer positiven oder negativen Krümmung der Membran führen kann.

9 Experimental procedures

9.1 Materials

9.1.1 Peptides

The KLAL (KLAL KLAL KAL KAAL KLA-NH₂), KLA1 (KLAL KLAL KAW KAAL KLA-NH₂) and the other D-amino acid analogues (**Table 4.1-1**) were synthesized using the Fmoc technique and purified by RP-HPLC (Dathe et al. 1996) and applied as HCl salt. The peptide solutions were freshly prepared in an aqueous Tris buffer by weighing the lyophilized samples, dissolving them in buffer, and diluting the samples to the required concentration. The one-letter code is used to give the sequences.

The synthetic peptides Ac-RW (Ac-RRWRF-NH₂) and C-RW (cyclo-RRWRF) were synthesized as described before (Dathe et al. 2004; Wessolowski et al. 2004). The peptide solutions were freshly prepared in an aqueous Tris buffer by weighing the lyophilized samples, dissolving them in buffer, and diluting the samples to the required concentration. The one-letter code is used to give the sequences.

8.1.2 Lipids

1-palmitoyl-2-oleoyl-*sn*-glycero-3-phosphoglycerol (POPG), 1,2-Dipalmitoyl-*sn*-glycero-3-phosphoglycerol (DPPG), 1,2-dimyristoyl-*sn*-glycero-3-phosphoglycerol (DMPG), 1,2-dimyristoyl-*sn*-glycero-3-phosphate-Na (DMPA), 1,2-dimyristoyl-*sn*-glycero-3-phosphocholine (DMPC), 1,2-dipalmitoyl-*sn*-glycero-3-phosphocholine (DPPC) and 1,2-dipalmitoyl-*sn*-glycero-3-phosphoethanolamine (DPPE) were purchased from Genzyme GmbH, Germany. The POPG and 1,2-diphytanoyl-*sn*-glycero-3-phosphocholine (DPhPC) used in the epifluorescence imaging and black lipid membrane experiments as well as 1-palmitoyl-2-oleoyl-*sn*-glycero-3-phosphocholine (POPC), 1-palmitoyl-2-oleoyl-*sn*-glycero-3-phosphoethanolamine (POPE), 1,2-dioleoyl-*sn*-glycero-3-phosphoethanolamine (DOPE), 1,2-dipalmitoyl-d₆₂-*sn*-glycero-3-phosphoglycerol (DPPG-d₆₂), 1,2-dipalmitoyl-d₆₂-*sn*-glycero-3-phosphoethanolamine (DPPE-d₆₂), 1,2-dimyristoyl-d₅₄-*sn*-glycero-3-phosphoglycerol (DMPG-d₅₄), 1,2-Dipalmitoyl-*sn*-glycero-3-phospho-L-serine (DPPS), 1,1',2,2'-tetramyristoyl cardiolipin (TMCL), 1,2-dipalmitoyl-*sn*-glycero-3-phosphoethanolamine-N-[7-nitro-2-1,3-benzoxadiazol-4-yl] (NBD-DPPE) and *E. Coli* polar lipid extract (67% PE, 23.2% PG, 9.8% cardiolipin) were purchased from Avanti Polar Lipids (Alabaster, AL, USA). All lipids were

used as received without any further purification or modification. The concentration was calculated from the weight of the dry lipid samples (w/v).

9.2 Methods

9.2.1 Monolayer trough and subphase

The used experimental setup is as described previously (Kerth et al. 2004). Prior to each experiment, the used troughs were washed with diluted Hellmanex® II solution (Hellma GmbH & Co. KG, Müllheim, Germany) and rinsed thoroughly with freshly deionised water. Both of the reference and sample compartments were filled with buffer and the temperature of the subphase was kept at $20^{\circ}\text{C} \pm 0.5^{\circ}\text{C}$. All monolayer experiments were carried out on an aqueous Tris buffer (10 mM Tris/Tris-HCl, 154 mM NaCl, pH 7.4). The Tris, Tris-HCl and NaCl were purchased from Sigma-Aldrich (Stienheim, Germany). The buffer was prepared using deionised water with a resistivity of $18.2 \text{ M}\Omega/\text{cm}$ (SG Wasseraufbereitung und Regenerierstation GmbH, Barsbüttel, Germany).

9.2.2 Adsorption experiments

Two types of experiments were performed; 1) a certain volume of KLA1 aqueous solution ($432 \mu\text{M}$) was injected in the subphase to achieve a bulk concentration of 100 nM , after which the increase in the surface pressure with time due to the accumulation of the peptide at the air/water interface was observed ($A = \text{cons}$). 2) The adsorption experiments were carried out by spreading a certain amount of lipids or lipid mixtures ($2.2 - 3.3 \text{ mM}$) from a chloroform/methanol 4:1 (v/v) stock solution on the aqueous subphase. Giving the lipid film time to equilibrate (15 min), the lipid film was compressed ($-0.02 \text{ nm}^2 \text{ lipid molecule}^{-1} \text{ min}^{-1}$) to achieve a surface pressure of $30 \text{ mN/m} \pm 0.2 \text{ mN m}^{-1}$ and held 15 min to relax. Upon the injection of KLA1 into the subphase and while maintaining the surface pressure constant at 30 mN/m ($\pi = \text{cons}$), the respective increase in the area per lipid molecule, due to the adsorption of KLA1, was monitored.

9.2.3 Cospreading experiments

The pure KLAL was dissolved in chloroform/methanol 4:1 (v/v) and the film was compressed with a speed of $-0.02 \text{ nm}^2 \text{ amino acid}^{-1} \text{ min}^{-1}$. In the case of lipid/KLAL mixtures and prior to the experiments, KLAL and the corresponding lipid or lipid mixture were premixed in chloroform/methanol 4:1 (v/v) in a ratio of 20:1 (lipid/KLAL). The lipid/KLAL film was spread on the buffer subphase, equilibrated for 30 min, and compressed with a speed

of $-0.02 \text{ nm}^2 \text{ lipid molecule}^{-1} \text{ min}^{-1}$. Thereafter, the π/A isotherm of the lipid/KLAL mixture was compared to the pure lipid isotherm, which was obtained using the same procedure.

9.2.4 Infrared reflection absorption spectroscopy

Our IRRAS setup was described previously (Kerth et al. 2004). The acquisition of IRRA spectra was carried out simultaneously while measuring the π/time ($A = \text{const}$) and A/time ($\pi = \text{const}$). Both perpendicular and parallel polarized radiation was applied with an angle of incidence, with respect to the normal of the subphase surface, of 40° . A total of 1000 or 2000 scans were averaged with a spectral resolution of 4 or 8 cm^{-1} using Blackman-Harris four-term apodization and a zero filling factor of 2. The reflection absorption spectrum was calculated using the equation $-\log(R/R_0)$, where R and R_0 being the single-beam reflectance spectrum of the monolayer of the sample trough and the single-beam reflectance spectrum of the reference trough surface, respectively. Spectral calculations were performed using a Visual Basic program with an implementation of the formalism published by (Flach et al. 1997; Mendelsohn et al. 1995).

9.2.5 Dynamic light scattering

The Dynamic light scattering measurements were performed by means of ALV-NIBS/HPPS high performance particle sizer (ALV-Laser Vertriebsgesellschaft m.b.H., Langen, Germany). The system is equipped with a HeNe laser of 3mW output power at a wavelength of 632.8 nm, a backscattering arrangement (the scattering angle is 173°) and an avalanche photodiode as a detection system. The temperature of the sample compartment was regulated by a software controlled Peltier device. 100 nm diameter LUVs were freshly prepared by extrusion prior to the experiments and the samples were prepared in an aqueous Tris buffer (10 mM Tris/Tris-HCl, 154 mM NaCl, pH 7.4). The titration experiments were carried out by 10 – 50 μl multi-step titrations of 1 mM vesicles suspension into $\sim 500\mu\text{l}$ of 5 – 10 μM peptide solution (starting volume and concentration) placed in a disposable 1 cm PMMA cuvette (Brand GmbH + Co. KG, Wertheim, Germany). After giving the samples $\sim 1\text{min}$ to equilibrate, the autocorrelation function was recorded for 180s (6 x 30s), which were then averaged. The data were fitted and analyzed using the ALV-5000/E/EPP software (Version 3.0) supplied with the instrument, which is based on CONTIN software package (Provencher 1982) that uses Laplace transforms for the inversion of the autocorrelation function. The normalized unweighted particle size distributions, which correlate the particle size with its respective scattering intensity, were determined using the linear regularized fit model.

9.2.6 Circular dichroism

Far UV-CD spectra were obtained using Jasco J810 spectropolarimeter equipped with a peltier device. The peptides (25 – 100 μM) and the 100 nm diameter extruded vesicles (1 mM) were prepared in an aqueous Tris buffer and mixed in a 0.1 cm cuvette to achieve an L/P ratio of 10 to 40. Thereafter, 10 to 20 accumulations of the CD spectra were recorded in the range of 190 – 260 nm. The spectra were corrected from the circular dichroism and differential scattering due to lipid vesicles, averaged and smoothed. The mean residual ellipticity $[\Theta]_{\text{MRW}}$ (in $\text{deg cm}^2 \text{mol}^{-1}$) was calculated using $[\Theta]_{\text{MRW}} = \Theta \cdot M_r / 10 \cdot d \cdot c \cdot N_A$, where Θ is the measured ellipticity in mdeg, M_r is the molecular mass of the peptide in g mol^{-1} , d is the optical path length in cm, c is the concentration in mg mL^{-1} and N_A is number of monomers in the peptide, namely 18.

9.2.7 Differential scanning calorimetry

For DSC experiments, the samples were prepared in an aqueous Tris buffer (10 mM Tris/Tris-HCl, 154 mM NaCl, pH 7.4). Tris-HCl and NaCl were purchased from Sigma-Aldrich (Steinheim, Germany). The vesicles of the pure lipids and lipid mixtures were prepared by sonication in a water bath at a temperature higher than the phase transition temperature of the lipid to obtain mostly unilamellar vesicles with an average diameter of 50 – 100 nm. The DSC measurements were carried out using VP-DSC from MicroCalTM Inc. (Northampton, MA). From the stock solution of the lipid vesicles and lipid mixtures, a final concentration of 1 – 2 mM lipid was prepared. The lipid-peptide mixtures with the desired ratio (5 – 200 μM peptide) were freshly pre-mixed prior to the DSC experiments. The samples were degassed for 10 minutes before being loaded. A scanning rate of 1°C min^{-1} was applied. The reference cell was filled with buffer. Several heating and cooling scans were performed to ensure the reproducibility of the thermograms.

9.2.8 Fourier transform infrared

The samples were prepared in an aqueous 100 mM NaCl solution. For experiments in D_2O (Sigma-Aldrich, Steinheim, Germany), the samples were reconstituted in $\sim 500\mu\text{l}$ D_2O and lyophilized for 3 times to ensure maximum H/D exchange. The lipid-peptide mixtures were sonicated for 60 minutes at a temperature higher than the transition temperature of the lipid to ensure equilibration of binding of the peptides to both sides of the membranes in the liposomes. The IR spectra were obtained using a Bruker Vector 22 spectrometer (Bruker GmbH, Germany) equipped with a DTGS detector. $15\mu\text{l}$ of 60 mM lipid or of 60 mM lipid/10 mM peptide mixture was placed between two CaF_2 windows with a 25 μm -thick Teflon

spacer. The sample holder was temperature-controlled by means of an external heating water bath (HAAKE Phoenix II C25P, Thermo Electron GmbH, Karlsruhe, Germany). At each temperature, the sample was equilibrated for at least 8 minutes and, thereafter, 64 scans were recorded with a resolution of 2 cm^{-1} and a zero filling factor of 2. For data processing, the Bruker OPUS FT-IR software was utilized. Spectra of a 100mM NaCl solution in H_2O or in D_2O were used as reference and subtracted from the sample spectra. Peak positions were determined by the second derivative method. Fitting the carbonyl bands in the IR spectra was carried out using the curve fitting command provided in OPUS software, where the Gaussian function and the values reported in (Blume et al. 1988), as a starting point for the peaks position, were applied.

9.2.9 *Isothermal titration calorimetry*

The ITC measurements were carried out using a VP-ITC from MicroCal™, Inc. (Northampton, MA). Regarding the titration experiments of KLA peptides, the LUV of lipids and lipid mixtures were freshly prepared by extrusion through a 100 nm diameter polycarbonate filter at a temperature higher than the phase transition temperature of the lipid or lipid mixture. The size distribution of the lipid vesicles was controlled by dynamic light scattering using ALV-NIBS/HPPS spectrometer (ALV-Laser Vertriebsgesellschaft m.b.H., Langen, Germany). Prior to each experiment, the sample cell and the syringe were washed with freshly distilled water, rinsed using chloroform/methanol 2:1 (v/v), and dried. The reference cell was filled with degassed water. The samples were prepared in an aqueous Tris buffer (10 mM Tris/Tris-HCl, 154 mM NaCl, pH 7.4). Unless otherwise specified, the 1.4ml reaction cell was loaded with the peptide solution (typical concentration 5 – 10 μM), whereas the injection syringe (nominal volume 250 μl) was filled with the vesicles suspension (typically 500 μM). The instrument was equilibrated at a temperature 5 °C below the experimental temperature with an initial delay of 60s. The reference power and the filter were set to 10 $\mu\text{cal s}^{-1}$ and 2s, respectively. After the point of the first injection was discarded, the titration curves were analyzed using the one binding-site model in the ORIGIN® software provided with the calorimeter.

The titration procedure of RRWWRF peptides was comparable to that with KLA peptides. However, the vesicles of the pure lipids and lipid mixtures were prepared by sonication in a water bath at a temperature higher than the phase transition temperature of the lipid for 30 - 60 minutes to obtain mostly unilamellar vesicles with an average diameter of 50 - 100 nm. Unless otherwise specified, the 1.4ml reaction cell was loaded with the peptide

solution (typical concentration 20-50 μM), whereas the injection syringe (nominal volume 250 μl) was filled with the vesicles suspension (typically 2.5-5 mM).

9.2.10 Planar supported bilayers

For the epifluorescence microscopy and FRAP experiments, quartz slides (40 mm x 25 mm x 1 mm) were purchased from Quartz Scientific (Fairport Harbor, OH). The following steps were used to clean the slides: 1) boiling in 10% Contrad 70 detergent (Fisher Scientific, Fair Lawn, NJ) for 10 min, 2) hot bath sonication in the detergent for 30 min, 3) thorough rinsing with Milli-Q water, 4) immersion in 95% H_2SO_4 /30% H_2O_2 (Fisher Scientific, Fair Lawn, NJ) 3:1 for 30 min to remove any organic residues, 5) extensive rinsing with Milli-Q water, and 6) the slides were kept in deionised water ready for use. Immediately prior to use, the slides were further cleaned for 5 - 10 min in an argon plasma sterilizer (Harrick Scientific, Ossining, NY).

The supported planar bilayers were prepared by one of three methods (Tamm and Tatulian 1997): vesicle fusion (Brian and McConnell 1984), Langmuir Blodgett/Langmuir Schaefer (Tamm and McConnell 1985), or combined Langmuir Blodgett/vesicle fusion (Kalb et al. 1992).

Vesicle fusion (VF): the desired lipids or lipid mixtures were co-solved with 1% NBD-DPPE in chloroform/methanol (Fisher Scientific, Fair Lawn, NJ) mixture. Thereafter, the solvent was evaporated under a stream of N_2 and kept under vacuum for at least 1 hour. The lipid residue was resuspended in aqueous Tris buffer (10 mM Tris/Tris-HCl, 154 mM NaCl, pH 7.4) and extruded to produce LUV (100 nm diameter). A clean quartz slide was placed in a custom-built flow-through chamber. 1.2 ml of 100 μM suspension of LUV was injected in the chamber and incubated for 30 to 60 min for the supported bilayer to form. The excess vesicles were flushed by rinsing the chamber with Tris buffer. If necessary, the lipid vesicles were premixed with CaCl_2 (Fisher Scientific, Fair Lawn, NJ), as a source for Ca^{+2} ions, to achieve final a concentration of 0.2 to 1 mM. Consequently, the excess vesicles/ Ca^{+2} were washed out using buffer contains ~ 20 mM EDTA (Fisher Scientific, Fair Lawn, NJ).

Langmuir Blodgett/Langmuir Schaefer (LB/LS): prior to each preparation, a Nima 611 Langmuir Blodgett trough (Nima, Coventry, U.K.) was rinsed extensively with distilled water. The trough was filled with deionised water and the lipid films were prepared at room temperature. A lipid monolayer containing 0.75% NBD-DPPE was spread from chloroform/methanol solution on the water surface to achieve a starting surface pressure of 0 to 5 mN m^{-1} . The film was given ~ 10 min to equilibrate and for the solvent to evaporate entirely. Thereafter, the film was compressed with a speed of 15 $\text{cm}^2 \text{min}^{-1}$ to reach a surface

pressure of $\sim 32 \text{ mN m}^{-1}$. Again, the film was given 10 min to equilibrate while the software maintained the surface pressure constant at 32 mN m^{-1} . A freshly cleaned quartz slide was rapidly (200 mm min^{-1}) dipped in the trough and slowly (5 mm min^{-1}) withdrawn, while the surface pressure was maintained at 32 mN m^{-1} , thereby depositing a LB lipid monolayer at each side of the slide. The same procedure could be repeated to deposit as many LB films as necessary using the same lipid film. The LS film was achieved through quick compression of the LB coated slide with its face down vertically against the lipid film to the trough. A suctioning tip was used to hold the slide. The slide was then pushed in the chamber that has previously been placed in the trough underneath the lipid film. The chamber was assembled and sealed under water to prevent air bubbles from entering the chamber. At last, the water in the chamber was carefully exchanged with Tris buffer.

Langmuir Blodgett/vesicle fusion (LB/VF): after an LB-coated slide was prepared and placed in the flow-through chamber, the vesicle suspension was injected in the chamber, incubated, and then rinsed as previously described.

9.2.11 Fluorescence microscopy

The epifluorescence imaging was carried out using two fluorescence microscopes that were described elsewhere (Kiessling et al. 2006; Kiessling and Tamm 2003; Wan et al. 2008): A) using a Zeiss Axiovert 35 fluorescence microscope (Carl Zeiss, Thornwood, NY) with a 40x water immersion objective (Zeiss; numerical aperture (N.A.) 0.75) and the Images ($520 \times 688 \text{ pixel}^2$, $139 \times 105 \text{ }\mu\text{m}^2$) were recorded by a charge-coupled device (CCD) cooled to -12°C (Sensicam QE, Cooke, Auburn Hills, MI), B) using a Zeiss Axiovert 200 fluorescence microscope (Carl Zeiss, Thornwood, NY) with a 63x water immersion objective (Zeiss; numerical aperture (N.A.) 0.95) and the images ($512 \times 512 \text{ pixel}^2$, $128 \times 128 \text{ }\mu\text{m}^2$) were recorded by an electron multiplying charge-coupled device (EMCCD) cooled to -60°C (iXon DV887AC-FI, Andor, Belfast, UK). The FRAP experiments were performed using the former setup. For the epifluorescence imaging, the NBD-DPPE-labelled bilayers were excited with a mercury lamp through a 546-nm band-pass filter (BP546/10, Schott Glaswerke, Mainz, Germany) and observed through a 610-nm band-pass filter (D610/60, Chroma, Brattleboro, VT). For FRAP experiments, NBD-DPPE was excited by an argon ion laser (Innova 300C, Coherent, Palo Alto, CA) at 488 nm and observed through a 535-nm band-pass filter (D535/40, Chroma). The intensity of the laser beam was computer controlled through an acousto-optic modulator (AOM-40, IntraAction, Bellwood, IL) or could be blocked entirely by a computer-controlled shutter. Fluorescence emission intensity was measured using a photomultiplier tube (Thorn EMI 9658A, Ruislip, UK). Data acquisition and image analysis

was done using homemade LabVIEW software (National Instruments, Austin, TX). Further image processing was performed using Adobe® Photoshop®.

9.2.12 Fluorescence recovery after photobleaching

In the FRAP experiments (Kiessling et al. 2006; Kiessling and Tamm 2003; Tamm and Kalb 1993) the NBD-DPPE labelled lipid bilayers were bleached in a pattern of parallel stripes (Smith and McConnell 1978). The $F(t) = F_{\infty} + (F_0 - F_{\infty}) \exp(-Da^2t)$ model was employed to fit the fluorescence (F) recovery versus time (t) data, where F_0 and F_{∞} are the initial and final fluorescence intensities after bleaching, respectively, $a = 2\pi/p$, p is the stripe period (12.7 or 3.2 μm), and D is the lateral diffusion coefficient. The mobile fraction mf , which reflects the % of observed fluorescence recovery within the time frame of a FRAP experiment (< 1 min), is given by $mf = 200 (F_{\infty} - F_0)/(F_{\text{pre}} - F_0)$, where F_{pre} is the fluorescence intensity before photobleaching. At least ten different regions were examined to determine lateral diffusion constant of the supported bilayer.

9.3 Important infrared absorption bands

Table 9.3-1 Important infrared absorption bands of lipids. Adapted from ref. (Lewis and McElhaney 1996; Mendelsohn and Mantsch 1986; Tamm and Tatulian 1997)

Assignment	Symbol	Approximate wavenumber (cm^{-1})
CH ₂ antisymmetric stretching	$\nu_{\text{as}}(\text{CH}_2)$	2916 – 2936 (s)
CH ₂ symmetric stretching	$\nu_{\text{s}}(\text{CH}_2)$	2843 – 2863 (s)
CD ₂ antisymmetric stretching	$\nu_{\text{as}}(\text{CD}_2)$	2190 – 2200 (s)
CD ₂ symmetric stretching	$\nu_{\text{s}}(\text{CD}_2)$	2085 – 2095 (s)
C=O stretching	$\nu(\text{CO})$	1730 – 1740 (s)
NH ₃ ⁺ antisymmetric bending	$\delta_{\text{as}}(\text{NH}_3^+)$	1630 (m)
COO ⁻ antisymmetric stretching	$\nu_{\text{as}}(\text{COO}^-)$	1623 (s)
NH ₃ ⁺ symmetric bending	$\delta_{\text{s}}(\text{NH}_3^+)$	1571 (m)
N ⁺ (CH ₃) ₃ antisymmetric bending	$\delta_{\text{as}}(\text{N}^+(\text{CH}_3)_3)$	1485 (m)
CH ₂ scissoring (hexagonal)	$\delta(\text{CH}_2)_n$	1467 – 1469 (m)
CH ₂ scissoring (triclinic)	$\delta(\text{CH}_2)_n$	1471 – 1473 (m)
CH ₂ scissoring (orthorhombic)	$\delta(\text{CH}_2)_n$	1465 and 1473 (m)
N ⁺ (CH ₃) ₃ symmetric bending	$\delta_{\text{s}}(\text{N}^+(\text{CH}_3)_3)$	1405 (m)
CH ₂ wagging band progression	$w(\text{CH}_2)$	1200 – 1400 (w)
PO ₂ ⁻ antisymmetric stretching	$\nu_{\text{as}}(\text{PO}_2^-)$	1200 – 1260 (s)
PO ₂ ⁻ symmetric stretching	$\nu_{\text{s}}(\text{PO}_2^-)$	1085 – 1110 (m)
CH ₂ rocking	$\gamma(\text{CH}_2)$	720 – 730 (m)
CD ₂ scissoring (hexagonal)	$\delta(\text{CD}_2)_n$	1088 (m)
CD ₂ scissoring (triclinic)	$\delta(\text{CD}_2)_n$	1093 (m)
CD ₂ scissoring (orthorhombic)	$\delta(\text{CD}_2)_n$	1083 and 1093 (m)

s, strong; m, medium; w, weak.

Table 9.3-2 Infrared absorption frequencies of liquid H₂O, HOD, and D₂O. Adapted from ref. (Tamm and Tatulian 1997).

Assignment	H ₂ O (cm ⁻¹)	HOD (cm ⁻¹)	D ₂ O (cm ⁻¹)
O-X antisymmetric stretching	3490 (s)	3380 ^a (s)	2540 (s)
O-X symmetric stretching	3280 (s)	2500 ^b (s)	2450 (s)
Association	2125 (w)		1555 (w)
Bending	1645 (s)	1450 (s)	1210 (s)

^aO-H, ^bO-D. s, strong; w, weak.

Table 9.3-3 Correlation between common protein secondary structures and the frequencies of Amide I and Amide II bands in H₂O and D₂O. Adapted from ref. (Arrondo et al. 1993; Goormaghtigh et al. 1994; Jackson and Mantsch 1995; Tamm and Tatulian 1997).

Secondary structure	Amide I band (cm ⁻¹)		Amide II band (cm ⁻¹)
	H ₂ O	D ₂ O	H ₂ O
Antiparallel β-sheet/ aggregated strands	1684 (1674 – 1695)	1679 (1672 – 1694)	
Turns/loops	1672 (1662 – 1682)	1671 (1653 – 1691)	
α-helix	1654 (1648 – 1657)	1652 (1642 – 1660)	1546 (1545 – 1550)
Random	1654 (1642 – 1657)	1645 (1639 – 1654)	
β-sheet	1633 (1623 – 1641)	1630 (1615 – 1638))	1528 (1525 – 1532)
Aggregated strands	1610 - 1628		

10 References

- Abraham T, Lewis RN, Hodges RS, McElhaney RN (2005a) Isothermal titration calorimetry studies of the binding of a rationally designed analogue of the antimicrobial peptide gramicidin S to phospholipid bilayer membranes. *Biochemistry* 44:2103-12
- Abraham T, Lewis RN, Hodges RS, McElhaney RN (2005b) Isothermal titration calorimetry studies of the binding of the antimicrobial peptide gramicidin S to phospholipid bilayer membranes. *Biochemistry* 44:11279-85
- Abrunhosa F, Faria S, Gomes P, Tomaz I, Pessoa JC, Andreu D, Bastos M (2005) Interaction and lipid-induced conformation of two cecropin-melittin hybrid peptides depend on peptide and membrane composition. *J. Phys. Chem. B* 109:17311-9
- Abuja PM, Zenz A, Trabi M, Craik DJ, Lohner K (2004) The cyclic antimicrobial peptide RTD-1 induces stabilized lipid-peptide domains more efficiently than its open-chain analogue. *FEBS Lett.* 566:301-6
- Adao R, Seixas R, Gomes P, Pessoa JC, Bastos M (2008) Membrane structure and interactions of a short Lycotoxin I analogue. *J. Pept. Sci.* 14:528-34
- Ambroggio EE, Kim DH, Separovic F, Barrow CJ, Barnham KJ, Bagatolli LA, Fidelio GD (2005) Surface behavior and lipid interaction of Alzheimer beta-amyloid peptide 1-42: a membrane-disrupting peptide. *Biophys. J.* 88:2706-13
- Andreu D, Rivas L (1998) Animal antimicrobial peptides: an overview. *Biopolymers* 47:415-33
- Andrushchenko VV, Vogel HJ, Prenner EJ (2007) Interactions of tryptophan-rich cathelicidin antimicrobial peptides with model membranes studied by differential scanning calorimetry. *Biochim. Biophys. Acta* 1768:2447-58
- Andrushchenko VV, Aarabi MH, Nguyen LT, Prenner EJ, Vogel HJ (2008) Thermodynamics of the interactions of tryptophan-rich cathelicidin antimicrobial peptides with model and natural membranes. *Biochim. Biophys. Acta* 1778:1004-14
- Appelt C, Eisenmenger F, Kuhne R, Schmieder P, Soderhall JA (2005a) Interaction of the antimicrobial peptide cyclo(RRWRF) with membranes by molecular dynamics simulations. *Biophys. J.* 89:2296-306
- Appelt C, Wessolowski A, Dathe M, Schmieder P (2008) Structures of cyclic, antimicrobial peptides in a membrane-mimicking environment define requirements for activity. *J. Pept. Sci.* 14:524-527
- Appelt C, Wessolowski A, Soderhall JA, Dathe M, Schmieder P (2005b) Structure of the antimicrobial, cationic hexapeptide cyclo(RRWRF) and its analogues in solution and bound to detergent micelles. *Chembiochem* 6:1654-62
- Arnt L, Rennie JR, Linser S, Willumeit R, Tew GN (2006) Membrane Activity of Biomimetic Facially Amphiphilic Antibiotics. *J. Phys. Chem. B* 110:3527-3532
- Arouri A (2004) Interaction between lipids and polyamines Institute of Chemistry, vol Project work, M.Sc. Martin-Luther-Universität Halle-Wittenberg, Halle (Saale)
- Arouri A, Garidel P, Kliche W, Blume A (2007) Hydrophobic interactions are the driving force for the binding of peptide mimotopes and Staphylococcal protein A to recombinant human IgG1. *Eur. Biophys. J.* 36:647-60
- Arrondo JL, Muga A, Castresana J, Goni FM (1993) Quantitative studies of the structure of proteins in solution by Fourier-transform infrared spectroscopy. *Prog. Biophys. Mol. Biol.* 59:23-56
- Atkinson D, Small DM (1986) Recombinant lipoproteins: implications for structure and assembly of native lipoproteins. *Annu. Rev. Biophys. Biophys. Chem.* 15:403-56

- Barman H, Walch M, Latinovic-Golic S, Dumrese C, Dolder M, Groscurth P, Ziegler U (2006) Cholesterol in negatively charged lipid bilayers modulates the effect of the antimicrobial protein granulysin. *J. Membr. Biol.* 212:29-39
- Bechinger B (1999) The structure, dynamics and orientation of antimicrobial peptides in membranes by multidimensional solid-state NMR spectroscopy. *Biochim. Biophys. Acta* 1462:157-83
- Bechinger B, Lohner K (2006) Detergent-like actions of linear amphipathic cationic antimicrobial peptides. *Biochim. Biophys. Acta* 1758:1529-39
- Bellomio A, Oliveira RG, Maggio B, Morero RD (2005) Penetration and interactions of the antimicrobial peptide, microcin J25, into uncharged phospholipid monolayers. *J. Colloid Interf. Sci.* 285:118-24
- Bhunia A, Domadia PN, Bhattacharjya S (2007) Structural and thermodynamic analyses of the interaction between melittin and lipopolysaccharide. *Biochim. Biophys. Acta* 1768:3282-91
- Binder H, Lindblom G (2003) Charge-dependent translocation of the Trojan peptide penetratin across lipid membranes. *Biophys. J.* 85:982-95
- Binder H, Lindblom G (2004) A molecular view on the interaction of the trojan peptide penetratin with the polar interface of lipid bilayers. *Biophys. J.* 87:332-43
- Blokzijl W, Engberts JBFN (1993) Hydrophobic effects. Opinions and facts. *Angew. Chem. Int. Edit.* 32:1545-1579
- Blondelle SE, Houghten RA (1996) Novel antimicrobial compounds identified using synthetic combinatorial library technology. *Trends Biotechnol.* 14:60-5
- Blondelle SE, Takahashi E, Dinh KT, Houghten RA (1995) The antimicrobial activity of hexapeptides derived from synthetic combinatorial libraries. *J. Appl. Bacteriol.* 78:39-46
- Blume A (1979) A comparative study of the phase transitions of phospholipid bilayers and monolayers. *Biochim. Biophys. Acta* 557:32-44
- Blume A (2004) Lipids. In: Walz D, Teissie J, Milazzo G (eds) *Bioelectrochemistry of membranes*. Birkhäuser Verlag, Basel, pp 60-152
- Blume A, Hübner W, Messner G (1988) Fourier transform infrared spectroscopy of ¹³C=O-labeled phospholipids hydrogen bonding to carbonyl groups. *Biochemistry* 27:8239-49
- Brauner JW, Mendelsohn R (1986) A comparison of differential scanning calorimetric and Fourier transform infrared spectroscopic determination of mixing behavior in binary phospholipid systems. *Biochim. Biophys. Acta* 861:16-24
- Breukink E, Ganz P, de Kruijff B, Seelig J (2000) Binding of Nisin Z to bilayer vesicles as determined with isothermal titration calorimetry. *Biochemistry* 39:10247-54
- Brian AA, McConnell HM (1984) Allogeneic stimulation of cytotoxic T cells by supported planar membranes. *Proc. Natl. Acad. Sci. USA* 81:6159-63
- Bringezu F, Majerowicz M, Maltseva E, Wen S, Brezesinski G, Waring AJ (2007a) Penetration of the antimicrobial peptide dicynthaurin into phospholipid monolayers at the liquid-air interface. *Chembiochem* 8:1038-47
- Bringezu F, Wen S, Dante S, Hauss T, Majerowicz M, Waring A (2007b) The insertion of the antimicrobial peptide dicynthaurin monomer in model membranes: thermodynamics and structural characterization. *Biochemistry* 46:5678-86
- Brogden KA (2005) Antimicrobial peptides: pore formers or metabolic inhibitors in bacteria? *Nat. Rev. Microbiol.* 3:238-50
- Brogden KA, De Lucca AJ, Bland J, Elliott S (1996) Isolation of an ovine pulmonary surfactant-associated anionic peptide bactericidal for *Pasteurella haemolytica*. *Proc. Natl. Acad. Sci. USA* 93:412-6

- Caffrey M, Cheng A (1995) Kinetics of lipid phase changes. *Curr. Opin. Struct. Biol.* 5:548-55
- Cai P, Flach CR, Mendelsohn R (2003) An infrared reflection-absorption spectroscopy study of the secondary structure in (KL₄)₄K, a therapeutic agent for respiratory distress syndrome, in aqueous monolayers with phospholipids. *Biochemistry* 42:9446-52
- Campelo F, Hernandez-Machado A (2007) Model for curvature-driven pearling instability in membranes. *Phys. Rev. Lett.* 99:088101-4
- Castano S, Desbat B, Dufourcq J (2000) Ideally amphipathic beta-sheeted peptides at interfaces: structure, orientation, affinities for lipids and hemolytic activity of (KL)_mK peptides. *Biochim. Biophys. Acta* 1463:65-80
- Cevc G (1990) Membrane electrostatics. *Biochim. Biophys. Acta* 1031:311-82
- Cevc G (1993) Appendix B: Thermodynamic parameters of phospholipids. In: Cevc G (ed) *Phospholipids Handbook*. Marcel Dekker, Inc., New York, pp 939-946
- Chan DI, Prenner EJ, Vogel HJ (2006) Tryptophan- and arginine-rich antimicrobial peptides: structures and mechanisms of action. *Biochim. Biophys. Acta* 1758:1184-202
- Chirgadze YN, Fedorov OV, Trushina NP (1975) Estimation of amino acid residue side-chain absorption in the infrared spectra of protein solutions in heavy water. *Biopolymers* 14:679-94
- Choung SY, Kobayashi T, Takemoto K, Ishitsuka H, Inoue K (1988) Interaction of a cyclic peptide, Ro09-0198, with phosphatidylethanolamine in liposomal membranes. *Biochim. Biophys. Acta* 940:180-7
- Cronan JE (2003) Bacterial membrane lipids: where do we stand? *Annu. Rev. Microbiol.* 57:203-24
- Cummings JE, Vanderlick TK (2007) Aggregation and hemi-fusion of anionic vesicles induced by the antimicrobial peptide cryptdin-4. *Biochim. Biophys. Acta* 1768:1796-804
- Dasher S, Liu S, Reynolds E (2007) Antimicrobial peptides and their potential as oral therapeutic agents. *Int. J. Pept. Res. Ther.* 13:505-516
- Dathe M, Meyer J, Beyermann M, Maul B, Hoischen C, Bienert M (2002) General aspects of peptide selectivity towards lipid bilayers and cell membranes studied by variation of the structural parameters of amphipathic helical model peptides. *Biochim. Biophys. Acta* 1558:171-86
- Dathe M, Nikolenko H, Klose J, Bienert M (2004) Cyclization increases the antimicrobial activity and selectivity of arginine- and tryptophan-containing hexapeptides. *Biochemistry* 43:9140-50
- Dathe M, Schumann M, Wieprecht T, Winkler A, Beyermann M, Krause E, Matsuzaki K, Murase O, Bienert M (1996) Peptide helicity and membrane surface charge modulate the balance of electrostatic and hydrophobic interactions with lipid bilayers and biological membranes. *Biochemistry* 35:12612-22
- Dathe M, Wieprecht T (1999) Structural features of helical antimicrobial peptides: their potential to modulate activity on model membranes and biological cells. *Biochim. Biophys. Acta* 1462:71-87
- Dathe M, Wieprecht T, Nikolenko H, Handel L, Maloy WL, MacDonald DL, Beyermann M, Bienert M (1997) Hydrophobicity, hydrophobic moment and angle subtended by charged residues modulate antibacterial and haemolytic activity of amphipathic helical peptides. *FEBS Lett.* 403:208-12
- Deshayes S, Morris MC, Divita G, Heitz F (2006) Interactions of amphipathic CPPs with model membranes. *Biochim. Biophys. Acta* 1758:328-35
- Dieudonne D, Gericke A, Flach CR, Jiang X, Farid RS, Mendelsohn R (1998) Propensity for Helix Formation in the Hydrophobic Peptides K₂(LA)_x (x = 6, 8, 10, 12) in

- Monolayer, Bulk, and Lipid-Containing Phases. Infrared and Circular Dichroism Studies. *J. Am. Chem. Soc.* 120:792-799
- Domanov YA, Kinnunen PK (2006) Antimicrobial peptides temporins B and L induce formation of tubular lipid protrusions from supported phospholipid bilayers. *Biophys. J.* 91:4427-39
- Domingues MM, Santiago PS, Castanho MA, Santos NC (2008) What can light scattering spectroscopy do for membrane-active peptide studies? *J. Pept. Sci.* 14:394-400
- Dowhan W, Bogdanov M (2002) Functional roles of lipids in membranes. In: Vance DE, Vance JE (eds) *Biochemistry of lipids, lipoproteins and membranes*. Elsevier, Amsterdam, pp 1-35
- Dufourcq J, Faucon JF, Fourche G, Dasseux JL, Le Maire M, Gulik-Krzywicki T (1986) Morphological changes of phosphatidylcholine bilayers induced by melittin: vesicularization, fusion, discoidal particles. *Biochim. Biophys. Acta* 859:33-48
- Dyck M, Kerth A, Blume A, Losche M (2006) Interaction of the Neurotransmitter, Neuropeptide Y, with Phospholipid Membranes: Infrared Spectroscopic Characterization at the Air/Water Interface. *J. Phys. Chem. B* 110:22152-22159
- Eisenberg D (1984) Three-dimensional structure of membrane and surface proteins. *Annu. Rev. Biochem.* 53:595-623
- El Jastimi R, Lafleur M (1999) Nisin promotes the formation of non-lamellar inverted phases in unsaturated phosphatidylethanolamines. *Biochim. Biophys. Acta* 1418:97-105
- Engelke M, Jessel R, Wiechmann A, Diehl HA (1997) Effect of inhalation anaesthetics on the phase behaviour, permeability and order of phosphatidylcholine bilayers. *Biophys. Chem.* 67:127-38
- Engelman DM (2005) Membranes are more mosaic than fluid. *Nature* 438:578-80
- Epanand RF, Mowery BP, Lee SE, Stahl SS, Lehrer RI, Gellman SH, Epanand RM (2008a) Dual mechanism of bacterial lethality for a cationic sequence-random copolymer that mimics host-defense antimicrobial peptides. *J. Mol. Biol.* 379:38-50
- Epanand RF, Schmitt MA, Gellman SH, Epanand RM (2006) Role of membrane lipids in the mechanism of bacterial species selective toxicity by two alpha/beta-antimicrobial peptides. *Biochim. Biophys. Acta* 1758:1343-50
- Epanand RM, Epanand RF (2008) Lipid domains in bacterial membranes and the action of antimicrobial agents. *Biochim. Biophys. Acta*
- Epanand RM, Rotem S, Mor A, Berno B, Epanand RF (2008b) Bacterial membranes as predictors of antimicrobial potency. *J. Am. Chem. Soc.* 130:14346-52
- Erbe A (2001) Sekundärstruktur eines Modellpeptids an Grenzflächen Institute of chemistry, vol Diplom. Martin-Luther-University Halle-Wittenberg, Halle
- Flach C, Cai P, Mendelsohn R (2006) IR reflectance-absorbance studies of peptide structure, orientation, and conformational flexibility in langmuir films: relevance for models of pulmonary surfactant action. In: Arrondo JLR, Alonso A (eds) *Advanced Techniques in Biophysics*, vol 10. Springer Berlin Heidelberg, pp 49-71
- Flach CR, Gericke A, Mendelsohn R (1997) Quantitative Determination of Molecular Chain Tilt Angles in Monolayer Films at the Air/Water Interface: Infrared Reflection/Absorption Spectroscopy of Behenic Acid Methyl Ester. *J. Phys. Chem. B* 101:58-65
- Freceer V (2006) QSAR analysis of antimicrobial and haemolytic effects of cyclic cationic antimicrobial peptides derived from protegrin-1. *Bioorg. Med. Chem.* 14:6065-74
- Freceer V, Ho B, Ding JL (2004) De novo design of potent antimicrobial peptides. *Antimicrob. Agents Chemother.* 48:3349-57
- Garidel P, Blume A (2000) Miscibility of phosphatidylethanolamine-phosphatidylglycerol mixtures as a function of pH and acyl chain length. *Eur. Biophys. J.* 28:629-638

- Garidel P, Blume A, Hubner W (2000) A Fourier transform infrared spectroscopic study of the interaction of alkaline earth cations with the negatively charged phospholipid 1, 2-dimyristoyl-sn-glycero-3-phosphoglycerol. *Biochim. Biophys. Acta* 1466:245-59
- Garidel P, Hildebrand A, Knauf K, Blume A (2007) Membranolytic activity of bile salts: influence of biological membrane properties and composition. *Molecules* 12:2292-326
- Garidel P, Johann C, Blume A (1997a) Nonideal mixing and phase separation in phosphatidylcholine-phosphatidic acid mixtures as a function of acyl chain length and pH. *Biophys. J.* 72:2196-210
- Garidel P, Johann C, Mennicke L, Blume A (1997b) The mixing behavior of pseudobinary phosphatidylcholine-phosphatidylglycerol mixtures as a function of pH and chain length. *Eur. Biophys. J.* 26:447-459
- Gennis RB (1989) *Biomembranes. Molecular structure and function.* Springer-Verlag, Heidelberg
- Gidalevitz D, Ishitsuka Y, Muresan AS, Konovalov O, Waring AJ, Lehrer RI, Lee KY (2003) Interaction of antimicrobial peptide protegrin with biomembranes. *Proc. Natl. Acad. Sci. USA* 100:6302-7
- Gifford JL, Hunter HN, Vogel HJ (2005) Lactoferricin: a lactoferrin-derived peptide with antimicrobial, antiviral, antitumor and immunological properties. *Cell. Mol. Life Sci.* 62:2588-98
- Ginsberg L (1978) Does Ca²⁺ cause fusion or lysis of unilamellar lipid vesicles? *Nature* 275:758-760
- Giuliani A, Pirri G, Nicoletto S (2007) Antimicrobial peptides: an overview of a promising class of therapeutics. *Cent. Eur. J. Biol.* 2:1-33
- Goncalves E, Kitas E, Seelig J (2005) Binding of oligoarginine to membrane lipids and heparan sulfate: structural and thermodynamic characterization of a cell-penetrating peptide. *Biochemistry* 44:2692-702
- Goni FM, Urbaneja MA, Arrondo JL, Alonso A, Durrani AA, Chapman D (1986) The interaction of phosphatidylcholine bilayers with Triton X-100. *Eur. J. Biochem.* 160:659-65
- Goormaghtigh E, Cabiaux V, Ruyschaert JM (1994) Determination of soluble and membrane protein structure by Fourier transform infrared spectroscopy. III. Secondary structures. *Subcell. Biochem.* 23:405-50
- Gordon YJ, Romanowski EG, McDermott AM (2005) A review of antimicrobial peptides and their therapeutic potential as anti-Infective drugs. *Curr. Eye Res.* 30:505-515
- Hac AE, Seeger HM, Fidorra M, Heimburg T (2005) Diffusion in two-component lipid membranes--a fluorescence correlation spectroscopy and monte carlo simulation study. *Biophys. J.* 88:317-33
- Hale JD, Hancock RE (2007) Alternative mechanisms of action of cationic antimicrobial peptides on bacteria. *Expert. Rev. Anti Infect. Ther.* 5:951-9
- Hallbrink M, Oehlke J, Papsdorf G, Bienert M (2004) Uptake of cell-penetrating peptides is dependent on peptide-to-cell ratio rather than on peptide concentration. *Biochim. Biophys. Acta* 1667:222-8
- Hallock KJ, Lee DK, Ramamoorthy A (2003) MSI-78, an analogue of the magainin antimicrobial peptides, disrupts lipid bilayer structure via positive curvature strain. *Biophys. J.* 84:3052-60
- Hancock RE (1997) Peptide antibiotics. *Lancet* 349:418-22
- Hancock RE, Chapple DS (1999) Peptide antibiotics. *Antimicrob. Agents Chemother.* 43:1317-23
- Hancock RE, Lehrer R (1998) Cationic peptides: a new source of antibiotics. *Trends Biotechnol.* 16:82-8

- Hasper HE, Kramer NE, Smith JL, Hillman JD, Zachariah C, Kuipers OP, de Kruijff B, Breukink E (2006) An alternative bactericidal mechanism of action for lantibiotic peptides that target lipid II. *Science* 313:1636-7
- Haug BE, Skar ML, Svendsen JS (2001) Bulky aromatic amino acids increase the antibacterial activity of 15-residue bovine lactoferricin derivatives. *J. Pept. Sci.* 7:425-32
- Hauser H, Shipley GG (1984) Interactions of divalent cations with phosphatidylserine bilayer membranes. *Biochemistry* 23:34-41
- Hawkey PM (2008) Molecular epidemiology of clinically significant antibiotic resistance genes. *Br. J. Pharmacol.* 153 Suppl 1:S406-13
- He K, Ludtke SJ, Huang HW, Worcester DL (1995) Antimicrobial peptide pores in membranes detected by neutron in-plane scattering. *Biochemistry* 34:15614-8
- Heerklotz H, Seelig J (2000) Titration calorimetry of surfactant-membrane partitioning and membrane solubilization. *Biochim. Biophys. Acta* 1508:69-85
- Heerklotz H, Seelig J (2007) Leakage and lysis of lipid membranes induced by the lipopeptide surfactin. *Eur. Biophys. J.* 36:305-14
- Heimburg T (2000) A model for the lipid pretransition: coupling of ripple formation with the chain-melting transition. *Biophys. J.* 78:1154-65
- Henriques ST, Melo MN, Castanho MA (2006) Cell-penetrating peptides and antimicrobial peptides: how different are they? *Biochem. J.* 399:1-7
- Heuer OE, Hammerum AM, Collignon P, Wegener HC (2006) Human health hazard from antimicrobial-resistant enterococci in animals and food. *Clin. Infect. Dis.* 43:911-6
- Hildebrand A, Beyer K, Neubert R, Garidel P, Blume A (2004) Solubilization of negatively charged DPPC/DPPG liposomes by bile salts. *J. Colloid Interf. Sci.* 279:559-71
- Hildebrand A, Neubert R, Garidel P, Blume A (2002) Bile salt induced solubilization of synthetic phosphatidylcholine vesicles studied by isothermal titration calorimetry. *Langmuir* 18:2836-2847
- Hinz A, Galla HJ (2005) Viral membrane penetration: lytic activity of a nodaviral fusion peptide. *Eur. Biophys. J.* 34:285-93
- Hoskin DW, Ramamoorthy A (2008) Studies on anticancer activities of antimicrobial peptides. *Biochim. Biophys. Acta* 1778:357-75
- Hoyrup P, Davidsen J, Jorgensen K (2001) Lipid Membrane Partitioning of Lysolipids and Fatty Acids: Effects of Membrane Phase Structure and Detergent Chain Length. *J. Phys. Chem. B* 105:2649-2657
- Huang C, Li S (1999) Calorimetric and molecular mechanics studies of the thermotropic phase behavior of membrane phospholipids. *Biochim. Biophys. Acta* 1422:273-307
- Huang HW (2006) Molecular mechanism of antimicrobial peptides: the origin of cooperativity. *Biochim. Biophys. Acta* 1758:1292-302
- Hunter HN, Jing W, Schibli DJ, Trinh T, Park IY, Kim SC, Vogel HJ (2005) The interactions of antimicrobial peptides derived from lysozyme with model membrane systems. *Biochim. Biophys. Acta* 1668:175-89
- Hussain H, Kerth A, Blume A, Kressler J (2004) Amphiphilic Block Copolymers of Poly(ethylene oxide) and Poly(perfluorohexylethyl methacrylate) at the Water Surface and Their Penetration into the Lipid Monolayer. *J. Phys. Chem. B* 108:9962-9969
- Hübner W, Blume A (1998) Interactions at the lipid-water interface. *Chem. Phys. Lipids* 96:99-123
- Ipsen JH, Mouritsen OG (1988) Modelling the phase equilibria in two-component membranes of phospholipids with different acyl-chain lengths. *Biochim. Biophys. Acta* 944:121-34
- Israelachvili J (1992) Intermolecular and surface forces: with applications to colloidal and biological systems. Academic Press, New York

- Ivanova VP, Makarov IM, Schaffer TE, Heimburg T (2003) Analyzing heat capacity profiles of peptide-containing membranes: cluster formation of gramicidin A. *Biophys. J.* 84:2427-39
- Jackson M, Mantsch HH (1995) The use and misuse of FTIR spectroscopy in the determination of protein structure. *Crit. Rev. Biochem. Mol. Biol.* 30:95-120
- Jean-Francois F, Castano S, Desbat B, Odaert B, Roux M, Metz-Boutigue MH, Dufourc EJ (2008) Aggregation of cateslytin beta-sheets on negatively charged lipids promotes rigid membrane domains. A new mode of action for antimicrobial peptides? *Biochemistry* 47:6394-402
- Jelinek R, Kolusheva S (2005) Membrane interactions of host-defense peptides studied in model systems. *Curr. Protein Pept. Sci.* 6:103-14
- Jing W, Hunter HN, Hagel J, Vogel HJ (2003) The structure of the antimicrobial peptide Ac-RRWWRF-NH₂ bound to micelles and its interactions with phospholipid bilayers. *J. Pept. Res.* 61:219-29
- Jing W, Prenner EJ, Vogel HJ, Waring AJ, Lehrer RI, Lohner K (2005) Headgroup structure and fatty acid chain length of the acidic phospholipids modulate the interaction of membrane mimetic vesicles with the antimicrobial peptide protegrin-1. *J. Pept. Sci.* 11:735-43
- Junkes C, Wessolowski A, Farnaud S, Evans RW, Good L, Bienert M, Dathe M (2008) The interaction of arginine- and tryptophan-rich cyclic hexapeptides with *Escherichia coli* membranes. *J. Pept. Sci.* 14:535-43
- Kaganer VM, Möhwald H, Dutta P (1999) Structure and phase transitions in Langmuir monolayers. *Rev. Mod. Phys.* 71:779-819
- Kalb E, Frey S, Tamm LK (1992) Formation of supported planar bilayers by fusion of vesicles to supported phospholipid monolayers. *Biochim. Biophys. Acta* 1103:307-16
- Kaliszan R (1998) Effect of separation conditions on chromatographic determination of hydrophobicity of acidic xenobiotics. *J Chromatogr B Biomed Sci Appl* 717:125-34
- Kandasamy SK, Larson RG (2006) Effect of salt on the interactions of antimicrobial peptides with zwitterionic lipid bilayers. *Biochim. Biophys. Acta* 1758:1274-84
- Kang JH, Lee MK, Kim KL, Hahm KS (1996) Structure-biological activity relationships of 11-residue highly basic peptide segment of bovine lactoferrin. *Int. J. Pept. Protein. Res.* 48:357-63
- Kates M, Syz JY, Gosser D, Haines TH (1993) pH-dissociation characteristics of cardiolipin and its 2'-deoxy analogue. *Lipids* 28:877-82
- Keller S, Heerklotz H, Jahnke N, Blume A (2006) Thermodynamics of lipid membrane solubilization by sodium dodecyl sulfate. *Biophys. J.* 90:4509-21
- Kerth A, Erbe A, Dathe M, Blume A (2004) Infrared reflection absorption spectroscopy of amphipathic model peptides at the air/water interface. *Biophys. J.* 86:3750-8
- Kiessling V, Crane JM, Tamm LK (2006) Transbilayer effects of raft-like lipid domains in asymmetric planar bilayers measured by single molecule tracking. *Biophys. J.* 91:3313-26
- Kiessling V, Tamm LK (2003) Measuring distances in supported bilayers by fluorescence interference-contrast microscopy: polymer supports and SNARE proteins. *Biophys. J.* 84:408-18
- Klocek G, Seelig J (2008) Melittin interaction with sulfated cell surface sugars. *Biochemistry* 47:2841-9
- Kononov O, Myagkov I, Struth B, Lohner K (2002) Lipid discrimination in phospholipid monolayers by the antimicrobial frog skin peptide PGLa. A synchrotron X-ray grazing incidence and reflectivity study. *Eur. Biophys. J.* 31:428-37
- Koynova R, Caffrey M (1998) Phases and phase transitions of the phosphatidylcholines. *Biochim. Biophys. Acta* 1376:91-145

- Krause E, Beyermann M, Dathe M, Rothemund S, Bienert M (1995) Location of an amphipathic alpha-helix in peptides using reversed-phase HPLC retention behavior of D-amino acid analogs. *Anal. Chem.* 67:252-8
- Langner M, Kubica K (1999) The electrostatics of lipid surfaces. *Chem. Phys. Lipids* 101:3-35
- Latal A, Degovics G, Epand RF, Epand RM, Lohner K (1997) Structural aspects of the interaction of peptidyl-glycylleucine-carboxamide, a highly potent antimicrobial peptide from frog skin, with lipids. *Eur. J. Biochem.* 248:938-46
- Leuschner C, Hansel W (2004) Membrane disrupting lytic peptides for cancer treatments. *Curr. Pharm. Des.* 10:2299-310
- Leventis R, Gagne J, Fuller N, Rand RP, Silvius JR (1986) Divalent cation induced fusion and lipid lateral segregation in phosphatidylcholine-phosphatidic acid vesicles. *Biochemistry* 25:6978-87
- Lewis RN, Kiricsi M, Prenner EJ, Hodges RS, McElhaney RN (2003) Fourier transform infrared spectroscopic study of the interactions of a strongly antimicrobial but weakly hemolytic analogue of gramicidin S with lipid micelles and lipid bilayer membranes. *Biochemistry* 42:440-9
- Lewis RN, McElhaney RN (1996) Fourier transform infrared spectroscopy in the study of hydrated lipids and lipid bilayer membranes. In: Mantsch HH, Chapman D (eds) *Infrared spectroscopy of biomolecules*. Wiley-Liss Inc., New York, Chichester, Brisbane, Toronto, Singapore, pp 159-202
- Lewis RN, Prenner EJ, Kondejewski LH, Flach CR, Mendelsohn R, Hodges RS, McElhaney RN (1999) Fourier transform infrared spectroscopic studies of the interaction of the antimicrobial peptide gramicidin S with lipid micelles and with lipid monolayer and bilayer membranes. *Biochemistry* 38:15193-203
- Lewis RN, Zweytick D, Pabst G, Lohner K, McElhaney RN (2007) Calorimetric, X-ray diffraction, and spectroscopic studies of the thermotropic phase behavior and organization of tetramyristoyl cardiolipin membranes. *Biophys. J.* 92:3166-77
- Liu D, DeGrado WF (2001) De novo design, synthesis, and characterization of antimicrobial beta-peptides. *J. Am. Chem. Soc.* 123:7553-9
- Liu F, Lewis RN, Hodges RS, McElhaney RN (2002) Effect of variations in the structure of a poly-leucine-based alpha-helical transmembrane peptide on its interaction with phosphatidylcholine bilayers. *Biochemistry* 41:9197-207
- Lohner K, Latal A, Lehrer RI, Ganz T (1997) Differential scanning microcalorimetry indicates that human defensin, HNP-2, interacts specifically with biomembrane mimetic systems. *Biochemistry* 36:1525-31
- Lohner K, Prenner EJ (1999) Differential scanning calorimetry and X-ray diffraction studies of the specificity of the interaction of antimicrobial peptides with membrane-mimetic systems. *Biochim. Biophys. Acta* 1462:141-56
- Lohner K, Sevcsik E, Pabst G, Liu AL (2008) Liposome-based biomembrane mimetic systems: implications for lipid-peptide interactions. *Advances in Planar Lipid Bilayers and Liposomes* 6:103-137
- Lohner K, Staudegger E, Prenner EJ, Lewis RN, Kriechbaum M, Degovics G, McElhaney RN (1999) Effect of staphylococcal delta-lysin on the thermotropic phase behavior and vesicle morphology of dimyristoylphosphatidylcholine lipid bilayer model membranes. Differential scanning calorimetric, ³¹P nuclear magnetic resonance and Fourier transform infrared spectroscopic, and X-ray diffraction studies. *Biochemistry* 38:16514-28
- Lopes DHJ, Meister A, Gohlke A, Hauser A, Blume A, Winter R (2007) Mechanism of islet amyloid polypeptide fibrillation at lipid interfaces studied by infrared reflection absorption spectroscopy. *Biophys. J.* 93:3132-3141

- Lundback T, Hard T (1996) Salt Dependence of the Free Energy, Enthalpy, and Entropy of Nonsequence Specific DNA Binding. *J. Phys. Chem.* 100:17690-17695
- Lupi S, Perla A, Maselli P, Bordi F, Sennato S (2008) Infrared spectra of phosphatidylethanolamine-cardiolipin binary system. *Colloids Surf. B Biointerfaces* 64:56-64
- Maget-Dana R (1999) The monolayer technique: a potent tool for studying the interfacial properties of antimicrobial and membrane-lytic peptides and their interactions with lipid membranes. *Biochim. Biophys. Acta* 1462:109-40
- Maget-Dana R, Lelievre D, Brack A (1999) Surface active properties of amphiphilic sequential isopeptides: Comparison between alpha-helical and beta-sheet conformations. *Biopolymers* 49:415-423
- Malcharek S, Hinz A, Hilterhaus L, Galla HJ (2005) Multilayer structures in lipid monolayer films containing surfactant protein C: effects of cholesterol and POPE. *Biophys. J.* 88:2638-49
- Maltseva E, Brezesinski G (2004) Adsorption of amyloid beta (1-40) peptide to phosphatidylethanolamine monolayers. *Chemphyschem* 5:1185-90
- Maltseva E, Kerth A, Blume A, Möhwald H, Brezesinski G (2005) Adsorption of Amyloid beta (1-40) Peptide at Phospholipid Monolayers. *Chembiochem* 6:1817-1824
- Mantsch HH, McElhaney RN (1991) Phospholipid phase transitions in model and biological membranes as studied by infrared spectroscopy. *Chem. Phys. Lipids* 57:213-26
- Marr AK, Gooderham WJ, Hancock RE (2006) Antibacterial peptides for therapeutic use: obstacles and realistic outlook. *Curr. Opin. Pharmacol.* 6:468-72
- Matsumoto K, Kusaka J, Nishibori A, Hara H (2006) Lipid domains in bacterial membranes. *Mol. Microbiol.* 61:1110-7
- Matsuyama K, Natori S (1990) Mode of action of sapecin, a novel antibacterial protein of *Sarcophaga peregrina* (flesh fly). *J. Biochem.* 108:128-32
- Matsuzaki K (1998) Magainins as paradigm for the mode of action of pore forming polypeptides. *Biochim. Biophys. Acta* 1376:391-400
- Matsuzaki K, Harada M, Funakoshi S, Fujii N, Miyajima K (1991) Physicochemical determinants for the interactions of magainins 1 and 2 with acidic lipid bilayers. *Biochim. Biophys. Acta* 1063:162-70
- Matsuzaki K, Murase O, Fujii N, Miyajima K (1996) An antimicrobial peptide, magainin 2, induced rapid flip-flop of phospholipids coupled with pore formation and peptide translocation. *Biochemistry* 35:11361-8
- Matsuzaki K, Sugishita K, Fujii N, Miyajima K (1995) Molecular basis for membrane selectivity of an antimicrobial peptide, magainin 2. *Biochemistry* 34:3423-9
- McDermott AM (2007) Cationic antimicrobial peptides. A future therapeutic option? *Arch. Soc. Esp. Oftalmol.* 82:467-70
- McElhaney RN (1982) The use of differential scanning calorimetry and differential thermal analysis in studies of model and biological membranes. *Chem. Phys. Lipids* 30:229-59
- McIntosh TJ (2004) Roles of bilayer structure and elastic properties in peptide localization in membranes. *Chem. Phys. Lipids* 130:83-98
- Mendelsohn R, Brauner JW, Gericke A (1995) External infrared reflection absorption spectrometry of monolayer films at the air-water interface. *Annu. Rev. Phys. Chem.* 46:305-334
- Mendelsohn R, Flach CR (2002) Infrared reflection-absorption spectroscopy of lipids, peptides, and proteins in aqueous monolayers. In: Sidney AS, Thomas JM (eds) *Current Topics in Membranes*, vol Volume 52. Academic Press, pp 57-88
- Mendelsohn R, Mantsch HH (1986) Fourier transform infrared studies of lipid-protein interaction. In: Watts A, de Pont JJHMM (eds) *Progress in protein-lipid interactions*, vol 2. Elsevier Science, Amsterdam, New York, Oxford, pp 103-146

- Miteva M, Andersson M, Karshikoff A, Otting G (1999) Molecular electroporation: a unifying concept for the description of membrane pore formation by antibacterial peptides, exemplified with NK-lysin. *FEBS Lett.* 462:155-8
- Momo F, Fabris S, Stevanato R (2000) Interaction of linear mono- and diamines with dimyristoylphosphatidylcholine and dimyristoylphosphatidylglycerol multilamellar liposomes. *Arch. Biochem. Biophys.* 382:224-31
- Murzyn K, Rog T, Pasenkiewicz-Gierula M (2005) Phosphatidylethanolamine-phosphatidylglycerol bilayer as a model of the inner bacterial membrane. *Biophys. J.* 88:1091-103
- Muta T, Fujimoto T, Nakajima H, Iwanaga S (1990) Tachyplesins isolated from hemocytes of Southeast Asian horseshoe crabs (*Carcinoscorpius rotundicauda* and *Tachyplesus gigas*): identification of a new tachyplesin, tachyplesin III, and a processing intermediate of its precursor. *J. Biochem.* 108:261-6
- Nagle JF, Tristram-Nagle S (2000) Structure of lipid bilayers. *Biochim. Biophys. Acta* 1469:159-95
- Nagpal S, Gupta V, Kaur KJ, Salunke DM (1999) Structure-function analysis of tritrypticin, an antibacterial peptide of innate immune origin. *J. Biol. Chem.* 274:23296-304
- Nakamura T, Furunaka H, Miyata T, Tokunaga F, Muta T, Iwanaga S, Niwa M, Takao T, Shimonishi Y (1988) Tachyplesin, a class of antimicrobial peptide from the hemocytes of the horseshoe crab (*Tachyplesus tridentatus*). Isolation and chemical structure. *J. Biol. Chem.* 263:16709-13
- Nollert P, Kiefer H, Jahnig F (1995) Lipid vesicle adsorption versus formation of planar bilayers on solid surfaces. *Biophys. J.* 69:1447-55
- O'Leary WM, Wilkinson SG (1988) Gram-positive bacteria. In: Ratledge C, Wilkinson SG (eds) *Microbial lipids*. Academic Press, London, pp 117-201
- Oehlke J, Lorenz D, Wiesner B, Bienert M (2005) Studies on the cellular uptake of substance P and lysine-rich, KLA-derived model peptides. *J. Mol. Recognit.* 18:50-9
- Ohki S (1984) Effects of divalent cations, temperature, osmotic pressure gradient, and vesicle curvature on phosphatidylserine vesicle fusion. *J. Membr. Biol.* 77:265-75
- Ohki S, Ohshima H (1985) Divalent cation-induced phosphatidic acid membrane fusion. Effect of ion binding and membrane surface tension. *Biochim. Biophys. Acta* 812:147-54
- Oliyntyk V, Jager M, Heimburg T, Buckin V, Kaatz U (2008) Lipid membrane domain formation and alamethicin aggregation studied by calorimetry, sound velocity measurements, and atomic force microscopy. *Biophys. Chem.* 134:168-77
- Oliyntyk V, Kaatz U, Heimburg T (2007) Defect formation of lytic peptides in lipid membranes and their influence on the thermodynamic properties of the pore environment. *Biochim. Biophys. Acta* 1768:236-45
- Papahadjopoulos D, Moscarello M, Eylar EH, Isac T (1975) Effects of proteins on thermotropic phase transitions of phospholipid membranes. *Biochim. Biophys. Acta* 401:317-35
- Papo N, Oren Z, Pag U, Sahl HG, Shai Y (2002) The consequence of sequence alteration of an amphipathic alpha-helical antimicrobial peptide and its diastereomers. *J. Biol. Chem.* 277:33913-21
- Papo N, Shai Y (2003) Can we predict biological activity of antimicrobial peptides from their interactions with model phospholipid membranes? *Peptides* 24:1693-703
- Parisien A, Allain B, Zhang J, Mandeville R, Lan CQ (2008) Novel alternatives to antibiotics: bacteriophages, bacterial cell wall hydrolases, and antimicrobial peptides. *J. Appl. Microbiol.* 104:1-13

- Pastrana-Rios B, Flach CR, Brauner JW, Mautone AJ, Mendelsohn R (1994) A direct test of the "squeeze-out" hypothesis of lung surfactant function. External reflection FT-IR at the air/water interface. *Biochemistry* 33:5121-7
- Pastrana-Rios B, Taneva S, Keough KM, Mautone AJ, Mendelsohn R (1995) External reflection absorption infrared spectroscopy study of lung surfactant proteins SP-B and SP-C in phospholipid monolayers at the air/water interface. *Biophys. J.* 69:2531-40
- Peschel A (2002) How do bacteria resist human antimicrobial peptides? *Trends Microbiol.* 10:179-86
- Pokorny A, Almeida PF (2004) Kinetics of dye efflux and lipid flip-flop induced by delta-lysine in phosphatidylcholine vesicles and the mechanism of graded release by amphipathic, alpha-helical peptides. *Biochemistry* 43:8846-57
- Pokorny A, Almeida PF (2005) Permeabilization of raft-containing lipid vesicles by delta-lysine: a mechanism for cell sensitivity to cytotoxic peptides. *Biochemistry* 44:9538-44
- Powers JP, Hancock RE (2003) The relationship between peptide structure and antibacterial activity. *Peptides* 24:1681-91
- Powers JP, Tan A, Ramamoorthy A, Hancock RE (2005) Solution structure and interaction of the antimicrobial polyphemusins with lipid membranes. *Biochemistry* 44:15504-13
- Pozo Navas B, Lohner K, Deutsch G, Sevcik E, Riske KA, Dimova R, Garidel P, Pabst G (2005) Composition dependence of vesicle morphology and mixing properties in a bacterial model membrane system. *Biochim. Biophys. Acta* 1716:40-8
- Pramanik A, Thyberg P, Rigler R (2000) Molecular interactions of peptides with phospholipid vesicle membranes as studied by fluorescence correlation spectroscopy. *Chem. Phys. Lipids* 104:35-47
- Prenner EJ, Lewis RN, Kondejewski LH, Hodges RS, McElhaney RN (1999) Differential scanning calorimetric study of the effect of the antimicrobial peptide gramicidin S on the thermotropic phase behavior of phosphatidylcholine, phosphatidylethanolamine and phosphatidylglycerol lipid bilayer membranes. *Biochim. Biophys. Acta* 1417:211-23
- Provencher SW (1982) CONTIN: a general purpose constrained regularization program for inverting noisy linear algebraic and integral equations. *Comput. Phys. Commun.* 27:229-242
- Radek K, Gallo R (2007) Antimicrobial peptides: natural effectors of the innate immune system. *Semin. Immunopathol.* 29:27-43
- Record MT, Jr., Anderson CF, Lohman TM (1978) Thermodynamic analysis of ion effects on the binding and conformational equilibria of proteins and nucleic acids: the roles of ion association or release, screening, and ion effects on water activity. *Q. Rev. Biophys.* 11:103-78
- Redfern DA, Gericke A (2004) Domain formation in phosphatidylinositol monophosphate/phosphatidylcholine mixed vesicles. *Biophys. J.* 86:2980-92
- Rennie J, Arnt L, Tang H, Nusslein K, Tew GN (2005) Simple oligomers as antimicrobial peptide mimics. *J. Ind. Microbiol. Biotechnol.* 32:296-300
- Rezansoff AJ, Hunter HN, Jing W, Park IY, Kim SC, Vogel HJ (2005) Interactions of the antimicrobial peptide Ac-FRWWHR-NH₂ with model membrane systems and bacterial cells. *J. Pept. Res.* 65:491-501
- Richter RP, Berat R, Brisson AR (2006) Formation of solid-supported lipid bilayers: an integrated view. *Langmuir* 22:3497-505
- Rosenfeld Y, Shai Y (2006) Lipopolysaccharide (Endotoxin)-host defense antibacterial peptides interactions: role in bacterial resistance and prevention of sepsis. *Biochim. Biophys. Acta* 1758:1513-22
- Rossi LM, Rangasamy P, Zhang J, Qiu XQ, Wu GY (2008) Research advances in the development of peptide antibiotics. *J. Pharm. Sci.* 97:1060-70

- Sanderson JM (2005) Peptide-lipid interactions: insights and perspectives. *Org. Biomol. Chem.* 3:201-12
- Sato H, Feix JB (2006) Peptide-membrane interactions and mechanisms of membrane destruction by amphipathic alpha-helical antimicrobial peptides. *Biochim. Biophys. Acta* 1758:1245-56
- Schladitz C, Vieira EP, Hermel H, Mohwald H (1999) Amyloid-beta-sheet formation at the air-water interface. *Biophys. J.* 77:3305-10
- Schneider MF, Marsh D, Jahn W, Kloesgen B, Heimburg T (1999) Network formation of lipid membranes: triggering structural transitions by chain melting. *Proc. Natl. Acad. Sci. USA* 96:14312-7
- Schote U, Ganz P, Fahr A, Seelig J (2002) Interactions of cyclosporines with lipid membranes as studied by solid-state nuclear magnetic resonance spectroscopy and high-sensitivity titration calorimetry. *J. Pharm. Sci.* 91:856-67
- Schwieger C (2008) Electrostatic and Non-Electrostatic Interactions of Positively Charged Polypeptides with Negatively Charged Lipid Membranes Institute of Chemistry, vol Ph.D. thesis. Martin-Luther-Universität Halle-Wittenberg, Halle (Saale)
- Schwieger C, Blume A (2007) Interaction of poly(L-lysines) with negatively charged membranes: an FT-IR and DSC study. *Eur. Biophys. J.* 36:437-50
- Seelig A, Seelig J (2002) Membrane structure. In: Meyers RA (ed) *Encyclopedia of Physical Science and Technology*. Academic Press, New York, pp 355-367
- Seelig J (2004) Thermodynamics of lipid-peptide interactions. *Biochim. Biophys. Acta* 1666:40-50
- Seelig J, Ganz P (1991) Nonclassical hydrophobic effect in membrane binding equilibria. *Biochemistry* 30:9354-9
- Sengupta D, Leontiadou H, Mark AE, Marrink SJ (2008) Toroidal pores formed by antimicrobial peptides show significant disorder. *Biochim. Biophys. Acta* 1778:2308-17
- Seto GW, Marwaha S, Kobewka DM, Lewis RN, Separovic F, McElhaney RN (2007) Interactions of the Australian tree frog antimicrobial peptides aurein 1.2, citropin 1.1 and maculatin 1.1 with lipid model membranes: differential scanning calorimetric and Fourier transform infrared spectroscopic studies. *Biochim. Biophys. Acta* 1768:2787-800
- Sevcsik E, Pabst G, Jilek A, Lohner K (2007) How lipids influence the mode of action of membrane-active peptides. *Biochim. Biophys. Acta* 1768:2586-95
- Shai Y (1999) Mechanism of the binding, insertion and destabilization of phospholipid bilayer membranes by alpha-helical antimicrobial and cell non-selective membrane-lytic peptides. *Biochim. Biophys. Acta* 1462:55-70
- Shai Y (2002) Mode of action of membrane active antimicrobial peptides. *Biopolymers* 66:236-48
- Shai Y, Oren Z (1996) Diastereoisomers of cytolysins, a novel class of potent antibacterial peptides. *J. Biol. Chem.* 271:7305-8
- Singer SJ, Nicolson GL (1972) The fluid mosaic model of the structure of cell membranes. *Science* 175:720-31
- Smith BA, McConnell HM (1978) Determination of molecular motion in membranes using periodic pattern photobleaching. *Proc. Natl. Acad. Sci. USA* 75:2759-63
- Som A, Vemparala S, Ivanov I, Tew GN (2008) Synthetic mimics of antimicrobial peptides. *Biopolymers* 90:83-93
- Sood R, Domanov Y, Pietiainen M, Kontinen VP, Kinnunen PK (2008) Binding of LL-37 to model biomembranes: insight into target vs host cell recognition. *Biochim. Biophys. Acta* 1778:983-96

- Sood R, Kinnunen PK (2008) Cholesterol, lanosterol, and ergosterol attenuate the membrane association of LL-37(W27F) and temporin L. *Biochim. Biophys. Acta* 1778:1460-6
- Spellberg B, Powers JH, Brass EP, Miller LG, Edwards JE, Jr. (2004) Trends in antimicrobial drug development: implications for the future. *Clin. Infect. Dis.* 38:1279-86
- Spaar A, Munster C, Salditt T (2004) Conformation of peptides in lipid membranes studied by X-ray grazing incidence scattering. *Biophys. J.* 87:396-407
- Staubitz P, Peschel A, Nieuwenhuizen WF, Otto M, Gotz F, Jung G, Jack RW (2001) Structure-function relationships in the tryptophan-rich, antimicrobial peptide indolicidin. *J. Pept. Sci.* 7:552-64
- Staudegger E, Prenner EJ, Kriechbaum M, Degovics G, Lewis RN, McElhaney RN, Lohner K (2000) X-ray studies on the interaction of the antimicrobial peptide gramicidin S with microbial lipid extracts: evidence for cubic phase formation. *Biochim. Biophys. Acta* 1468:213-30
- Stella L, Mazzuca C, Venanzi M, Palleschi A, Didone M, Formaggio F, Toniolo C, Pispisa B (2004) Aggregation and water-membrane partition as major determinants of the activity of the antibiotic peptide trichogin GA IV. *Biophys. J.* 86:936-45
- Strom MB, Haug BE, Skar ML, Stensen W, Stiberg T, Svendsen JS (2003) The pharmacophore of short cationic antibacterial peptides. *J. Med. Chem.* 46:1567-70
- Strom MB, Rekdal O, Svendsen JS (2002) Antimicrobial activity of short arginine- and tryptophan-rich peptides. *J. Pept. Sci.* 8:431-7
- Sugar IP, Monticelli G (1985) Interrelationships between the phase diagrams of the two-component phospholipid bilayers. *Biophys. J.* 48:283-8
- Tamm LK (1986) Incorporation of a synthetic mitochondrial signal peptide into charged and uncharged phospholipid monolayers. *Biochemistry* 25:7470-6
- Tamm LK (2002) Peptide-Lipid Interactions in Supported Monolayers and Bilayers. In: Sidney AS, Thomas JM (eds) *Current Topics in Membranes*, vol Volume 52. Academic Press, pp 191-202
- Tamm LK, Kalb E (1993) Microspectrofluorometry on supported planar membranes. In: Schulmann SG (ed) *Molecular luminescence spectroscopy*, part 3. John Wiley and Sons, New York, pp 253-305
- Tamm LK, McConnell HM (1985) Supported phospholipid bilayers. *Biophys. J.* 47:105-13
- Tamm LK, Tatulian SA (1997) Infrared spectroscopy of proteins and peptides in lipid bilayers. *Q. Rev. Biophys.* 30:365-429
- Tamm LK, Tomich JM, Saier MH, Jr. (1989) Membrane incorporation and induction of secondary structure of synthetic peptides corresponding to the N-terminal signal sequences of the glucitol and mannitol permeases of *Escherichia coli*. *J. Biol. Chem.* 264:2587-92
- Taylor KMG, Craig DQM (2003) Physical methods of study: differential scanning calorimetry. In: Weissig V, Torchilin VP (eds) *Liposomes: a practical approach*. Oxford University Press, Oxford pp 79-104
- Terzi E, Holzemann G, Seelig J (1997) Interaction of Alzheimer beta-amyloid peptide(1-40) with lipid membranes. *Biochemistry* 36:14845-52
- Teuber M (2001) Veterinary use and antibiotic resistance. *Curr. Opin. Microbiol.* 4:493-9
- Tew GN, Liu D, Chen B, Doerksen RJ, Kaplan J, Carroll PJ, Klein ML, DeGrado WF (2002) De novo design of biomimetic antimicrobial polymers. *Proc. Natl. Acad. Sci. USA* 99:5110-4
- Thennarasu S, Lee DK, Poon A, Kawulka KE, Vederas JC, Ramamoorthy A (2005) Membrane permeabilization, orientation, and antimicrobial mechanism of subtilisin A. *Chem. Phys. Lipids* 137:38-51
- Tomita M, Takase M, Bellamy W, Shimamura S (1994) The active peptide of lactoferrin. *Acta Paediatr. Jpn* 36:585-91

- Tossi A, Sandri L, Giangaspero A (2000) Amphipathic, alpha-helical antimicrobial peptides. *Biopolymers* 55:4-30
- Tsamaloukas AD, Keller S, Heerklotz H (2007) Uptake and release protocol for assessing membrane binding and permeation by way of isothermal titration calorimetry. *Nat. Protocols* 2:695-704
- Tuchtenhagen J, Ziegler W, Blume A (1994) Acyl chain conformational ordering in liquid-crystalline bilayers: comparative FT-IR and ²H-NMR studies of phospholipids differing in headgroup structure and chain length. *Eur. Biophys. J.* 23:323-35
- van Kan EJ, Ganchev DN, Snel MM, Chupin V, van der Bent A, de Kruijff B (2003) The peptide antibiotic clavanin A interacts strongly and specifically with lipid bilayers. *Biochemistry* 42:11366-72
- Virtanen JA, Cheng KH, Somerharju P (1998) Phospholipid composition of the mammalian red cell membrane can be rationalized by a superlattice model. *Proc. Natl. Acad. Sci. U S A* 95:4964-9
- Vogel H (1987) Comparison of the conformation and orientation of alamethicin and melittin in lipid membranes. *Biochemistry* 26:4562-72
- Volinsky R, Kolusheva S, Berman A, Jelinek R (2006) Investigations of antimicrobial peptides in planar film systems. *Biochim. Biophys. Acta* 1758:1393-407
- Wan C, Kiessling V, Tamm LK (2008) Coupling of cholesterol-rich lipid phases in asymmetric bilayers. *Biochemistry* 47:2190-8
- Wang S, Huang J, Song Q, Fu H (2007) Characterizing assembly morphology changes during solubilization process of dimyristoyl phosphocholine vesicles by n-dodecyl triethylammonium bromide. *J. Colloid Interf. Sci.* 311:296-302
- Wen S, Majerowicz M, Waring A, Bringezu F (2007) Dicynthaurin (ala) monomer interaction with phospholipid bilayers studied by fluorescence leakage and isothermal titration calorimetry. *J. Phys. Chem. B* 111:6280-7
- Wenk MR, Seelig J (1998) Magainin 2 amide interaction with lipid membranes: calorimetric detection of peptide binding and pore formation. *Biochemistry* 37:3909-16
- Wessolowski A, Bienert M, Dathe M (2004) Antimicrobial activity of arginine- and tryptophan-rich hexapeptides: the effects of aromatic clusters, D-amino acid substitution and cyclization. *J. Pept. Res.* 64:159-69
- White DA (1973) The phospholipid composition of mammalian tissues. In: Ansell GB, Hawthorne JN, Dawson RMC (eds) *Form and function of phospholipids*. Elsevier, Amsterdam, pp 441-482
- White SH, Wimley WC (1998) Hydrophobic interactions of peptides with membrane interfaces. *Biochim. Biophys. Acta* 1376:339-52
- Wieprecht T, Apostolov O, Beyermann M, Seelig J (1999a) Thermodynamics of the alpha-helix-coil transition of amphipathic peptides in a membrane environment: implications for the peptide-membrane binding equilibrium. *J. Mol. Biol.* 294:785-94
- Wieprecht T, Apostolov O, Beyermann M, Seelig J (2000a) Interaction of a mitochondrial presequence with lipid membranes: role of helix formation for membrane binding and perturbation. *Biochemistry* 39:15297-305
- Wieprecht T, Apostolov O, Beyermann M, Seelig J (2000b) Membrane binding and pore formation of the antibacterial peptide PGLa: thermodynamic and mechanistic aspects. *Biochemistry* 39:442-52
- Wieprecht T, Apostolov O, Seelig J (2000c) Binding of the antibacterial peptide magainin 2 amide to small and large unilamellar vesicles. *Biophys. Chem.* 85:187-98
- Wieprecht T, Beyermann M, Seelig J (1999b) Binding of antibacterial magainin peptides to electrically neutral membranes: thermodynamics and structure. *Biochemistry* 38:10377-87

- Wieprecht T, Beyermann M, Seelig J (2002) Thermodynamics of the coil-alpha-helix transition of amphipathic peptides in a membrane environment: the role of vesicle curvature. *Biophys. Chem.* 96:191-201
- Wieprecht T, Seelig J (2002) Isothermal titration calorimetry for studying interactions between peptides and lipid membranes. In: Sidney AS, Thomas JM (eds) *Current Topics in Membranes*, vol Volume 52. Academic Press, pp 31-56
- Wilkinson SG (1988) Gram-negative bacteria. In: Ratledge C, Wilkinson SG (eds) *Microbial lipids*. Academic Press, London, pp 299-488
- Willumeit R, Kumpugdee M, Funari SS, Lohner K, Navas BP, Brandenburg K, Linser S, Andra J (2005) Structural rearrangement of model membranes by the peptide antibiotic NK-2. *Biochim. Biophys. Acta* 1669:125-34
- Yang L, Gordon VD, Mishra A, Som A, Purdy KR, Davis MA, Tew GN, Wong GC (2007) Synthetic antimicrobial oligomers induce a composition-dependent topological transition in membranes. *J. Am. Chem. Soc.* 129:12141-7
- Yang L, Harroun TA, Weiss TM, Ding L, Huang HW (2001) Barrel-stave model or toroidal model? A case study on melittin pores. *Biophys. J.* 81:1475-85
- Yeaman MR, Yount NY (2003) Mechanisms of antimicrobial peptide action and resistance. *Pharmacol. Rev.* 55:27-55
- Zandomenighi G, Krebs MR, McCammon MG, Fandrich M (2004) FTIR reveals structural differences between native beta-sheet proteins and amyloid fibrils. *Protein Sci.* 13:3314-21
- Zelezetsky I, Tossi A (2006) Alpha-helical antimicrobial peptides--using a sequence template to guide structure-activity relationship studies. *Biochim. Biophys. Acta* 1758:1436-49
- Zhang F, Rowe ES (1994) Calorimetric studies of the interactions of cytochrome c with dioleoylphosphatidylglycerol extruded vesicles: ionic strength effects. *Biochim. Biophys. Acta* 1193:219-25
- Zhang L, Falla TJ (2004) Cationic antimicrobial peptides - an update. *Expert. Opin. Investig. Drugs* 13:97-106
- Zhang YM, Rock CO (2008) Membrane lipid homeostasis in bacteria. *Nat. Rev. Microbiol.* 6:222-33

11 List of Figures and Tables

11.1 List of Figures

- Figure 1.1-1 The plasma membrane structure of eukaryotic cells according to the model of Singer and Nicolson 1972. Adapted from ref. (Dowhan and Bogdanov 2002). ----- 1
- Figure 1.1-2 Schematic presentation of the molecular structure of bacterial cell membranes. Gram-negative bacteria consist of an outer membrane and a cytoplasmic membrane, whereas Gram-positive bacteria possess only a cytoplasmic membrane protected by a peptidoglycan layer that also exists in the periplasmic space of Gram-negative bacteria. Adapted from ref. (Lohner et al. 2008). ----- 3
- Figure 1.3-1 A DSC thermogram of DPPC showing the various thermotropic phase transitions. The illustrations exhibit the bilayer structure at different phases. ----- 7
- Figure 2.2-1 The classical models for the mode of action of antimicrobial peptides. The red part of the peptides represents the hydrophilic region, whereas the blue shows the hydrophobic part. (A) Barrel-stave model, (B) Carpet model, (C) Toroidal pore model, (D) Molecular electroporation model, (E) Sinking raft model. Adapted from refs. (Chan et al. 2006; Pokorny and Almeida 2005). ----- 12
- Figure 4.1-1 View of the α -helix (top) and the twisted β -sheet single strand (bottom) structures of KLAL. In the side view of the α -helix, the atoms N, O, C and H are coloured blue, red, dark gray, and light gray, respectively. In the Connolly surface of the peptide, Lys (K) is coloured blue, Leu (L) is coloured green, Ala (A) is coloured grey, and the backbone is coloured light gray. ----- 20
- Figure 4.2-1 (A) The development of surface pressure over time after the injection of KLA1 in the subphase (10 mM Tris, 154 mM NaCl, pH 7.4) at 20°C. The starting bulk concentration was 100 nM. (B) The IRRA spectra of KLA1 film at the respective positions a-e. The IRRA spectra were recorded with *p*-polarized light at an angle of incidence of 40°. ----- 23
- Figure 4.2-2 (A) ΔA versus time course of various lipid monolayers after the injection of KLA1 in the subphase (10 mM Tris, 154 mM NaCl, pH 7.4) at 20°C. The surface pressure of the lipid films was kept at 30 mN m⁻¹, and the starting bulk concentration of KLA1 was 49 nM. (B) The IRRA spectra of the different films at the respective positions a-d. The solid black lines belong to the peptide-associated lipid films, whereas the dotted red lines are from pure lipid films. The IRRA spectra were recorded with *p*-polarized light at an angle of incidence of 40°. ----- 26
- Figure 4.2-3 (A) The influence of KLA1 bulk concentration (25 – 98 nM) on ΔA versus time course of POPG monolayers after the injection of the peptide in the subphase (10 mM Tris, 154 mM NaCl, pH 7.4) at 20°C. (B) The dependence of the relative area increase ($\Delta A/A_0$) of POPG monolayers on the KLA1 bulk concentration, where A_0 is the initial area per lipid. During the experiments, the surface pressure of the films was kept constant at 30 mN m⁻¹. ----- 28
- Figure 4.2-4 The influence of POPG fraction in the mixed monolayers on the maximum ΔA achieved after the injection of KLA1 in the subphase (10 mM Tris, 154 mM NaCl, pH 7.4) at 20°C. The surface pressure of the lipid films was kept at 30 mN m⁻¹, and the starting bulk concentration of KLA1 was 49 nM. ----- 30
- Figure 4.2-5 (A) Surface pressure versus area per one peptide molecule compression isotherm of KLAL spread on the surface of the subphase (10 mM Tris, 154 mM NaCl, pH 7.4) at 20°C. (B) IRRA spectra of the film at the respective positions a-d. The IRRA spectra were recorded with *s*-polarized light at an angle of incidence of 40°. ----- 33

- Figure 4.2-6 (A) Surface pressure versus area per one lipid molecule compression isotherm of POPG and POPG/KLAL 20:1 spread on the surface of the subphase (10 mM Tris, 154 mM NaCl, pH 7.4) at 20°C. The area was scaled to the lipid molecular area. (B) IRRA spectra of the films at the respective positions a-e. The IRRA spectra were recorded with *p*-polarized light at an angle of incidence of 40°. ----- 35
- Figure 4.2-7 (A) Surface pressure versus area per one lipid molecule compression isotherm of POPC and POPC/KLAL 20:1 spread on the surface of the subphase (10 mM Tris, 154 mM NaCl, pH 7.4) at 20°C. The area was scaled to the lipid molecular area. (B) IRRA spectra of the films at the respective positions a-e. The IRRA spectra were recorded with *p*-polarized light at an angle of incidence of 40°. ----- 37
- Figure 4.2-8 (A) Surface pressure versus area per one lipid molecule compression isotherm of POPE and POPE/KLAL 20:1 spread on the surface of the subphase (10 mM Tris, 154 mM NaCl, pH 7.4) at 20°C. The area was scaled to the lipid molecular area. (B) IRRA spectra of the films at the respective positions a-e. The IRRA spectra were recorded with *p*-polarized light at an angle of incidence of 40°. ----- 38
- Figure 4.2-9 Comparison of surface pressure versus area per one peptide molecule compression isotherms of pure KLAL and that of the peptide in the different mixed lipid-KLAL films. ----- 40
- Figure 4.2-10 Unweighted distribution of hydrodynamic radii obtained from DLS measurements of DPPG (left) and DPPC (right) vesicles (1 mM, ~ 50 nm radius) before and after the multi-step addition to KLA1 and $k_{9,a10}$ -KLAL solutions (500 μ l, 10 μ M) at 25°C. The samples were prepared in buffer (10 mM Tris, 154 mM NaCl, pH 7.4). ----- 44
- Figure 4.2-11 Unweighted distribution of hydrodynamic radii obtained from DLS measurements of free DPPG vesicles and of $l_{11,k12}$ -KLAL-bound DPPG (L/P 24:1) at 25°C, which shows the changes in the size of DPPG vesicles after 0, 360 and 720 min of the addition of the peptide. The samples were prepared in buffer (10 mM Tris, 154 mM NaCl, pH 7.4). ----- 45
- Figure 4.2-12 CD spectra of KLAL (peptide concentration 10^{-5} M) in Tris buffer, 50% TFE in buffer (v/v), buffered POPG SUV suspension (lipid concentration 2.3 mM) and buffered POPC SUV suspension (lipid concentration 2.0 mM). Adapted from ref. (Dathe et al. 1996)----- 46
- Figure 4.2-13 (Left) CD spectra of KLA peptides (25 – 100 μ M) in DPPG LUV suspension (~ 50 nm radius, 1 mM, L/P 10 to 40) at 20°C. (Right) The influence of temperature on DPPG/KLA1 and DPPG/ $l_{11,k12}$ -KLAL mixtures with L/P ratio of 10. The mixtures were heated from 20 to 70°C and then cooled back to 20°C. The samples were prepared in buffer (10 mM Tris, 154 mM NaCl, pH 7.4).----- 47
- Figure 4.2-14 First (solid lines) and second (dashed lines) heating DSC curves of DPPG LUV (2 mM) before (black lines) and after the addition of (A) KLA1, (B) $k_{1,l2}$ -KLAL, (C) $k_{9,a10}$ -KLAL, and (D) $l_{11,k12}$ -KLAL peptides with L/P ratios of 200 to 10. The samples were prepared in buffer (10 mM Tris, 154 mM NaCl, pH 7.4).----- 48
- Figure 4.2-15 First and second heating DSC curves of a premixed and a preloaded DPPG/KLA1 (2 mM/100 μ M) 20:1 mixture. The samples were prepared in buffer (10 mM Tris, 154 mM NaCl, pH 7.4). ----- 53
- Figure 4.2-16 Amide I vibrational band (left) and its second derivative (right) of 10 mM KLA1 in D₂O (100 mM NaCl) at various temperatures through the heating phase from 20°C to 76°C and the cooling back to 20°C.----- 54
- Figure 4.2-17 Amide I vibrational band (left) and its second derivative (right) of 10 mM KLA1 premixed with 60 mM DPPG-d₆₂ (L/P = 6) in D₂O (100 mM NaCl) at various temperatures through the heating phase from 20°C to 76°C and the cooling back to 20°C. ----- 55

- Figure 4.2-18 (Top) Temperature dependence of the wavenumber of the antisymmetric CD₂-stretching band of 60 mM DPPG-d₆₂ without and with 14.3 mol% KLA peptides (L/P = 6). The samples were prepared in H₂O (100 mM NaCl). (Bottom) First derivative of the curves shown in the top diagram. ----- 57
- Figure 4.2-19 Carbonyl stretching vibrational bands ($\nu(\text{CO})$) of 60 mM DPPG-d₆₂ (left) and of 60 mM/ 10 mM DPPG-d₆₂/KLA1 (L/P 6:1) complex (right) in D₂O (100 mM NaCl) through the heating phase from 20 and 76°C and the cooling back to 20°C. The experimental bands (black lines) were resolved into two Gaussians representing the hydrated (red lines) and the non-hydrated states (green lines). The relative integral of each peak is shown underneath it as a percentage, whereas the original peaks positions are illustrated with dotted lines. ----- 58
- Figure 4.2-20 The experimental power signals (top) and the integrated peaks as a function of DPPG/peptide ratio (bottom) of the titration of DPPG LUV (500 μM) in the syringe into KLA peptides (5 μM) and buffer in the reaction cell at 15°C. The samples were prepared in buffer (10 mM Tris, 154 mM NaCl, pH 7.4). ----- 62
- Figure 4.2-21 The experimental power signals of the binding of KLA1 (5 μM) to DPPG/DPPC (left) and DPPG/DPPE (right) LUV mixed vesicles (total lipid concentration 500 μM) as well as to the single components (500 μM) at 15°C. The samples were prepared in buffer (10 mM Tris, 154 mM NaCl, pH 7.4). ----- 66
- Figure 4.2-22 (Left) The experimental power signals of the binding of KLA1 (5 μM) to DPPG LUV (500 μM) at different NaCl concentrations (154 to 1000 mM) at 15°C. The samples were prepared in buffer (10 mM Tris, 154 mM NaCl, pH 7.4). (Right) The salt concentration dependence of the binding parameters of KLA1 to DPPG LUV at 15°C. The linear dependence of K_{app} on NaCl concentration was linearly fitted to determine K_{T} , the binding constant at 1M NaCl. ΔH° becomes zero at ~ 727 mM NaCl. ----- 68
- Figure 4.2-23 The experimental power signals (top) and the integrated peaks as a function of DPPG/KLA1 ratio (bottom) of the titration of DPPG LUV (500 μM) in the syringe into KLA1 peptide (5 μM) in the reaction cell at temperatures of 5 to 25°C (left) and of 30 to 50°C (right) The samples were prepared in buffer (10 mM Tris, 154 mM NaCl, pH 7.4). ----- 70
- Figure 4.2-24 The temperature dependence of the binding parameters K_{app} , N , ΔH° , $-\Delta S^\circ$ and ΔG° of KLA1 to DPPG LUV. The linear temperature dependence of ΔH° was linearly fitted to determine the change in specific heat capacity ΔC_p . ----- 71
- Figure 4.2-25 (Left) The experimental power signal at 15°C (top) and the integrated peaks as a function of POPG/KLA1 ratio at 5 to 50°C (bottom) of the interaction of KLA1 (5 – 10 μM) with POPG LUV (0.5 - 1 mM). The samples were prepared in buffer (10 mM Tris, 154 mM NaCl, pH 7.4). (Right) The temperature dependence of the binding parameters K_{app} , N , ΔH° , $-\Delta S^\circ$ and ΔG° of KLA1 to POPG LUV. The linear temperature dependence of ΔH° was linearly fitted to determine the change in specific heat capacity ΔC_p . ----- 73
- Figure 5.1-1 View of the amphipathic structure of Ac-RW, where the arginine (R) residues are oriented in one direction and the aromatic amino acids tryptophan (W) and phenylalanine (P) are aligned in the opposite direction. ----- 77
- Figure 5.1-2 (A and B) Ac-RW peptide in the presence of DPC and SDS micelles, respectively. (C and D) C-RW peptide in the presence of DPC and SDS micelles, respectively. The structures were determined by means of NMR (Appelt et al. 2005b; Jing et al. 2003). Tryptophan residues are highlighted in pale-green, Phenylalanine is shown in orange, and Arginine residues are presented in blue colour. Adapted from ref. (Chan et al. 2006) ----- 79
- Figure 5.2-1 Unweighted distribution of hydrodynamic radii obtained from DLS measurements of DPPG (left) and DPPC (right) vesicles (1 mM, ~ 50 nm radius) before

- and after the multi-step addition to Ac-RW and C-RW solutions (500 μ l, 5 μ M) at 25°C. The samples were prepared in buffer (10 mM Tris, 154 mM NaCl, pH 7.4). ----- 80
- Figure 5.2-2 DSC curves of DMPC, DPPG, and DPPE LUV (lipid concentration 1 – 2 mM) with and without added peptides Ac-RW and C-RW (L/P 20:1). The samples were prepared in buffer (10 mM Tris, 154 mM NaCl, pH 7.4). ----- 81
- Figure 5.2-3 DSC curves of DPPS, DMPA, TMCL and DPPG LUV (lipid concentration 1 – 2 mM) before (black lines) and after the addition of 2.4 mol% C-RW (red lines) (L/P 40:1). The samples were prepared in buffer (10 mM Tris, 154 mM NaCl, pH 7.4). ----- 82
- Figure 5.2-4 Transition temperature of DPPG (1 – 2 mM) as a function of peptide concentration. ----- 85
- Figure 5.2-5 DSC curves of DPPG/DMPC mixtures (total lipid concentration 1 – 2 mM) without and with added peptides Ac-RW and C-RW (L/P 15:1). The samples were prepared in buffer (10 mM Tris, 154 mM NaCl, pH 7.4). ----- 86
- Figure 5.2-6 DSC curves of DPPG/DPPE mixtures (total lipid concentration 1 – 2 mM) without and with added peptides Ac-RW and C-RW (L/P 15:1). The samples were prepared in buffer (10 mM Tris, 154 mM NaCl, pH 7.4). ----- 88
- Figure 5.2-7 DSC curves of TMCL/DPPG mixtures (total lipid concentration 1 – 2 mM) without and with added peptides Ac-RW and C-RW (L/P 15). The samples were prepared in buffer (10 mM Tris, 154 mM NaCl, pH 7.4). ----- 90
- Figure 5.2-8 DSC curves of TMCL/DPPE mixtures (total lipid concentration 1 – 2 mM) without and with added peptides Ac-RW and C-RW (L/P 15:1). The samples were prepared in buffer (10 mM Tris, 154 mM NaCl, pH 7.4). ----- 91
- Figure 5.2-9 DSC curves of the ternary TMCL/DPPG/DPPE 1:1:1 mixture (total lipid concentration 1 – 2 mM) without and with added peptides Ac-RW and C-RW (L/P 15:1). The samples were prepared in buffer (10 mM Tris, 154 mM NaCl, pH 7.4). ----- 92
- Figure 5.2-10 (Top) Temperature dependence of the wavenumber of the antisymmetric CD₂-stretching band of 60 mM DPPG-d₆₂ liposomes without and with 14.3 mol% C-RW (L/P 6:1). The samples were prepared in H₂O (100 mM NaCl). (Bottom) First derivate of the curves shown at the top. ----- 94
- Figure 5.2-11 Amide I and guanidinium vibrational bands (left) and their second derivative (right) of 10 mM Ac-RW and C-RW, respectively, in D₂O (100 mM NaCl) at various temperatures through the heating phase from 20°C to 76°C and the cooling back to 20°C. ----- 95
- Figure 5.2-12 Amide I and guanidinium vibrational bands (left) and their second derivative (right) of 10 mM Ac-RW and C-RW peptides, respectively, premixed with 60 mM DPPG-d₆₂ (L/P 6:1) in D₂O (100 mM NaCl) at various temperatures through the heating phase from 20°C to 76°C and the cooling back to 20°C. ----- 95
- Figure 5.2-13 (Top) Temperature dependence of the wavenumber of the symmetric CH₂-stretching band (left ordinate) and of the wavenumber of the CH₂-scissoring band (right ordinate) of TMCL (60 mM) without (full symbols) and with 14.3 mol% added peptide C-RW (L/P 6:1) (open symbols). The samples were prepared in H₂O (100 mM NaCl). (Bottom) First derivative of the curves shown in the top diagram. ----- 96
- Figure 5.2-14 (Top) Temperature dependence of the wavenumber of the antisymmetric CH₂-stretching band of DMPC (left ordinate) and of the wavenumber of the antisymmetric CD₂-stretching band of DPPG-d₆₂ (right ordinate) in a DPPG-d₆₂/DMPC 1:1 mixture (total lipid concentration 60 mM) without (full symbols) and with 14.3 mol% added peptide C-RW (L/P 6:1) (open symbols). The samples were prepared in H₂O (100 mM NaCl). (Bottom) First derivative of the curves shown in the top diagram. ----- 97
- Figure 5.2-15 (Top) Temperature dependence of the wavenumber of the antisymmetric CH₂-stretching band of DPPE (left ordinate) and of the wavenumber of the antisymmetric CD₂-stretching band of DPPG-d₆₂ (right ordinate) in a DPPG-d₆₂/DPPE 1:1 mixture

- (total lipid concentration 60 mM) without (full symbols) and with 14.3 mol% added peptide C-RW (L/P 6:1) (open symbols). The samples were prepared in H₂O (100 mM NaCl). (Bottom) First derivative of the curves shown in the top diagram. ----- 98
- Figure 5.2-16 (Top) Temperature dependence of the wavenumber of the symmetric CH₂-stretching band of TMCL (left ordinate) and of the wavenumber of the symmetric CD₂-stretching band of DPPE-d₆₂ (right ordinate) in a TMCL/DPPE-d₆₂ 1:1 mixture (total lipid concentration 60 mM) without (full symbols) and with 14.3 mol% added peptide C-RW (L/P 6:1) (open symbols). The samples were prepared in H₂O (100 mM NaCl). (Bottom) First derivative of the curves shown in the top diagram. ----- 99
- Figure 5.2-17 (Top) Temperature dependence of the wavenumber of the symmetric CH₂-stretching band of TMCL (left ordinate) and of the wavenumber of the symmetric CD₂-stretching band of DPPG-d₆₂ (right ordinate) in a TMCL/DPPG-d₆₂ 1:1 mixture (total lipid concentration 60 mM) without (full symbols) and with 14.3 mol% added peptide C-RW (L/P 6:1) (open symbols). The samples were prepared in H₂O (100 mM NaCl). (Bottom) First derivative of the curves shown in the top diagram. ----- 100
- Figure 5.2-18 (Top) Temperature dependence of the wavenumber of the symmetric CH₂-stretching band of TMCL (left ordinate) and of the wavenumber of the symmetric CD₂-stretching band of DMPG-d₅₄ (right ordinate) in a TMCL/DMPG-d₅₄ 1:1 mixture (total lipid concentration 60 mM) without (full symbols) and with 14.3 mol% added peptide C-RW (L/P 6:1) (open symbols). The samples were prepared in H₂O (100 mM NaCl). (Bottom) First derivative of the curves shown in the top diagram. ----- 101
- Figure 5.2-19 (Top) Temperature dependence of the wavenumber of the symmetric CH₂-stretching band of TMCL/DPPG 1:1 mixture (left ordinate) and of the wavenumber of the symmetric CD₂-stretching band of DPPE-d₆₂ (right ordinate) in a TMCL/DPPG/DPPE-d₆₂ 1:1:1 ternary mixture (total lipid concentration) without (full symbols) and with 14.3 mol% added peptide C-RW (L/P 6:1) (open symbols). The samples were prepared in H₂O (100 mM NaCl). (Bottom) First derivative of the curves shown in the top diagram. ----- 102
- Figure 5.2-20 (Top) Temperature dependence of the wavenumber of the symmetric CH₂-stretching band of TMCL/DPPE 1:1 mixture (left ordinate) and of the wavenumber of the symmetric CD₂-stretching band of DPPG-d₆₂ (right ordinate) in a TMCL/DPPE/DPPG-d₆₂ 1:1:1 ternary mixture (total lipid concentration 60 mM) without (full symbols) and with 14.3 mol% added peptide C-RW (L/P 6:1) (open symbols). The samples were prepared in H₂O (100 mM NaCl). (Bottom) First derivative of the curves shown in the top diagram. ----- 103
- Figure 5.2-21 (Top) Temperature dependence of the wavenumber of the symmetric CH₂-stretching band of TMCL/DMPG 1:1 mixture (left ordinate) and of the wavenumber of the symmetric CD₂-stretching band of DPPE-d₆₂ (right ordinate) in a TMCL/DMPG/DPPE-d₆₂ 1:1:1 ternary mixture (total lipid concentration 60 mM) without (full symbols) and with 14.3 mol% added peptide C-RW (L/P 6:1) (open symbols). The samples were prepared in H₂O (100 mM NaCl). (Bottom) First derivative of the curves shown in the top diagram. ----- 103
- Figure 5.2-22 (Top) Temperature dependence of the wavenumber of the antisymmetric CH₂-stretching band of TMCL/DPPE 1:1 mixture (left ordinate) and of the wavenumber of the antisymmetric CD₂-stretching band of DMPG-d₅₄ (right ordinate) in a TMCL/DPPE/DMPG-d₅₄ 1:1:1 ternary mixture (total lipid concentration 60 mM) without (full symbols) and with 14.3 mol% added peptide C-RW (L/P 6:1) (open symbols). The samples were prepared in H₂O (100 mM NaCl). (Bottom) First derivative of the curves shown in the top diagram. ----- 104
- Figure 5.2-23 (Top) Temperature dependence of the wavenumber of the symmetric CH₂-stretching band of POPE (left ordinate) and of the wavenumber of the symmetric CD₂-

- stretching band of DPPG-d₆₂ (right ordinate) in a DPPG-d₆₂/POPE 1:1 mixture (total lipid concentration 60 mM) without (full symbols) and with 14.3 mol% added peptide C-RW (L/P 6:1) (open symbols). The samples were prepared in H₂O (100 mM NaCl). (Bottom) First derivative of the curves shown in the top diagram. ----- 105
- Figure 5.2-24 The experimental power signals (top) and the integrated peaks as a function of DPPG/peptide ratio (bottom) of the titration of DPPG LUV (5 mM) in the syringe into Ac-RW (left) and C-RW (right) peptide solutions (20 μM) in the reaction cell, respectively, at 15°C. The samples were prepared in buffer (10 mM Tris, 154 mM NaCl, pH 7.4). ----- 107
- Figure 5.2-25 The experimental power signals (A) and the integrated peaks as a function of DPPG/C-RW ratio (B) of the titration of DPPG LUV (2.5 mM) in the syringe into C-RW peptide solution (40 μM) in the reaction cell at different NaCl concentrations (154 to 500 mM) at 25°C. The samples were prepared in buffer (10 mM Tris, 154 mM NaCl, pH 7.4). ----- 109
- Figure 5.2-26 The experimental power signals of the titration of DPPG/DPPC and DPPG/DPPE mixed LUV (total lipid concentration 5 mM) as well as of the single components (5 mM) in the syringe into C-RW peptide solution (20 - 50 μM) in the reaction cell at 25°C. The samples were prepared in buffer (10 mM Tris, 154 mM NaCl, pH 7.4). ----- 110
- Figure 5.3-1 Cartoon illustrating the C-RW-induced demixing in a bilayer of mixed PG/PE, represented by red and blue balls, respectively. C-RW segregates PG from PE creating defects between the formed domains. The hydrophobic amino acids Trp and Phe of the peptide are somewhat buried in the membrane core while the arginine residues interact with the PG headgroup region. ----- 114
- Figure 6.2-1 Epifluorescence image showing the aggregation of POPG LUV (NBD-DPPE 1 mol%) at the quartz substrate upon the premixing with 1 mM CaCl₂. The addition of Ca⁺² ions facilitated the adsorption of POPG vesicles to the acidic substrate but no supported membranes were formed. ----- 117
- Figure 6.2-2 (A) SLB prepared by VF of POPG/POPC 1:3 LUV (NBD-DPPE 1 mol%) premixed with 200 μM CaCl₂. (B) The SLB after the addition of 1 μM C-RW. ----- 118
- Figure 6.3-1 SLB prepared by LB/LS of the pure lipids POPC (A), POPE (B), POPG (C), POPG/POPC 1:1 (D), POPG/POPE 1:1 (E), and *E. coli* lipid extract (F). The lipid preparations were premixed with 0.75 mol% NBD-DPPE. The dark spots represent dye-depleted domains. ----- 119
- Figure 6.3-2 SLB prepared by LB/LS of POPG (A) and POPE (B). The figure shows the segregation of the dye molecules (NBD-DPPE 0.75 mol%) at the domains boundaries. ----- 121
- Figure 6.3-3 SLB prepared by LB/LS of POPG/POPE 1:1 (NBD-DPPE 0.75 mol%) showing the domains uncoupling between the two leaflets of the supported membrane. ----- 121
- Figure 6.4-1 SLB prepared by LB/LS of POPG (NBD-DPPE 0.75 mol%). The figures illustrate the effect and morphological changes over time (0 to 60 min) of adding 1 μM C-RW into the buffer. The subsequent images became darker as compared to the control image due to the photobleaching effect. The inset in (D) is a magnification of the pearl-chain instability. ----- 123
- Figure 6.4-2 SLB prepared by LB/LS of POPG (NBD-DPPE 0.75 mol%). The figures illustrate the effect and morphological changes over time (0 to 39 min) of adding 4 μM C-RW into the buffer. The subsequent images became darker as compared to the control image due to the photobleaching effect. The insets in (D) are magnifications of some structures in the image. ----- 124
- Figure 6.4-3 A proposed mechanism for the tubular outgrowth from SLB induced by the binding of amphipathic helical peptides. The α-helical peptides are represented by

<p>cylinders with their hydrophobic sides shaded gray. (A) Lipid segregation and membrane thinning induced at low peptide concentration. (B) The formation of fibrils that consists of lipids and peptides at high peptide concentration. Adapted from ref. (Domanov and Kinnunen 2006) -----</p>	125
<p>Figure 6.4-4 SLB prepared by LB/LS of POPG/POPC 1:1 (NBD-DPPE 0.75 mol%) before (A) and 8 min after the addition of 1 μM C-RW into the buffer (B).-----</p>	125
<p>Figure 6.4-5 SLB prepared by LB/LS of POPG/POPC 1:1 (NBD-DPPE 0.75 mol%). The figures illustrate the effect and morphological changes over time (0 to 169 min) of adding 4 μM C-RW into the buffer. The inset in (C) is a magnification of some structures in the image. -----</p>	126
<p>Figure 6.4-6 SLB prepared by LB/LS of POPG/POPE 1:1 (NBD-DPPE 0.75 mol%). The figures illustrate the effect and morphological changes over time (0 to 79 min) of adding 4 μM C-RW into the buffer. -----</p>	127
<p>Figure 6.4-7 SLB prepared by LB/LS of <i>E. coli</i> lipid extract (NBD-DPPE 0.75 mol%) before (A) and 45 min after the addition of 1.2 μM C-RW into the buffer (B). The difference in brightness between both images is due to the gray scaling applied upon processing both pictures.-----</p>	128
<p>Figure 6.5-1 SLB prepared by LB/LS of POPC (left) and POPE (right) (NBD-DPPE 0.75 mol%) before (A and C, respectively) as well as 60 and 90 min after the addition of 4 μM KLA1 into the buffer (B and D, respectively). -----</p>	130
<p>Figure 6.5-2 SLB prepared by LB/LS of POPG (NBD-DPPE 0.75 mol%). The figures illustrate the effect and morphological changes over time (0 to 22 min) of adding 4 μM KLA1 into the buffer. The bright lines in the SLB shown in (B) and (C) are most probably membrane deformations that were formed, initially, during the peptide injection process. -----</p>	131
<p>Figure 6.5-3 SLB prepared by LB/LS of POPG/POPC 1:1 (NBD-DPPE 0.75 mol%). The figures illustrate the effect and morphological changes over time (0 to 99 min) of adding 4 μM KLA1 into the buffer. -----</p>	132
<p>Figure 6.5-4 SLB prepared by LB/LS of POPG/POPE 1:1 (NBD-DPPE 0.75 mol%). The figures illustrate the effect and morphological changes over time (0 to 14 min) of adding 4 μM KLA1 into the buffer. -----</p>	133
<p>Figure 6.5-5 SLB prepared by LB/LS of <i>E. coli</i> lipid extract (NBD-DPPE 0.75 mol%) before (A) and 31 min after the addition of 5 μM KLA1 into the buffer (B). -----</p>	134

11.2 List of Tables

<p>Table 1.1-1 Phospholipid composition of red blood cells (percentage of total phospholipid) from various organisms listed according to increasing sphingomyelin content. Adapted from refs. (Lohner et al. 2008; White 1973). -----</p>	2
<p>Table 1.1-2 Phospholipid composition of some selected species of Gram-negative and Gram-positive bacteria (percentage of total phospholipid). Adapted from refs. (Lohner et al. 2008; O’Leary and Wilkinson 1988; Wilkinson 1988).-----</p>	4
<p>Table 1.2-1 The general chemical structure of phospholipids showing the hydrophilic headgroup and the hydrophobic tail regions. The phospholipids may differ in the headgroup structure as well as in the length, symmetry, degree of unsaturation and branching of the acyl chains.-----</p>	5
<p>Table 4.1-1 The nomenclature and sequence of KLA peptides. The modified amino acids as compared to KLAL are underlined. The one letter code is used to give the sequence; K: lysine, L: leucine, A: alanine, W: tryptophan. The capital and small letters are used to show L-amino acids and D-amino acids, respectively. Adapted from refs. (Dathe et al. 1996; Krause et al. 1995).-----</p>	18

Table 4.1-2 The different properties and activities of KLA peptides. Adapted from refs. (Dathe et al. 1996; Dathe et al. 1997; Krause et al. 1995) -----	19
Table 4.2-1 Summary of ΔA , KLA1 adsorption ratio and L/P ratio at the interface in dependence on film fluidity, KLA1 bulk concentration, POPG fraction in the mixed films, and POPG surface concentration. The surface pressure of the lipid films was kept at 30 mN m^{-1} . -----	31
Table 4.2-2 The different properties of pure KLAL film and of the peptide in the different lipid-KLAL premixed films. The structure of KLAL in POPC and DOPE premixed films was anticipated from the area per peptide molecule (see Figure 4.2-9) -----	40
Table 4.2-3 Comparison of the stretching vibrational bands (CH_2 , PO_2^- , CO) of the mixed lipid-peptide films at 30 mN m^{-1} and of the peptide adsorbed to lipid monolayers, whose pressure was kept at 30 mN m^{-1} , for the lipids POPG, DPPG, POPC and POPE. -----	42
Table 4.2-4 The thermodynamic parameters of the interaction of KLA peptides with lipid vesicles at different conditions. The helicity of the peptides is as following: $k_{1,12}$ -KLAL 74%, KLA1 54%, $l_{11,k_{12}}$ -KLAL 47%, and $k_{9,a_{10}}$ -KLAL 48%. The helicity was determined in POPG SUV suspension using $10 \mu\text{M}$ peptide (see Table 4.1-2). -----	63
Table 5.1-1 The biological and bilayer permeabilizing activities and hydrophobic parameters of Ac-RW and C-RW peptides. Adapted from refs. (Dathe et al. 2004; Wessolowski et al. 2004) -----	77
Table 5.2-1 The thermodynamic parameters of the DSC thermograms presented in Figure 5.2-3 of DPPG, TMCL, DMPA and DPPS before and after the addition of 2.4 mol% C-RW. -----	83
Table 5.2-2 The thermodynamic parameters of the interaction of C-RW with lipid vesicles at different conditions. -----	108
Table 9.3-1 Important infrared absorption bands of lipids. Adapted from ref. (Lewis and McElhaney 1996; Mendelsohn and Mantsch 1986; Tamm and Tatulian 1997) -----	147
Table 9.3-2 Infrared absorption frequencies of liquid H_2O , HOD, and D_2O . Adapted from ref. (Tamm and Tatulian 1997). -----	148
Table 9.3-3 Correlation between common protein secondary structures and the frequencies of Amide I and Amide II bands in H_2O and D_2O . Adapted from ref. (Arrondo et al. 1993; Goormaghtigh et al. 1994; Jackson and Mantsch 1995; Tamm and Tatulian 1997). ---	148

12 Acknowledgement

While this thesis is of necessity singularly authored, its production was ultimately a collaborative effort, and I would like to take this opportunity to thank those essential to its completion.

Of foremost, I owe my gratitude to my supervisor Prof. Alfred Blume for providing me the opportunity to undertake my Ph.D. in his group as well as for the intellectual stimulation, encouragement, support, and personal guidance throughout my postgraduate career.

I am obliged to Dr. Margitta Dathe (Forschungsinstitut für Molekulare Pharmakologie, Berlin) for providing the peptides, for the valuable contributions to my work, and for the fruitful cooperation.

I would like to acknowledge Prof. Lukas Tamm (Department of Molecular Physiology and Biological Physics, University of Virginia, VA) for giving me the opportunity to carry out part of this research in his lab and for his guidance, as well as to his group for all sorts of help. In addition, I would like to thank Dr. Luiz C. Salay for performing the BLM measurements (not included here) and Dr. Volker Kiessling for his essential assistance with the preparation of the supported lipid membranes and with the epifluorescence imaging and FRAP experiments.

I am indebted to Dr. Andreas Kerth for his essential assistance with the monolayer techniques, and IRRAS and FT-IR spectroscopies, Dr. Anton Hauser for performing the AFM experiments (not included here), and Dr. Günter Förster for performing the X-ray experiments (not included here) as well as for the extensive discussions.

I would like also to thank Dr. Hauke Lilie and Konstantin Kuppe (Institut für Biochemie und Biotechnologie, MLU) for their assistance with the CD measurements, as well as Dr. Willi Rettig and Mrs. Martina Mannd (Institut für Pharmazie, MLU) for performing low temperature DSC experiments (not included here).

I am extremely grateful to all members of the DFG Graduiertenkolleg 1026 “conformational transitions in macromolecular interactions”, particularly Mrs. Mechtild Wahle and Prof. Milton Stubbs, for the stimulating atmosphere and for the continuous help and support.

The technical assistance of Mr. Andreas Lonitz, Mrs. Bettina Fölting, and Mrs. Ingrid Schaller is much appreciated.

My sincere thanks are due to Dr. Annette Meister, Dr. Andreas Kerth, Dr. Christian Schwieger, and Dr. Martin Schiewek as well as to the other members of our group for the convenient atmosphere and for their valuable advices and friendly help in a variety of ways in the course of this research.

The financial support from Deutsche Forschungsgemeinschaft (DFG) is gratefully acknowledged.

Finally, a very special debt of gratitude goes to my family and friends. Without their support this work could never be done.

13 Curriculum vitae

13.1 Personal data

Surname: Arouri

First name: Ahmad

Date of birth: 20.03.1979

Place of birth: London

13.2 Education and research experience

1997 Secondary Certificate, Scientific Branch. Sweleh Secondary School, Amman/Jordan.

1997 –2002 B.Sc. Pharmacy, Faculty of Pharmacy, University of Jordan, Amman/Jordan.

2003 –2005 M.Sc. “Applied Polymer Science”, Department of Engineering Sciences, Martin-Luther-University Halle-Wittenberg, Halle (Saale)/Germany.

2004 Project Work in the workgroup of Prof. Alfred Blume: “Interactions between lipids and polyamines”. Martin-Luther-University Halle-Wittenberg, Halle (Saale)/Germany.

2004 –2005 Master Thesis in the workgroup of Prof. Alfred Blume: “IgG1 interactions with peptide mimotopes and *Staphylococcal* protein A: a calorimetric study using ITC and DSC”. In cooperation with Boehringer Ingelheim Pharma GmbH & Co. KG. Martin-Luther-University Halle-Wittenberg, Halle (Saale)/Germany.

2005 - 2008 Ph.D. Student, Faculty of Natural Sciences II (Chemistry and Physics), Martin-Luther-University Halle-Wittenberg, Halle (Saale)/Germany.

2007 Financial support from DFG for an integrated action with the Lab of Prof. Lukas Tamm, University of Virginia, VA/USA: “Epifluorescence imaging of the interaction of antimicrobial peptides with supported lipid membranes”.

13.3 Publications

- ❖ **Ahmad Aroui**, Margitta Dathe, Alfred Blume. Peptide induced demixing in PG/PE lipid mixtures: a mechanism for the specificity of antimicrobial peptides towards bacterial membranes?, *Biochim. Biophys. Acta* (2009), doi:10.1016/j.bbamem.2008.11.022.
- ❖ **Ahmad Aroui**, Patrick Garidel, Werner Kliche, Alfred Blume. Hydrophobic interactions are the driving force for the binding of peptide mimotopes and *Staphylococcal* protein A to recombinant human IgG1, *Eur. Biophys. J.* 36, 647-660 (2007).

13.4 Oral contributions

- ❖ **Ahmad Aroui**, Günter Förster, Luiz C. Salay, Volker Kiessling, Lukas Tamm, Margitta Dathe, Alfred Blume. Peptide-induced lipid demixing: a new mechanism of action of antimicrobial peptides? 11th Naples workshop on bioactive peptides, Naples (Italy), 24-27 May, 2008.
- ❖ **Ahmad Aroui**, Margitta Dathe, Alfred Blume. The effect of the antimicrobial peptide RRWRF on the behaviour of DPPG/DPPE and DPPG/DMPC mixed membranes as revealed by DSC and FT-IR. Fall meeting of the Graduiertenkolleg 1026 “Conformational transitions in macromolecular interactions”, Wittenberg (Germany), 6-8 September, 2007.
- ❖ **Ahmad Aroui**, Christian Schwieger, Margitta Dathe, Alfred Blume. Differential scanning calorimetry to monitor antimicrobials-induced changes in the thermotropic phase behaviour of lipid vesicles. Spring meeting of the Graduiertenkolleg 1026 “Conformational transitions in macromolecular interactions”, Oppurg (Germany), 8-10 March, 2007.
- ❖ **Ahmad Aroui**, Andreas Kerth, Margitta Dathe, Alfred Blume. Thermodynamics of the interaction of model antimicrobial peptides with model lipid membranes. Fall meeting of the Graduiertenkolleg 1026 “Conformational transitions in macromolecular interactions”, Potsdam (Germany), 4-6 October, 2006.
- ❖ **Ahmad Aroui**, Andreas Kerth, Margitta Dathe, Alfred Blume. The influence of the lipid model on the behaviour of amphipathic peptides at the air/water interface as

studied by Infra-Red Reflection-Absorption Spectroscopy (IRRAS). Spring meeting of the Graduiertenkolleg 1026 “Conformational transitions in macromolecular interactions”, Weimar (Germany), 17-19 March 2006.

- ❖ **Ahmad Aroui**, Patrick Garidel, Werner Kliche, Alfred Blume. IgG1 interactions study using ITC. Fall meeting of the Graduiertenkolleg 1026 “Conformational transitions in macromolecular interactions”, Wittenberg (Germany), 2-4 September 2005.
- ❖ **Ahmad Aroui**, Patrick Garidel, Werner Kliche, Alfred Blume. IgG1 interactions with peptide mimotopes and *staphylococcal* protein A: a calorimetric study using ITC. Workshop in biological physics, physics of life: from single molecules to networks, Humlebæk (Denmark), 21-27 August, 2005.

13.5 Poster contributions

- ❖ **Ahmad Aroui**, Luiz C. Salay, Lukas Tamm, Margitta Dathe, Alfred Blume. Peptide-induced lipid demixing: a new mechanism of action of antimicrobial peptides. International meeting of the Graduiertenkolleg 1026 “Conformational transitions in macromolecular interactions”, Halle (Germany), 28-1 February-March, 2008.
- ❖ **Ahmad Aroui**, Margitta Dathe, Alfred Blume. The interaction of polyamines and CAMPs with negatively charged lipid membranes: a calorimetric study. The 6th EBSA European Biophysics Congress, London (U.K.), July 14 –18, 2007 (Eur Biophys J (2007) 36 (Suppl 1):S51–S248).
- ❖ **Ahmad Aroui**, Andreas Kerth, Margitta Dathe, Alfred Blume. A comparison of the interaction of antimicrobial peptides with PE and PC containing lipid membranes. 2nd Workshop on Biophysics of Membrane-active Peptides, Lisbon (Portugal), April 1-4, 2007.
- ❖ **Ahmad Aroui**, Christian Schwieger, Margitta Dathe, Alfred Blume. Differential scanning calorimetry to monitor antimicrobials-induced changes in the thermotropic phase behaviour of lipid vesicles. Membrane interacting lipids and proteins, Halle/Saale (Germany), 28-31 March, 2007.
- ❖ **Ahmad Aroui**, Andreas Kerth, Margitta Dathe, Alfred Blume. Interaction of antimicrobial peptides with PE and PC containing lipid membranes. Annual Meeting of the German Biophysical Society, Mainz (Germany), 24-27 September, 2006.

- ❖ **Ahmad Arouri**, Andreas Kerth, Margitta Dathe, Alfred Blume. Amphipathic model peptide-lipid mixtures at the air/water interface. International Workshop on dynamics of artificial and biological membranes, Gomadingen (Germany), 20-22 March, 2006.
- ❖ Christian Schwieger, **Ahmad Arouri**, Alfred Blume. Interaction of negatively charged Membranes with Polyamines. Annual meeting of the German Biophysical Society, Freiburg (Germany), 12-15 September, 2004.

14 Statement of originality

This work has not been previously submitted for a degree in any university.

To the best of my knowledge and belief, this thesis contains no previously published or written by another person expect where due reference is made in the thesis itself.

Ahmad Arouri

Halle, December 2008